ANALYSIS OF DYNAMIC LOADING BEHAVIOUR FOR PAVEMENT ON SOFT SOIL

Dissertation

Slamet Widodo

Technische Universität Bergakademie Freiberg

Freiberg, 2013

ANALYSIS OF DYNAMIC LOADING BEHAVIOUR FOR PAVEMENT ON SOFT SOIL

To the Faculty of
Geowissenschaften, Geotechnik und Bergbau
of the Technische Universität Bergakademie Freiberg
approved

THESIS

to attain the academic degree of

DOKTOR-INGENIEUR
DR.-ING.

Submitted

By Magister Teknik in Pavement Engineering, Slamet Widodo
Born on the 23rd December 1967 in Surabaya, Indonesia

Reviewers: Prof. Dr.-Ing. Herbert Klapperich, Freiberg
Prof. Dr.rer.nat. Rafig Azzam, Aachen
Prof. Dr. Masyhur Irsyam, Bandung-Indonesia

Date of the award: 19-11-2013

ACKNOWLEDGMENTS

The author wishes to express his sincere gratitude to Prof. Dr.-Ing. Herbert Klapperich, the chairperson of his dissertation committee, for his very kind encouragement, guidance, friendship and inspiration given throughout the graduate work. The author is also grateful to the other dissertation committee members, Prof. Dr.rer.nat. Rafig Azzam and Prof. Dr. Masyhur Irsyam for their very precious time for reading this dissertation.

The author is very grateful to Dr.-Ing. Habil. Nandor Tamaskovics for his kind encouragement, competent guidance, care and always inspires him. Thanks to all of the author's colleagues and staff at Soil Mechanics laboratory, Institut für Geotechnik for their help, co-operation and valuable discussions and especially to Dr.-Ing. Ernst-Dieter Hornig and Frau Helga Vanselow and also Hong Shen, Abdelazim Ibrahim, Jinyang Fu, Phan Luu Minh Phuang, Irina, Anastasia Alferova, Ahmed Mohamed, and Sebastian Althoff.

Special thanks is addressed to some generous people who permit him using their data in part of this thesis namely Suzanne van Eekelen, Prof. Marcio S.S. Almeida, Abdullah C. Hassandi and Cao Wei-ping.

The financial support of the Overseas Scholarship Program of Master/PhD for Academic Staff of Tanjungpura University with contract No. 1725.35/D4.4/2009 during the author's studies at the Technische Universität Bergakademie Freiberg is gratefully acknowledged. The support by the GraFA (Graduierten-und Forschungsakademie) is also gratefully acknowledged. Likewise, join working with DFG-Research Project is really helpful. The author honored to thank to Prof. Dr. Chairil Effendy, the former Rector of Tanjungpura University and Prof. Dr. Thamrin Usman as the Rector of Tanjungpura University.

Thanks warmly to the author's Indonesian friends in Freiberg who made his years enjoyable: families of Arief Wijaya, Herry Permana, Toni and Eki, Nazaruddin, Heru, Annisa, Anesia, Miranti, Annas, Anto, and Linda. Also, special thanks goes to Adang Budiman that improves his English and Prof. Zhuang for correcting the final manuscript.

The author is very grateful to his parents, special thanks to the author's parents, Suhadi and Sutrinah and also mother-in-law, Nurjanah who always pray for the success, happiness and moral support, and encouragement.

Finally, the author is overwhelmed in thanking his wife, Juliana and his children, Basith, Retnoayu, and Satrio, for their understanding and patience throughout the period of his study. Also, special thanks goes to Fajar Indaharti, from her he learn deep patience and sincerity.

ABSTRACT

The increasing need for regional development has led engineers to find safe ways to construct the infrastructure of transportation on soft soils. Soft soil is not able to sustain external loads without having large deformations. The geotechnical properties of soft soil which is known for its low bearing capacity, high water content, high compressibility and long term settlement as well.

In pavement engineering, either highway or runway as an infrastructure, a pavement encompasses three important parts namely *traffic load*, *pavement* and *subgrade*. Traffic load generated from tire pressure of vehicle and/or airplane wheels are usually around 550 kPa even more on the surface of the pavement. Pavement generally comprises granular materials with unbounded or bounded materials located between traffic load and subgrade, distributing the load to surface of subgrade.

One of the promising soil improvement techniques is a *piled embankment*. When geosynthetics layer is unrolled over piles, it is known as *geosynthetics supported piled embankment*. Particularly in deep soft soil, when piles do not reach a hard stratum due to large thickness of the soft soil, the construction is an embankment on floating piles. Furthermore, because of different stiffness between piles and subsoil, soil arching effect would be developed there.

By using Finite Element analysis, some findings resulted from experimental works and several field tests around the world as field case studies are verified. Some important findings are as follows: the stress concentration ratio is not a single value, but it would be changed depending on the height of embankment, consolidation process of subsoil, surcharge of traffic load, and tensile modulus of geosynthetics as well. Ratio height of embankment to clear piles spacing (h/s) around 1.4 can be used as a critical value to distinguish between low embankment and high embankment. When geosynthetics is applied to reinforce a pavement/embankment, the vertical distance of geosynthetics layers and number of geosynthetics layers depend on the quality of pavement material. The lower layer of geosynthetics withstands a tensile stress higher than upper layer. Primary reinforcements for geosynthetics in piled embankments are located at span between piles with maximum strains at zones of adjacent piles. Traffic load that passes through on the surface of the pavement can reduce the soil arching, but it can be restored during the off peak hours. Settlements of embankments on floating piles can accurately be modelled using the consolidation calculation type, whereas the end-bearing piles may be used the plastic calculation type. Longer piles can be effectively applied to reduce a creep. By applying length of floating piles more than 20% of soft soil depth, it would have a significant impact to reduce a creep on a deep soft soil.

TABLE OF CONTENTS

CHAPTER 3. CHARACTERIZATION OF MATERIALS AND LOADING

CHAPTER 4. EXPERIMENTAL WORKS AND FIELD CASE STUDIES

LIST OF FIGURES

LIST OF TABLES

LIST OF NOTATIONS

a	width of the pile cap
A	total cross-sectional area of the 'unit cell' attributed to each column
a	radius of the circular footing
A,B,C,D	fitting parameters
A/A_c	reciprocal area replacement ratio
A_1	reduction factor for creep
A_2	reduction factor for damage caused by transport, installation, compression
A_3	reduction factor for processing connection
A_4	reduction factor for environmental influences (weather, chemical, micro-organism)
A_c	cross-sectional area of one column
A_G	plan area of pile group including the soil between the piles
a_s	area replacement ratio or coverage ratio
B	width of underground structure
$2B$	width of strip
b_{Ers}	width of column
C	competency ratio
c	viscous damping constant
C_1 , C_2	material constant
CBR	California Bearing Ratio
CBR_{bc}	CBR value of the base course
CBR_{sg}	CBR value of the subgrade soil
C_c	soil arching coefficient depending on H and a $C_c = 1.5\ H / a - 0.07$ for floating piles $C_c = 1.95\ H / a - 0.18$ for end-bearing piles
C_c	coefficient of curvature
c_c	compression index
c_h	average coefficient of horizontal consolidation
c_r	recompression index
c_s	swelling index
CR	compression ratio
CSR	column stress ratio
C_u	coefficient of uniformity
c_u	undrained cohesion
c_v	consolidation coefficient
c_α	swelling index
d	diagonal pile spacing
D	Euler's stretching tensor an
D	damping ratio
d	thickness of pavement (or concrete layer),
D	column diameter
d	depth
D	flexural rigidity of the plate strip
D	strain rate
D	thickness of stabilized clay layer (or sub-layer)

d*	underlying stratum
D_{10}	diameter of grains passing sieve at 10 percentage
D_{60}	diameter of grains passing sieve at 60 percentage
$\mathbf{D}^{acc}$	given accumulation rate
d_e	equivalent diameter
d_i	reinforced depth
d_i	stratum (or sub-layer) thickness within the reinforced depth
D_{max}	maximum diameter of grains
D_{min}	minimum damping ratio
E	modulus of elasticity
E	Young's modulus,
E	efficacy
E	elastic stiffness
e	void ratio
E_1, E_2	elastic modulus of first and second layer
E_{50}	secant modulus
E_{50}^{ref}	reference stiffness modulus corresponding to the reference stress p^{ref}
E_c	modulus deformation of the columns
E_c	Young's modulus of concrete
e_d, e_c and e_i	reference void ratio corresponding to the non-zero stress
E_k	horizontal outward-thrust
e_{max}	maximum void ratio
e_{min}	minimum void ratio
e_o	initial void ratio
E_{oed}	oedometer compression modulus
E_{oed}^{ref}	reference tangent stiffness for primary oedometer loading
ESAL	equivalent single axle load
E_{ur}^{ref}	reference un-/reloading modulus corresponding to the reference pressure σ^{ref}
f	yield function
F_b	flexural strength
f_B	low frequency
f_c	partial factor for construction safe
f_c'	characteristic compressive strength 28 day
F_c	compressive strength of perpendicular fiber
f_c	factor for bearing capacity of subgrade soil
F_c	tensile strength for perpendicular fiber
f_{cf}	flexural-tensile strength 28 day
f_d	partial factor for mechanical damage
F_d	permissible long term tensile strength
f_{env}	partial factor for environment
f_{fs}	partial load factor for soil unit weight
F_k	short term tensile strength
F_k	vertical load
f_m	partial factor for extrapolation of tensile strength
f_q	partial load factor for applied external load
f_s	factor for rutting depth of 75 mm
$F_{s,G,k}$	vertical load at static loading

$F_{s,G+Q,k}$	vertical load at static and variable-dynamic loading
F_t	tensile strength for parallel fiber
F_v	shear strength
g	plastic potential function
G	shear modulus of material
G	specific gravity
G	specific gravity of wooden material
G_0	initial shear modulus
G_0^{ref}	elastic small strain shear modulus at reference pressure p^{ref}
G_{max}	maximum shear modulus of material
G_o	initial shear modulus of material
h	height of embankment
H	thickness of soil above the point
h	required base course thickness
H	thickness of soil above the point
h	thickness of the first layer
H	thickness of fill granular material
h	thickness of first layer
H	thickness of soil layer
h/s	ratio of embankment height to clear spacing
H_c	critical height of embankments without ground treatment
h_g	height of arching $h_g = h$ for $h < s / 2$ $h_g = s / 2$ for $h \geq s / 2$
h'_o	thickness of unreinforced aggregate base
H_r	thickness of reinforced granular material
H_u	thickness of unreinforced granular material
I	moment inertia of beam
I_o	Bessel function of the first kind and order of zero
I_p	placticity index
J	geogrids aperture stability modulus
J_k	tensile stiffness of geosynthetics
K	earth pressure coefficient
k	modulus of subgrade reaction
k	foundation stiffness
k	reaction modulus of subgrade
k	stiffness of geosynthetics
k_1, k_2,k_3	regression coefficients obtained from regression analysis
K_a	active earth pressure coefficient ($K_a = \tan^2 (45+\phi/2)$
K_{agh}	active lateral earth pressure coefficient according to DIN 4085
K_b	empirical bearing capacity factor
k_i	permeability
K_{krit}	critical ratio of major stress = $\tan^2 [45^o + \phi'_k / 2]$
K_o^{NC}	K_o-value for normal consolidation
K_p	coefficient of passive earth pressure
k_v	permeability
K_w	coefficient instead of K
L	length of span

L	length of the column
L	pile length
L	column length
$\mathcal{L}$	fourth order constitutive tensor
l	radius of relative stiffness
L/d	to optimum column aspect ratio
LL	liquid limit
L_w	clear spacing
m	power for stress-level dependency of stiffness
m	dimensionless parameter
M	slope of critical state line
m	mass per unit length of the beam
M_E	compressibility modulus
M_V	rigidity modulus
M_r	resilient modulus
M_{soil}	oedometer compression modulus of surrounding soil
m_v	coefficient of compressibility of untreated soft clay
$\boldsymbol{M}$	fourth-order tangent stiffness tensor of the material
n	number of piles
$\mathbf{N}$	second order constitutive tensor
N	number of axle passes
N	number of blows from Standard Penetration Test (SPT)
N	number of cycles
N	number of passes of axle load
n	porosity
n	stress concentration ratio
N_c	factor of bearing capacity
OC	organic content
OCR	state of preconsolidation stress
P	constant concentrated vertical with moving load
P	wheel load
p	total applied pressure of the embankment
p	mean principle stress
p	support pressure from roof above underground structure
p	tire inflation pressure
p^*	normalized loading (p/p_o)
P_A	axle load
P_a	reference pressure (atmospheric pressure)
P_{av}	average load on a pile within group
P_{axle}	axle load
p_c	vertical stress on the column
p^{eq}	constant on the ellipse in the p-q plane
$p_{G,k}$	static loading
$p_{G+Q,k}$	static and variable loading
P_i	actual axle load
PI	plasticity index
P_o	equivalent standard axle load of 80 kN

p_o	nominal overburden total stress at the elevation of underground
p_o	pressure on the circular footing
p_z	vertical pressure on the circular footing
q	distributed surcharge load
q	surcharge acting at the surface of the soil
q	ultimate vertical stress in a stone column
q	vertical stress at the subgrade surface
Q	design dynamic load
q_a	quantity
q_c	cone tip resistance
q_f	ultimate deviatoric stress
Q_r	required design vertical load
q_u	unconfined compressive strength
q_u	unconfined compressive strength
r	column radius
r	horizontal distance from centerline
R	radius of equivalent tire contact area
R	aspect ratio of the group
R	radius of circular area
R,β_r,χ,m_R,m_T	five addtional parameters for iIntergranular strain concept
R_f	failure ratio
RSR	relative settlement reduction
s	diagonal pile spacing
s	allowable rutting depth
s	column spacing
s	pile spacing
s	rut depth
S	settlement of embankment supported by piles
S	stiffness coefficient
s/d	ratio of pile spacing to pile cap diameter
S_0	embankment settlement constructed on soft soil without the support of piles
S_1	compression of the stabilized volume for case 1
S_1	settlement of a single pile under unit load
S_2	compression of stabilized volume for case 2
s-a	width of strip
S_c	settlement of the columns
S_o	settlement of untreated soil subjected to the actual load of embankment
S_p	primary settlement
S_r	degree of saturation
SRR	stress reduction ratio
S_s	settlement of untreated soil subjected to reduced pressure
S_s	secondary settlement
s_u	undrained shear strength
t	time
T	corrected thickness of base course
t_1	time in first step
t_2	time in next step
$\boldsymbol{T_{eff}}$	effective aggregate thickness

T_o	initial aggregate thickness
T_{RP}	tension in geosynthetics
$\dot{\mathbf{T}}$	Jaumann stress rate
V	constant velocity
v	Poisson's ratio
v_{cr}	critical velocity
v_{ur}	un-/reloading Poisson's ratio
V_s	shear wave
w	lateral deflection of plate strip
w	water content
w	deformation at interface between two layers
$w(r)$	vertical displacement of the surface
w_i	settlement of a pile *i* within a group of *n* piles
W_n	water content
W_T	equivalent vertical load
z	thickness of the soil overlying the element
$\epsilon^{acc\ v}$	volumetric strain
$\Delta\ d_{stab}$	consolidation settlement of stabilized ground
Δd	consolidation settlement of unstabilized ground
ΔP	different stress
ΔS_r	differential settlement between the columns and the untreated soil
Φ	state 'compaction' $\Phi = \Delta\ n\ /n_0$
α_{ij}	interaction factor for pile *i* due to any other pile *j* within the group
α	influencing factor due to the presence of geosynthetics layer
β	settlement reduction ratio
δ	maximum sag (vertical deflection) of geosynthetics
δ	settlement of roof
δ	intergranular strain tensor
δ^*	normalized displacement (δ / B)
$\varepsilon^{acc}(N)$	average accumulation curve
ε^{ampl}	strain amplitude
$\underline{\dot{\varepsilon}}^{e}$	elastic strain rate
$\dot{\varepsilon}_q^{acc}$	accumulation of deviatoric strain
$\dot{\varepsilon}_v^{acc}$	accumulation of volumetric strain
ε^{e}	elastic strain
ε^{p}	plastic strain
$\underline{\dot{\varepsilon}}^{p}$	plastic strain rate
ε	strain
ε_v	vertical strain
ε_k	strain in geosynthetics
ϕ'	effective internal friction angle
ϕ_c, h_s, n, e_{d0}, e_{c0}, e_{i0}, α, β,	eight material parameters for hypoplastic model
ϕ_{max}	peak secant angle of shearing resistance
ϕ	internal friction angle of the soil

γ	unit weight of the soil
γ	partial safety coefficient for the consideration of possibility
γ_k	unit weight of embankment
γ	unit weight of the soil
γ^{ampl}	shear strain amplitude
γH	nominal vertical stress at the base of embankment
γ^{p}	plastic shear strain
γ	unit weight
η^{av}	average stress ratio
η_1	creep factor
η_2	installation damage factor
η_3	biological and chemical degradation factor
κ^*	modified swelling index
λ	plastic multiplied factor
λ^*	modified compression index
μ	Poisson's ratio
μ^*	modified creep index
μ_1, μ_2	Poisson's ratio of first and second layer
ρ	density of soil
σ	average stress of applied embankment plus surcharge at level of top piles
σ_a	allowable strength
σ_3	confining stress
σ_c	stress on the columns
σ_c	vertical stress on the pile cap
σ_d	deviatoric stress
σ_{creep}^{col}	creep strength of column
σ_h'	effective horizontal pressure on the columns
σ_h	horizontal stress
σ_i	radial (vertical) stress acting immediately beneath the crown of the arch
σ_{pile}	vertical stress on piles
σ_{rz}	vertical stress at interface between two layers with radius = r
σ_s	reduced pressure on the untreated soil due to embankment
σ_s	stress on the subsoil
σ_{soil}	vertical stress on soil
σ_u	ultimate strength
σ_v	vertical stress
σ_z	vertical stress at interface between two layers with radius = 0
$\sigma_{flexural}$	flexural strength of wooden material
σ'_{ro}	free-field lateral effective stress
$\sigma_{\_I\_compressive}$	compressive strength of wooden material
$\sigma_{// comp or tensile}$	tensile strength of wooden material
θ	bulk stress ($\sigma_1 + \sigma_2 + \sigma_3$)
τ	shear strength
τ_{oct}	octahedral shear stress
$\tau_{u,col}$	undrained shear strength of the columns

$\tau_{//}$	shear strength of wooden material
(x_0 , z)	fixed coordinates along the length of strip and in the vertical direction

CHAPTER 1

Introduction

The increasing need for infrastructure development has led engineers to find an alternative on soft soils. Engineers are continually faced with maintaining and developing pavement infrastructure with limited financial resources. Traditional pavement design and construction practices require high-quality material for fulfilment of construction standards. In many areas of the world, quality materials are unavailable or in short supply. Due to these restrictions, engineers seek alternative designs or innovative design practices.

Weak foundation soils have always been a challenge to geotechnical engineers when designing infrastructure. Low bearing capacity, slope stability, lateral pressure, movements and differential settlements are some major concerns. However, a variety of techniques are available to address these issues, including preloading, deep mixing columns, stone columns, use of lightweight fill and soil replacement. Flexible pavement layered system is shown in Fig.1-1. Meanwhile, vertical load distribution induced by a moving wheel load is illustrated in Fig. 1-2.

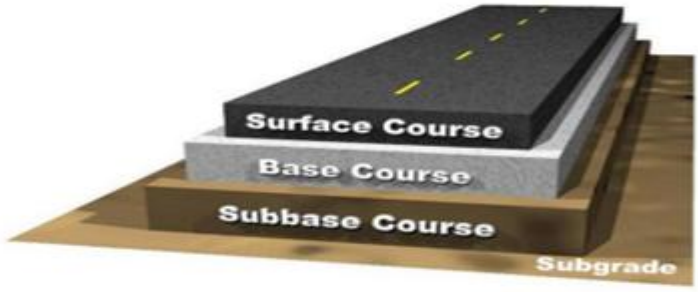

Fig. 1-1 Cross-section of flexible pavement system (after Muench, 2006)

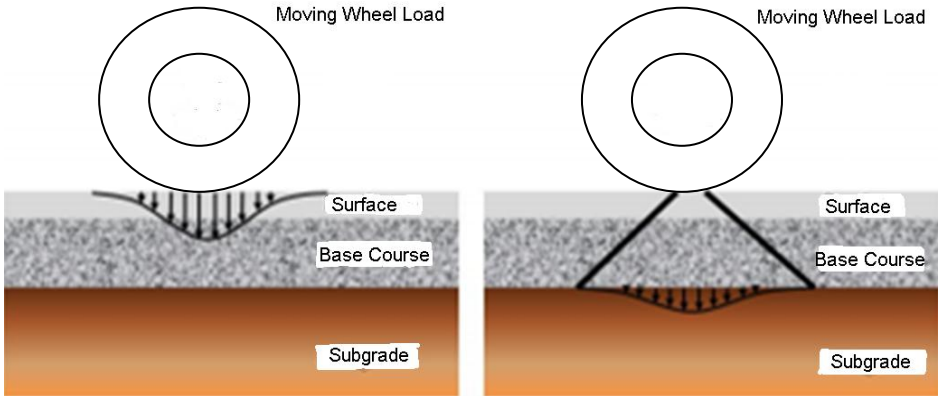

(a) (b)

Fig. 1-2 Stress distribution with depth in a flexible pavement, (a) High stress area directly under wheel load (b) Reduced load at subgrade level

1.1. Reinforced Base Course

Fig. 1-3 shows a typical section of reinforced base course, which consists of an aggregate base layer, a subgrade and a reinforcement layer usually placed between the base course and subgrade. The base course and geogrid transmit the traffic load to the top of the subgrade. Under repeated load, the behaviour of the base-geogrid-subgrade system is complicated. The overall behaviour depends on the properties of geosynthetics, soil characteristics, and the interaction between the soil and the reinforcement.

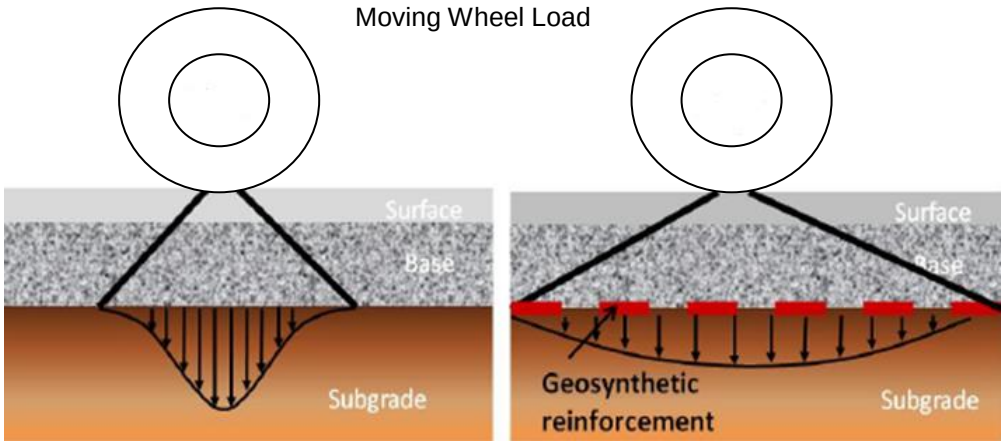

(a) (b)

Fig. 1-3 Relative load magnitude at subgrade layer level (a) Unreinforced flexible pavement (b) Geosynthetics-reinforced flexible pavement

1.2. Piles Supported Embankment

Soil alone is only able to carry compressive and shear forces. However, through the use of geosynthetics as reinforcing elements, soil structures can be built to carry tensile forces. It is real vision that the reinforcement of soil with geogrids will be common in the future as reinforcement of concrete with steel mesh is nowadays. In roadway, runway and railway applications the insertion of horizontal geogrid layers in granular base course provide an increased modulus, hence it provides lateral confinement to the system.

For soft soils, one of the most promising solution to these problems is to use piled embankments. In many cases, this method appears to be the most practical, efficient (low long-term cost and short construction time) and environmentally-friendly solution for construction on soft soil. Field applications are mainly highways and railways.

Piles are installed through the soft subsoil and transfer load to deeper subsoil. The majority of the load from embankments and surcharge (pavements and live load) are carried by the piles and thus there is relatively little load on the soft subsoil. Piles are typically arranged in square or triangular patterns in the field. By using a piled embankment technique, the construction can be undertaken in a single stage without having to wait for the soft soil to consolidate.

Settlements and differential settlements are also significantly reduced once the technique is used successfully.

Geosynthetics-reinforced piles supported embankment is a promising technique when it is constructed over weak soil as depicted in Fig. 1-4. It is also valuable in two ways; if there is adjacent structure that is sensitive to differential settlement and if there is a need for accelerated construction. This complex foundation system consists of strong piles in soft soil and compressible soil. A bridging layer is placed above the columns consisting of coarse grained soil and one or more layers of geosynthetics is situated on the bridging layer.

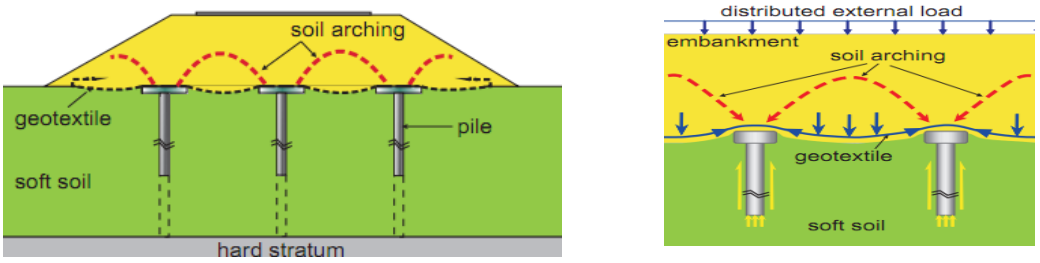

(a) (b)

Fig. 1-4 Geosynthetics-reinforced piles supported embankment (after Satibi, 2009)

1.3. Motivation

Stiff soils are preferable as a foundation for buildings, roadways and other infrastructures. However, these types of foundation soil are not always available on site. In tropic regions like Indonesia, soft soil deposits (peat, organic and inorganic soft soil) occur in lowland and highland areas and generally termed as basin and valley of peat. In some places, the depth of soft soil can reache 30 meters or even more.

Soft soil exhibits very low bearing capacity and it is not suitable for constructing embankment, highway, runway, railway, building or any other load bearing engineering structure. Organic soft soil in its natural state consists of water and decomposing plant fragments with virtually no measurable bearing strength. Peat and organic soil are considered as soft soil because they have high settlement value and even under moderately applied load.

The most extensive areas of peat soil are located in the northern hemisphere. It is estimated about 1 billion acres of the world are peat or equal to 4.5% of total land area. In United States peat is found in 42 states, with a total area of 30 million hectares. Canada has 170 million hectares and the former USSR has 150 million hectares. In Japan, peat is widely distributed throughout Hokaido with an area approximately 200 thousand hectares (Alwi, 2007).

The world tropical peat land is located in Asia, South Africa and Latin America covering around 30 million hectares. Around two thirds (66%) are in Southeast Asia (Global Environtment Centre). While in Indonesia peat soil covers about 20 million hectares of the country land. Most extensive areas are located across eastern Sumatra, western and southern Kalimantan and southern Papua. The soft areas are mostly dominated by peat overlaying soft clay soils, whereas there are mainly soft clay soils spreading out in other places as depicted in Fig. 1-5.

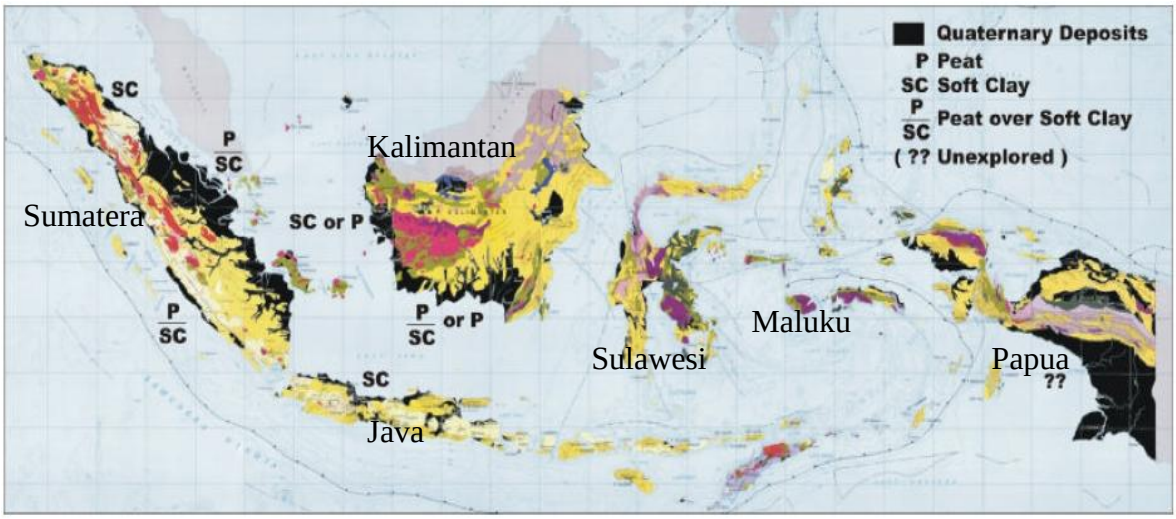

Fig. 1-5 Location of soft soil in Indonesia (after Puslitbang, 2001)

The total area of soft soils (peat and soft clay soil) in Indonesia is about 60 million hectares, which contribute around 30 percent of the total land area (Satibi**,** 2009). Distribution of peat soils in some regions or provinces in Indonesia is reported by Radjaguguk (1991) resulted from a study conducted by Euroconsult in 1983 and the final report by BB Litbang (2008). This is shown in Table 1-1. Meanwhile, Table 1-2 illustrates the depth distribution of peat soils.

Table 1-1 Distribution of peat soils in Indonesia

Islands / Provinces	Area of peat soils in Indonesia (hectares)	
	After Radjaguguk, 1991	After BB Litbang, 2008
Sumatera Island		
Nanngroe Aceh	270	-
North Sumatera	335,000	-
West Sumatera	31,000	-
Riau	1,704,000	4,043,600
Jambi	900,000	716,839
South Sumatera	990,000	1,483,662
Bengkulu	22,000	-
Lampung	24,000	-
Kalimantan Island		
West Kalimantan	4,610,000	1,729,980
Central Kalimantan	2,162,000	3,010,640
South Kalimantan	1,484,000	331,629
East Kalimantan	1,053,000	-
Sulawesi Island		
Central Sulawesi	15,000	-
South Sulawesi	1,000	-
Southeast Sulawesi	18,000	-
Maluku Archipelago	20,000	-
Papua Island	4,600,000	7,001,239
Java Island	25,000	-
	17,994,270	18,317,589

Source: Radjaguguk, 1999; BB Litbang, 2008

Table 1-2 Distribution of thickness for peat soils in Indonesia

Province	Distribution based on thickness of peat (%)			Total area (hectares)
	Shallow 0-150 cm	Intermediate 100-200 cm	Deep >200 cm	
Riau	8.6	10.7	80.7	486,339
Jambi	33.4	9.3	57.3	168,163
South Sumatera	63.0	11.5	25.5	317,784
West Kalimantan	39.5	34.6	25.9	100,754
South & Central Kalimantan	62.6	19.6	17.8	190,145
			Total	1,263,185

Source: Radjaguguk, 1991

1.4. Geological Indonesia

The biogeography of the whole Indonesian archipelago and the distribution of its soil, plants and animals have been determined by the geological and climatic history. Fig. 1-6 shows a story of plate tectonics and continental drift, climatic events and changing sea levels (MacKinnon et al., 1996).

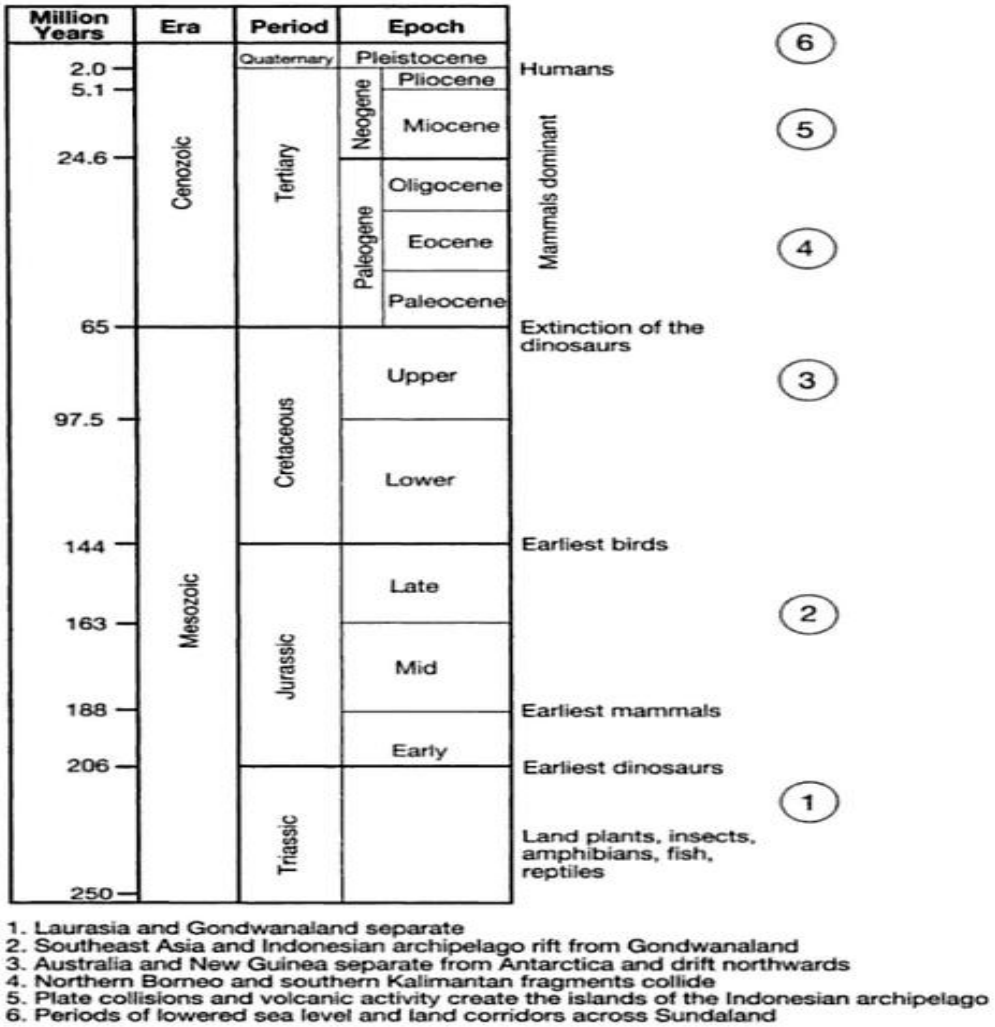

Fig. 1-6 Geological time scale showing the appearance of life forms and the occurrence of major geological events (after MacKinnon et al., 1996)

As recently as of 25 million years ago, very recently on the geological time scale as in Fig. 1-6, the Indonesian archipelago as we know it today simply did not exist, but the story began much earlier than that.

The continental land masses are by no means permanent and the earth is in a dynamic state. The outer solid part of the earth, the crust, is quite thin, like the rind of an orange. The are two kinds of crust: oceanic and continental. Oceanic crust is usually young (0-200 millions years), thin (5-15 km) and composed mostly of dense volcanic rocks. Continental crust often has a core of older rocks (200 to 3,500 million years), is thicker (20-50 km) and is less dense than oceanic crust, composed of rocks such as sandstones and granites. Western Indonesia, comprised of Kalimantan, Sumatra, and West and Central Java, is composed predominantly of continental crust, as is much of the shallow sea floor between these islands. Below the crust of the earth is a zone where the rock is hotter and more plastic. Continental and oceanic plates float on a fluid, underlying material (Simandjuntak, 1993).

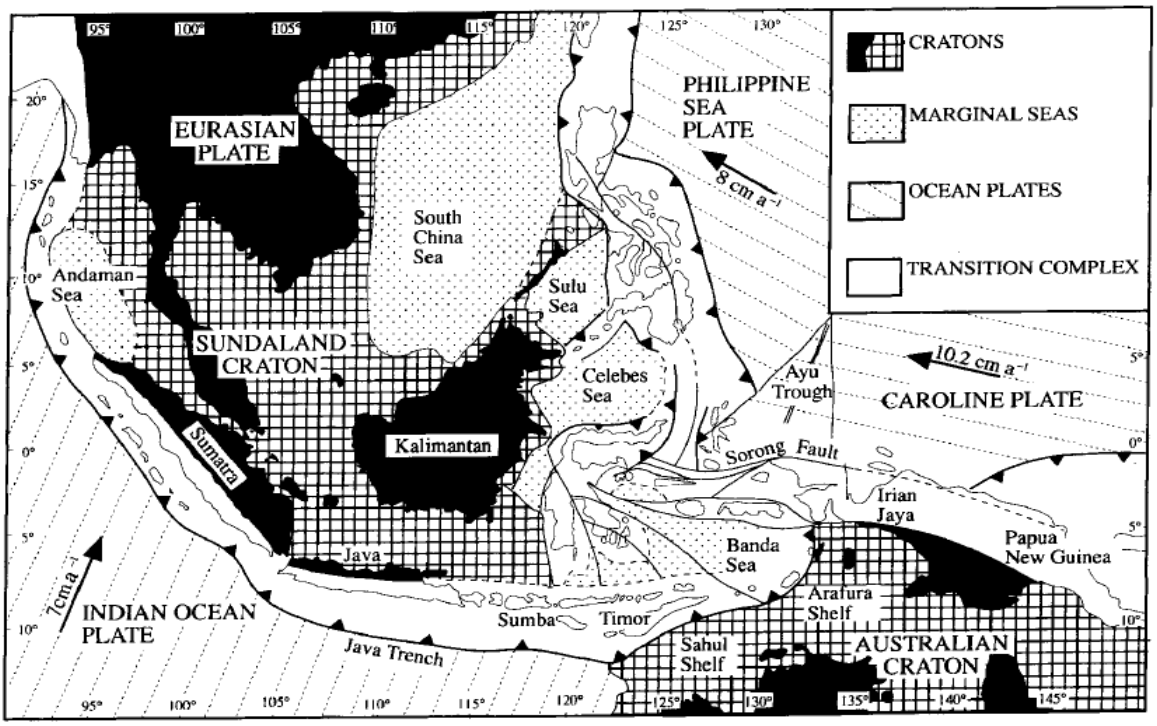

Fig. 1-7 Neotectonic profile of Indonesia archipelago (after Simandjuntak, 1993)

Plate movements are very slow, only a few centimeters per year, but over a 60-million year period (the time since the dinosaurs became extinct) a plate drifting only 1 cm per year would have moved 600 km. The Indonesian region is dominated by three major plates, namely Southeast Asian plate, the Indo-Australian plate and the Pacific plate, as well as several smaller platelets that have sheared off Irian Jaya. The process is still continuing today (Gorsel, 2012).

Soil conditions are very important in affecting the distribution of vegetation. There are five factors in soil formation: lithology, climate, topography, biological organisms and time. In Kalimantan, the majority of its soils have developed on the rolling plains and dissected hills

on sedimentary and old igneous rock. These soils range from strongly weathered and acid ultisols to young inceptisols. In the south, extensive alluvial plains and peat soils extend into the Java Sea. Weathering is strong in the humid tropics, favoured by both warmth and moisture. Because of the high rainfall, soils are constantly wet and soluble constituents are removed. This process is called leaching. High levels of weathering, leaching and biological activity (degradation of organic matter) are characteristics of many Bornean soils (van Gorsel, 2012).

1.5. Floating Fondation

Choosing floating foundation is economic and effective in the presence of deep soft soils more than 30 meters below the surface. Traditional floating foundation using wooden piles is still commonly used today‘s construction on soft soil in Indonesia, particularly in Kalimantan. Mini wooden piles ranging in size from about 10 to 17 cm in diameter and approximately 400 to 1500 cm in length are widely used as a foundation to support construction of building, e.g. houses and shopping centres.

For highway or road constructions, there are two ways to install the wooden piles over soft soils. The first is similar to a mattress foundation where wooden piles are laid down horizontally over the ground surface and transversely axis of the road. The second using wooden piles are driven into the ground surface vertically and lay square board caps at the top piles.

1.5.1. Wooden Mattress Foundation

In the past, wooden mattress foundations were usually used for road access or temporary constructions and for low volume traffic. After completing the installation of piles, selected material would be filled over this foundation. After that base course and asphaltic layers can be performed over the embankment. Later on, in accordance with the increased traffic volume and axle load, this kind of construction is rarely performed anymore besides some drawbacks such as weathering of material because the piles are not submerged fully under water. Figure 1-8 illustrates wooden mattress foundation technique located on soft soil in West Kalimantan.

Fig. 1-8 Wooden mattress foundation

1.5.2. Wooden Piled Foundation

Nowadays, embankment of granular soils supported by piles are often used for road and railway constructions. The required load carrying capacity of the pile is typically less than around 30 tonnes. This implies that the piles used for soil improvement are micropiles, i.e. a pile with diameter less than 30 cm. At Kyoto Road in Netherlands, wooden pile 18 cm in diameter is connected with concrete cap 30 cm in diameter and 40 cm deep (Eekelen et al., 2009).

In West Kalimantan, the mini pile with board cap is sometimes used in highway construction even for runway construction. A mini pile with 10 to 17 cm in diameter and 400 to 1500 cm long is driven into the ground surface with piles spacing ranging between 40 and 50 cm. Later on, a square board cap around 20 cm in diameter is nailed to the top of the pile. Post levelling the ground surface as high as the top surface of board caps, geosynthetic sheets can be unrolled over this surface and followed by a selected material or granular material. Even in some cases, construction of piled embankment without using pile cap can be done. This technique is illustrated in Figure 1-9.

Fig. 1-9 Wooden piled foundation

1.5.3. Cementitious Piled Foundation

The piled embankment supported by piles with geogrids has been considered as an advantageous alternative metod for solving problem some transport infrastructures over soft soil deposits. Piles and/or pile caps can be cementitious material which gives more high compressive strength to support higher vertical stress when being subjected to a load on surface of pile caps. Some places in the world have applied this type of construction to overcome some problems related to soft soils.

These types of piles are generally installed in the field by driving them downward using machine. When a depth of soft layer is shallow, bottom tip of piles can be driven until hard stratum of soil in order to reach maximum bearing capacity. Otherwise, floating piles become alternative way if hard stratum of soil is deep enough. After installation is completed, geosynthetics can be readily unrolled over them before filling up embankment material. Figure 1-10 shows cementitious piled foundation techniques.

Fig. 1-10 Cementitious piled foundation (after Scottwilson, 2009)

1.6. Research Aims

This research is focused on understanding behaviour of dynamic loading on pavement over deep soft soil. Some topics are studied, including soil arching analysis, geosynthetics reinforcement, piled embankments, settlements of construction and stress analysis on pavement (improved subgrade or embankment) resulted from static and/or live load. Several methods are used for approaches such as Giroud-Han, British Standar BS8006, Nordic Standard, German Method EBGEO 2010 and Finite Element Method. Behaviour of loading over pavement or embankment is analyzed comprising of static loading, moving load and repeated loading.

1.7. Lay Out of Thesis

Thesis is arranged into 8 chapters as indicated below:

Chapter 2 reviews some terminologies which include arching concept, capping ratio, the stress concentration ratio, stress reduction factor and efficacy. Thus, providing theoretical approaches in geosynthetic reinforcement and piled embankments. Followed by describing the method by calculating of settlement and differential settlement for piled embankment.

Chapter 3 reviews characteristics of soft soil such as physical and mechanical properties and also describing properties of embankment material. Meanwhile, properties of geosynthetics as reinforcing material is provided, particularly tensile strength and also presented compression strength of pile materials such as wooden pile, concrete pile, stone column and soil cement column and characteristic of dynamic loading on pavement as well.

Chapter 4 presents some experimental works in laboratories and field case studies for various situations over the world in handling the soft soil. This chapter describes some problems and simultaneously solves on the pertaining realm in soft soil such as excessive settlement, horizontal thrust, vertical distance of geosynthetics layer, various kinds of piles, static and cyclic loading.

Chapter 5 provides some analytical approaches of rutting on the surface of the pavement as material response under static and moving load as well settlement on foundation. Moreover, some constitutive models are introduced that can be applied in finite element analysis. Moreover, geometrical idealization is needed to transform the real geometric shapes to finite element analysis.

Chapter 6 discusses some interesting findings in Chapter 4 and then verified with numerical analysis using Plaxis software package. Some important findings is presented such as optimal vertical distance of geosynthetics layer in base course, influence of very soft soil against soil arching and/or stress concentration ratio, determining critical height of embankment, various types of load transfer platform, tensile strain of geosynthetics in piled embankment and creep phenomenon in soft soil.

Chapter 7 elaborates excessive settlements of pavement construction supported by floating piles over deep soft soil of two case studies in Supadio Airport Pontianak regarding with runway reconstruction work and apron widening project.

Chapter 8 presents the main findings and concludes this study. Later on, recommendation for further works is highlighted.

CHAPTER 2

Literature Review

2.1 Basic Definitions of Soft Soil

2.1.1. Classification System for Soil

The word of soil, in civil engineering, will refer to material that is not petrified, not bedrock, composed of mineral grains, organic matter, has a shape and size, water and gas. Commonly, soil consists of peat, organic soil, clay, silt, sand and gravel. Soil itself has been classified by the United States, known as the Unified Classification (Unified Soil Classification System or USCS). This system is classified based on particle size, distribution and properties of fine grain. The USCS divides the soil into three main categories: coarse grained soil, fine grained soil and high-yield organic soil. Meanwhile, inorganic soil is divided into sub-classification of gravel, sand, silt and clay.

2.1.2. Fine-Grained Inorganic Soil

Fine-grained inorganic soil is divided into sub-groups i.e. silt (M) and clay (C). Silt is a fine-grained soil that has a liquid limit and plastic index if it is plotted into Fig. 2-1 the line-A, whereas the clay will be above the line.

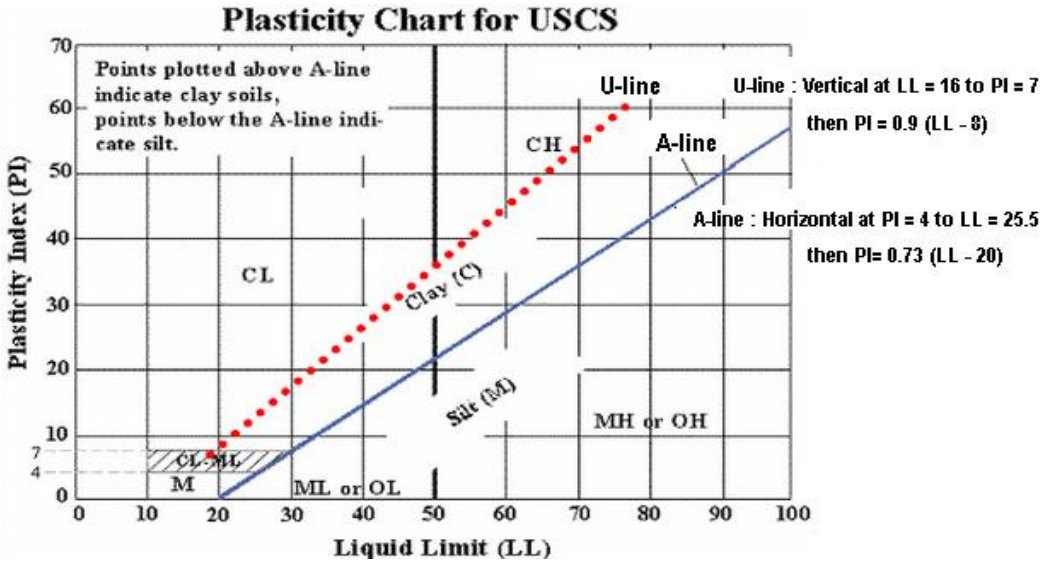

Fig. 2-1 Atterberg limit for organic and inorganic soils (after Puslitbang, 2001)

2.1.3. Organic Soil and Peat

There is also fine grained soil, in which Indonesian Geotechnical Guide-1, 2001 divides into three groups based on their organic content, as shown in Table 2-1. Organic soil (O) is the soil which has the organic content 25 to 75%. Organic soil is categorised into OL and OH appropriate level of plasticity. Peat is a soil that has organic content more than 75%. Based on its fiber content, peat soil is grouped into two: amorphous with fiber content less than 20% and fibrous with the fiber content exceeds of 20%.

Table 2-1 Soil classification based on organic content

Organic content	Soil group
>75% 25 - 75% < 25%	Peat Organic soil Low organic soil

Source: Indonesian Geotechnical Guide-1, 2001)

Peat as used today includes a vast range of peat, peaty organic soils, organic soils and soils with organic content (Landva et al., 1983). According to the ASTM standard D 2487-00, organic clay/silt with sufficient organic content will influence the soil properties. By classification, an organic soil is a soil that would be classified as a clay/silt except that its liquid limit value after oven drying is less than 75% of its liquid value before.

2.1.4. Soft Soil

There are two types of soft soil: soft clay and peat. Soft clay has clay minerals and a high moisture content causing low shear strength. The undrained shear strength (c_u) for the clay soil as indicated in the following Table 2-2.

Table 2-2 Consistency of clay
(after Indonesian geotechnical guide-4, 2001)

Consistency	c_u (kPa)
Very soft Soft Medium Stiff Very stiff Hard	< 12.5 12.5 - 24 25 - 49 50 - 99 100 - 200 > 200

In geotechnical engineering, soft terms specify to clay with shear strength ranging from 12.5 to 25 kPa, whereas the very soft clay is below 12.5 kPa. Table 2-3 gives some clues of an indication of the shear strength when it was identified in the field (Indonesian Geotechnical Guide-4, 2001).

Table 2-3 Field indicator of undrained shear strength for soft clay

Consistency	Field indication
Soft Very soft	It can be formed easily with fingers If squeezed it will be out between fingers

Source: Indonesian Geotechnical Guide-4, 2001)

Indonesian Public Works (1999) defines the soft soil as the soil that can be penetrated with the thumb a minimum 25 mm or has the undrained shear strength less than 40 kPa on the basis of field vane shear test. Soft soil may compose of inorganic and organic soil. Inorganic soft soil generally consists of clay or silt and it has organic content between 0 and 25% or ash content ranging from 75 to 100%. Whereas organic soft soil consists of clay or silt and organic content between 25 and 75%, or ash content ranging from 25 to 75%.

Peat is a soil-forming consisting of the primary of the remaining plants and the organic content exceeding 75%. Basically, all types of soil are Resen old in geological terms that are less than 10000 years old. The geological period is also commonly known as the Holocene.

2.1.5. Parameters for Soft Soil

Realistic parameter values for soft soil are important to be well prepared before taking the samples from field work and testing them into the laboratory. This would assist in anticipating if result gained from laboratory or field test varies from site to others. Varied results that are measured from some parameters like water content, unit weight, Atterberg limits, soil strength, coefficient of compressibility, consolidation index and permeability are common when taking testing in the laboratory or field works.

Table 2-4 Range of realistic values for parameters of soft soil

Soil parameter	Unit	Clay	Organic clay	Fibrous peat
Water content, w	%	20 – 150	100 – 500	100 – 4000
Unit weight, γ	kN/m^3	14 – 17	12 – 15	10 – 12
Organic content	%	< 25	25 – 75	> 75
Undrained cohesion, c_u	kPa	5 – 50	5 – 50	10 – 50
Liquid Limit	%	60 – 120	-	-
Plasticity Index	%	40 -80	-	-
Friction angle, ϕ'	[^{o}]	21 – 27	25 – 35	30 – 40
Compression index, c_c	[-]	1– 2.5	1 – 5	1 – 20
Consolidation coeff.,c_v	m2/year	1 – 10	5 – 50	10 – 100
Swelling Index, c_α	cm/s	(0.03 -0.05) c_c	(0.04 – 0.06) c_c	1 – 4
Permeability, k_i	cm/s	10^{-8} – 10^{-9}	100 – 10^{-12}	100 – 10^{-12}

Source: Indonesian Geotechnical Guide-1, 2001

Undrained shear strength is an important parameter. This parameter for soft clay around the surface in Indonesia ranges from 10 to 20 kPa. Undrained shear strength of 10 kPa is only able to support an embankment about 2 m high.

2.1.6. Factors Affecting Behaviour of Clay

2.1.6.1. Organic Content

Organic content of clay or peat is generally derived from crop residues remaining on the surface of the earth. Clay with low organic content values, for example below 10%, can be found in clay estuarine and shallow marine sediments. Paul and Barras (1999) identified the existence of this estuarine clay in the area Bothkenaar Scotland where the organic content ranges from 2 to 4%. The influences of organic content of soil are: increased levels of saturated water, high compressibility and low permeability.

Hobbs (1987) emphasized that the organic content can be calculated based on the weight but the effect on soil properties also depend on its volume. He concluded that if the organic content of about 27% by weight or about 55% of the volume, the material will give a great influence on the properties of clay.

2.1.6.2. Sedimentation Rate

On sedimentary clay, rapid addition of layer thickness caused by high sedimentation rate will cause pore water pressure. Sedimentation rate for the clay on a delta turned out to be a little

clay underconsolidated (Cox, 1970). Although Barry and Rachlan (2001) concluded there is no existence of such phenomena.

Skempton (1970) presented the variation curves for a large number of clay deposits from the present until the Pliocene period. Clay said as normally consolidated if the soil never experienced the pressure is greater than the effective stress on it. Otherwise, over consolidated clay. The process of sedimentation of clay in salt water occurs at high rate. For Indonesia, sedimentation rate is 120 to 300 cm per 1000 years (Cox, 1970).

2.1.6.3. Chemical Weathering

Weathering is defined as a process leading to structural disintegration and decomposition of geological materials due to direct influence of hydrosphere and atmosphere (Kenney, 1976). Bjerrum (1967) explained the effects of weathering on shear strength and compressibility of which shear strength and compressibility decrease due to weathering.

2.1.6.4. Freshwater Leaching

Leaching can be defined as a process caused by hydraulic or by a diffusion gradient that removes material in solution (e.g. salt) from a passage in the soil profile. Rosenqvist (1953) considered the process of leaching also occurred in the area of sediment under water (sub-aquatic) from ground water when mixing with salt water steadily.

On soft clay deposits located in a flat delta plain of southeast Asia, leaching process is largely caused by rains and floods from overflowing rivers. Therefore, salt concentration on the surface will be low and tended to increase with depth. Salinity will also be lower with increasing distance to the coastline.

2.1.6.5. Clay in Southeast Asia

According to Rahadian (1992) some properties of soft organic mineral in Southeast Asia encompass water content varying from 60 through 150 %, having high plasticity, content of clay ranging from 35 % and 60 % with ilite, caolynite and monmorilonite. In Bangkok, clay mineral is dominantly ilite, meanwhile in Singapore is Caolynite and in peninsular Malaysia is monmorilonite. Organic content varies from 2 and 5%, and the 22.5% organic content founded in Peninsular Malaysia. Value of pH is between 3.1 and 8. Sensitivity of this soil ranges from 1.5 to 18 (or medium quick clay). Compression index varies from 0.02 through 1.5. The overconsolidated ratio is less than 1.6. Effective internal friction angle varies from 20 to 25 degrees and leads to be reduced with increasing of the plasticity index.

In Indonesia, engineering properties along the coastline is generally close to the soft soil in Southeast Asia such as natural water content, specific gravity and unit weight. Soft soil in Sumatera and Java Island is mainly silty clay. Atterberg limit for this kind of soil has a liquid limit between 40% and 160%. Generally, plasticity index is above or nearby A-line of Cassagrande or in USCS so called CH OH soil. Compressibility of Indonesian marine clay is high enough. Compression index varies from 0.5 to 2.

2.1.7. Factors Affecting Behaviour of Peat

2.1.7.1. Specific Gravity

Mineral soil generally has a specific gravity of 2.7 and soil containing organic matter ranges from 1.4. Therefore, gravity influenced by organic content (Skempton and Petley, 1970). Similarly to soils in Indonesia, specific gravity varied 2.7 to 2.9 while the peat varied between 1.4 and 1.7 (Rahadian et al. 2001).

Besides specific gravity, the physical property of peat is bulk density. According to Adhi W. (1984) peat soil is characterized by bulk density of 0.6 to 0.1 g/cm^3. Moreover, further experiment was undertaken using a ring sample method ranging from 0.14 g/cm^3 to 0.22 g/cm^3 (Muslihat, 2003).

2.1.7.2. Liquid Limit

Liquid limit testing requires adequate soil crushing. Therefore this test has very limited value as a guide, especially peat properties of fibrous peat exist in Indonesia. According to data on the area Berengbengkel for organic clay, it was confirmed that high organic content showed a high liquid limit (Farrell et al., 1994). In terms of weight loss on heating, it was assumed to be equal to the organic content of the missing.

2.1.7.3. Compressibility

Farrell et al. (1994) showed that the compression index Ireland peat associated with liquid limit according to equation:

$$c_c = k\ (W_L - 10) \qquad (2\text{-}1)$$

where: k = 0.007 to 0.009

For fibrous peat the equation above cannot be applied. Consolidation tests on fibrous peat in Barengbengkel show the value of c_c up to 20. The vertical compression index is almost twice of horizontal compression index values. Keep in mind that the value of high compression index (c_c) cannot be applied to the conventional calculation in small strain. Peat compression index will decrease with increasing stress.

2.1.7.4. Permeability

Barry et al. (1992) performed the pumping test to support permeability in the forests of Riau and revealed that the permeability between 10^{-2} and 10^{-4} m/s. They also compared it with other research, as indicated in Table 2-5.

Table 2-5 Permeability values for peat soils

Discription of peat	Permeability (m/s)	Sources
At the surface	$> 10^{-1}$	Hobbs (1986)
On the bottom	3×10^{-5}	-idem-
Fen Acrotelm in Russia		
near surface	3×10^{-5}	-idem-
near bottom	6×10^{-7}	-idem-
Peat soils in Irlandia	3×10^{-8} to 10^{-7}	-idem-
Sphagnum peats		
H8 to H10	6×10^{-8}	-idem-
H3	10^{-5}	-idem-
Sedge peat, H3 to H5	10^{-5}	-idem-
Brushwood, H3 to H6	10^{-5}	-idem-
Fibrous acidic Malaysia peat	2×10^{-5} to 6×10^{-8}	Toh et al. (1990)

After Barry et al., 1992 and Hobbs, 1986

2.1.7.5. Properties of Peat Soil in Indonesia

In Indonesia, soft soil is widespread in the big islands, namely Sumatera, Kalimantan, and Papua. Property of peat soil in Papua island is rarely found caused by lack of infrastructures

development in this region. Some properties of peat soil both islands of Sumatera and Kalimantan as reported Soepandji (1996, 1998) are depicted in Table 2-6.

Table 2-6 Properties of peat soils in Sumatera and Kalimantan islands

Properties	Kalimantan		Sumatera		
	Pontianak	Banjarmasin	Duri	Desa Tampan	Musi
Ash Content (%)	1.2	3.29	21.96	25.2	50.7
Water Content (%)	632	198	235	338	235.4
Specific Gravity	1.42	1.47	1.6	1.55	1.82
Liquid Limit (%)	260	182	440	236	274
Plastic Limit (%)	196	148	377	309	194
Shrinkage Limit (%)	-	28	-	59	-
pH value	4.8	6.5	3.9	3.6	3.3
Bulk Density	-	-	1.084	0.95	1.12
Compression Index, Cc	-	-	2.5-3.2	2.11	1.57
Recompression Index, Cr	-	-	0.07-0.13	0.107	0.05
Classification ,ASTM D4427-92 (1997)	low ash, acidic	low ash, acidic	organic soil	organic soil	organic soil

After Soepandji et al., 1996, 1998 cited Eka Priadi, 2008

2.2. Bearing Capacity of Soft Soil

2.2.1. Bearing Capacity at Ground Surface of Soft Soil

Before a complete failure of soft soil subgrade occurs, local over-stressing in shear takes place and results in punching shear failure or local shear failure in the soil (Rodin, 1965). The bearing capacity of subgrade under such condition is low and can be quantified by the equation:

$$q_u = \pi\, c_u \tag{2-2}$$

where c_u is undrained shear strength of subgrade. On pavement engineering, the bearing capacity is well known as California Bearing Ratio (CBR). For soft soil an empirical relation between CBR value and undrained shear strength is:

$$c_u = 30\ \text{CBR (kPa)} \tag{2-3}$$

When a general shear failure can be reached using reinforcement or a localized shear failure of the subgrade can be prevented, the bearing capacity of the subgrade can be increased maximum almost twice from previous state to:

$$q_u = 2\pi\, c_u \tag{2-4}$$

2.2.2. Contact Area and Tire Pressure

Wheel load of vehicular traffic over the surface of the pavement for rubber tired vehicle (single, dual, or tandem wheel) is equal to half of the axle load as depicted in Fig 2-2. Vertical stress on the pavement surface is distributed downward to subgrade surface. Vertical stress on the surface of subgrade is smaller than vertical stress on the surface of the pavement depending on thickness (H) and stiffness of the base course.

Therefore design dynamic load, Q, for this situation is:

$$Q = P_{axle} / 2 \tag{2-5}$$

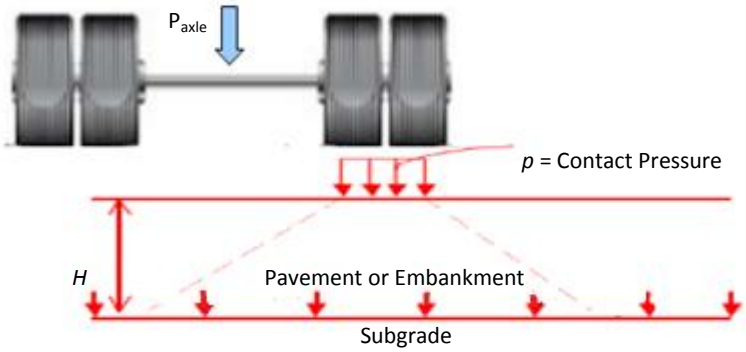

Fig. 2-2 Contact area and tire pressure (after TENAX, 2001)

For single or dual wheel, contact pressure (p) is equal to their tire inflation pressure. The contact pressure is assumed to be a circular area and its radius is calculated by:

$$R = \sqrt{\frac{Q}{\pi . p}} \tag{2-6}$$

2.2.3. Determination of Fill Thickness

Boussinesq equations can be used here to calculate fill thickness. The criterion for calculating the fill thickness is that the thickness of the fill must be large enough to allow the stress transferred to subgrade surface is within the bearing capacity of subgrade as Equation (2-2) and Equation (2-4).

For rubber tired traffic loading, the contact area of the wheel is assumed to be a circular form and in this condition, the vertical stress at the subgrade surface, q, transferred from uniform loading (contact pressure) can be provided:

$$q = p\left\{1 - \left[\frac{1}{1+\left(\frac{R}{H}\right)^2}\right]^{3/2}\right\} \tag{2-7}$$

Re-writing equation (2-7) we find:

$$H^2 = \frac{R}{\left(1-\frac{q}{p}\right)^{-2/3}-1} \tag{2-8}$$

The required thickness for an unreinforced section is:

$$H_u = \sqrt{\frac{\frac{Q}{\pi\, p}}{\left(1-\frac{\pi\, c_u}{p}\right)^{-2/3}-1}} \tag{2-9}$$

It is similarly that the required thickness for a section reinforced using geosynthetics is:

$$H_r = \sqrt{\frac{\frac{Q}{\pi\, p}}{\left(1-\frac{2\,\pi\, c_u}{p}\right)^{-2/3}-1}} \tag{2-10}$$

Magnitudes of bearing capacity of the subgrade soft soil both unreinforced and reinforced are different between methods each other as shown in Table 2-7.

Table 2-7 Comparison of bearing capacity in different design methods

Method	Unreinforced section	Reinforced section	Material
Giroud-Noiray (1981)	3.14 c_u	5.14 c_u	Geotextile
Giroud-Han (2004)	3.14 c_u	5.14 c_u 5.71 c_u	Geotextile Geogrid
USACE (2003)	2.8 c_u	3.6 c_u 5.8 c_u	Geotextile Geogrid
Barenberg (1975)	3.0 c_u	6.0 c_u	Geotextile
DuPont Typar (2010)	3.14 c_u	5.14 c_u	Geotextile
Philips (1987)	2.8 c_u	5.0 c_u	Geotextile
Rodin (1965)	3.1 c_u	6.2 c_u	Geogrid
Roadex III (2008)	4.0 c_u	-	-

2.2.4. Settlement Analysis

Estimation of settlement must involve both primary and secondary. For soft clay and organic clay, Terzaghi consolidation theory can be applied.

Primary settlement for normally consolidated clay:

$$S_p = H.\frac{c_c}{1+e_0}\log\frac{P_0+\Delta P}{P_0} \tag{2-11}$$

Primary settlement for over consolidated clay:

$$S_p, P_o + \Delta P < P_c = H.\frac{c_s}{1+e_0}\log\frac{P_0+\Delta P}{P_0} \tag{2-12}$$

$$S_p, P_o + \Delta P > P_c = H\ c_s \log\frac{P_o+\Delta P}{P_o} + H.\frac{c_c}{1+e_0}\log\frac{P_0+\Delta P}{P_0} \tag{2-13}$$

Secondary settlement:

$$S_s = H\ c_\alpha \log\frac{t_2}{t_1} \tag{2-14}$$

2.3. Quasi-Static and Dynamic Loading

2.3.1. Definition of Terms

A cyclic loading on a foundation soil may be caused by moving vehicles (e.g. aircrafts, trains, cars), by wind (e.g. wind power plant), or by waves (e.g. coastal structures). If the cycles are applied with a low loading frequency f_B, the inertia forces are not considered or negligible and it is spoken of a *quasi-static cyclic* loading. Whereas if loading frequency is large so inertia forces are relevant and loading is *dynamic*. Border between quasi-static and dynamic loading also depends on an amplitude of the cycles. This amplitude dependence is ignored and the border is said to lay at $f_B \approx 5$ Hz (Wichtmann, 2005). At a certain strain amplitude test up to $f_B \approx 30$ Hz in the literature and Wichtmann's test showed no influence of loading frequency f_B on the secant stiffness (elastic portion of the strain).

Sources of dynamic actions are described in Fig. 2-3.

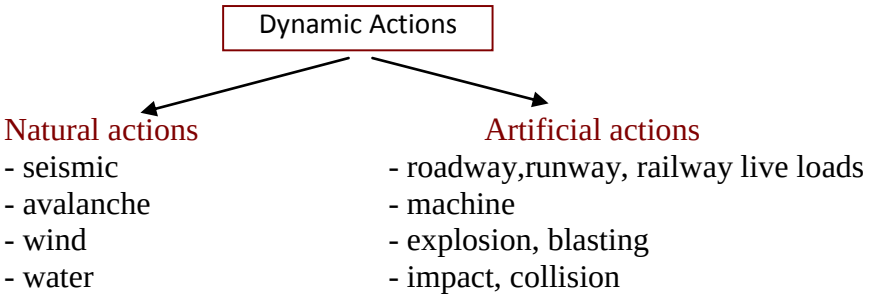

Fig. 2-3 Sources of dynamic actions (after EBGEO, 2010)

The actions in terms of DIN 1054 can be differentiated into dynamic, cyclic, and shock-like actions. Dynamic actions refer to high frequency. Inertia forces are not negligible and it can critically influence system behavior. Cyclic actions refer to low frequency actions where the inertia forces can generally be ignored (frequencies ≤1 to 2 Hz). The shock-like actions refer to actions acting over a short period only. The time may be in the range of milliseconds up to several second. Their upper bound is not fixed and inertia forces may also act.

Additional distinguishing criteria include load-time history characteristic, effective spatial direction, source and frequency of occurrence. Load time history is shown in Fig. 2-4.

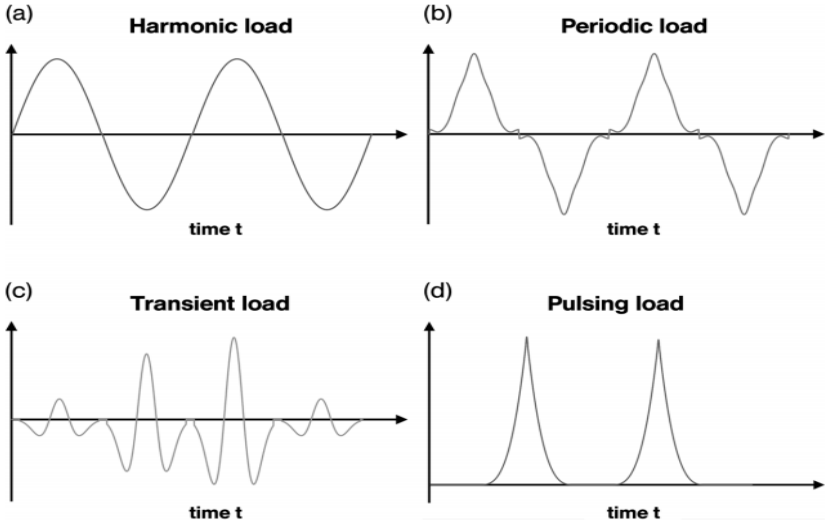

Fig. 2-4 Typical of load time history (after EBGEO, 2010)

2.3.2. Stress Distribution on Unbounded Material

Generally, load from vehicle wheels at the surface of granular pavement will be distributed on top of the subgrade layer taking assumption the circular form for the spreading angle of 45 degrees. Range of vertical stress magnitude on the formation level (on top of the subgrade layer) was just between 20 kPa to 120 kPa. Meanwhile, horizontal stress due to a pavement system having around 0.25 to 0.75 m total thickness on the formation level was around 30 kPa (Sasongko, H., 1996). Fig. 2-5 presents load distributions on granular material.

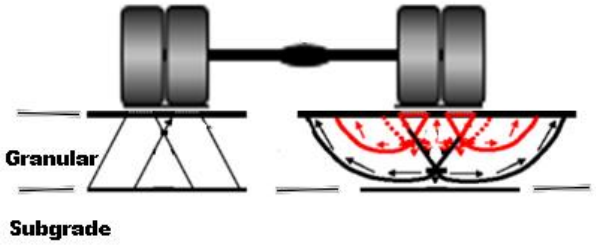

Fig. 2-5 Load distribution on granular material (after Giroud et al., 1981)

2.3.3. Stress Distribution on Bounded Material

It is different pattern with granular materials that induced by vehicle wheels at the surface of bounded material of pavement, e.g. slab of Portland cement concrete or bituminous layer, will be distributed on top of subgrade layer taking assumption the circular form with a radius of relative stiffness, *l*, as indicated in Equation (2-15).

$$l = \sqrt[4]{\frac{Ed^3}{12(1-\mu^2)k}} \tag{2-15}$$

Where: E = Young's modulus, k = the reaction modulus of subgrade, d = the thickness of pavement (or concrete layer), μ = Poisson's ratio.

2.3.4. Magnitude of Loading

Transportation infrastructure such as roadway, railway and runway is always subjected to moving load. For vehicles crossing on streets, all kinds of vehicles refer to Equivalent Single Axle Load (ESAL) 18 kips (or 8.12 tonnes) with tire pressure 85 psi (550 kPa). Meanwhile, airplane passing at runway surface which loading coming from an airplane depends on weight, tire pressure, wheel configuration (single, dual, tandem) of the airplane. Tire pressures for airplanes vary from 140 psi to 200 psi.

In Germany, according to Ril 836 for rail infrastructure, the subgrade or improved subgrade has to be able to support the load above this surface layer at least around 52 kPa as described in Fig. 2-6. High speed trains from 100 to 300 km/h need the additional layer around 1 to 2 of the superstructure thickness (Muncke et al., 1999; Kempfert et al., 1999).

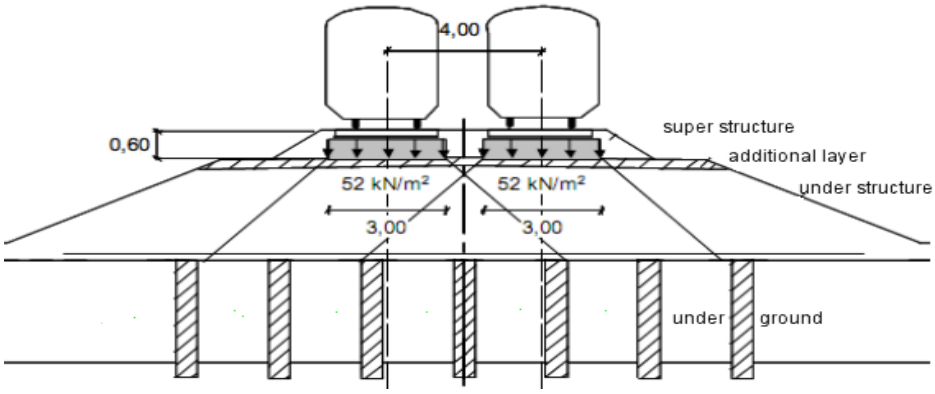

Fig. 2-6 Cross-section for rail track (after Ril 836)

Standard axle load is different for each country. In Greece, Beskou et al. (2011) reports that for a locomotive (or engine) is around 210 kN and 150 kN for carriage. In Indonesia, railway infrastructure is subjected to a maximum axle load of 180 kN (Kepmenhub, 2000).

2.4. Geosynthetics Reinforcement

2.4.1. Type of Geosynthetics

Geosynthetics for earth reinforcement purpose is divided into two groups: permeable matter (geotextile, geogrid, geocomposite and geolinier) and impermeable matter (geomembrane and intermembrane). For ground improvement or earth reinforcement, it must have some properties such as shear strength, tensile strength, and punch strength (Suryolelono, 1997). Types of geosynthetics used in earth reinforcement are shown in Table 2-8.

Table 2-8 Type of geosynthetics used in reinforced earth (after Suryolelono, 1997)

Material	Type	Form
Geosynthetics	Geotextile	Woven and Unwoven
	Geogrid	Uniaxial and Biaxial
	Geolinier	Bar
	Geostrip	Strip/tape
	Geocell	Assembled cell

When designing geosynthetics as earth reinforcement, some reduction factors have to be considered. Design tensile strength of geosynthetics follows this equation:

$$F_d = \frac{F_k}{(A_1 \cdot A_2 \cdot A_3 \cdot A_4 \cdot \gamma)} \quad (2\text{-}16)$$

where: F_d is permissible long term tensile strength
F_k is short term tensile strength
A_1 is reduction factor for creep
A_2 is reduction factor for damage caused by transport, installation, compression
A_3 is reduction factor for processing connection
A_4 is reduction factor for environmental influences (weather, chemical, micro-organism)
γ is partial safety coefficient for the consideration of possibility

2.4.2. Geosynthetics Reinforcement Mechanism

Some small and full-scale studies have been performed to better understand how geosinthetics interact with fill material to contrast their performance with unreinforced conditions in a variety of civil engineering applications. Koerner (1998) discussed this interaction and providing basic definition through geogrid. A geogrid is defined as a geosynthetics material consisting of connected parallel sets of tensile ribs with apertures of sufficient size to allow strike-through of the sorrounding soil, stone or other geotechnical material (Koerner, 2005). Commercial geogrid products marketed and sold include extruded punched-and-drawn geogrids, woven and coated geogrids, welded geogrids, and geogrids composites. Structural biaxial geogrids can be used to reinforce earth fill over soft soil ground and provide a stable subgrade under flexible and rigid pavements, unpaved roads, railroad track beds, parking yards, work platforms and building foundations.

Subgrade soil beneath a paved or unpaved surface can fail under load in two ways: localized shear failure and deeper-seated bearing capacity failure (ultimate failure). The subgrade beneath an unreinforced fill will fail in the localized shear failure at around a half of stress level than the ultimate bearing capacity of the subgrade. Geogrid reinforcement of granular fills over soft soil ground can prevent the localized shear failure of the subgrade.There are

three primary mechanisms as being relevant to the interaction of geogrid and pavement materials: lateral restraint, improved bearing capacity and tensioned membrane effect (Perkins and Ismeik, 1997a).

2.4.2.1. Restraint and Confinement

There are two types of restraint as shown in Fig. 2-7. The first is related to the reverse curvature of the geosinthetics outside the wheel path where a downward pressure is created. This has the effect of a surcharge load, which levels out the deformation and enforces the compression of the soil. Secondly, when aggregate particles attempt to move away under the load, this provides tensile reinforcement to aggregate layer.This confinement of aggregate increases its strength and modulus, which in turn decrease the compressive stress on subgrade by spreading the load better underneath the wheel load.

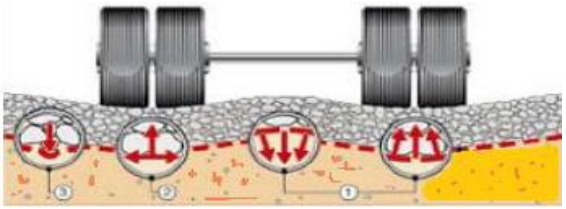

Fig. 2-7 Three stabilization mechanisms (after Perkins and Ismeik, 1997)

2.4.2.2. Membrane Mechanism

Membrane mechanism is effective when a geosynthetic is laid on deformable soil and vertical loads are applied. In plane, tensile stress develops in the geosynthetics, relieving the soil which is not capable of absorbing it. This is plane force induces a component of stress perpendicular to the plane of the geosynthetic sheet, in the direction of the force. Therefore, this is of great significance in temporary road construction, where it can reduce rutting the tremendously. The use of the higher modulus of geosynthetics will reduce the rutting on the surface of the pavement.

2.4.2.3. Local Reinforcement

Loads on individual stones can cause spot failure in the subgrade. A high initial modulus of geosynthetics allows to distribute the load and reduce the vertical stress as well as provide resistance to displacement. A high elongation avoids local puncturing of geosynthetics to stretch around a penetrating aggregate/stone.

2.4.3. Geosynthetics Reinforcement Methods

More attention has been given to the important practical application of geogrid reinforcement incorporated at the base of a layer granular fill placed on a soft clay subgrade. This kind of construction is commonly used for low-cost unpaved roads such as temporary site access roads, low embankments, car parks and the working platform. The purpose of the fill is to provide a suitable operating surface on which concentrated loads may be carried without the subgrade failing or deforming excessively. It is now common practice to use a layer of polymer geosynthetics at the base of the fill layer in order to separate the fill from the soft soil beneath and to improve its load-carrying capacity.

The behaviour of such a system is complex and a number of procedures for the design have been proposed, notably by Barenberg et al. (1975), Giroud and Noiray (1981), Sellmeijer et al. (1982), Giroud et al. (1984). These procedures which are based on simplified deformation

mechanisms and some empiricism have provided the basis for satisfactory design. Some methods work better than others for certain site conditions, material and traffic volume. However, none is principles of plasticity and fully addresses the significance of shear forces acting between the base and the subgrade. In 2004 Giroud and J. Han introduced a method and improve the previous method. Also US Army Corps of Engineer in 2003 launched a method particularly for low volume.

2.4.3.1. Giroud-Noiray Method (1981)

Giroud-Noiray method (1981) is often used as a reference. The equation for this method is:

$$h_0' = \frac{125.7 \log N + 496.52 \log P_A - 291.14\, s - 2412.42}{(c_u)^{0.63}} \quad (2\text{-}17)$$

Where: h'_o is thickness of unreinforced aggregate base (m); N is number of passes of axle load; P_A is axle load (Newton); s is rut depth (m) and c_u is undrained cohesion of subgrade soil (Pascal).

2.4.3.2. Giroud-Han Method 2004

Recognizing a need to advance geosynthetic design for unpaved surface, J.P. Giroud and Jie Han, published a design method in the August 2004 edition of the American Society Civil Engineers (ASCE). Their approach combines bearing capacity theory with empirical data from full-scale test sections and monitored unpaved roads.

Some distinctions of the methods relative to conventional geosynthetics road design practice including the following :

- considering of the effects of variation in base course strength
- considering of number and size of load cycles and desired roadway performance
- considering load distribution angle within the base course changes with time
- to recognize that geotextiles and geogrids perform differently in roads
- to recognize that not all geogrids perform the same
- to calibrate and validate of theoretical results with laboratory and full-scale test

Equation for Giroud-Han method is:

$$h = \frac{0.868 + \left(0.661 - 1.006\, J^2\right)\left(\frac{r}{h}\right)^{1.5} \log N}{\left[1 + 0.204\left(\frac{3.48\, CBR_{bc}^{0.3}}{CBR_{sg}} - 1\right)\right]} \left(\sqrt{\frac{\frac{P}{\pi r^2}}{\frac{s}{f_s}\left[1 - 0.9 e^{-\left(\frac{r}{h}\right)^2}\right] N_c f_c CBR_{sg}}} - 1 \right) r \quad (2\text{-}18)$$

where: h = required base course thickness (m)
J = geogrids aperture stability modulus (m-N/degree)
N = number of axle passes
P = wheel load (kN)
r = radius of equivalent tire contact area (m)
CBR_{sg} = CBR value of the subgrade soil
CBR_{bc} = CBR value of the base course
s = allowable rutting depth (mm)
f_s = factor for rutting depth (75 mm)
f_c = factor for bearing capacity of subgrade soil (30 kPa)
N_c = 3.14 and J=0 for unreinforced base course
N_c = 5.14 and J=0 for geotextile-reinforced base course

N_c = 5.71 and J=0.32 m-N/degree for Tensar BX 1100 reinforced base course
N_c = 5.71 and J=0.65 m-N/degree for Tensar BX 1200 reinforced base course

2.4.3.3. US Army Corps of Engineers Method (2003)

In February 2003, Corps of Engineers published a design method consideration use of geogrids and geotextiles for paved and unpaved roads. Its approach for unpaved surface is based on methodology originally developed by U.S. Forest Service. This method distinguishes the performance of geotextiles and geogrids as reinforcement component in subgrade improvement applications.

When using Corps of Engineers method, engineers have to select an appropriate bearing capacity factor, N_c, for the geosynthetics type being considered. The Corps of Engineers method recommended the following N_c values:

N_c = 2.8 without a geosynthetics
N_c = 3.6 with a geotextile for conservative designs
N_c = 5.8 with a geogrid

The first step in designing an effective reinforced pavement system is to determine the properties of the subgrade including the grain-size distribution, Atterberg limits and in situ shear strength or bearing capacity. The in situ shear strength can be measured directly using vane shear devices or indirectly using a correlation from California Bearing Ratio (CBR) using Dynamic Cone Penetrometer device. The design subgrade strength is defined as the 75th percentile strength of the top 18 in (45 cm) of the subgrade. Besides CBR value, cone index value can be converted to shear strength using a chart as depicted in Fig. 2-8.

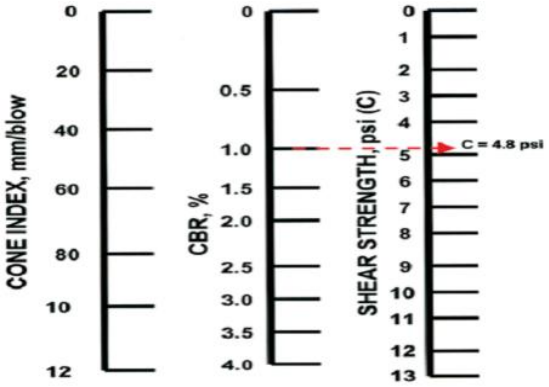

Fig. 2-8 Correlation between Cone index, CBR, and Shear strength (after Archer, 2008)

Next step is to determine the subgrade bearing capacity using equation below:

$$\text{Subgrade bearing capacity} = \text{C}.\ N_c\ (\text{psi}) \qquad (2\text{-}19)$$

Once the subgrade bearing capacity has been determined, the engineer or designer can refer to one of the three relevant design charts (single wheel, dual wheel and tandem wheel).

2.4.3.4. DuPont Method (2008)

Degradation of pavement is caused by some factors including contamination of aggregate base by fine-grained subgrade under dynamic loading so called pumping effect. This causes a substantial reduction of the shear resistance of the aggregate. The thickness of 'clean' aggregate is reduced down to unacceptable levels. Others are lack of subsurface drainage and unpredicted traffic increase. Use of geotextile using DuPont guide will prevent aggregate contamination. This guide uses the CBR value as a measure of soil strength. The correlation

factors between CBR, c_u (undrained shear strength), M_V (rigidity modulus), M_E (compressibility modulus) are given by a chart as shown in Fig. 2-9.

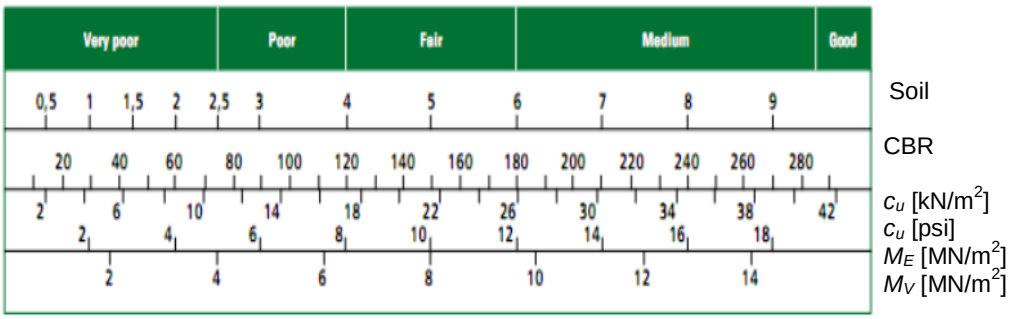

Fig. 2-9 Correlation chart for estimating the subgrade value (after Barenberg, 1975)

An unpaved road normally consists of unbound aggregate base. Inclusion geotextile between subgrade and aggregate base allows for better aggregate compaction, subgrade consolidation, reinforcement of the structure and to increase the ultimate bearing capacity of subgrade around $(2+\pi)\ c_u$.

The first procedure is to determine initial aggregate thickness ($\mathbf{T_O}$) according to load and subgrade conditions and then consider service life and aggregate efficiency. Fig. 2-10 below describes this stage easily. The left side of the chart is the subgrade CBR and axle load P_i to determine $\mathbf{T_O}$ or alternatively using right one.

(a) (b)

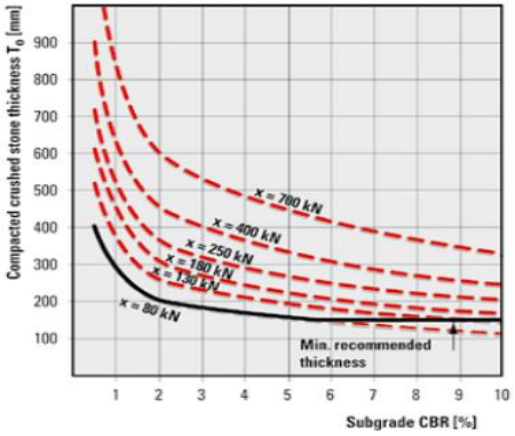

CBR [%]	P_1 [kN]	P_2 [lbs]
0,5	45.31	0.119
1	32.37	0.085
1.5	25.89	0.068
2	22.47	0.059
3	20.56	0.054
4	18.66	0.049
5	17.14	0.045
6	16.00	0.042
7	14.85	0.039
8	13.71	0.036
9	12.95	0.034
10	12.19	0.032

T_o (mm) = $P_1\sqrt{\text{Axle Load (kN)}}$

T_o (in) = $P_2\sqrt{\text{Axle Load (lbs)}}$

Fig. 2-10 Design chart DuPont method (a) Compacted crushed stone thickness for 1000 axle loads, (b) Factor to determine curve P_i

The second step is to make an adjustment of $\mathbf{T_O}$ for service life or corrected thickness of base course ($\mathbf{T}$) using equation (2-20).

$$\mathbf{T} = C\ .\ \mathbf{T_O} = [\ 0.27 \log (\Sigma\ Ni\ .\ ESAL) + 0.19\ ]\ .\ \mathbf{T_O} \qquad (2\text{-}20)$$

$$ESAL = (\ P_i\ /\ P_o\ )^{3.95} \qquad (2\text{-}21)$$

The service life is expressed as the total number of 80 kN axle load application. The actual axle load (P_i) is first converted to an equivalent standard axle load (P_o=80 kN).

The last step is to adjust the use of different kind of material. This difference is accounted for by using the aggregate efficiency α. Angular crushed aggregate is the best because it

interlocks well and provides a high bearing capacity. Depending on availability, other materials or blends can be used and Table 2-8 indicates typical thickness efficiency factors of various surfacing and base materials.

Table 2-8 Aggregate efficiency

Material	Efficiency α
Paving Stone	2
Hot Mix / Dense-Macadam	2
Dense Surface Course	2
Soil-cement > 5 MPa compression	1.5
Soil bitumen	1.5
Hard crushed stone aggregate-'standard'	1.0
Medium crushed stone aggregate (CBR > 80%)	0.8
Hard round stone aggregate (CBR > 80%)	0.8
Medium round stone aggregate	0.5
Sandy gravel (CBR = 20-30%)	0.5
Crushed limestone	0.5
Loose gravel, compactable sand	0.4

Source: DuPont method, 2008

The effective aggregate thickness ($\mathbf{T_{eff}}$) can be expressed:

$$\mathbf{T_{eff}} = \Sigma\, T_i / \alpha_i \qquad (2\text{-}22)$$

2.5. Piled Embankments

2.5.1. Conventional Piled Embankments

The development of infrastructure is moving rapidly to a life cost analysis approach, in which the whole initial capital and on-going maintenance cost are balanced to ensure the best performance of the structure. Since, the first used in Europe in the 1970's, piled embankments have provided an excellent method of supporting embankments. The initial capital cost associated with piled embankments has been higher than other techniques. Typical piled embankment is illustrated in Figure 2-11.

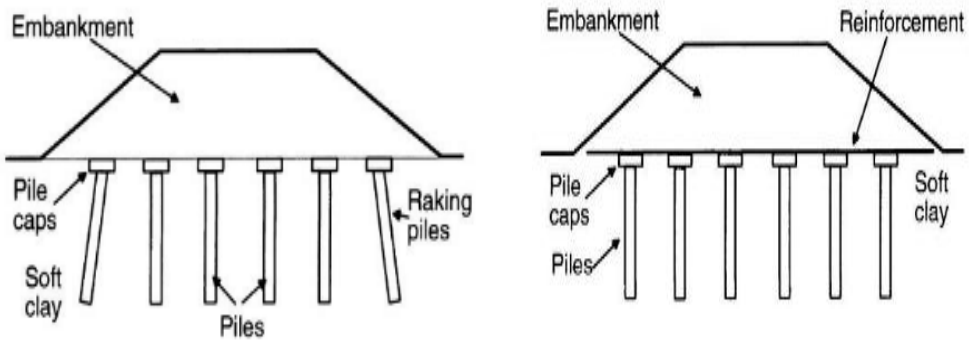

(a) (b)

Fig. 2-11 Typical piled embankments (a) Conventional piled embankment (b) Piled embankment with basally reinforcement

The conventional pile-supported system or piled embankments without reinforcement requires large pile caps and very close piles. This relies on soil arching in the embankment fill and can lead to punching failure. It is essential thing to transfer the large embankment loads to the piles and to avoid surface deformation due to large differential settlement between caps. Consideration required to ensure the edges piles can take the lateral loads imposed by lateral thrust, whereas piled embankment with reinforcement the reinforcement take places the lateral embankment thrust loads so raking piles not required anymore.

A survey of various projects (Han, 1999) found that in conventional piled embankments the coverage ratio (the ratio area of pile caps to total foundation area) is 60-70%, whereas in geosynthetics reinforced piled supported embankments is reduced to about 10-20%.

2.5.2. Geosynthetics-Reinforced Piled Embankment

Piled embankment with large pile caps and no reinforcement materials was firstly used in the late 1960-70's in Finland. This was to overcome the problem at the interface of a rigid bridge abutment and the adjacent embankment on soft soil. This construction method proved very successful and in the 1970's was modified to include high strength geosynthetics material. This material, firstly, can reduce the size of the pile caps, as vertical load would be transferred by tension in the geosynthetics spanning between pile caps. Secondly, it removes the need for expensive raking piles as the geosynthetics would resist outward lateral movement of the embankment side slopes.

A piled embankment is a complex soil-structure interaction problem consisting of piles, generally on a square grid, driven through the soft soil to a firm-bearing stratum. Due to the higher stiffness of piles in relation to the surrounding soft soil, the vertical stress from the embankment and surcharge load are concentrated on piles. Then, soil arching develops as a result of different settlement between the stiff pile heads and the soft ground. Meanwhile several methods currently exist for estimating the magnitude of arching (Kempfert et al. (2004); Russel et al. (2003); Jenner et al. (1998); Hewlett & Randolph (1988); Guido (1987); and Terzaghi (1943).

During more than three decades in many places in the world over 30 years have applied this kind of system as shown in Table 2-10. Piles are generally installed on a square grid, whereas triangular arrangements greatly complicate the analysis of the arching mechanism.

Table 2-10 Piled embankments geometry used over the past 35 years

Reference	Year of construction	Country	Piles spacing (m)	Pile caps (m)	Height (m)
Reid & Buchanan (1984)	1973	Scotland	3.0 – 4.5	1.1 – 1.5	6
Holmberg (1978)	1978	Thailand	1.5	0.8	3.0 – 6.0
O'Riordan (1996)	1985	Ireland	3	1	8.6
Jones et al. (1998)	1989	UK	2.75	1.4	4
Rogbeck et al. (1998)	1996	Sweden	2.4	1.2	1.7
Habib et al. (2002) Van Eekelen et al (2007)	2000 2004	Netherlands	2.5 1.27	0.7 0.3	1.55 1.15
Marchi et al. (2006)	2003	Italy	2	0.5	5.5
Almeida et al.(2008)	2004	Brazil	2.5	0.8	1.2

2.5.3. Soil Arching Concept

Arching is defined by Mc Nulty (1965) as ''*the ability of a material to transfer loads from one location to another in response to a relative displacement between the locations. A system of shear stress is the mechanism by which the loads are transferred* ''. Consider soil on a rigid base, there is no tendency for differential movement and hence no soil arching as in Figure 2-12 (a) the stress acting at point of **a** is the overburden stress (γH), where γ is the unit weight of the soil and H is the height of the soil prism. When one of the local supports at the point **a** is removed, the point **a** is in tension and a roof tension arch is formed. The true arch collapses as the soil is not in equilibrium as depicted in Figure 2-12(b) meanwhile in the next stage as in Figure 2-12(c) the soil settles in an inverted arch, the adjacent soil develops the required shear strength and the soil reaches equilibrium state. The transfer of pressure from the yielding portion to the stationary portion is so-called 'arching'.

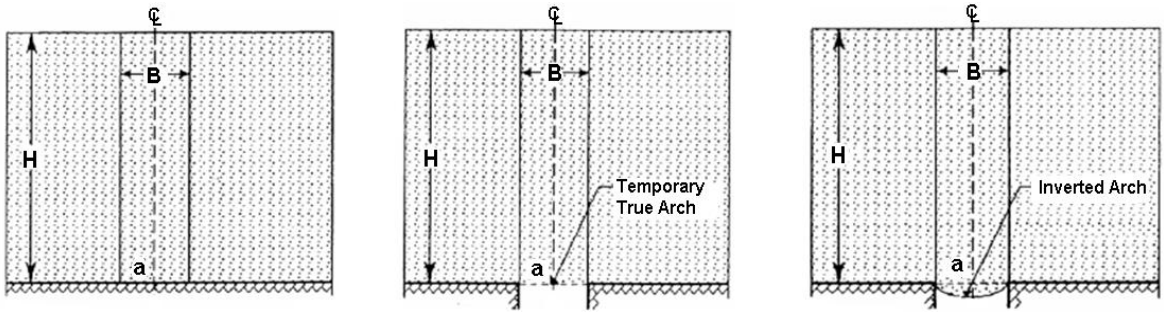

(a) (b) (c)

Fig. 2-12 Soil arching concept (after Mc Nulty, 1965)

Deformation-based design is widely used in foundation engineering. It is currently used in the design of such applications as foots, piles and drilled shafts. In order to accurately use deformation-based design, there must be reliable ways to calculate the differential settlements in the ground. The equal strain assumption is sometimes also a contributing factor to the inaccurate calculation of differential settlements. This method implies that the settlements in the soft clay and at top columns are equal, which implies that there is no stress concentration in the bridging layer. This is inconsistent with the stress concentrations in the columns. Therefore, it violates the vertical stress equilibrium. If equilibrium is violating, the settlements are not being calculated accurately.

2.5.3.1. Rectangular Prism: Terzaghi (1943)

Terzaghi (1943) considered the equilibrium of a differential element and then integrates this through the depth (z) of the moving soil mass. See Fig. 2-13 below where a rectangular soil element, having a thickness (dH) and weight (dW) is depicted.

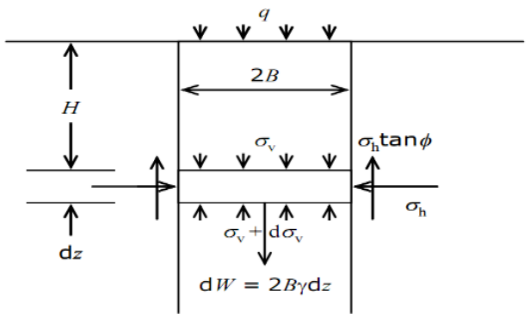

Fig. 2-13 Stress state of a differential element (after Terzaghi, 1943)

The vertical stress applied to its upper surface is:

$$\sigma_v = \gamma H + q \tag{2-23}$$

where: σ_v = the vertical stress (kN/m^2)
γ = the unit weight of the soil (kN/m^3)
H = the thickness of soil above the point (m)
q = the surcharge acting at the surface of the soil (kN/m^2)

The corresponding normal stress (horizontal stress) on the vertical surface of sliding (σ_h) is given by:

$$\sigma_h = K.\ \sigma_v \tag{2-24}$$

where: σ_h = the horizontal stress (kN/m^2)
K = the earth pressure coefficient (dimensionless parameter)

The shear strength of the soil (assuming the soil to be cohesionless) is determined by:

$$\tau = \sigma_h\ .\ tan\ \phi \tag{2-25}$$

where: τ = the shear strength (kN/m^2)
ϕ = the internal friction angle of the soil (degree)

When the element is in equilibrium, the summation of the vertical forces must be equal to zero. Therefore, the vertical equilibrium can be expressed as:

$$d\sigma_v/dz = \gamma - K.\ \sigma_v\ tan\ \phi\ /\ B \tag{2-26}$$

where: $2B$ = the width of strip (m)
z = the thickness of the soil overlying the element (m)

Using the boundary condition that $\sigma_v = 0$ for z = 0, the partial differential equation can be solved as follows (Terzaghi, 1943 and later McKelvey, 1994).

$$\sigma_v = \frac{\gamma\ B}{K \tan\varphi}\left(1 - e^{-K \tan\varphi\ .\ z/B}\right) + q e^{-K \tan\varphi\ .\ z/B} \tag{2-27}$$

Krynine (1945) derived the earth pressure coefficient, K, as depicted below.

$$K = \frac{1-sin^2\varphi}{1+sin^2\varphi} \tag{2-28}$$

Handy (1985) proposed that the shape of the arched soil is catenary and suggested the use of the coefficient K_w instead of K, by considering an arch of minor principal stress.

$$K_w = 1.06\ (\cos^2\ \theta + K_a \sin^2\ \theta) \tag{2-29}$$

where: $\theta = 45 + \varphi/2$

Russell et al. (2003) proposed that K could be conservatively taken as 0.5 and Potts & Zdravkovic (2008) proposed that K = 1.0 gave good correspondence with the results of plane strain finite element.

2.5.3.2. Rectangular Pyramid: Guido Method (1987)

This method is quite different from other methods of analysis for soil arching. The so-called 'Guido' design method is based on empirical evidence from model test carried out with geogrid reinforced granular soil beneath a footing continued in a rigid box (see Fig. 2-14).

The results suggest that multiple layers of geogrid reinforcement increase the bearing capacity, which could be interpreted as an improved angle of friction for the composite soil-geogrid material (Slocombe&Bell, 1998). The 'load spread' angle in the reinforced soil beneath the footing was proposed to be 45^o (Bell et al., 1994).

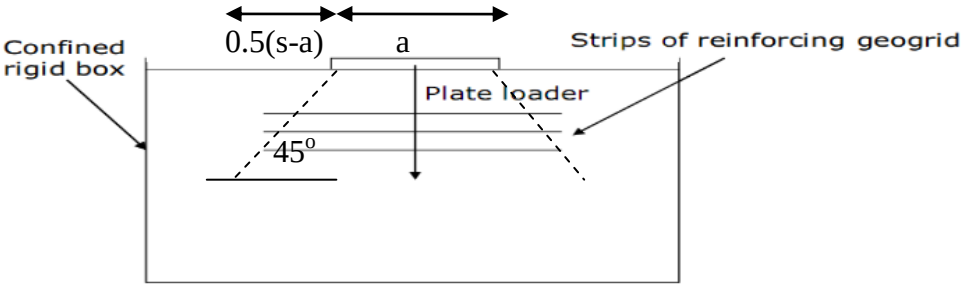

Fig. 2-14 Guido's experimental set-up (after Guido, 1987)

The stress on the subsoil (σ_s) resulted from self weight of the unsupported soil mass is equal to the volume of triangle/pyramid multiplied by the soil unit weight (γ). Then, it is divided by the area over which the soil prism acts. For the two dimensional situation, the stress acting on the subsoil is:

$$\sigma_s = \gamma (s\text{-}a) / 4 \qquad (2\text{-}30)$$

Meanwhile, for the three dimensional situation, the equation is modified to:

$$\sigma_s = \gamma (s\text{-}a) / 3\sqrt{2} \qquad (2\text{-}31)$$

where: s-a = the width of strip (m)

From the equations above that the height of the embankment has no effect on the pressure acting on the subsoil. Moreover, the friction angle of the fill material is not considered in this case. Love&Milligan (2003) suggest that the Guido method may experience difficulties when dealing with situations where support of the existing subsoil is very low. The Guido method concentrates more on reinforcement rather than arching process.

2.5.3.3. Semicircular Arch: Hewlett & Randolph (1988)

Hewlett&Randolph (1988) derived theoretical solutions based on observations from experimental tests of arching in a granular soil. Their analysis attempts to consider actual arches in the soil as shown in Fig. 2-15.

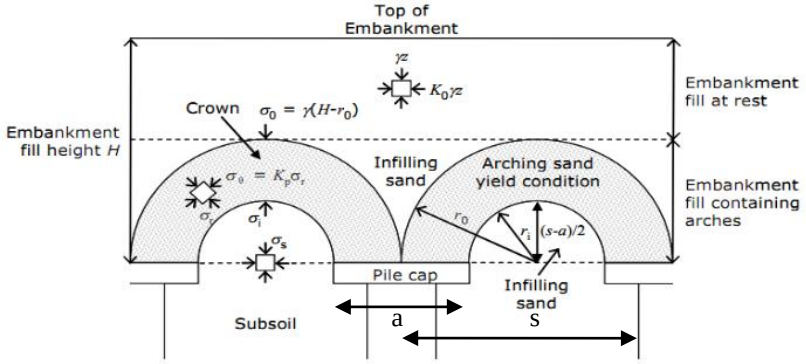

Fig. 2-15 Arching through a piled embankment (after Hewlett&Randolph, 1988)

The 'arches of sand' transmit the majority of embankment load onto the pile caps, with the subsoil carrying load predominantly from the 'infill' material below the arches. The arches are assumed to be semi circular (in 2D) uniformly without overlapping.

The analysis considers equilibrium of an element at the 'crown' as in Fig. 2-16. Here the tangential (horizontal) direction is the direction of major principal stress and the radial (vertical) direction is the minor principal stress. Yielding is in the 'passive' condition since the horizontal stress is the major principal stress.

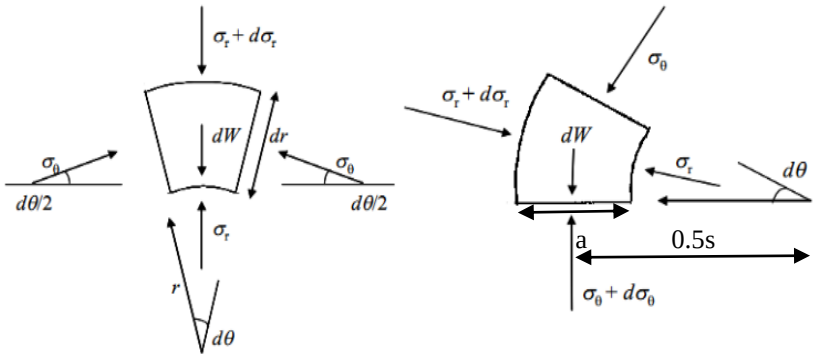

(a) An element of sand at the crown of arch

(b) An element of sand above the pile cap

Fig. 2-16 Stress on an element of soil arching (after Hewlett&Randolph, 1988)

By using the boundary condition, considering vertical equilibrium, that the stress at the top of arching layer is equal to the weight of material above acting on the outer radius of arch will give a solution for the radial (vertical) stress acting immediately beneath the crown of the arch (σ_i). The vertical stress acting on the subsoil is then obtained by adding the stress due to the infilling material beneath the arch, based on the maximum height of infill (s-a)/2.

$$\sigma_s = \sigma_i + \gamma(s\text{-}a) / 2 \tag{2-32}$$

When considering the three dimensional solution the equation above is modified to:

$$\sigma_s = \sigma_i + \gamma(s\text{-}a) / \sqrt{2} \tag{2-33}$$

The vertical stress (σ_s) is considered uniform here. Though, Low et al. (1994) introduced this parameter to allow a possible non uniform vertical stress on the soft ground.

In case at the pile cap, the tangential (vertical) stress is the major principal stress and the radial (horizontal) stress is the minor principal stress. In conjunction with overall vertical equilibrium of the embankment, a value of σ_s is obtained in the limit when the ratio of the major and minor principal stress is K_p. In fact, yielding occurs in an ’active’ condition, since the vertical stress is the major principal stress.

2.5.3.4. Positive Projecting Subsurface Conduits: BS 8006-1 (2010)

The method used in the British Standard (BS 8006) for strengthened/reinforced soils and other fills to design geosynthetics over piles was initially developed by Jones et al. (1990). A 2 dimensional geometry was assumed, which implies 'walls' in the soil rather than piles. This method uses a modified form of Marston's equation for positive projecting subsurface conduits to obtain the ratio of the vertical stress acting on top of the piles caps to the average vertical stress at the base of the embankment ($\sigma_s = \gamma H$).

The equation proposed by Marston was derived from field tests at the Engineering Experiment Station at Iowa State College in 1913. The equation is normally used to calculate the reduced loads on buried pipes (see Fig. 2-17).

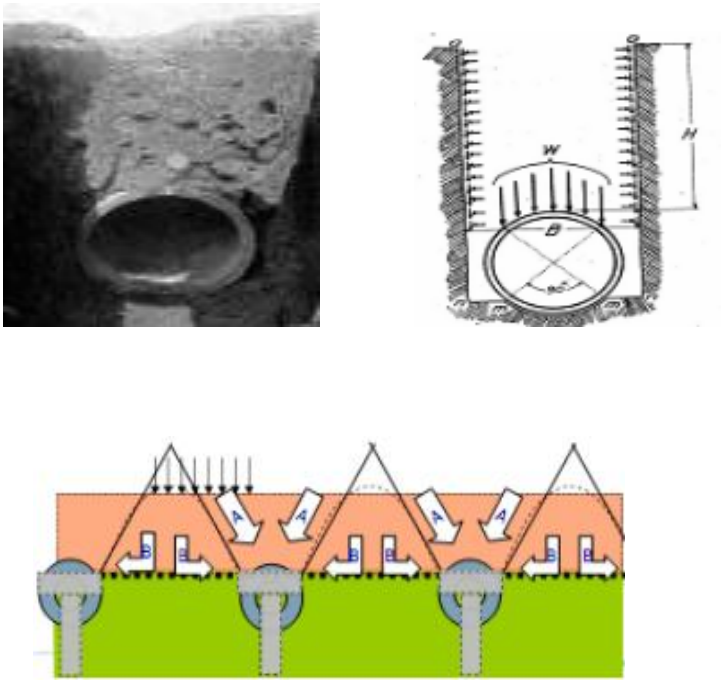

Fig. 2-17 Stress distribution of sub-surface conduit (after Marston et al., 1913)

For the two dimensional situation the Marston's equation is:

$$\frac{\sigma_c}{\gamma H} = \frac{C_c a}{H} \tag{2-34}$$

Meanwhile, the three dimensional analysis is modified to:

$$\frac{\sigma_c}{\gamma H} = \left(\frac{C_c a}{H}\right)^2 \tag{2-35}$$

where: σ_c = the vertical stress on the pile cap (kN/m^2)
γ = the unit weight of the soil (kN/m^3)
a = the width of the pile cap (m)
H = the thickness of soil above the point (m)
γH = the nominal vertical stress at the base of embankment (kN/m^2)
C_c = the soil arching coefficient depending on H and a
$C_c = 1.95\ H / a - 0.18$ for end-bearing piles
$C_c = 1.5\ H / a - 0.07$ for floating piles

2.5.3.5. Multi Vaulted-Dome: German Standard (EBGEO, 2010)

In EBGEO 2010 for a three dimensional arching model proposed by Kempfert et al. (1997), it appears similar to the Hewlett&Randolph (1988) approach. However, the average vertical pressure acting on the soft subsoil was obtained by considering the equilibrium of dome shaped arches of varying size in the 'infill' material beneath a hemisphere (see Fig. 2-18).

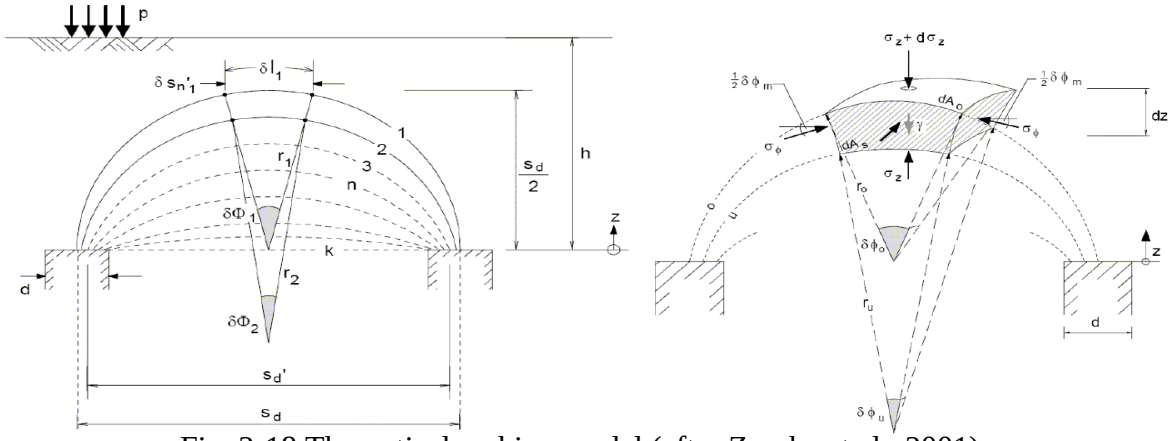

Fig. 2-18 Theoretical arching model (after Zaeske et al., 2001)

EBGEO (2010) recommends the use of geosynthetics reinforcement but the arching effect and the membrane tension are dissociated. After arching on embankments, it will develop a redistribution of vertical stress at the surface between piles ($\sigma_{zo,k}$) and vertical stress at surface of piles ($\sigma_{zs,k}$) as depicted in Fig. 2-19.

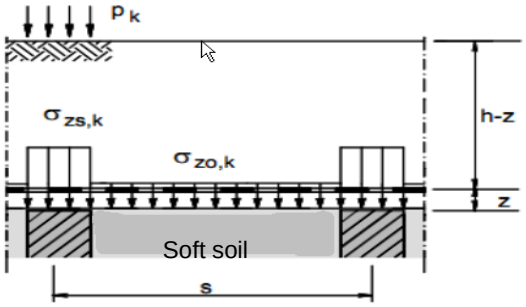

Fig. 2-19 Vertical stress redistribution on arching (after EBGEO, 2010)

Vertical stress at the surface between piles after arching on embankments is divided into two groups, namely the vertical stress for static loading ($\sigma_{zo,G,k}$) and vertical stress for static and variable-dynamic loading ($\sigma_{zo,G+Q,k}$).

$$\sigma_{zo,G,k} = \lambda_1^{\chi}.\left(\gamma_k + \frac{p_{G,k}}{h}\right).\left(h.\left(\lambda_1 + h_g^2.\lambda_2\right)^{-\chi} + h_g.\left(\left(\lambda_1 + \frac{h_g^2.\lambda_2}{4}\right)^{-\chi} - \lambda 1 + hg2.\lambda 2^{-\chi}\right.\right. \quad (2\text{-}36)$$

$$\sigma_{zo,G+Q,k} = \lambda_1^{\chi}.\left(\gamma_k + \frac{p_{G+Q,k}}{h}\right).\left(h.\left(\lambda_1 + h_g^2.\lambda_2\right)^{-\chi} + h_g.\left(\left(\lambda_1 + \frac{h_g^2.\lambda_2}{4}\right)^{-\chi} - \lambda 1 + hg2.\lambda 2^{-\chi}\right.\right. \quad (2\text{-}37)$$

where: γ_k = unit weight of embankment (kN/m^3)
$p_{G,k}$ = static loading (kN/m^2)
$p_{G+Q,k}$ = static and variable loading (kN/m^2)
h_g = height of arching (m)
h_g = s / 2 for $h \geq s / 2$
h_g = h for $h < s / 2$

h = height of embankment (m)
s = diagonal pile spacing (m)
d = diagonal pile spacing (m)
K_{krit} = critical ratio of major stress = $\tan^2 [45^o + \phi'_k / 2]$
χ = $d.\,(K_{krit\,-}\,1) / (\lambda_2 . s)$
λ_1 = $(s - d)^2 / 8$
λ_2 = $(s^2 + 2\,d.\,s - d^2) / 2\,s^2$

Furthermore, the vertical stress at the surface of piles after arching on embankments resulted from surcharge divided into two groups, namely the vertical stress for static loading ($\sigma_{zs,G,k}$) and vertical stress for static and variable-dynamic loading ($\sigma_{zs,G+Q,k}$).

$$\sigma_{zs,G,k} = [\,(\gamma_k . h + p_{G,k}) - \sigma_{zo,G,k}\,]\,A_E/A_s + \sigma_{zo,G,k} \quad (2\text{-}38)$$

$$\sigma_{zs,G+Q,k} = [\,(\gamma_k . h + p_{G+Q,k}) - \sigma_{zo,G+Q,k}\,]\,A_E/A_s + \sigma_{zo,G+Q,k} \quad (2\text{-}39)$$

Where A_E is the area of one cell pile embankment and A_s is a support surface for point and/or linear bearing elements.

Vertical loads or forces on bearing element as:

$$F_{s,G,k} = \sigma_{zs,G,k} . A_s \quad (2\text{-}40)$$

$$F_{s,G+Q,k} = \sigma_{zs,G+Q,k} . A_s \quad (2\text{-}41)$$

Generally, the resultant force on bearing element conservatively is calculated using:

$$F_{s,G,k} = (\gamma_k . h + p_{G,k}) . A_E \quad (2\text{-}42)$$

$$F_{s,G+Q,k} = (\gamma_k . h + p_{G+Q,k}) . A_E \quad (2\text{-}43)$$

2.5.3.6. Arching Evolution

A novel approach for determining the vertical loading on underground structure in granular soils has been developed (Iglesia et al. 1999). As can be seen in Fig. 2-20, it is proposed that as the trap door is gradually lowered, the arch evolves from an initially curved shape (1) to a triangular one (2), before ultimately collapsing with the appearance of a prismatic sliding mass with two vertical shear planes (3).

Compared to analysis of a piled embankment the structure is analogous to subsoil. The curved arch is similar to Hewlett&Rundolph's semi-circular arch. The triangular arch is similar to Guido's triangular arch and prismatic sliding mass is similar to Terzaghi's sliding block.

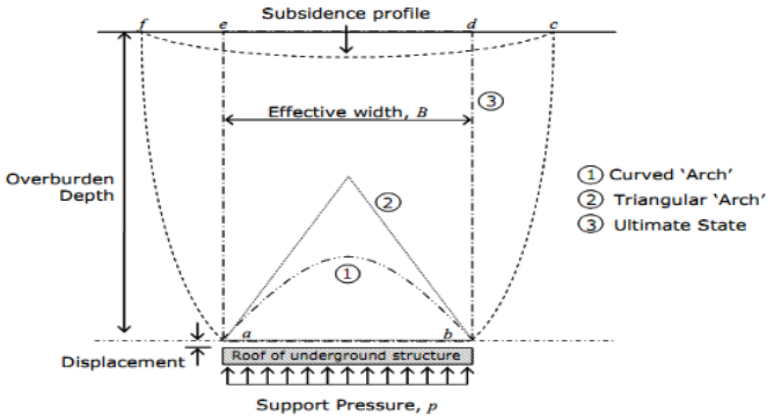

Fig. 2-20 Arching evolution (after Iglesia et al., 1999)

A methodology has been proposed by Iglesia et al. (1999) not only for determining the vertical loading on the structure, but also for relating to this movement of the roof of an underground structure. This is referred to as a 'Ground Reaction Curve' (GRC) for overlying soil. This is used dimensionless plotting of normalized loading (p*) vs. normalized displacement (δ*).

$$p^* = \frac{p}{p_o} \tag{2-44}$$

$$\delta^* = \frac{\delta}{B} \tag{2-45}$$

where : p = the support pressure from roof above underground structure (kN/m^2)
p_o = the nominal overburden total stress at the elevation of underground (kN/m^2)
δ = the settlement of roof (kN/m^2)
B = the width of underground structure (m)

As shown in Fig. 2-21 that the GRC is divided into four parts namely the initial arching phase, maximum arching, loading of the recovery stage, and the ultimate state.

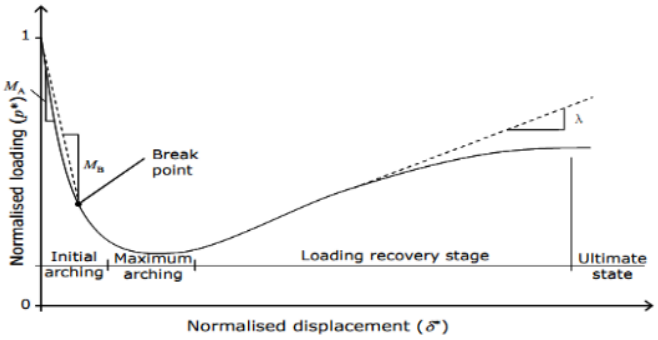

Fig. 2-21 Generalized ground reaction curve (after Iglesia et al., 1999)

2.5.4. Definition of Terms

There are four terms commonly used to relate the total applied embankment pressure, the pressure acting on top of the pile, and the pressure acting on the soil surface between piles spacing.

1. the stress concentration ratio, *n*
2. the column stress ratio, *CSR*, or competency ratio, *C*,
3. the efficacy, *E*
4. the stress reduction ratio, *SRR*

2.5.4.1. Stress Concentration Ratio

The stress concentration ratio (n) is a parameter that is used to quantify load transfer. It is defined as the ratio of the stress on the pile (caps) to the soil between the piles (caps). Ooi et al., (1987) cited in Han (1999) indicated that the value of stress concentration ratio for conventional pile embankments ranges between 1.0 to 8,0. This ratio increased with the increase in ratio of the embankment height to the net spacing between pile caps. For structure using Geosynthetics Reinforced Pile Supported (GRPS) embankments on vibro-concrete and concrete piles, this value ranged from 8 to 25 which is much higher than conventional piled embankments (Reid et al., 1993; Maddisson et al., 1996). This increase in n is due to the inclusion of the geosynthetics layer and depends on the stiffness or rigidity of foundation.

$$n = \frac{\sigma_{pile}}{\sigma_{soil}} \quad (2\text{-}46)$$

2.5.4.2. Column Stress Ratio

The ratio between the stress on the top of the columns, σ_{pile}, and the average applied embankment plus surcharge stress at the level of the top of the piles, σ, is referred as the column stress ratio, *CSR*.

$$CSR = \frac{\sigma_{pile}}{\sigma} \quad (2\text{-}47)$$

Low et al. (1994) use term of ''competency ratio'' using the symbol of *C* to refer the same meaning for column stress ratio.

2.5.4.3. Efficacy

Hewlett &Randolph (1988); Low et al. (1994) defined efficacy, *E*, as the proportion of the embankment weight carried by the piles rather than the subsoil. Efficacy increase (tending towards 1.0) as the effect of arching increases.

$$E = \frac{\sigma_{pile} . a_s}{\sigma} \quad (2\text{-}48)$$

where: a_s = area replacement ratio or coverage ratio which is defined as:

$$a_s = \frac{area\ of\ pile}{total\ tributary\ area} = \frac{A_{pile}}{A_{pile}+A_{soil}} \quad (2\text{-}49)$$

2.5.4.4. Stress Reduction Ratio

Soil arching causes vertical stress to be transferred from the soft soil to the columns (Han and Gabr, 2002). The stress reduction ratio (*SRR*) is defined as the ratio of stress applied to the foundation soil between the columns, σ_{soil}, to the average stress applied by the embankment plus surcharge, σ. A *SRR* of 1.0 implies no arching and the SRR reduces ultimately tending to zero as the effects of arching increase.

$$SRR = \frac{\sigma_{soil}}{\sigma} \quad (2\text{-}50)$$

Mainly current methods such as Terzaghi, Hewlett &Randolph, Guido, and Carlsson have a main assumption that the geosynthetics reinforcement takes the entire load between the columns and that none of the load is carried by the foundation soil (Russel and Pierpoint 1997). As stated previously, there is a large discrepancy in results from each of these methods.

All parameters above have a close relationship to each other as expressed in equations below.

$$SRR = \frac{1}{1+(n-1).a_s} = \frac{1-CSR\ .a_s}{1-a_s} \quad (2\text{-}51)$$

$$CSR = \frac{n}{1+(n-1).a_s} = \frac{1-SRR\ .(1-a_s)}{a_s} \quad (2\text{-}52)$$

$$E = CSR\ .\ a_s = 1 - SRR(1 - a_s) \quad (2\text{-}53)$$

$$SRR = \frac{(1-E)}{(1-a_s)} \quad (2\text{-}54)$$

Arching in the embankment plays an important role in the behaviour of column-supported embankments. For the condition of no soil arching, there is no reduction of pressure on the

foundation soil between the columns and hence the values of *n*, *SRR*, and *CSR* are equal to one. If complete soil arching hypothetically develops, the entire applied embankment load would be carried by the columns and no load would be carried by the soil between columns. Relationship of the parameters is shown in Fig 2-22.

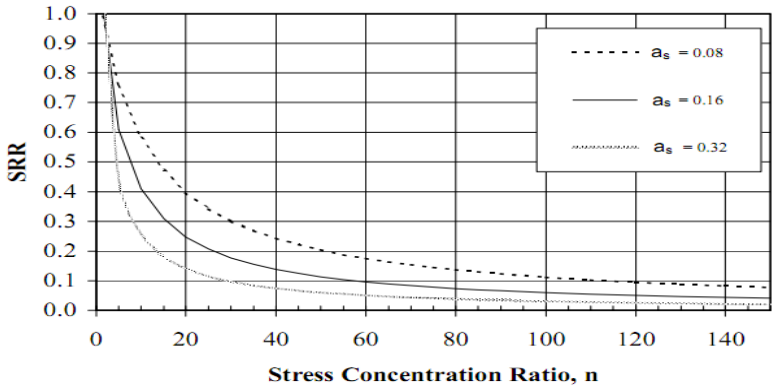

Fig. 2-22 Relationship between *n* and *SRR* (after Smith, 2006)

2.5.5. Load Transfer Mechanism

The inclusion of geosynthetics layer (see Fig. 2-23) is expected to reduce the differential settlement between two piles. A single layer of reinforcement may be used at or near the base of the embankment. Generally it is not placed directly on the pile caps due to the risk of damage. A single geosynthetics layer acts as a tension membrane or catenary, whereas a multi-layer system can interlock better with the surrounding soil and acts as a stiffened beam or plate.

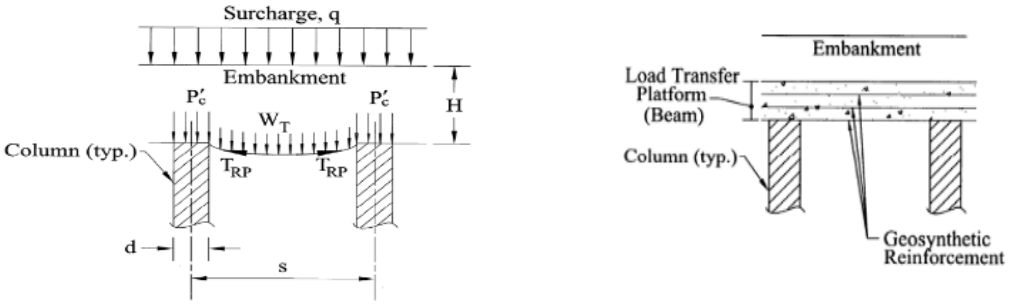

(a) Catenary (b) Beam

Fig. 2-23 Load transfer mechanism (after Collin, 2004)

The design of the load transfer platform (Collin, 2004) based on the use of multiple layers is a refinement of a method referred to Guido method. The primary assumptions for the beam theory are:

1. a minimum of three layers of reinforced is applied to create the platform
2. spacing between layers is 200-450 mm
3. platform thickness is greater than or equal to one half the clear spacing piles
4. soil arching is fully developed within the depth of the platform

When one or more layers of geosynthetics reinforcement are placed in the fill above the columns, the stress that would otherwise be applied to the foundation soil between columns is

assumed to be carried by geosynthetics. Thus, the *SRR* value can be used to represent the portion of embankment load carried by geosynthetics reinforcement.

2.5.5.1. BS 8006 Method

This method has adopted the empirical method developed for design of geosynthetic reinforced piled embankment that was developed by Jones et al. (1990). The plan area of the unit cell is s^2 and the area not supported by columns is s^2-a^2, as shown in Fig. 2-24.

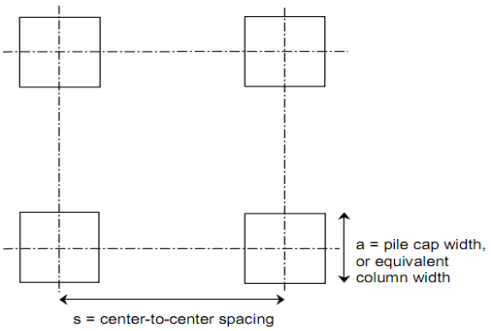

Fig. 2-24 Unit cell utilization (after Jones et al., 1990)

BS8006 defines a critical embankment height equal to 1.4(s-a). If the embankment height is below the critical height, arching is not fully developed. The embankment and surcharge load is converted to an equivalent vertical load, W_T, between the piles which triangle load with W_T as maximum value at the centre of span, as determined by using equation:

$$W_T = \frac{s\,(\gamma H+q)}{s^2-a^2}\left[s^2 - a^2\left(\frac{p_c'}{\gamma H+q}\right)\right],\ for\ H \leq 1.4(s-a) \qquad (2\text{-}55)$$

If the embankment heights is greater than the critical height assumed that all load above the critical height are transferred directly to columns as a result of arching in the embankment fill (Kempton et al.1998).

$$W_T = \frac{1.4\,s\,\gamma\,(s-a)}{s^2-a^2}\left[s^2 - a^2\left(\frac{p_c'}{\gamma H+q}\right)\right],\ for\ H > 1.4(s-a) \qquad (2\text{-}56)$$

where: p_c = vertical stress on the column
γ = unit weight of the embankment fill
H = embankment height
q = surcharge load

The stress reduction ratio, *SRR*, may be determined using the following equation:

$$SRR = \frac{2\,W_T\,(s-a)}{(s^2-a^2)(\gamma H+q)} \qquad (2\text{-}57)$$

2.5.5.2. Adapted Guido Method

Guido et al., (1987) presented that the inclusion of biaxial geogrids within granular soil below spread footing could improve the bearing capacity of foundation soils. Angle of load spread through the geogrid reinforcedless soil can conservatively be taken as 45 degrees. Bell et al. (1994) applied this finding to perform with two layers of geosynthetic reinforced supported on vibro-concrete columns. Russel and Pierpoint (1997) also assumed that geosynthetics caries a pyramid of soil that not supported by column with angle of 45 degrees from the horizontal level.

The *SRR* value for the Adapted Guido Method is based on the interior area of the unit cell, i.e., $(s\text{-}a)^2$ rather than $s^2\text{-}a^2$.

$$SRR = \frac{(s-a)\,\gamma}{3\sqrt{2}\,(\gamma H+q)} \tag{2-58}$$

2.5.5.3. Adapted Nordic Method

This method adopted a triangular soil arching model of Carlsson's work (1987). This method is similar to the Adapted Guido method but a wedge with an internal angle at the apex of the wedge is equal to 30 degrees as shown in Fig. 2-25 .The Nordic method adopts a critical height of 1.87 (*s*-a) and additional overburden above the top wedge will be directly transferred to the columns.

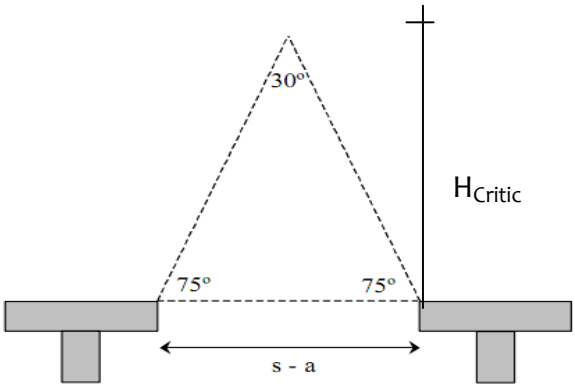

Fig. 2-25 Triangular soil arching of Nordic method (after Nordic guideline,2003)

The stress reduction ratio for the two dimensional approach, SRR_{2D}, is given as:

$$SRR_{2D} = \frac{s-a}{4\,H\tan 15^o} \tag{2-59}$$

Rogberck et al. (1998) provide a correction factor used to compute the geosynthetics tension for an embankment supported by square piles caps. The net effect of this correction factor for the three-dimensional stress reduction is the same as the two dimensional value and when a surcharge load considered, the equation above is:

$$SRR_{2D} = \frac{(s-a)\,\gamma}{4\,(\gamma\,H+q)\tan 15^o} \tag{2-60}$$

Equation 2-59 is applicable for embankment height greater than or equal to the critical height and for lower embankments. The upper part of the triangle must be truncated to calculate the stress reduction ratio.

2.5.5.4. Adapted Terzaghi Method

Russell and Pierpoint (1997) adapted Terzaghi's arching theory to develop a stress reduction ratio. The settling mass is assumed to be cruciform in plan. The three-dimensional stress reduction ratio is expressed as:

$$SRR_{3D} = \frac{(s^2-a^2)}{4\;H\;a\;K\tan 15^o}\cdot\left(1-exp\left(\frac{-4\;H\;a\;K\tan\varphi}{(s^2-a^2)}\right)\right) \tag{2-61}$$

where: K = coefficient of lateral earth pressure, and ϕ = internal friction angle of embankment fill. The K value is assumed to be equal to one and the equation above is referred as Adapted Terzaghi's method 1.

Several years later Russell et al. (2003) presented a modified version of the previous method. They assume that the portion of the embankment fill that settles as a cruciform has a height of n.*H* and the embankment fill above the settling cruciform is treated as surcharge. The stress reduction ratio from latter method (Adapted Terzaghi Method 2) is expressed as:

$$SRR_{3D} = \frac{(s^2-a^2)\gamma}{4\ a\ (\gamma H+q)\ K \tan 15^o} \cdot \left(1 - exp\left(\frac{-4\ a\ H\ n\ K \tan\varphi}{(s^2-a^2)}\right)\right) + \frac{\gamma(1-n)H+q}{(\gamma H+q)} \cdot exp\left(\frac{-4\ a\ H\ n\ \tan\varphi}{(s^2-a^2)}\right) \quad (2\text{-}62)$$

where: q = embankment surcharge, *K*= coefficient of lateral earth pressure which Russel et al.(2003) assumes to be equal to 0.5 , n = 1.0 for ultimate limit state (ULS) conditions and 0.8 for serviceability limit state (SLS) conditions.

2.5.5.5. Hewlett and Randolph Method

Hewlett and Randolph (1988) stated that the dome regions will fail either at the crown of the arch or at the top of the column, but not elsewhere (see Fig. 2-26). Hewlett and Randolph (1988) evaluated the load transfer mechanisms in terms of efficacy.

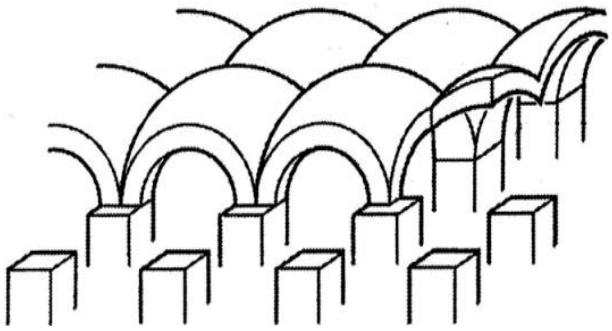

Fig. 2-26 Dome soil arching model (after Hewlett &Randolph,1988)

Efficacy at the arch crown is:

$$E = 1 - \left(1 - \left(\frac{a}{s}\right)^2\right) \cdot \left[\left(1 - \frac{a}{s}\right)^{2(K_p-1)} \cdot \left(1 - \frac{2\ s\ (K_p-1)}{\sqrt{2}\ H\ (2K_p-3)}\right) + \left(\frac{(s-a)\ 2(K_p-1)}{\sqrt{2}\ H\ (2K_p-3)}\right)\right] \quad (2\text{-}63)$$

Efficacy at the top of pile is:

$$E = \frac{\beta}{1+\beta} \quad (2\text{-}64)$$

$$\beta = \left(\frac{2K_p}{K_p+1}\right) \cdot \left(\frac{1}{1+\frac{a}{s}}\right) \cdot \left[\left(1 - \frac{a}{s}\right)^{-K_p} - \left(1 + \frac{a}{s}K_p\right)\right] \quad (2\text{-}65)$$

where: K_p = coefficient of passive earth pressure

The stress reduction ratio may be determined efficacy and its value at the arch crown is:

$$SRR = \left[\left(1 - \frac{a}{s}\right)^{2(K_p-1)} \cdot \left(1 - \frac{2\ s\ (K_p-1)}{\sqrt{2}\ H\ (2K_p-3)}\right) + \left(\frac{(s-a)\ 2(K_p-1)}{\sqrt{2}\ H\ (2K_p-3)}\right)\right] \quad (2\text{-}66)$$

The stress reduction ratio at the top of the pile is:

$$SRR = \frac{1}{\left(\frac{2K_p}{K_p+1}\right)\left[\left(1-\frac{a}{s}\right)^{(1-K_p)}-\left(1-\frac{a}{s}\right)\left(1+\frac{a}{s}.K_p\right)\right]+\left(1-\frac{a^2}{s^2}\right)} \quad (2\text{-}67)$$

2.5.5.6. German Method (EBGEO 2010)

In the German method, it is adopted from Kempfert et al. (2004). The arching theory from Zaeske's work (2004) has been developed based upon plasticity theory, laboratory pilot scale tests and numerical analysis.

The vertical stress on soft soil in between columns is expressed as:

$$\sigma_{soil} = \lambda_1^{\chi}.\left(\gamma + \frac{q}{H}\right).\left[H\left(\lambda_1 + h_g^2.\lambda_2\right)^{-\chi} + h_g.\left(\left(\lambda_1 + \frac{h_g^2.\lambda_2}{4}\right)^{-\chi} - \right.\right.$$
$$\lambda 1 + hg2.\lambda 2 - \chi \quad (2\text{-}68)$$

Kempfert et al. (2004) recommend using the equation to determine the load on the top of geosynthetics reinforcement. Soil support from the subgrade beneath geosynthetics layer also can be taken into account. The stress reduction ratio may be determined as follows:

$$SRR = \frac{1}{(1+\lambda)^{\chi}} + \frac{h_g}{H}.\left[\frac{1}{\left(1+\frac{\lambda}{4}\right)^{\chi}} - \frac{1}{(1+\lambda)^{\chi}}\right] \quad (2\text{-}69)$$

2.5.6. Column Design

The embankment and/or any surcharge load is typically assumed to be carried by the columns. The selection of column type is most often based on workability, load capacity and cost. For purposes of determining the design vertical load in the column, it is convenient to associate the tributary area of soil surrounding each column as illustrated in Fig. 2-27.

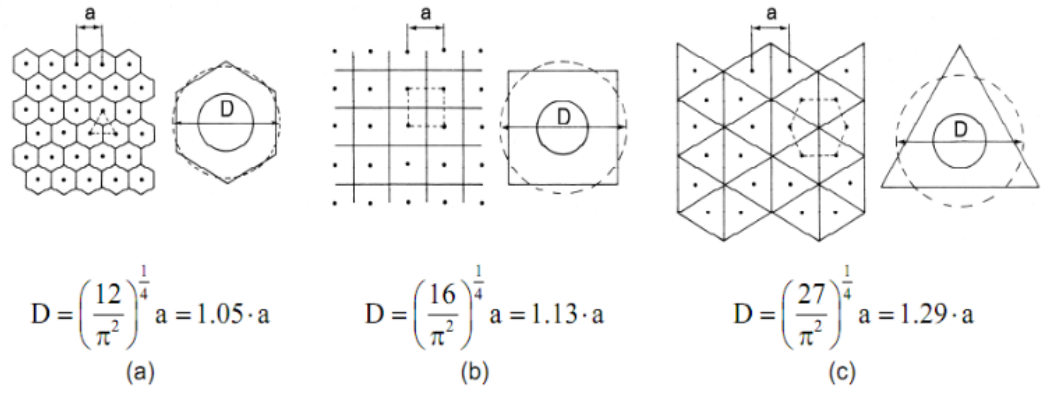

Fig. 2-27 Effective tributary area of column,
(a) Triangular spacing (b) Square spacing (c) Hexagonal spacing

The required design vertical load, Q_r, in the column is determined according to the following equation:

$$Q_r = \pi \left(\frac{D}{2}\right)^2 (\gamma H + q) \quad (2\text{-}70)$$

2.5.7. Tension in Geosynthetics Reinforcement due to Vertical Stress

Geosynthetics reinforcement is commonly used in soil by placing at the base of the embankment. The tension will provide support between the pile caps (see Fig.2-28). Geosynthetics reinforcement helps to transfer the weight of the embankment directly on to the columns or piles (Lawson, 1992). At the edges of embankment it also prevents lateral spreading (Hewlett&Rundolph, 1988). However, these two functions are normally considered independently.

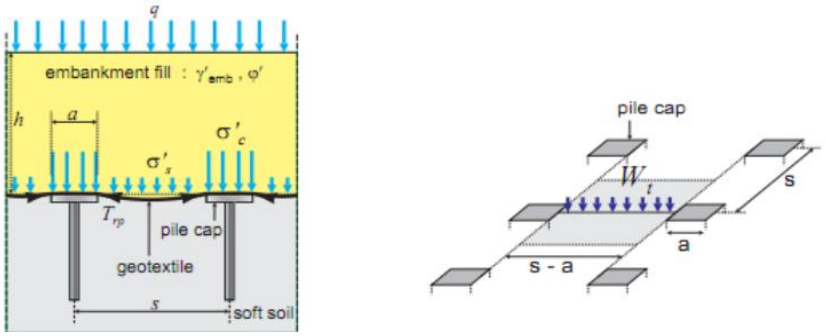

Fig. 2-28 Tension on geosynthetics reinforcement (after Satibi, 2009)

The effect of additional capacity to carry a vertical load could be added based on purely tensile response. They proposed that assuming the geosynthetics was subjected to a uniform vertical load and deforms as a parabola.

$$T_{RP} = \frac{W_T \cdot L^2}{8\,\delta} \tag{2-71}$$

where : T_{RP} = the tension in geosynthetic (kN/m)
W_T = the uniform stress acting on the geosynthetics (kN/m^2)
L = (s-a) the length of span (m)
δ = the maximum sag (vertical deflection) of geosynthetic (m)

The average strain based on the total extension in the geosynthetics, ε, can be expressed in terms of the maximum sag as follows:

$$\varepsilon = \frac{8}{3}.\left(\frac{\delta}{l}\right)^2 \tag{2-72}$$

As can be seen in equation (2-72) that the strain, ε, increases as the square of δ. The tension in the geosynthetics is assumed as linear response against strain as below:

$$T_{RP} = k.\varepsilon \tag{2-73}$$

where: k = the stiffness of geosynthetics and in another expression:

$$T_{RP} = k.\frac{8}{3}\left(\frac{\delta}{L}\right)^2 \tag{2-74}$$

This can be re-arranged to express how the load which can be carried theoretically increase with the sag:

$$W_T = 64\ \frac{k}{3L}\left(\frac{\delta}{L}\right)^3 \tag{2-75}$$

Giroud, J.P. (1995) presented a correlation between deflection and strain in geosynthetics, it is similar to Eq. 2-71, and re-writing it as follows:

$$\delta = (s - a).\sqrt{\frac{3\varepsilon}{8}} \quad (2\text{-}76)$$

2.5.7.1. BS8006 Method

The BS8006 method assumes that the geosynthetics reinforcement is placed above columns installed in a square grid pattern. It is assumed that the embankment fill load is distributed along the horizontal span of geosynthetics between pile caps and the entire load between pile caps is carried by the geosynthetics and there is no support from the foundation soil. The tensile load T_{RP} per meter 'run' generated in the reinforcement resulting from the distributed load W_T is given by:

$$T = \frac{W_T(s-a)}{2a}.\sqrt{1 + \frac{1}{6\varepsilon}} \quad (2\text{-}77)$$

The tension in the reinforcement is calculated taking into consideration the maximum allowable strain in the reinforcement. Six percent of strain is considered the upper limit for transferring the load to the piles. The upper limit should be reduced for shallow embankments to prevent differential movement on the surface of the embankment. To avoid long term localized deformations at the surface of the embankment, the long term strain should be kept to a minimum and a maximum creep strain of 2% is permitted for permanent construction.

2.5.7.2. EBGEO 2010 Method

The EBGEO 2010 method adopted Kempfert's work for evaluating the tension and strain in geosynthetics reinforcement. For practical application, the strain in geosynthetics reinforcement is determined using dimensionless design charts and then the tension is determined by multiplying the strain by the geosynthetics stiffness. The force on the geosynthetics, F_k, is equal to the vertical stress over subsoil, σ_{soil} , multiply by a tributary area associated with the strip of geosynthetics spanning between adjacent pile caps. The resistance of foundation soil is included by using a modulus of subgrade reaction, *k*. The modulus of subgrade reaction is the ratio of the pressure applied to the soil over a loaded area divided by the resulting displacement.

The maximum stress in the geosynthetics reinforcement occurs over a width equal to b_{Ers} . For a circular columns have to be converted to b_{Ers} of 0.886 d_c, where d_c = diameter of column. Plan view of foundation and geosynthetics is as shown in Fig. 2-29.

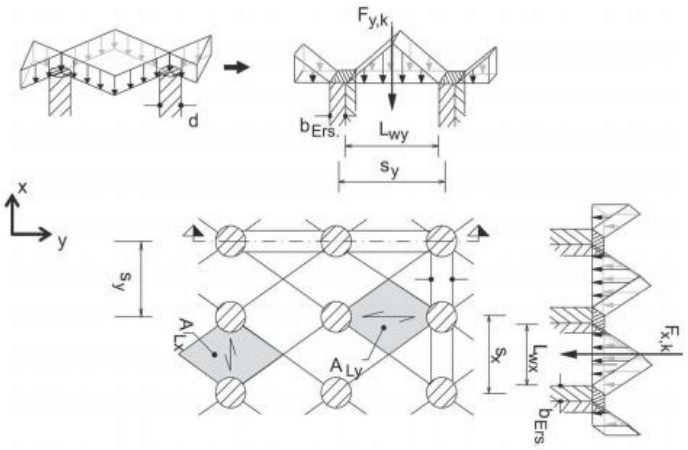

Fig. 2-29 Plan view of foundation and geosynthetics (after Kempfert et al., 2004)

The maximum strain in the geosynthetic reinforcement is dependent upon the tensile stiffness of geosynthetic, J_k, the modulus of subgrade reaction, k, the vertical load, F_k, clear spacing, L_w, and width of column, b_{Ers} . The value of strain in geosynthetics, ε_k, can be determined using the design chart in Fig. 2-30.

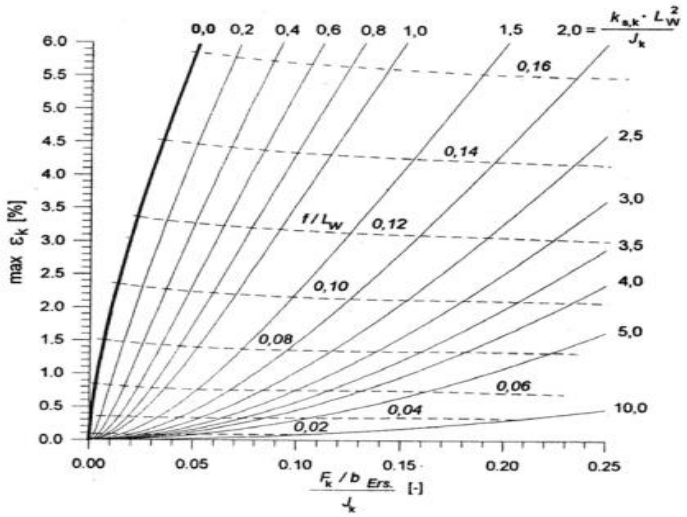

Fig. 2-30 Chart to determine strain in geosynthetics (after Kempfert et al., 2004)

The tensile force in the reinforcement can be calculated using the following equation:

$$T_{RP} = \varepsilon_k \ . J_k \qquad (2\text{-}78)$$

When applied two layers of geosynthetics, the calculated tensile force is divided with respect to the ratio of their tensile moduli (Kempfert et al. 2004).

2.5.8. Soil Resistance

Most current design methods for piled embankment ignore any support from the subsoil between the pile caps. This is conservative and over estimate the magnitude of tension in the reinforcement (Russell et al., 2001). Strain and deformation compatibility is required between each layer (embankment fill, geosynthetics and subsoil). In practice, there will be some support provided by soil below. This will considerably reduce the tension in the geosynthetics reinforcement. Reid and Buchman (1983) found from their study that the resistance from the subsoil is around 0.18 γH. John (1987) found the soil resistance to be 0.15 γH.

2.5.9. Tension in Geosynthetics Reinforcement due to Lateral Sliding

The reinforcement should resist the horizontal force due to lateral sliding. This tensile should be generated at strain which compatible with allowable lateral pile movements. The need for raking of the piles is eliminated. The reinforcement tensile load needed to resist the outward thrust on the embankment in accordance with BS 8006 is:

$$T_{ds} = 0.5\, K_a\, (f_{fs}.\, \gamma.\, H + 2f_q.\, q)\, H \qquad (2\text{-}79)$$

where : K_a = the active earth pressure coefficient ($K_a = \tan^2 (45+\phi/2)$
q = the uniformly distributed surcharge load (kN/m^2)
f_{fs} = the partial load factor for soil unit weight
f_q = the partial load factor for applied external load

γ = the unit weight of embankment fill (kN/m^3)

H = the height of embankment fill (m)

In EBGEO 2010, it is similar to the equation above, but any little bite different for coefficient of active earth pressure (see Fig.2-31).

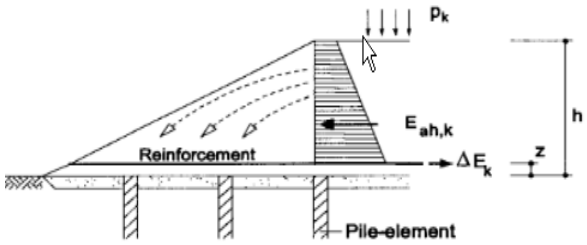

Fig. 2-31 Horizontal outward-thrust resisted by geosynthetics (after EBGEO, 2010)

$$E_k = [\ 0.5.\ \gamma_{embk}\ .\ (h\text{-}z).\gamma_G + p_k\ .\gamma_Q\ ]\ .(h\text{-}z).\ K_{agh} \qquad (2\text{-}80)$$

Where K_{agh} is the active lateral earth pressure coefficient according to DIN 4085, which is defined as :

$$K_{agh} = [\ \cos\ \phi'\ /\ (1+A_s)\ ]^2 \qquad (2\text{-}81)$$

$$A_s = [\ (\sin(\phi' + \delta_{s,k}).\ \sin\ \phi'\ )\ /\ \cos\ \delta_{s,k})\ ]^{1/2} \qquad (2\text{-}82)$$

where: γ_G = the partial load factor for soil unit weight

γ_Q = the partial load factor for applied external load

ϕ' = the internal friction angle (degree)

2.5.10. Settlements Analysis

2.5.10.1. Different Settlement on the Surface of Embankment

Because of difference in stiffness between piles and soft soil, it possible occur a differential settlement at the surface of the embankment. BS 8006 states that a plane of equal settlement exists at an embankment height of 1.4 (*s*-a) from the top of the piles caps in which ***s*** is spacing of pile caps and **a** is the width of the pile caps. Terzaghi (1943) carried out laboratory tests and found that the plane of equal settlements exists at 1.5 – 2.5 times the width of the void. As can be seen in Fig. 2-32 that δ_s is the settlement of subsoil at the midpoint between piles. δ_{ec} is the settlement at the surface of the embankment at the centerline above the pile cap. δ_{em} is the settlement at the surface of the embankment at the midpoint between the pile caps.

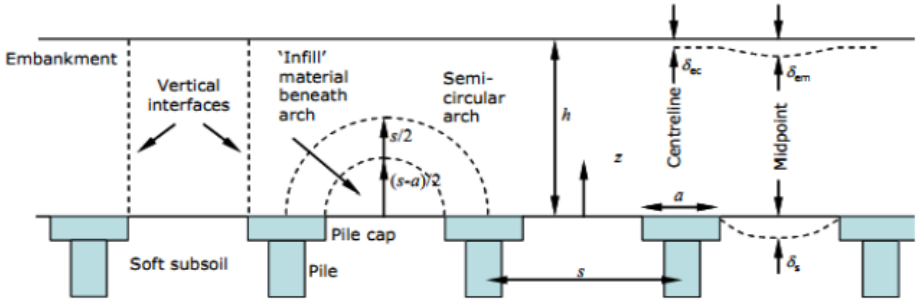

Fig. 2-32 Piled embankments showing arching soil, notations for geometry and settlement (after Zhuang, 2009)

When a height of embankment is lower than the critical height, the differential settlement potentially develops there and vice versa. Table 2-11 below shows the critical height of some design methods.

Table 2-11 Critical height for different design methods

Method	Critical Height, Hc
Terzaghi (1943)	2.5 (*s*-a)
Carlsson (1987)	1.87 (*s*-a)
Hewlett&Randolph (1988)	1.4 (*s*-a)
BS8006 (1995)	1.4 (*s*-a)
Horgan & Sarby (2000)	1.54 to 1.92 (*s*-a)
Kempfert et al. (2004)	s_g / 2

2.5.10.2. Settlement on the Bottom of Embankment

Soft clay and other compressible soils have a tendency to settle under heavy loading. There are some techniques of soil improvement used to prevent these settlements. Piles, stone columns, vibro-concrete columns and deep mixed columns are some of the commonly used techniques.

Poulos (2005) reviewed the evolution of settlement analysis for pile groups and the transition from research to practice over the past 30 years. Many methods exist for estimating the settlement of piled foundation, ranging from empirical methods, through simple hand calculation methods, to sophisticated numerical finite element and finite difference analysis. There are a number of approaches commonly adopted for the estimation of the settlement of pile groups:

- Methods which employ the concept of interaction factors and principle of superposition;
- Methods which involve the modification of a single pile load-settlement curve, to take account of group interaction effects;
- The settlement ratio method, in which the settlement of a single pile at the average load level is multiplied by a groups settlement ratio (R_s), which reflects the effects of group interaction;
- The equivalent raft method, in which the pile groups is represented by an equivalent raft acting at some characteristic depth along the piles;
- The equivalent pier method, in which the pile group is represented by a pier containing the piles and the soil between them. The pier is treated as a single pile of equivalent stiffness in order to compute the average settlement of the group;
- Numerical methods such as the finite element method (FEM) and finite difference method (FDM).

2.5.10.2.1. Interaction Factor Method

The interaction factor, denoted by α_{ij}, is defined as the additional displacement at the top of pile *i* due to a loaded adjacent pile *j*, divided by the settlement of pile *j* under its own load, and its application based on the theory of elasticity. Poulos (1994) had already successfully employed the interaction factor for predicting the response characteristics of pile groups or piled raft foundation. In this method as shown in Fig. 2-33, the settlement w_i of a pile *i* within a group of *n* piles is given as follows:

$$w_i = \Sigma P_{av} \,.\, S_1 \,.\, \alpha_{ij} \qquad (2\text{-}83)$$

where: P_{av} = average load on a pile within group; S_1 = settlement of a single pile under unit load; α_{ij} = interaction factor for pile *i* due to any other pile *j* within the group, corresponding to the spacing s_{ij} between pile *i* and *j*.

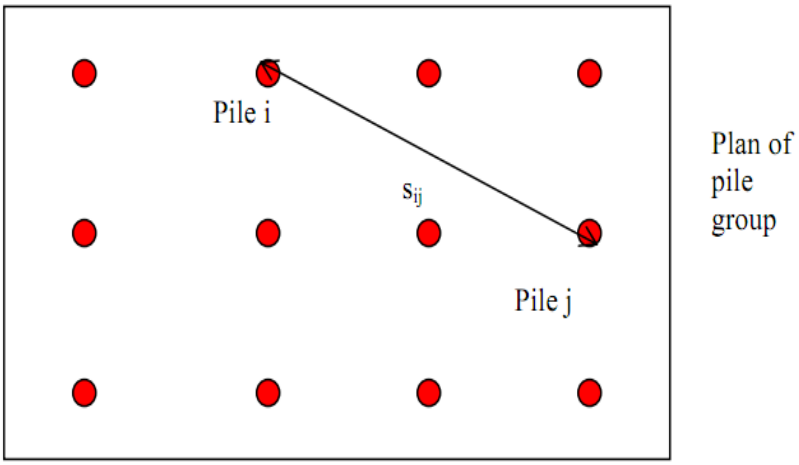

Fig. 2-33 Superposition via the interaction factor method (after Poulos and Davis, 1980)

Simplified or closed-form expressions for the interaction factors have been developed, thus enabling a simpler computer analysis. Mandolini and Viggiani (1997) have developed the following expressions for the interaction factor, in one of the following forms:

$$\alpha = A\,(\,s\,/\,\mathrm{d}\,)^B \qquad (2\text{-}84)$$

or $$\alpha = C + D\,ln\,(\,s\,/\,\mathrm{d}\,) \qquad (2\text{-}85)$$

where: *A,B,C,D* = fitting parameters
s/d = ratio of pile spacing to pile cap diameter

The value of *A* ranged between 0.57 and 0.98, while the range of *B* was -0.60 to -1.20. The value of C is equal to 1.0 and D = -0.26.

The original interaction factors published by Poulos (1968) were based on the assumption that the soil was a homogenous elastic medium, having a constant modulus with depth. This was clearly a great simplification of reality, and in subsequent years, some significant improvements and extensions have been made including non-uniform soil modulus, influence of bearing stratum and interaction between two dissimilar piles.

Influence of non-homogeneity (see Fig. 2-34) compares relationship between interaction factor and *s*/d for three cases, namely a homogeneous soil layer with a constant modulus E_s with depth, a soil where the surface modulus (E_{s0}) is 3 times that at the base (E_{sL}), and a non-homogeneous soil layer whose modulus varies linearly with depth from zero at the surface (a Gibson soil) but which has the same average modulus as the uniform layer. Influence of stiffness of the bearing stratum against interaction factor which is effect of the stiffness of bearing stratum E_{s2} as a multiple of the overlying soil E_{s1}.

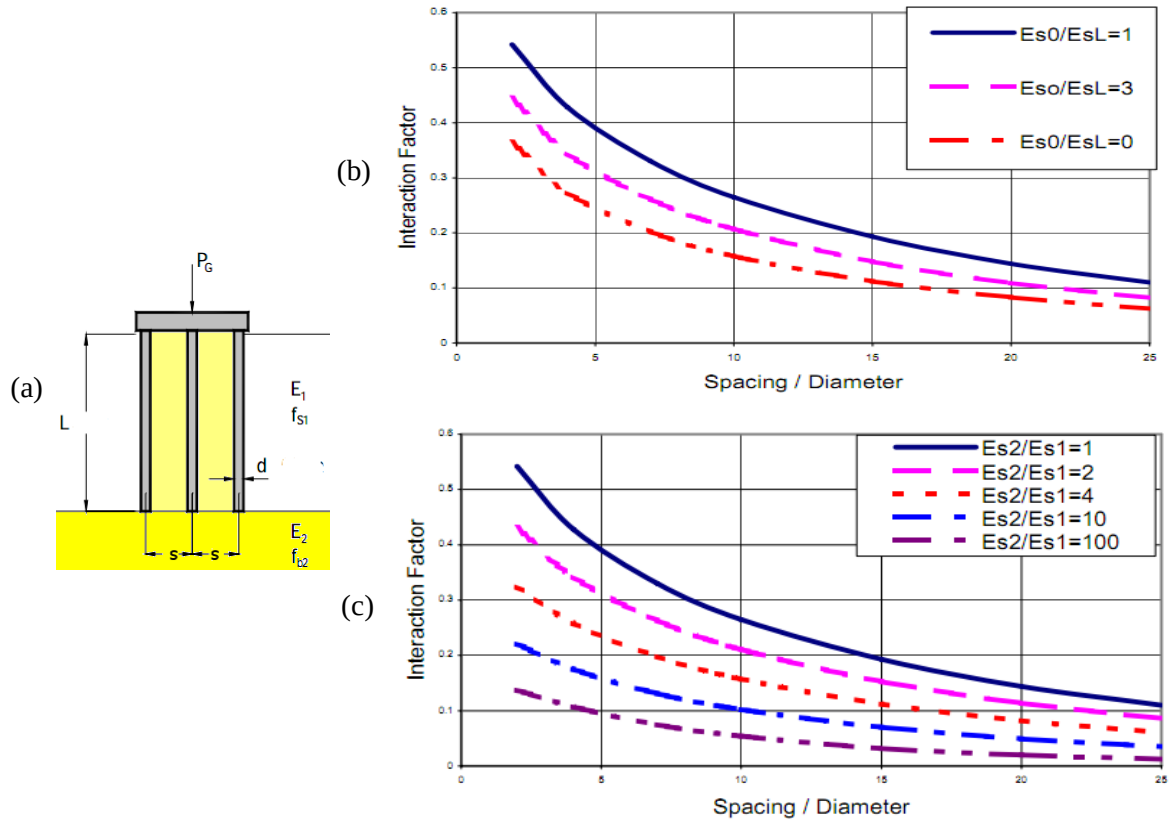

Fig. 2-34 Interaction factor, (a) Simplified case (b) Influence factor for non-homogeneity for soil layer (c) Influence factor for bearing stratum (after Poulos,1968)

2.5.10.2.2. Equivalent Raft Method

The equivalent raft method has been used extensively for estimating pile group settlements. It relies on the replacement of the pile group by raft foundation of some equivalent dimensions, acting at some representative depth below the surface. There are many variants of this method, but the one suggested by Tomlinson (1986) appears to be a convenient and useful approach. In this approach, the representative depth varies from 2*L*/3 to *L*, depending on the assessed founding conditions; the former applies to floating pile groups, while the latter value is for end-bearing groups. The load is spread at an angle which varies from 1 in 4 for friction piles, to zero for end bearing groups. Once the equivalent raft has been established, the settlement can be computed from normal shallow foundation analysis.

Poulos (1993) has examined the applicability of the equivalent raft method to friction and end-bearing pile group and concluded that this method gives a reasonably accurate prediction for pile group containing more than about 16 piles with spacing of 3 times of pile diameter. This method should be limited to cases in which the pile cross-sections exceed about 10% of the plan area of the group (van Impe, 1991).

2.5.10.2.3. Equivalent Pier Method

The pile group is replaced by a pier of similar length to the piles in the group, and with an equivalent diameter, d_e, estimated as follows (Poulos, 1993):

$$d_e = (1.13 \text{ to } 1.27) \, . \, A_G^{0.5} \qquad (2\text{-}86)$$

where: A_G = plan area of pile group including the soil between the piles

The lower value is more relevant to predominantly bearing piles, while the larger one is more applicable to predominantly friction or floating piles. Randolph (1994) has related the accuracy of equivalent pier method to the aspect ratio R of the group, where:

$$R = (n s / L)^{0.5} \quad (2\text{-}87)$$

where: n = number of piles, s = pile spacing, L = pile length. The equivalent pier method tends to overestimate stiffness for values of R less than about 3, for values of R of 1 or more provide that the pile spacing is not greater than 5 diameters.

2.5.10.2.4. Piled Raft Method

Piled raft foundations are often used to improve the bearing capacity or to reduce the differential deflection in the foundation structure. For preliminary estimates of piled raft behavior, a convenient method of estimating the load-settlement behavior has been developed by combining the approaches described by Poulos and Davis (1980) and Randolph (1994). The method is described as the Poulos-Davis-Randolph (PDR) method. There are two main steps: firstly, it is the estimation of the ultimate load capacity and secondly, it is the estimation of the load-settlement behavior via a simple tri-linear relationship.

2.5.10.2.5. Japanese Method

Deep mixing method is also applied in Japan to improve soft clay and organic soils (Takenaka, 1995; Bergado et al., 1999; Porbaha, 2000; CDIT, 2002). Because the deep mix elements are stiffer than the surrounding soft soil, the stress concentration ratio develops there. It is different with the dry deep mixing method which the stress concentration ratio may be on the order of 4 to 6 (Kaiqiu, 2000), whereas the wet deep mixing method for soil-cement is typically to be about 10 to 20 (CDIT, 2002).

The consolidation settlement of soil stabilized by deep mixed columns is determined the following equation (CDM, 1985):

$$\Delta d_{stab} = \beta \, . \, \Delta d \quad (2\text{-}88)$$

where: Δd_{stab} = consolidation settlement of stabilized ground, Δd = consolidation settlement of unstabilized ground, and β = settlement reduction ratio.

The settlement reduction ratio is identically as stress reduction ratio, *SRR*. The stress concentration ratio, n, and area replacement ratio, a_s, are used to determine the settlement reduction ratio as follows:

$$\beta = SRR = \sigma_{soil} / \sigma = 1 / [1 + (n-1) a_s] \quad (2\text{-}89)$$

The consolidation settlement of the unstabilized ground, Δd, is calculated as follows:

$$\Delta d = m_v \, . \, \sigma \, . \, D \quad (2\text{-}90)$$

where: m_v = coefficient of compressibility of untreated soft clay, D = thickness of stabilized clay layer (or sub-layer)

For shallow soft soils we have a possibility to build the piled embankment using end-bearing piles which bottom of columns is located on the hard stratum, but for deep soft soil it is not so effective and economic if we construct this kind of structure. Therefore, the floating piles are the best choice to overcome this problem. Though, settlement on soft soil is too high because of high compressibility and creep is also the main problem.

2.5.10.2.6. Public Works Research Center Method

Public Works Research Center method (2000) as cited Han (2003) has come up with a design method for reinforced embankments on deep mixed column.

Settlement of the columns is given as:

$$S_c = \sigma_c \, . \, L \, / \, E_c \tag{2-91}$$

where: S_c = settlement of the columns
σ_c = stress on the columns
L = length of the columns
E_c = modulus deformation of the columns

Modulus deformation has a correlation with unconfined compression strength (q_u) of the column depending on a kind of column.

$$E_c = 100 \, q_u \tag{2-92}$$

The settlement of the untreated soil is given by:

$$S_s = S_o . \, \sigma_s \, / \, p \tag{2-93}$$

where: S_s = settlement of untreated soil subjected to reduced pressure, σ_s
S_o = settlement of untreated soil subjected to the actual load of embankment, p
σ_s = reduced pressure on the untreated soil due to embankment
p = total applied pressure of the embankment

The differential settlement illustrated in Fig. 2-35 between the soil and the columns in the absence of geosynthetics reinforcement is given by:

$$\Delta S = S_s - S_c \tag{2-94}$$

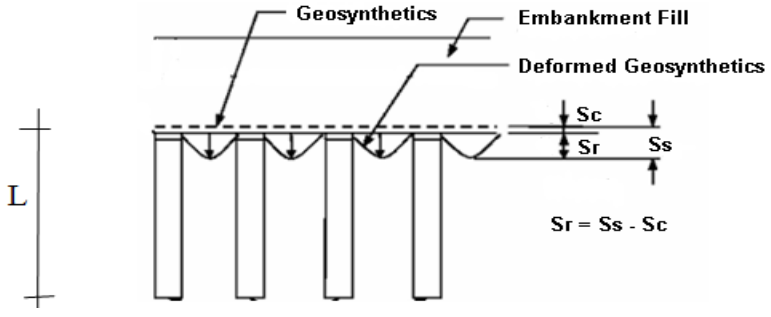

Fig. 2-35 Settlement on the end-bearing piles (after PWRC method, 2000)

When there is an inclusion of geosynthetics layer, the differential settlement can be given into account an influence factor due to the inclusion of the reinforcement.

$$\Delta S_r = S_s \, / \, [1 + 2 \, \alpha \, (S_s \, / \, p)] \tag{2-95}$$

where: ΔS_r = differential settlement between the columns and the untreated soil
α = influence factor due to the presence of geosynthetics layer

This influence factor is related to the tensile stiffness of geosynthetics reinforcement. The relation between the two factors can be seen in Fig.2-36.

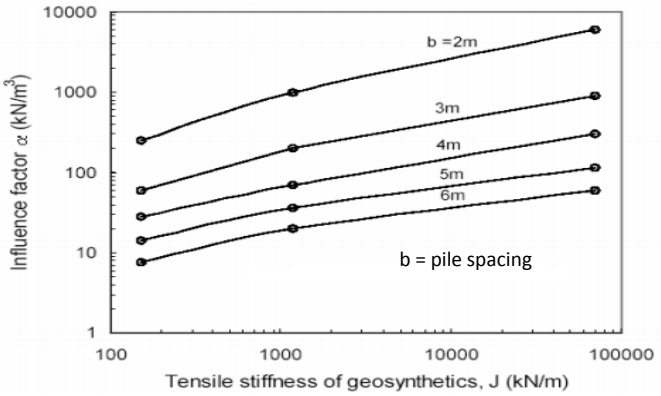

Fig. 2-36 Influence factor (α), (after Han, 2003)

2.5.10.2.7. Scandinavian Method

Lime/cement and cement columns installed by the dry method of deep mixing have been used extensively to support road and railroad embankment in Scandinavia country. In Sweden almost 90% of all columns are installed to increase the stability and reduce the settlement of embankments constructed on soft soils (Holm 1999; Broms 2003). It assumed that the same strain occurs in the columns and the soil at every level (Broms, 1999) is shown in Fig. 2-37 below.

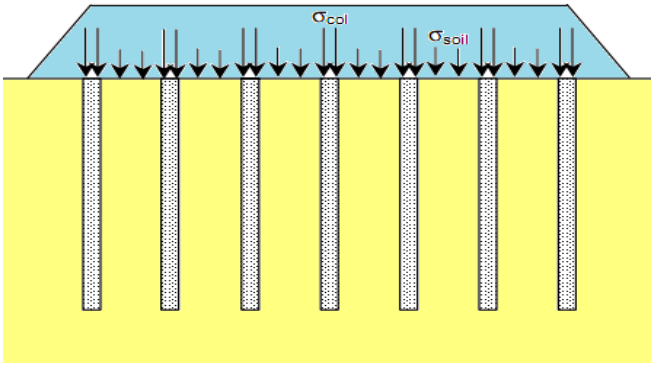

Fig. 2-37 Stress distributions for columns of deep mixed foundation (after Smith,2005)

The stress concentration in the stiffer column must greater than stress in the surrounding soil, and then re-writing Eq. 2-46 for the stress concentration ratio, *n*. and coverage ratio, a_s, from Eq. 2-49.

$$n = \frac{\sigma_{col}}{\sigma_{soil}} \tag{2-96}$$

where: a_s = area replacement ratio or coverage ratio which is defined as:

$$a_s = \frac{area\ of\ column}{total\ tributary\ area} = \frac{A_{col}}{A_{col}+A_{soil}} \tag{2-97}$$

The load applied on embankment is carried by both the column and the soft soil. The average stress applied by embankment, σ, may be expressed as:

$$\sigma = \sigma_{col}\, a_s + \sigma_{soil}\, (1\text{-}a_s) \tag{2-98}$$

The vertical stress is carried by column and the surrounding soil as illustrated in Fig. 2-37 above as follows:

$$\sigma_{soil} = \frac{\sigma}{[1+(n-1)\, a_s]} \tag{2-99}$$

$$\sigma_{col} = \frac{n\, \sigma}{[1+(n-1)\, a_s]} \tag{2-100}$$

Depending on stiffness of column material, for lime/cement and soil-cement columns in Sweden and Finland the stress concentration ratio of five is often used in design purpose (Carlsten and Ekstrom, 1997). Based on large-scale field test performed on soil-cement columns installed by the dry method Kaiqiu (2000) reported that stress concentration ratio ranged from 4.7 to 5.7 under embankment loading.

The load deformation behavior of a dry mixed column is assumed to take place as shown in Fig. 2-38. The load-deformation curve is linear up to long-term strength or creep strength and the slope of the curve is equal to the modulus of elasticity of the column, E_{pile}. Once, the creep strength of the column is reached, additional loads are carried by the soil. The creep strength is less than the column ultimate (or failure) strength, namely 65% to 90% of the ultimate strength (Broms, 1999).

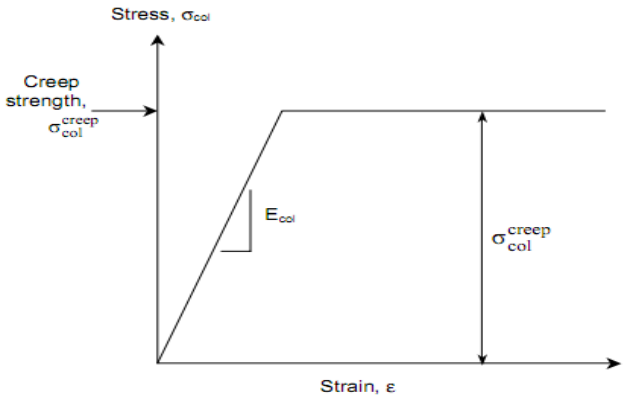

Fig. 2-38 Stress-strain relationship in dry mixed column (after Broms, 1999)

The column ultimate strength can be empirically determined using equation:

$$\sigma_{col}^{ult} = 2\, \tau_{u,col} + 3\sigma_h' \tag{2-101}$$

Where: $\tau_{u,col}$ = the undrained shear strength of the columns and σ_h' = the effective horizontal pressure on the columns. For the Scandinavian applications, the undrained shear strength is limited to 22 psi or 150 kPa (EuroSoilStab, 2002).

The compression of a volume of stabilized soil column is evaluated by considering two load cases. The first one is when the creep strength of the columns is not reached and the second case is when the creep strength of columns is reached. In the first case, the compression, S_1, and corresponding vertical strain, ε_v, within the stabilized area are calculated based on the following equations:

$$S_1 = \sum \frac{\sigma_{col}}{E_{col}} . d_i = \sum \frac{\sigma_{soil}}{M_{soil}} d_i = \sum \varepsilon_v d_i \tag{2-102}$$

$$\varepsilon_V = \frac{\sigma}{a_s E_{col} + (1-a_s) M_{soil}} \tag{2-103}$$

Where: S_1 = the compression of the stabilized volume for case 1, d_i = stratum (or sub-layer) thickness within the reinforced depth, M_{soil} = oedometer compression modulus of surrounding soil. From both equations above that settlement of the stabilized volume decreases with increasing area replacement ratio and with increasing the column stiffness.

In the second case when the creep limit of the columns is reached. The columns cannot take load anymore. Therefore, subsequent loads carried by the unstabilized soil between columns govern the settlement. Compression of the stabilized volume is calculated using the following equation:

$$S_2 = \sum \frac{\sigma - \sigma_{creep}^{col} \cdot a_s}{1 - a_s} \cdot \frac{d_i}{M_{soil}} \qquad (2\text{-}104)$$

where: S_2 = the compression of stabilized volume for case 2, σ_{creep}^{col} = the creep strength

Broms (2003) suggests that the observed settlement can often be larger than the calculated settlement. The differences between estimated and observed settlements generally increase with increasing column lengths.

For partly penetrating columns or floating piles, the compression of a stratum of thickness d* below the reinforced depth can be estimated for both cases. For case 1, the applied load is assumed to be transferred directly down through the reinforced depth, d_i, and then it is distributed through the underlying layer, d*, with angle of 1H:2V as shown in Fig. 2-39. The compression of the underlying stratum, d*, and the reinforced depth, d_i, are the total settlement.

For case 2 when the column creep strength is reached, the load be carried by columns is transferred directly down through the reinforced depth (d_i) and then it is distributed through the underlying layer (d*) at angle of 1H:2V. Meanwhile, the applied load that exceeds the creep strength of the columns is applied to the ground surface and distributed through the underlying soil at angle of 1H: 2V.

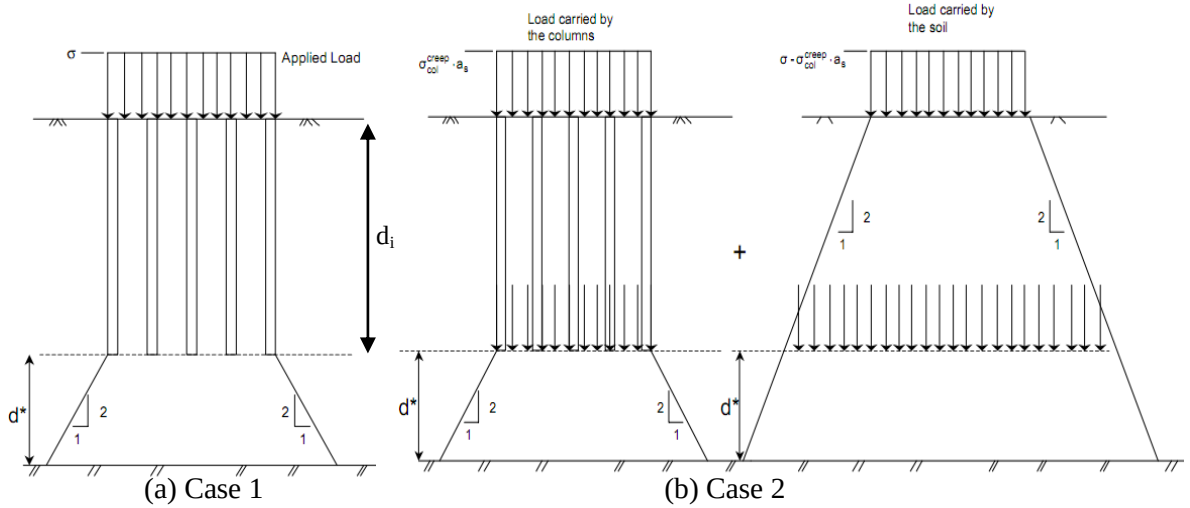

(a) Case 1 (b) Case 2

Fig. 2-39 Stress distributions beneath the stabilized columns for both cases (after Broms, 1999)

For all methods mentioned above, settlement is a procress of water dissipation from soil body in which it consists of lot of fine grained soil. Some methods can be applied to accelerate this process such as vertical drains, pre-loading, vacuum technique, and electro-osmosis. Zhuang

et al. (2006) conducted electro-osmotic consolidation test for small-scale model. They concluded that soil properties like c, ϕ , γ_{max} exhibit increasing after treatment of electro-kinetic geosynthetics (EKG).

2.5.10.3. Relative Settlement Reduction (RSR)

A piled embankment using end-bearing piles is known as an effective method for soft soil improvement. However, the end-bearing piles can be applied only when the soft soil thickness is relatively shallow, e.g. up to 15 m. But, in many regions such as in Scandinavia and some places in Southeast Asia, the soft soil thickness can be very deep up to 30 m or even more. In such case, it is not possible economically to use the end-bearing piles. Effectiveness of embankments on floating piles can be determined using its relative settlement reduction (*RSR*). This terminology is defined as:

$$RSR = \frac{S_0 - S}{S_0} \tag{2-105}$$

Where S_0 is embankment settlement constructed on soft soil without the support of piles and S is the settlement of an embankment supported by piles.

CHAPTER 3

Characterization of Materials and Loading

There are four kinds of material to be characterized regarding the topic research: subsoil, embankment, geosynthetics, and piles. It is important to know well some properties of them. Because stress and strain relationship in material is induced by loading either static or dynamic loading, and the characteristic of loading, including the magnitude and movement of loading on transportation infrastructure is necessary to be understood.

3.1. Characteristic of Soft Soil in Indonesia

3.1.1 Physical Properties

A soil comprises of three basic constituents i.e. solids, liquids and gasses. Solids may be either mineral or organic matter or both with their spaces filled with water and/or air. The soil is saturated when all of pore spaces are filled with water. The purpose of the physical properties testing is to obtain adequate information related to soil behavior. Some parameters to describe the soil are as follows: water content W_n, unit weight γ, Atterberg limits (LL, PL, PI), sieve analysis, degree of saturation S_r, organic content *OC*.

3.1.1.1. Physical Properties of Soft Soil in Java Island

Characteristic of soft soils at some sites in several provinces in Java Island as reported in Development of Guidance for Roadway Construction over Expansive Soil (2003). Evaluation for this soil is aimed to know characteristics and classification of soil as summarized in Table 3-1.

Table 3-1 Characteristics of soft soils in Java island

Parameters	Provinces and Links of the observed roads								
	Central Java				D.I.Y	East Java			W. Java
	Semarang - Purwodadi	Dempet - Godong	Demak-Kudus	Wirosari-Cepu	Yogya-Wates	Ngawi - Caruban	Surabaya -Gresik	Gresik-Lamongan	Jakarta-Cikampek
1. Unit weigth (gr/cm3)	1.63-1.76	1.68-1.75	1.67-1.74	1.75 – 1.86	1.68 – 1.73	1.63-1.89	1.61-1.79	1.73	1.59 – 1.71
2. Clay content (%)	22-43	25-40	24-34	30 - 52	30 -52	30-61	23-45	44	25 - 58
3. Liquid limit (%)	80-110	72-108	83-94	53 -107	53 - 107	72-130	62-90	81	82 -104
4. Plastic Index (%)	52-79	40-74	44-58	24 - 57	24 - 97	39-79	28-45	48	46 - 62
5. Linear shrinkage (%)	18-22	12-26	-	-	18	15-27	-	-	-
6. Water content (%)	32-48	37-53	29-49	24 - 40	27 -32	40-55	38-53	34	34 - 52
7. Passing # 200 (%)	83-98	82-98	95-98	73 - 96	76-96	92-98	89-94	97	92 - 94
8. Classification of soil	CH, clay	CH,clay	CH	CH,Silty clay	CH, clay	CH, silty clay	CH,clay	CH,clay	MH,Silt
9. Mineral of clay	Montmori lonite	Montmori lonite	Montmori lonite	Montmori lonite	Montmori lonite	Montmori lonite, 60 %	Montmori lonite 45 %	Montmori lonite	Montmori lonite, 10 %
10.Colour	Browny grey	Browny grey	Blackish grey	Greyey black	Greyey black	Blackish grey	Blackish grey	Blackish grey	Blackish grey
Location : - Depth (m)	2.0 -.3.0	1.0 -3.0	2.0 -5.0	1.0 - 4.0	2.0 – 5.0	1.0 -.4.0	1.0 -3.0	1.0 -2.0	1.0 - 3.0
- Site (KM)	36-43	13.8	38.8	37.5 – 58.25	23.0 -27.0	5..0 – 19.0	12.8 – 14.45	16.50	25.50 – 69.60

Source: Final Report of Guidance for Roadway Construction over Expansive Soil, 2003

Soft soils are widespread in a lot of locations in Indonesia. In Java island, the soft soils mostly consist of clay and/or silt, whereas in Sumatra and Kalimantan they are not only soft clay but some regions covered by peat soils. Java Island is most dense in population and the

island has many infrastructures particularly roadways, railways and runways constructed over the soft soil.

Chen (1975) uses a single index based on plasticity index to identify expansive soil. For Plasticity Index (PI) values ranging from 20 to 55 are high for swelling level and very high for PI values more than 55. Whilst Seed et al. (1962) use equation Ac = PI / (CF-10) to identify activity level of soil. For value of Ac that more than 1.25 the soil has high level of activity.

3.1.1.2. Physical Properties of Soft Soil in Pontianak

Most of Pontianak soil samples were blackish, blackish grey to dark in colour and had an acidic smell. Organic content (*OC*) of about 10% was found (Priadi, 2008). These are classified as fine grain soils because most of the samples having an average 84% pass through sieve no. 200. Plasticity Index (*PI*) and the liquid limit (*LL*) varied widely from 5 to 35% and 20 to 70% respectively. According to ASTM standard D2487-00 and USCS based on visually observation, organic content and distribution of grain size, these soils are classified as organic soil. Organic clay deposits seem dominantly near the ground surface. Sandy soil layer is founded 15 to 30 m in depth. The water content (W_n) varies widely ranging from 25 to 200%, but decrease with greater depth. Generally, water content of Pontianak soft organic soil was higher than its liquid limit. Furthermore, a cohesive soil with water content higher than the liquid limit is defined as *super soft soil* clay.

Based on soil investigation for the project of Supadio airport runway expansion (2009) will be a complement for data soil in Pontianak. The existing runway 2.250 m long and 30 m wide would be extended 2.600 m long and 45 m wide, respectively. There were 10 sites of taken samples using cone penetrometer test and the standard penetration test. As a comparison and supplement that the testing of physical properties for Pontianak soil taken at a 1.5 m depth has also been done in Geotechnical Laboratory TU Bergakademie Freiberg. Furthermore, physical and mechanical properties of soils as described in Table 3-2.

Table 3-2 Subsoil properties at several zones in Pontianak

Parameters	Unit	Priadi's data	Project data of Supadio's runway	Sample of Pontianak soil	Values in range of all data
		Range of value	Range of value	Range of value	
1. Soil classification	-	Low organic	Low organic	Low organic	Low organic
2. Water content, *W*n	%	58.22-169.98	35 – 91	81.6-109.4	81.6-91
3. Organic content, *OC*	%	10	-	11.88	10-11.9
4. Specific gravity , Gs	-	2.2-2.6	2.36 – 2.70	2.611	2.4-2.6
5. Unit weight, γ (kg/m3)	kN/m3	12.3-16.49	13.9 – 18.5	13.94-14.31	13.9-14.3
6. Liquid Limit, *LL*	%	20-70	17.10 - 62.46	84.52-99.25	62.5
7. Plastic Limit, *PL*	%	17-35	14.62 – 38.44	39.6-50.22	35-39
8. Plasticity Index, *PI*	%	5-35	2.48 – 29.67	34.3-59.6	29.7-35
9. Void ratio, e	%	1.02-3.30	0.88 – 2.65	-	1-2.6
10. Cohesion (UD), c	kN/m2	6-16.5	7.2-19.8	0.38-8.08	7.2-8
11. Friction angle (UD), ϕ	o	1.0-20.3	3.03-13.66	13.61-27.26	13.6-13.7
12. Compression index, *C*c	-	0.16-0.34	0.278-1.663	-	0.28-0.34
13. Coeff. of compressibility	-	-	1.4E-3 to 7E-3	-	1.4E-3 to 7E-3
14. Permeability, k_v	m/day	4.4E-6 to 7.8E-4	-	-	4.4E-6 to 7.8E-4
15. Unconf. comp. strength	kN/m2	-	8.4-65.5	-	8.4-65.5
16. Oedometer modulus	kN/m2	550	-	-	550
17. Young's modulus	kN/m2	650-1166	-	-	650-1166

Based on Chen (1975) approach, for soil in this region with *PI* value average 19.5 can be classified as high for swelling level.

3.1.2. Mechanical Properties

Mechanical properties are a necessary thing when investigating strength and deformation of soil during loading. Shear strength of cohesive soil can be determined by using shear tests and/or triaxial tests in which parameters cohesion, c, and internal friction angle, ϕ, can be measured. Whilst in predicting the rate of settlement for the soil can be carried out by using a consolidation test or oedometer testing in the other to obtain consolidation index, c_c.

3.1.2.1. Direct Shear Strength

Normally, specimens of around 20 mm height and 40 cm^2 cross-sectional circle surface are utilized in the direct shear test, but some problems emerge when doing the kind of test for very soft material. A little adjustment is an important thing in this case based on previous experiences which the height of specimen needs to be higher than in the normal situation. For consolidated drained (CD) shear test, height of the specimen around 30 mm was mounted to overcome the high compressibility of soil in other to avoid friction between upper and lower ribs in the shear box. The consolidated drained shear tests were conducted with normal stresses 50, 75, 100, 150, 200 kN/m^2 respectively and consolidation time was set up for 2 days before running shearing tests.

3.1.2.2. Compression

When soil undergoes a loading, because of their relatively low permeability, their compression is controlled by the rate at which water is squeezed out of the pores. The slope e against log σ' plotted in normally consolidated soil is referred to as the compression index, c_c. The load increment ratio was uniform where the loading was from 25 to 800 kN/m^2. The compression index, c_c, varies widely with the increasing depth, however, the depth does not influence of c_c.

Priadi (2008) characterized the Pontianak soft organic soil compressibility behavior that the top layer (around 10 m deep) is highly compressible ranging from 0.5 to 1.38 with an average value of about 0.8, whereas at below this layer ranging from 0.2 to 0.5 with an average value is about 0.3. Meanwhile, the recompression index, c_s, ranges widely from 0.03 to 0.25. Some of the 1-D Oedometer test results are shown in Fig. 3-1.

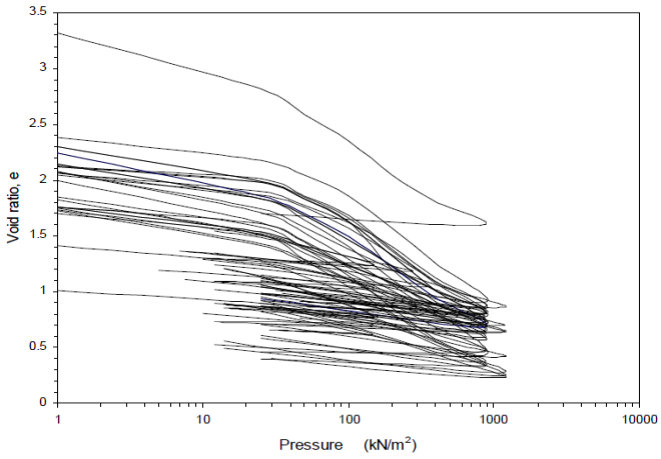

Fig. 3-1 Oedometer test of Pontianak soft organic soil (after Priadi, 2008)

The over consolidated ratio, *OCR*, is defined as the ratio between the pre-consolidation stress and the effective in-situ stress. *OCR* is a state parameter that indicates the amount of over-consolidation of the soil (Brinkgreve, 2001). This value notably reduces with a depth. Pontianak soft organic soils are heavily over consolidated from the ground surface to about 5 m depth due to the wetting and drying cycles during deposition. The over consolidation ratio ranges from 2 to 11 at this layer, whereas *OCR* values range from 1.3 to 2 are found at 5 to 20 m depth.

3.1.3. Bearing Capacity

Bearing capacity for subsoil particularly undrained condition can be expressed by several parameters such as shear strength (s_u), unconfined compressive strength (q_u) and California Bearing Ratio (CBR). The three parameters mentioned above have a correlation with each other. In case soft soil, subsoil is a cohesive material, generally like this, and also undrained condition. Shear strength is approximately value of cohesion because the internal friction angle is very small. Even, it is equal to zero when soil is the unconsolidated undrained condition.

Unconfined compressive strength is nearly twice of shear strength (Braja M. Das, 1995). When a bearing capacity is expressed as CBR, the empirical correlation is that shear strength is 30 times of CBR (Barenberg, 1975).

Bearing capacity of subsoil can be improved by inserting piles. It can be the bored piles and also the driven piles. After inserting piles with a certain depth, bearing capacity of soil in an area that is replaced by the pile can be represented by the pile. This value depends on the cone tip resistance linearly.

When pile is inserted in subsoil to support load over top of pile, estimation from Bustamante and Gianeseli (1982) can be proposed to determine the bearing capacity (q_u) from the cone tip resistance (q_c). In which q_c is the required force to penetrate the cone divided by base area of the cone. The equation is as follows:

$$q_u = K_b . q_c \tag{3-1}$$

where K_b is an empirical bearing capacity factor that varies from 0.15 to 0.60 depending on the soil type and pile installation procedure as depicted in Table 3-3.

Table 3-3 Empirical bearing capacity factor

Soil Type	Bored piles	Driven piles
Clay-silt	0.375	0.60
Sand-gravel	0.15	0.375
Chalk	0.20	0.40

After Bustamante & Gianeseli (1982)

3.2. Embankment Materials

3.2.1. Material Properties

Materials for embankment should have some properties such as durability, fire resistant and compacted ability. Various materials can be used as embankment fills as shown in Table 3-4. However, these materials have to fulfill some requirements if a good result wants to be achieved.

Table 3-4 Various materials for embankments

No.	Materials	Unit weight (kN/m^3)
1	Sand	18-22
2	Cohesive soil	16-19
3	Corduroy	7.0
4	Rubber slag	4.0-6.0
5	Pumice	10.9
6	Dreg saws	< 10.0
7	Peat bales	< 10.0
8	Expanded polystyrene (*EPS*)	0.2-0.4

Source: Indonesian Geotechnical Guidance-4 (2001)

The Indonesian Geotechnical Guidance-4 (2001) gives the design parameters when using material as embankment fill as depicted in Table 3-5.

Table 3-5 Design parameters for embankment material

Parameters	Unit	Geographical Zone	
		A	B
Unit weight, γ	kN/m^3	18	20
Undrained shear strength, S_u	kN/m^2	100	100
Cohesion, c'	kN/m^2	10	5
Internal friction angle, ϕ'	[^{O}]	35	30

Source: Indonesian Geotechnical Guidance-4(2001)

A Java island (vulcanic rocks)

B Sumatra, Kalimantan, Sulawesi. Papua island (sedimentary and metamorphic rocks)

3.2.2 Strength of Material

As illustrated in Table 3-4 above, the higher values for unit weight, γ, internal friction angle, ϕ, and shear strength, s_u, will give a good result regarding with soil arching on embankment. Usually, embankment fill is a cohesionless material or very small cohesion.

In pavement engineering, particularly flexible pavement system, there are some important layers namely surface course, base course and/or subbase course and subgrade. Rosyidi et al. (2004) reported the elastic modulus of pavement materials in situ measurement. These values are in the range 3,000 to 7,200 MPa, 1.000 to 2,400 MPa, 480 to 600 MPa for surface course, base course and subbase course respectively.

The concept of resilient modulus has been used to explain the nonlinear stress-strain characteristics of soils. Generally, regarding with bearing capacity, the strength of pavement materials can be expressed in *CBR* (California Bearing Capacity) or Modulus reslient, M_r. Heukelom and Klomp (1962) reported a correlation between *CBR* value using dynamic compaction and the in situ resilient modulus of soil. It has been extensively used for fine grained soils with a soaked CBR of 10% or less.

$$M_r(psi) = 1500\ CBR \quad (3\text{-}2a)$$

$$M_r(MPa) = 10\ CBR \quad (3\text{-}2b)$$

Webb et al. (1986) have reported a number test of cohesionless soils in repeated load triaxial test following the AASHTO procedure as equations follows:

$$M_r(psi) = 3116\ CBR^{0.4779707} \quad (3\text{-}3a)$$

$$M_r(MPa) = 21.485\ CBR^{0.4779707} \quad (3\text{-}3b)$$

Sasongko (1996) also reported a correlation between *CBR* and Mr using repeated load triaxial test in laboratory as shown equations follows:

$$M_r(MPa) = 10\ CBR\ (at\ CBR\ of\ 6.5\%) \quad (3\text{-}4a)$$

$$M_r(MPa) = 4\ CBR\ (at\ CBR\ of\ 28\%) \quad (3\text{-}4b)$$

$$M_r(MPa) = 4\ CBR\ (at\ CBR\ of\ 45\%) \quad (3\text{-}4c)$$

NCHRP (2004) provided a correlation between *CBR* and Mr for a number of cohesionless soils in repeated load triaxial test following the AASHTO procedure. A typical equation for medium clay sand is shown equation (3-5).

$$M_r(psi) = 2{,}555\ CBR^{0.64} \quad (3\text{-}5a)$$

$$M_r(MPa) = 17.60\ CBR^{0.64} \quad (3\text{-}5b)$$

Several constitutive models have been proposed by many researchers for modeling resilient moduli of soils and aggregates. Dunlap (1963) suggested the following relationship for presenting resilient modulus:

$$M_r = k_1 \left(\frac{\sigma_3}{P_a}\right) k_2 \quad (3\text{-}6)$$

where k_1, k_2 = regression coefficients obtained from regression analysis
P_a = reference pressure (atmospheric pressure)
σ_3 = confining stress

Seed et al. (1967) suggested a relation where resilient modulus is a function of bulk stress (θ), also known as the *K–θ* model. This model, generally adopted for granular soils, uses θ as the main attribute in the model.

$$M_r = k_1 \left(\frac{\theta}{P_a}\right)^{k_2} \quad (3\text{-}7)$$

where θ = bulk stress ($\sigma_1 + \sigma_2 + \sigma_3$)

The main drawback of this model is that it does not account for shear stresses and shear strains developed during loading. Moossazadeh and Witczak (1981) proposed a relation known as the deviatoric stress model recommended for cohesive soil, known as *K*-σ_d model.

$$M_r = k_1 \left(\frac{\sigma_d}{P_a}\right)^{k_2} \quad (3\text{-}8)$$

where σ_d = deviator stress (σ_1 - σ_3)

May and Witczak (1981) proposed a model to describe the non-linear behavior revealed in the repeated load triaxial test. This model considers the effects of shear stress, confining stress and deviatoric stress with the model formulated in terms of bulk and deviatoric stress.

$$M_r = k_1 P_a \left(\frac{\theta}{P_a}\right)^{k_2} \left(\frac{\sigma_d}{P_a}\right)^{k_3} \quad (3\text{-}9)$$

Uzan (1992) introduced the octahedral shear stress in place of deviator stress in equation (3-9), which provided a better explanation for the stress state of the material, in which the

normal and shear stress change during loading. The proposed model is known as the k_1- k_3 model. The universality of this model stems from its ability to conceptually represent all types of soils from pure cohesive soils to non-cohesive soils.

$$M_r = k_1 P_a \left(\frac{\theta}{P_a}\right)^{k_2} \left(\frac{\tau_{oct}}{P_a}\right)^{k_3} \quad (3\text{-}10)$$

where $\tau_{oct} = \frac{1}{3}[(\sigma_1 - \sigma_2)^2 + (\sigma_1 - \sigma_2)^2 + (\sigma_1 - \sigma_2)^2]^{1/2}$

The coefficients k_1, k_2, and k_3 are constants, depending on the state and quality of unbound granular materials. Since coefficient k_1 is proportional to Young's modulus, it should always be positive as M_r can never be negative. The coefficient k_2 should be positive, because increasing the volumetric stress produces stiffening or hardening of the material, yielding higher modulus. The coefficient k_3 should be negative because an increase in the shear stress softens the material, thereby yielding lower modulus. If nonlinear property coefficients k_2 and k_3 are set to zero, then the model can be simplified as linear elastic. If k_3 is zero, the behavior could be non-linear hardening and if k_2 is zero, the behavior is non-linear softening.

3.2.3. Maximum Height of Embankment

Stability for maximum or critical height of embankment for road according Roadex III (2008) without ground treatment can be calculated using equation (3-11).

$$H_c = \frac{4C_u}{\gamma} \quad (3\text{-}11)$$

where γ is unit weight of embankment fill and c_u is the undrained shear strength of subsoil beneath embankments.

3.2.4. Dynamic Properties

Shear modulus, damping ratio and shear wave velocity profiles are an important input parameter in site response analysis. Jafari, M.K. et al. (2002), based on field geoseismic investigation data for fine grained soil in Tehran, present new correlation for Shear-wave (V_s) and Number of blows (N) from Standard Penetration Test (SPT). Some researchers also give some equations for the correlation between V_s and N.

Shear wave velocity can be obtained directly from field investigation or laboratory testing of soil samples of the studied area, but it is not always economical solution. However, when the direct measurement of shear wave velocity for soil layers is not available, the existing or developed correlations between N values of SPT and the shear wave velocity could be used. Some researchers have carried out some correlation between the shear wave velocity and number of blows from Standard Penetration Test for some kinds of material for both cohesion and cohesionless material as shown in Table 3-6.

The behaviour of soil under cyclic loading is non-linear and dependent on some factors including soil type, confining pressure, number of loading cycles and amplitude of loading. Non linear hysteretic soil behaviour is commonly characterized by a viscous damping and equivalent shear modulus (Seed and Idriss, 1970; Hardin and Drenevich, 1972). Definition of damping is a measure of energy dissipation. It increases with increasing magnitude of cyclic shear strain, whereas shear modulus decrease with increasing magnitude of cyclic shear strain. It is also known that dynamic properties of soil are influenced by the plasticity index, void ratio, relative density and number of cycles (Cabalar and Cevik, 2008).

Table 3-6 Correlation between V_s and N

Author(s)	Soil type	Shear wave velocity, V_s (meter/second)
Kanai, et al. (1966)	All	$V_s = 19\ N^{0.6}$
Shibata (1970)	Sand	$V_s = 32\ N^{0.5}$
Ohba & Toriuma (1970)	Alluvial	$V_s = 85\ N^{0.31}$
Ohta, et al. (1972)	Sand	$V_s = 87\ N^{0.36}$
Ohsaki & Iwasaki (1973)	All Cohesionless	$V_s = 82\ N^{0.39}$ $V_s = 59\ N^{0.47}$
Imai & Yoshimura (1975) Imai, et al. (1975) Imai (1977) Imai & Tonouchi (1982) Imai & Yoshimura (1990)	All All All All All	$V_s = 92\ N^{0.329}$ $V_s = 90\ N^{0.341}$ $V_s = 91\ N^{0.337}$ $V_s = 97\ N^{0.314}$ $V_s = 76\ N^{0.33}$
Ohta & Goto (1978)	All Sands Gravels	$V_s = 85\ N^{0.348}$ $V_s = 88\ N^{0.34}$ $V_s = 94\ N^{0.34}$
JRA (1980)	Clays Sand	$V_s = 100\ N^{0.333}$ $V_s = 80\ N^{0.333}$
Seed & Idriss (1981) Seed, et al. (1983)	All Sands	$V_s = 61\ N^{0.5}$ $V_s = 56\ N^{0.5}$
Sykora & Stokoe (1983)	Granular	$V_s = 100\ N^{0.29}$
Okamota, et al. (1989)	Dilluvial sands	$V_s = 125\ N^{0.3}$
Lee (1990)	Sands Clay Silts	$V_s = 57\ N^{0.49}$ $V_s = 114\ N^{0.31}$ $V_s = 106\ N^{0.32}$
Yokota, et al. (1991)	All	$V_s = 121\ N^{0.27}$
Jafary, et al. (1997)	All Clayey soils Silty soils Clayey & Silty	$V_s = 22\ N^{0.85}$ $V_s = 27\ N^{0.73}$ $V_s = 22\ N^{0.77}$ $V_s = 19\ N^{0.85}$

Source: Jafary et al., (2002)

Once shear wave velocity is determined, and then shear modulus of material, G, is obtained using equation $G=\rho .V_s^{\ 2}$, which ρ is the density of soil.

Shear modulus of air dry clean sands at a certain level of shear strain, γ, can be represented approximately by the following empirical equation irrespectively of kinds of sands.

$$(\gamma = 10^{-6}) \qquad G = 900\frac{(2.17-e)^2}{1+e}p^{0.38} \tag{3-12}$$

$$(\gamma = 10^{-5}) \qquad G = 850\frac{(2.17-e)^2}{1+e}\mathrm{p}^{0.44} \tag{3-13}$$

$$(\gamma = 10^{-4}) \qquad G = 700\frac{(2.17-e)^2}{1+e}p^{0.50} \tag{3-14}$$

Where G is shear modulus in kg/cm^2, p is mean principle stress in kg/cm^2 and e is the void ratio. Eq. 3-5 is identical to the empirical equation for round Ottawa-sand proposed by Hardin, et al. (1972).

All tests demonstrated the well known dependence of G_{max} on effective confining pressure σ'_o and density expressed in terms of the void ratio e. In other to an analytical expression for the $G_{max} = G_{max}(\sigma'_o)$ relationship, the general equation suggested by Hardin (1972) is adopted.

$$G_{max} = \frac{S}{0.3+0.7\,e^2} p_a^{1-n} (\sigma_o')^n \tag{3-15}$$

Where: S is a stiffness coefficient. The experimental results are closely approximated by setting S= 420 and n= 0.6. It should be noticed that the value of the exponent n is higher than widely used for cohesive and cohesiveless soils which ranges between 0.4 and 0.5. The variation of shear modulus with shear strain amplitude as expressed in the following equation.

$$G = \frac{G_{max}}{1+200\,\gamma} \tag{3-16}$$

Damping ratio D was found to be essentially independent on confining pressure and density. An average value D_{min}=2% was determined from all tests. The increase of damping with shear strain amplitude γ may be approximately expressed by:

$$\frac{D}{D_{min}} = \frac{A}{1+\alpha/\gamma} \tag{3-17}$$

with A = 6.2 and α = 6.5.10^{-4}.

The soil starts to exhibit hysteretic and non-linear behaviour in the shear strain range between 10^{-6} and 10^{-3}, where the secant stiffness decreases with the increasing of the strain level. Various authors have suggested several equations to connect the damping ratio and the shear modulus when both are functions of the shear strain. Hardin and Drnevich (1972) derived the simple relationship equation.

$$D = D_{\max}\left(1 - \frac{G}{G_o}\right) \tag{3-18}$$

where: G is the secant modulus and G_o is the initial shear modulus.

Park and Stewart (2001) have proposed equations for sandy soils and clayey soil respectively.

For sandy soils $$D = 32.85\left[0.54\left(\frac{G}{G_o}\right)^2 - 1.53\frac{G}{G_o} + 1\right] \tag{3-19}$$

For clayey soils $$D = 17.83\left[0.56\left(\frac{G}{G_o}\right)^2 - 1.39\frac{G}{G_o} + 1\right] \tag{3-20}$$

3.3. Geosynthetics

3.3.1. Material Properties

The geosynthetics terminology may be based on the subdivision by PrEN ISO 10318. According to this standard "*Geosynthetics*" is a generic term describing a product at least one of whose components is made from a synthetic or natural polymer, in the form of a sheet, a strip or a three dimensional structure, used in contact with soil and/or other materials in geotechnical and civil engineering applications. As depicted in Fig. 3-2 that geosynthetics can be differentiated into permeable and impermeable products.

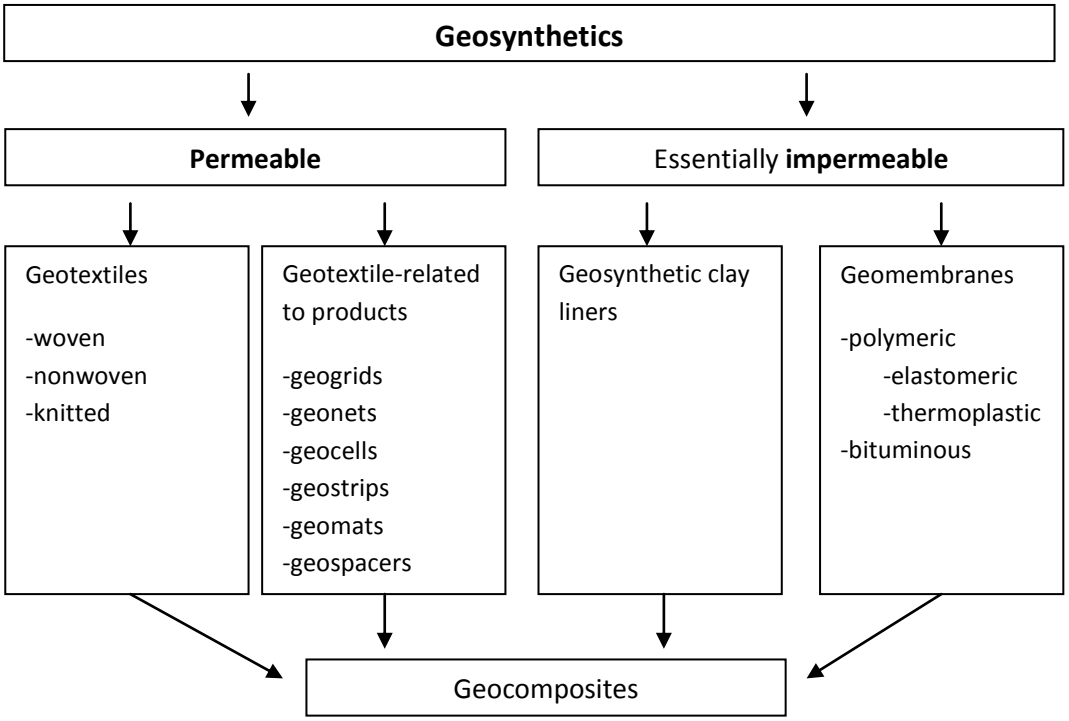

Fig. 3-2 Geosynthetics subdivision (after PrEN ISO 10318)

The use of a geosynthetics in pavement system reinforcement is to aid in support of the traffic load. Traffic loads may be vehicular loads experienced over the life of the pavement. B*ase (or subbase) reinforcement* is a treatment using of a geosynthetics as a tensile element at the bottom of base (or subbase) or within a base course and is designed to address the pavement distress mode of pavement surface deformation or rutting and asphalt fatigue cracking.Whilst *subgrade restraint* is the use of geosynthetics at the subgrade/subbase or subgrade/base interface to increase the support of construction over a weak or low strength subgrade (Barenberg, 1980; Steward et al., 1977; Giroud and Noiray, 1982; Holz et al., 1987).

The following benefits of using geosynthetics in roadways are identified (TenCate Mirafi, 2010):

1. Reducing the intensity of stress on subgrade (function: separation).
2. Preventing subgrade fines from pumping into the base (function: filtration).
3. Preventing contamination of the base materials allowing more open graded, free-draining aggregates to be considered in the design (function : filtration).
4. Reducing the depth of excavation required for removal of unsuitable subgrade materials (function: separation and reinforcement).
5. Reducing the thickness of aggregate required to stabilize the subgrade (function: separation and reinforcement).
6. Minimizing disturbance of the subgrade during construction (function separation and reinforcement).
7. Assisting the increase in subgrade strength over time (function: filtration).
8. Minimizing the differential settlement of roadway, which helps maintain pavement integrity and uniformity (function: reinforcement).
9. Minimizing maintenance and extending the life of the pavement (function: all).

Others important findings from laboratory and/or field studies include the following:

1. An optimum benefits when the geosynthetics was placed at the bottom of a 200-300 mm thick base layer.
2. For thicker base sections, the most beneficial reinforcement location appeared to be in the middle of the base, where geogrids were found to perform best.
3. For thin bases (less than 200 mm), lack of separation was noted as a potential problem for geogrids. Geogrid-geotextile composites tend to perform better for thin bases, especially where subgrade strengths were below a CBR of 3%.
4. Reinforcement benefits were observed with subgrade strengths up to a CBR of 8%.

Benefits using geosynthetics as reinforcement can be defined by *TBR* (*traffic benefit ratio*) and *BCR* (*Base course reduction*) as shown in Table 3-7. The *TBR* is defined as the ratio of number of cycles necessary to reach the same rut depth for a test section containing reinforcement to unreinforced section with the same section thickness and subgrade properties. Furthermore, *BCR* is expressed as a percentage savings of the unreinforced base course thickness.

Table 3-7 TBR and BCR resulted from laboratory and field test

Materials	TBR	BCR
Geotextiles: Range Typical value	 1 – 220 1.5 – 10	 22 – 33 %
Geogrids: Range Typical value	 0.8 – 670 1.5 – 70	 30 – 50 %

After TenCate Mirafi, 2010

Besides the ratio coefficients (*TBR*, *BCR*), the following properties are considered to influence performance : tensile strength at 1%, 2% and 5% strain, coefficients of pullout and direct shear, aperture size (grids) and percent open area (geotextiles) and stiffness properties including the flexural rigidity and aperture stability. For subgrade restraint applications, the properties of tensile strength at 2% and 5% strain are primarily related to geosynthetics performance.

3.3.2. Position of Geosynthetisc in Pavement Design Practice

There are three general applications for the use of geosynthetisc reinforcement in pavements. Therefore, the appropriate application with the ultimate objective of maximizing performance as the following guidance for these three distinct applications:

1. Weak Subgrade (CBR <3), For Thin (≤250 mm) Base Sections and Thick (>250 mm) Base Sections.

When a weak subgrade exists, woven geotextile should be placed at the surface interface. In addition, if the required base course is greater than 250 mm (10 in), a second layer of reinforcement, biaxial geogrid, should be placed in the middle of the base course section.

2. Firm Subgrade (CBR >3), For Thin (≤250 mm) Base Sections and Thick (>250 mm) Base Sections.

For a firm subgrade and relatively thin base course section is designed biaxial geogrid at the subgrade interface. While geogrid can be placed in the middle of the base course when firm subgrade and relatively thick base course section is designed.

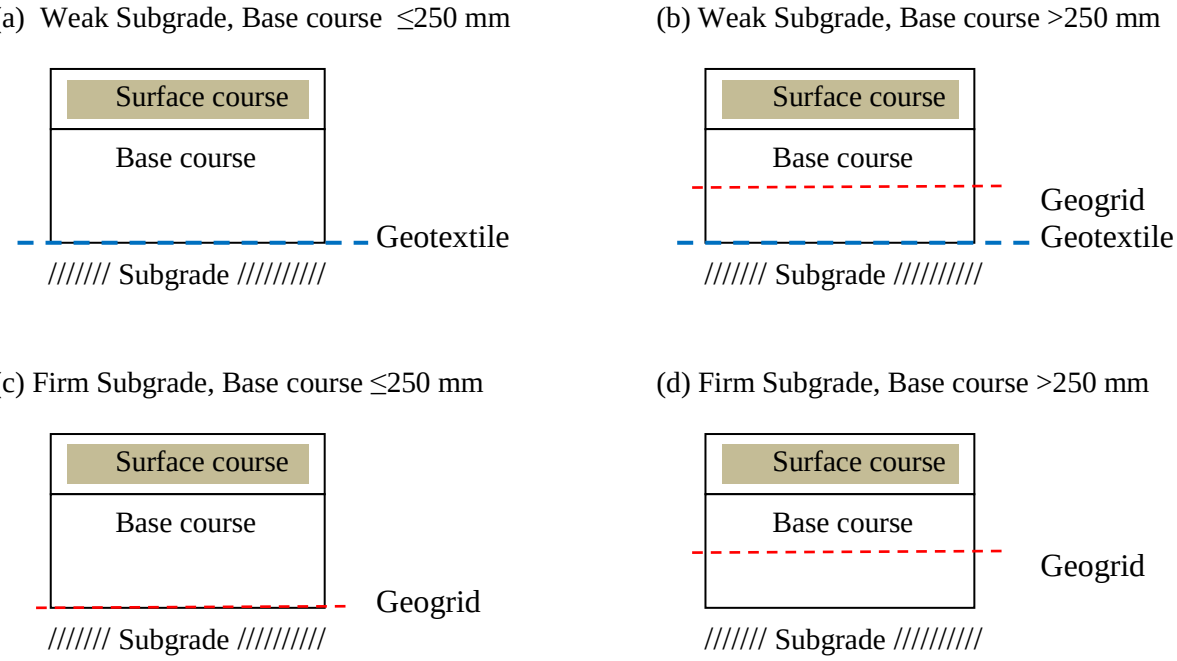

Fig. 3-3 Position of geosynthetics in pavement design practice (after Mirafi, 2010)

3.3.3. Tensile Strength of Geosynthetics

Tensile strength of geosynthetics depends on raw material of geosynthetic such as aramid or polyamide (PA), polyethylene of high density (PE-HD), polyester (PET), polypropylene (PP) and polyvinyl alcohol (PVA). Range of tensile strength from various raw materials of geosynthetics is shown in Fig. 3-4.

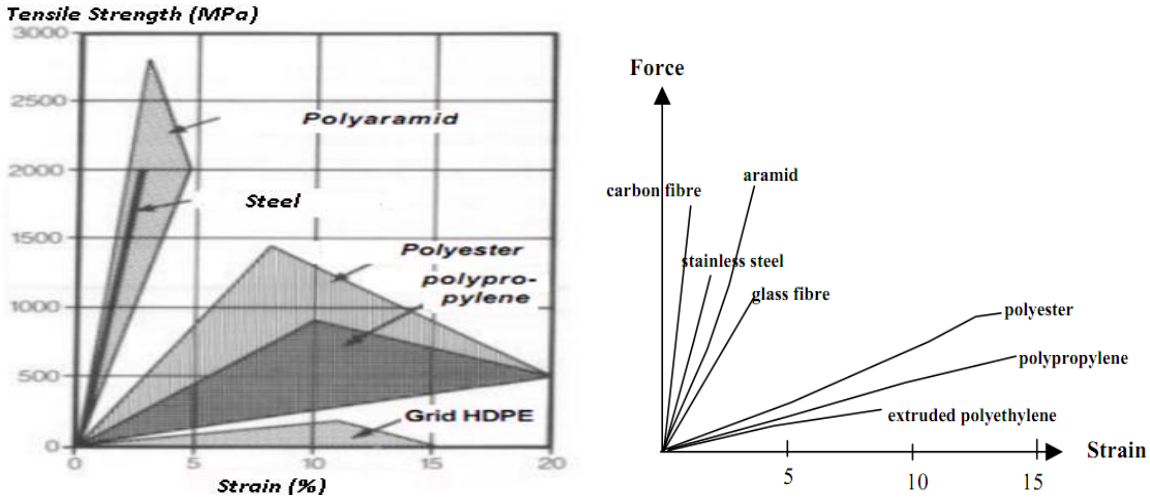

(a) (b)

Fig. 3-4 Typical strain vs. Force behaviour of reinforcement (a) Exxon, 1989 (b) Carlson, 1987

Typical short term strength of geosynthetics is described in Table 3-8 for various raw materials (EBGEO, 2010; Althoff, 2011).

Table 3-8 Tensile strengths of geosynthetics (after EBGEO, 2010)

Raw material	Product types	Typical short term strengths [kN/m]			Typical elongation at failure [%]	
		from	to	max.	from	to
AR (aramides)	Woven geogrids Woven geotextile	40 100	1200 1400	2200 300	2 2	4 4
PE (polyethylene)	Woven geogrids Extruded geogrids Woven geotextile	20 40 30	150 150 200	300 200 400	15 10 15	20 15 20
PET (polyester)	Woven geogrids Bonded geogrids Woven geotextile	20 20 100	800 400 1000	1200 500 1600	8 6 8	15 10 15
PP (polypropylene)	Woven geogrids Bonded geogrids Extruded geogrids Woven geotextile	20 20 20 20	200 200 50 200	500 400 - 600	8 8 8 8	15 15 20 20
PVA (polyvinyl alcohol)	Woven geogrids Woven geotextile	30 30	1000 900	1600 1800	4 4	5 5

When choosing geosynthetics for reinforcement, there are two factors that must be considered well namely internal and external factor. Internal factors such as tensile strength, creep properties, whereas external factors such as kind of embankment fill, endurance against environment (ultra violet, acidic or alkaline matter, micro-organism. In other to cover all conditions, strength of geosynthetics has to be adjusted using some partial factors. According to Nordic guideline (2003) some conversion factors for design purpose are listed in Table 3-9 through Table 3-11.

Table 3-9 Conversion factors of geosynyhetic reinforcements
(after Nordic guideline, 2003)

Conversion parameters	Conversion factor
Creep factor Installation damage Biological and chemical degradation	η_1 η_2 η_3

Table 3-10 Conversion factors η_1 for long-term properties
(after Nordic guideline, 2003)

Conversion parameters	Conversion factor, η_1	Material factor, f_m
Steel	0.8	1.25
Polyester (PET)	0.4	2.5
Polypropylene (PP)	0.2	5
Polyamide (PA)	0.35	2.8
Polyethylene (PE)	0.2	5

Table 3-11 Conversion factors η_2 for damage during installation (after Nordic guideline, 2003)

Conversion parameters	Conversion factor, η_2	Material factor, f_d
Clay/silt	0.91	1.1
Sand	0.83	1.2
Gravel (Natural)	0.77	1.3
Gravel (Broken)	0.72	1.4
Chrused Rockfill	0.67	1.5

According to Swedish Road Administration publication 1992:10, the material factors for biological and chemical degradation, f_{env}, may be assumed 1.1 as long as the pH value ranges between 4 and 9, which gives a conversion factor of $\eta_3 = 0.91$.

Allowable tensile strength of geosynthetics for reinforcement design is defined as ultimate tensile strength divided by *the reduction factor* (or *partial factor*).

$$\sigma_a = \sigma_u \left\{ {}^1/_{f_d}, {}^1/_{f_{env}}, {}^1/_{f_m}, {}^1/_{f_c} \right\} \quad (3\text{-}21)$$

where: σ_a = allowable strength
σ_u = ultimate strength
f_d = partial factor for mechanical damage
f_{env}= partial factor for environment
f_m = partial factor for extrapolation of tensile strength
f_c = partial factor for construction safe

3.4. Characteristic of Piles

There are three classifications of columnar foundation include (Han and Wayne, 2000) namely:

- flexible column (such as stone columns and lime columns)
- semi-rigid columns (such as lime-cement and soil-cement columns)
- rigid piles (such as concrete pile, timber piles, and vibro-concrete piles)

3.4.1. Wooden Pile

Strength of wooden material can be grouped into four classes of strength and type of stress as in Table 3-12 (PKKI, 1961). Wooden material with Class 1 and 2 is usually used in construction demand.

Table 3-12 Strength class for wooden material (after PKKI, 1961)

No.	Type of stress	Strength class of wood (kg/cm^2)			
		1	2	3	4
1	$\sigma_{flexural}$	150	100	75	50
2	$\sigma_{// comp or tensile}$	130	85	60	45
3	$\sigma_{\perp compressive}$	40	25	15	10
4	$\tau_{//}$	20	12	8	5
5	Young's modulus, E (kg/cm^2)	125000	100000	80000	60000

According to the new code SNI 2002 (Indonesian National Standardization, 2002), quality of wooden material or *quality code* use mixed Letter and Number to declare Elastic Modulus as in Table 3-13.

Table 3-13 Quality code for wooden material (after SNI, 2002)

Code of quality	Young's modulus [MPa]	Flexural strength F_b [MPa]	Tensile strength parallel fiber F_t [MPa]	Tenslie strength perpendic. fiber F_c [MPa]	Shear strength F_v [MPa]	Compr. strength perpendic. F_c [MPa]
E26	25000	66	60	46	6.6	24
E25	24000	62	58	45	6.5	23
E24	23000	59	56	45	6.4	22
E23	22000	56	53	43	6.2	21
E22	21000	54	50	41	6.1	20
E21	20000	50	47	40	5.9	19
E20	19000	47	44	39	5.8	18
E19	18000	44	42	37	5.6	17
E18	17000	42	39	35	5.4	16
E17	16000	38	36	34	5.4	15
E16	15000	35	33	33	5.2	14
E15	14000	32	31	31	5.1	13
E14	13000	30	28	30	4.9	12
E13	12000	27	25	28	4.8	11
E12	11000	23	22	27	4.6	11
E11	10000	20	19	25	4.5	10
E10	9000	18	17	24	4.3	9

Elastic modulus or Young's modulus of wooden material can be estimated using equation below (SNI, 2002).

$$E \text{ (MPa)} = 16{,}000\, G^{0.7} \tag{3-22}$$

Where: G is specific gravity of wooden material at water content 15%.

3.4.2. Concrete Pile

It is similar to wooden material that for *cementitious pile* (or concrete pile) Young's modulus is an important parameter. Cemented material such as concrete column, it is able to be subjected to high compressive stress. Young's modulus can be estimated using compressive strength of concrete.

$$E_c = 14{,}850\, f_c'^{0.5} \text{ (kg/cm}^2\text{)} \tag{3-23}$$

Relationship between characteristic compressive strength and flexural strength as described in Eq. 3-24.

$$f_{cf} = K\, f_c'^{0.5} \text{ (MPa)} \tag{3-24a}$$

$$f_{cf} = 1.13\, K\, f_c'^{0.5} \text{ (kg/cm}^2\text{)} \tag{3-24b}$$

where: E_c = Young's modulus of concrete
f_c' = characteristic of 28-day-compressive strength
f_{cf} = flexural-tensile strength of 28-day
K = 0.7 for gravel and 0.75 for crushed stone

3.4.3. Stone Column

Hughes and Withers (1974) performed pioneering laboratory studies of sand columns within a cylindrical chamber containing clay and used radiography to track the deformations occurring within and outside the columns. They found that CCET (cylindrical cavity expansion theory) represented the measured column behaviour very well and proposed that the ultimate vertical stress (q) in a stone column could be predicted by:

$$q = \frac{1-\sin\phi'}{1-\sin\phi'}(\sigma'_{ro} + 4c) \quad (3\text{-}25)$$

where: ϕ' is the friction angle of stone infill, σ'_{ro} is the free-field lateral effective stress and c is the undrained shear strength.

The equation above is widely used in practice today. There are alternative approaches for estimating the bearing capacity of a single column and column group, such as that recently published by Etezad et al. (2006). The authors report an analytical treatment of bearing capacity failure mechanisms. Failure mechanisms adopted are based upon the output from a combination of finite element analysis and field trials.

Absolute and differential settlement restrictions usually govern the length and spacing of columns, and the preferred method of estimating post-treatment in European practice was developed by Priebe (1995). Although, this method is strictly applicable to infinite array of columns and has some empiricism in its development.

Priebe's settlement improvement factor, n, defined as:

$$n = \text{settlement without treatment} / \text{settlement with treatment} \quad (3\text{-}26)$$

It is a function of the friction angle of stone ϕ', the soil's Poisson's ratio and an area replacement ratio dictated by the column spacing. The area replacement ratio is defined as A_c/A, where A_c = cross-sectional area of one column and A = total cross-sectional area of the 'unit cell' attributed to each column. A_c/A is related geometrically to the column radius, r, and column spacing, s, according to:

$$\frac{A_c}{A} = k\left(\frac{r}{s}\right)^2 \quad (3\text{-}27)$$

Where: k is π and $2\pi/\sqrt{3}$ for square and triangular column grids respectively.

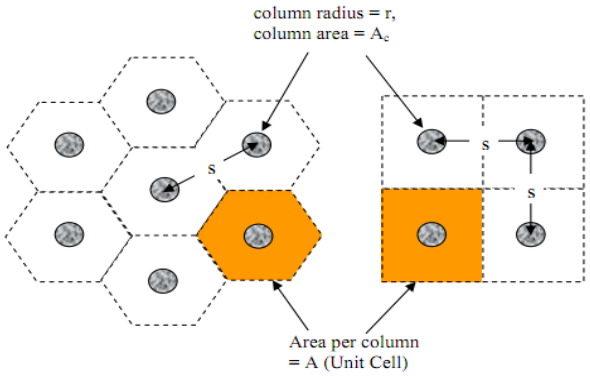

Fig. 3-5 Typical of columns arrangements: Triangular and Square grids (after Priebe, 1995)

Priebe's *'basic improvement factor*' may be derived from the chart as shown in Fig. 3-6. Need to be noted that the reciprocal area replacement ratio A/A_c is used on the chart.

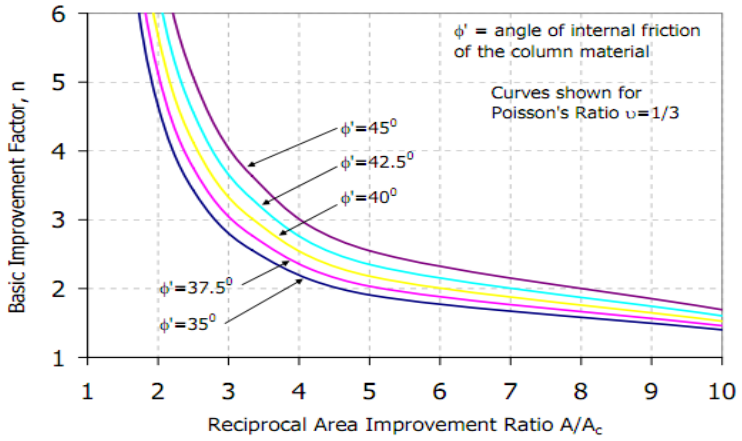

Fig. 3-6 Priebe's basic improvement factor (after Priebe, 1995)

A lower limit to the undrained strength of c_u = 15 kPa is suggested for treatment with stone column, although there have been situations where softer soils have been successfully improved (Raju et al., 2004). In other hands, UK National House Building Council (NHBC, 1988) suggests that stone columns should not be used when I_p >40%. Wood et al., (2002) conducted what is considered to be the most comprehensive laboratory model investigations of large groups of columns. The results suggest that significant improvement in the bearing capacity requires an area replacement ratio of 25 % or greater.

McKelvey et al. (2004) used a transparent medium with 'clay-like' properties to allow visual monitoring of the columns throughout the foundation loading. The main findings of this research relate to optimum column aspect ratio *L/d* (*L*=column length, *d*=column diameter) that in the case of 'short column' (i.e. *L/d*=6), bulging took place over the entire length of column. The 'long column' (*L/d*=10) deformed significantly in the upper region whereas the bottom portion remained undeformed. McKelvey et al. (2004) postulated a 'critical column length' of *L/d*=6, which is in keeping with earlier work (Hughes and Withers, 1974; Muir Wood et al. 2004).

3.4.4. Soil Cement Column

The deep mixing method is a technology that mixes in-situ soils with cementitious materials to form a vertical stiffness in the ground. The deep mixing method (DMM) utilizes quicklime, slaked lime, cement, fly ash, and/or other agents. The agents, widely referred to as 'binders', may be introduced in the form of either a dry powder or slurry.

In the late 1960's, Japan and Sweden independently began research and development of deep soil mixing techniques using granular quicklime. The Japanese were focusing on soil improvement techniques suited to large marine and estuarine projects, while Sweden was primary focusing on soil improvement of soft clay for road and railway projects. The method in which dry powdered lime and cement are used as the stabilizing agents is generally known as the 'Dry Method of Deep Mixing', whereas the use of stabilizing agents in slurry form referred to as the 'Wet Method of Deep Mixing' by the mid 1970's, in effort to improve the uniformity of soil treated by deep mixing. Typical operating parameters of the Japanese mixing machines are summarized in Table 3-14.

Table 3-14. Typical Japanese mixing installation parameters (after Kaiqiu, 2000)

Description	Single drive shaft	Double drive shaft	Multibarrel drive shaft
Depth of stabilization	49 ft (15 m)	> 49 ft (15 m)	98-131 ft (30 - 40 m)
Penetration velocity	2 - 3.3 ft/m 0.6 - 1.0 m/min	0.7 - 3.3 ft/m 0.2 - 1.0 m/min	3.3 - 6.6 ft/m 1.0 - 2.0 m/min
Withdrawal velocity	2 - 3.3 ft/m 0.6 - 1.0 m/min	0.7 - 3.3 ft/m 0.2 - 1.0 m/min	3.3 - 6.0 ft/m 1.0 - 1.5 m/min
Rotating speed	50 rpm	46 rpm	20 - 30 rpm (penetration) 40 - 60 rpm (withdrawal)

Deep mixing methods in the U.S. have been used on several projects either dry or wet method. In general, dry mixed stabilization is appropriate for sites with relatively deep deposits of very soft soil, and sufficient groundwater to hydrate both the lime and cement (Esrig and Mac Kenna, 1999). Cohesive soils with moisture contents between 60% and 200% are best suited for dry mixing.

While several different types of laboratory tests are used to evaluate the shear strength and stiffness of deep mixed columns, the most frequently used is the *unconfined compression test*, mainly because of the simplicity of the test. Many factors affect the unconfined compressive strength because of a wide variety of soil types and binder mixes. The 28-day unconfined-compressive strengths for soil treated by the wet method may range from 140 to 27000 kPa (Haley&Aldrich, 2000; Kaiqiu, 2000; Tatsuoka&Kobayashi, 1983) whereas using the dry method range from 14 to 2700 kPa (Hebib&Farrell, 2002; Jacobson et al, 2002; Kaiqiu, 2000). Unconfined compressive strengths, q_u, for three projects in the U.S. are presented in Table 3-15.

Table 3-15 Specified values of q_u on deep mixing projects in the U.S.

Projects	Soil types / binder amount	Specified q_u	Reference(s)
Oakland Airport Roadway, California	Wet method; Loose sandy fill and soft soil; 160-240 kg/m3 cement	At 28 days, Average q_u > 1035 kPa, Minimum q_u > 690 kPa	Yang et al,2001
Central Artery Project, Boston	Wet method; Fill and organic soft clay; 220-300 kg/m3 cement	At 56 days, Maximum q_u > 26900 kPa, Minimum q_u > 2100 kPa	Lambrechts et al,1998; Maswoswe,2001
I-95 Route 1, Alexandria	Wet method; Soft organic clay; 300 kg/m3 cement	At 28 days, Average q_u > 1100 kPa, Minimum q_u > 690 kPa	Shiells et al,2003; Lambrechts et al,1998

Source, M. Smith, 2008

Stabilization of soft organic soils with cement columns using the mix-in-place technique (MIP) for a railway embankment at section of Büchen-Hamburg was upgrade in 2003 by the German Railway company (Deutsche Bahn) to allow a train speed of 230 km/h (Schwarz&Raithel, 2005). The cement columns (diameter 0.63 m and 5-8 m length) were installed in a square 1.5×1.5 m grid, containing 2.5 to 3% cement, which can be characterized

as a wet deep mixing technique, the composition of binder (water, cement and bentonite) and the water binder ratio (approx. 1.0). Each of 500 m^3-treated soil, 6 unconfined compression tests, was carried out after 28 days. According to the test, unconfined compressive strength after 28 days of all samples exceeds the design criteria of $q_u \geq 2.2$ Mpa.

For cemented columns installed by the wet method, Takenaka (1995) reported that undrained shear strength is equal to one-half of the unconfined compressive strength for those values below several hundred kPa and become less than one-half when they are greater than several hundred kPa. As a rule of thumb, Takenaka (1995) recommended that undrained shear strength be taken as one-third of the unconfined compressive strength. Kivelo (1997) found that the undrained shear strength can be less than one-half the unconfined compressive strength at low confining pressures. However, when the total confining pressure exceeds 150-250 kPa, the undrained shear strength becomes almost constant at a value equal to one half of the unconfined compressive strength.

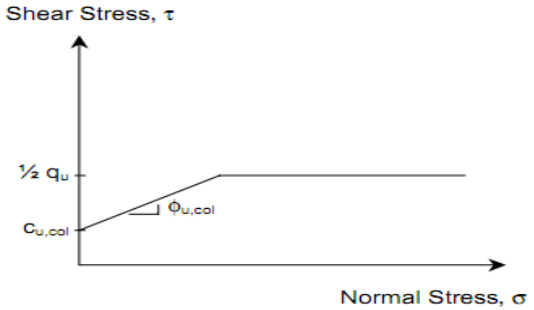

Fig. 3-7 Undrained shear strength of lime/cement column (after Kivelo, 1997)

The peak strength is typically reached at strains 0f 1% to 2% and decrease in strength once the peak strength is exceeded (Kivelo, 1998). The residual strength of soil-cement is 65% to 90% of the unconfined compressive strength (Tatsuoka&Kobayashi, 1983).

The undrained secant modulus of elasticity, E_{50}, which evaluated at 50% of the peak strength, is a measure of soil-cement compressibility. Some researchers correlate E_{50} to unconfined compressive strength for columns installed the dray method (Braker, 2000; Broms, 2003; Jacobson et al., 2003; Navin&Filz, 2005). Whilst for cement treated soils using the wet method also have been performed and presents relatively higher values of secant modulus of elasticity than those using the dry method (Kawasaki et al., 1981, Navin&Filz, 2005, Fang et al., 2001). The relationship between E_{50} and q_u is provided in Table 3-16.

Table 3-16 Relationship between E_{50} and q_u

Binder types	E_{50}	Reference(s)
Dry lime/cement	50 - 180 q_u 75 q_u	Baker, 2000; Broms, 2003 Jacobson et al., 2003
Dry cement	65 - 250 q_u 300 q_u	Baker, 2000; Broms, 2003 Navin and Filz, 2005
Wet cement	350 - 1000 q_u 30 - 300 q_u 150 q_u 300 q_u	Kawasaki et al., 1981 Fang et al., 2001 Mc Ginn and O'Rouke, 2003 Navin and Filz, 2005

Source:M. Smith, 2008

When the modulus of elasticity is used in design analysis, the secant modulus E_{50} is typically used as the design value of column E_{col}. The modulus of elasticity on samples prepared in the laboratory is typically higher than modulus determined from coring test obtained in situ actual columns (Broms, 2003).

The oedometer compression modulus E_{oed} is related to modulus of elasticity E_{col} and Poisson's ratio ν as follows:

$$E_{oed} = \frac{E_{col}(1-\nu)}{(1+\nu)(1-2\nu)} \quad (3\text{-}28)$$

Generally the Poisson's ratio of deep mixed treated soil is around 0.25 to 0.45 (Terashi, 2003). Therefore, E_{oed} is equal to 1.2 to 3 E_{col}.

The total unit weight of treated soil using the dry method increases from 3% to 15% above the untreated soil. Whilst tensile strength of soil improved by the wet method, it is 10% to 20% of unconfined compressive strength. Moreover, permeability of treated soil ranges from 10^{-7} to 10^{-8} m/s is routinely achievable.

3.5. Characteristic of Loading

Transport infrastructure such as roadway, railway and runway is mainly subjected by moving load. Although at a certain situation they are static loading such as car parking at the parking lot, airplane parking on a parking stand at the apron. When a vehicle passes through a roadway, time loading at certain point on the surface of the roadway section depends on velocity of the vehicle. Load repetition induced by wheels of the vehicles on the surface is able to result in a rut depth during a service period of roadway.

3.5.1. Vehicular Traffic

When vehicles crossing on the roadway, all kinds of vehicle refer to Equivalent Single Axle Load (ESAL) of 18 kips (or 8.12 ton) with inflation pressure 80 psi (560 kPa). Wheel configuration may be single, dual wheels and tandem. Meanwhile, light vehicles (passenger cars) have an inflation pressure around 32 psi (225 kPa).

3.5.2. Airplane

Compared to a wheel load generated by traffic on the roadway, the wheel load of airplane has quite higher in magnitude than that of on the roadway. It depends on weight, tire pressure, wheel configuration of airplane. Tire pressures of the airplane vary from 0.5 MPa to more than 1.5 MPa.

Because weight of the airplane is quite heavy that will be transferred to the surface of the pavement, wheel configuration plays an important role. For light aircraft, it uses a single wheel configuration. Dual wheel configuration can be seen for a moderately weight of the airplane. Furthermore, another configuration for heavy weight of the airplane is tandem and also dual tandem.

In other to accommodate the various airplanes for operational movement, it needs to provide aerodrome areal as shown in Table 3-17. The aerodrome reference code uses number and letter codes to express class of airport (ICAO, 1999). Maximum allowable tire pressure category consists of *High* (no pressure limit), *Medium* (pressure limited to 1.50 MPa), *Low* (pressure limited to 1.00 Mpa) and *Very low* (pressure limited to 0.50 MPa. The higher tire pressure indicates the heavier weight of the airplane.

Table 3-17 Aerodrome reference code (after ICAO, 1999)

Code element 1		Code element 2		
Code number	Aeroplane reference field length	Code letter	Wingspan	Outer main gear wheel span *
[1]	[2]	[3]	[4]	[5]
1	Less than 800 m	A	Up to but not including 15 m	Up to but not including 4.5 m
2	800 m up to but not including 1200 m	B	15 m up to but not including 24 m	15 m up to but not including 24 m
3	1200 m up to but not including 1800 m	C	24 m up to but not including 36 m	6 m up to but not including 9 m
4	1800 m and over	D	36 m up to but not including 52 m	9 m up to but not including 14 m
		E	52 m up to but not including 65 m	9 m up to but not including 14 m
		F	65 m up to but not including 80 m	14 m up to but not including 16 m

** Distance between the outside edges of the main gear wheels*

3.5.3. Trains

In Germany, according to Ril 836 for rail infrastructure, the subgrade or improved subgrade has to be able to support a load above this surface layer with bearing capacity at least around 52 kPa. For high speed trains from 100 to 300 km/h, it needs the additional layer around 1 to 2 times of the superstructure thickness (Muncke et al., 1999; Kempfert et al., 1999).

It is different for each country with respect to a standard axle load. For instance in Greece, Beskou et al., (2011) reported that locomotive (or engine) is around 210 kN and 150 kN for carriage. In Indonesia, railway infrastructure is subjected to axle load maximum 180 kN (Indonesian Railway Code, 2003).

CHAPTER 4

Experimental Works and Field Case Studies

4.1. General

To understand well the pavement behaviour and/or embankment overlying soft soil, some researchers have performed some experimental works either in laboratories using small scale approach or monitoring full-scale directly in the field (Zaeske, 2001); Heitz, 2006; Wei-ping et al., 2007; Hassandi et al., 2005; Schwarz et al., 2005; Djarwadi, 2006; Almeida et al., 2008; Eekelen, 2009). Treatments for ground improvement in this study only focus on horizontally inclusion of geosynthetics, vertically inclusion of piles and the combined technique both of them. Meanwhile, some tests have been done to know an influence of geosynthetics into granular soil (Bussert, 2006; Ruiken&Ziegler, 2008; Ruiken et al., 2010). Furthermore, some intensive tests regarding with geosynthetics-soil interaction behaviour have been carried out using interaction testing device (ITD) at Geotechnical Institute of Technical University Bergakademie Freiberg (Aydogmus&Klapperich, 2004; Aydogmus, 2006; Tamaskovics&Klapperich, 2010; Althoff, 2010, 2011).

4.2. Experimental Work at the Laboratory

4.2.1. Geosynthetics

4.2.1.1. Horizontal pressure experiment

Ruiken and Ziegler (2008) performed a test to know the influence of inclusion of geosynthetics in unbounded granular material. Tubular sample of diameter 500 mm and height 1100 mm consisting of gravel d_{50}=12 mm and sand d_{50}=0.5 mm was compacted around 95-100% standard proctor. Geogrids with tensile strength of 30 kN/m and aperture 32 cm were inserted horizontally from only a layer until 7 layers in tubular sample. There were 9 tape gauges installed to measure the radial deformation of the sample. Vertical stress with constant speed of 1 mm/min (0.1% per minute) was applied. Fig. 4-1 is showing the setup test.

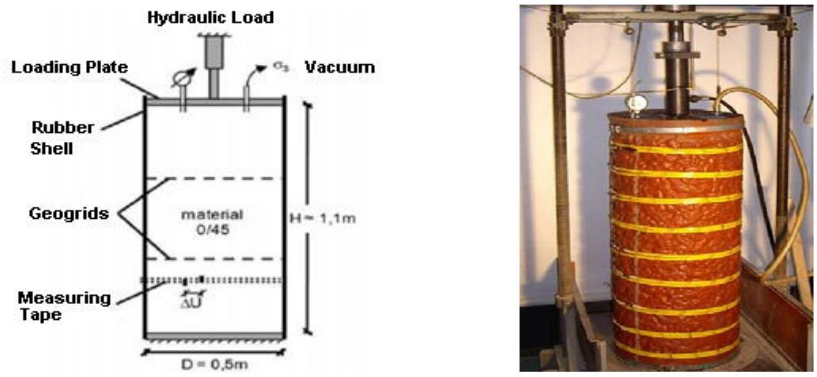

Fig. 4-1 Setup of sample in laboratory test
(after Ruiken and Ziegler, 2008)

Ruiken and Ziegler (2008) reported their result test that the inclusion of geosynthetics can reduce the radial deformation. The more number of layers will reduce the magnitude of radial deformation as shown in Fig. 4-2. This result indicated that more than 3 layers did not give significant impact on radial strains. It suggests a hint that distance of geogrid probably was effectively applied in range 280-360 mm because the radial deformations resulted from 2 to 3 layers of geogrids are very close.

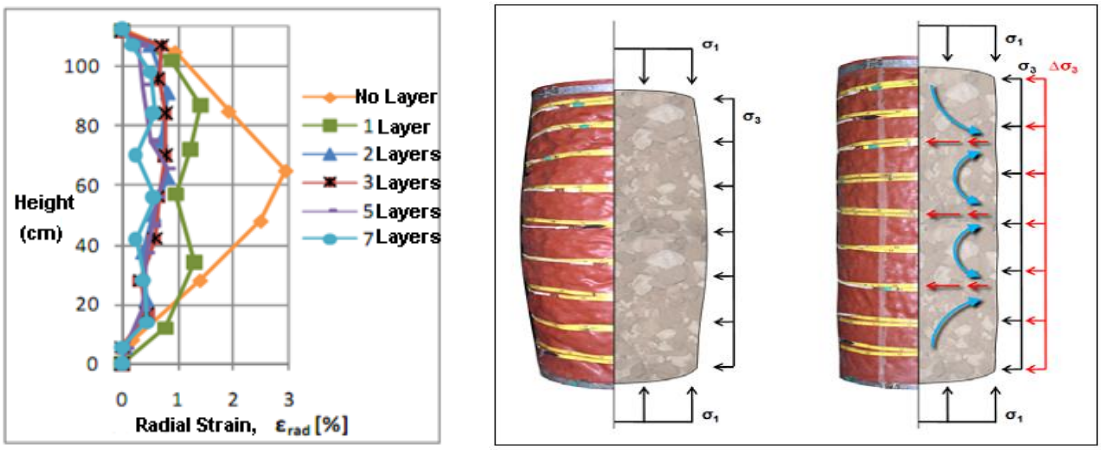

Fig. 4-2 Radial strains in laboratory test (after Ruiken and Ziegler, 2008)

Some studies to observe the horizontal deformation subjected to a vertical load has been performed by researchers (Clayton et al., 1993; Soong & Koerner, 1997; Yang et al, 2009). Ruiken and Ziegler (2010) also performed the deformation by inclusion geosynthetic as shown in Figure 4-3. A sand sample in box sized (H×B×L) 1m×1m×0.45m compacted up to 100% standard proctor was used to do the experiment as shown in Fig. 4-3. A couple side was made of steel and another couple side was glass with 106 mm thick. To reduce friction between sand and glass, a thin latex membrane inserted in between and a uniform load up to 50 kN/m^2 was applied at the surface of the sample box.

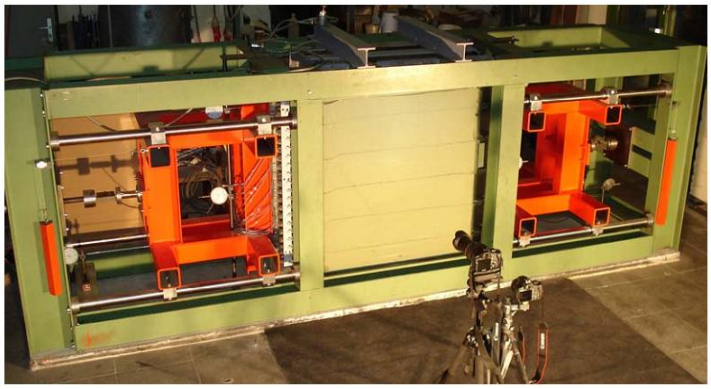

Fig. 4-3 Installation for measuring horizontal pressure (after Ruiken et al., 2010)

Inclusion of geogrid from one up to 5 layers has been applied and then the experiment result was a curve correlating between horizontal deformation of vertical movable plane and horizontal outward pressure on the vertical plane as depicted in Fig. 4-4. It was interesting

that for 2 and 3 inclusion of geogrids they almost coincided with each other. Moreover, using of 5 layers did not give lower horizontal pressure than that of using 4 layers. Overall, more and more numerous layers suggest that horizontal outward pressure was reduced.

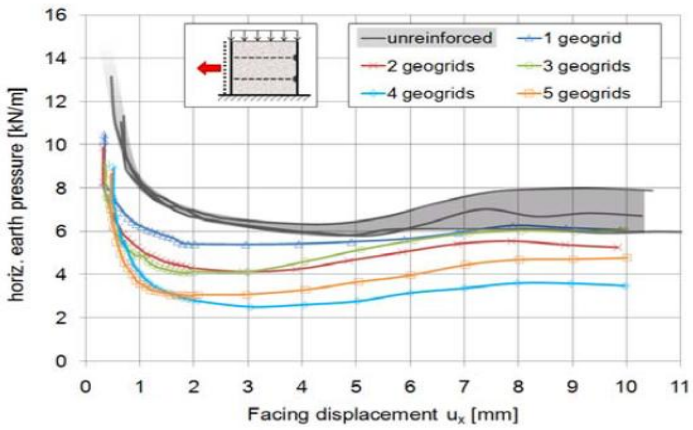

Fig. 4-4 Horizontal outward-pressure (after Ruiken et al., 2010)

4.2.1.2. Load transfer mechanism experiment

Bussert (2006) performed a research for studying the load transfer mechanism by soil/geogrid with 'insoil' testing using setup with movable front wall and introducing forces from the soil into the forcing geogrids. Fig. 4-5 is showing the test setup.

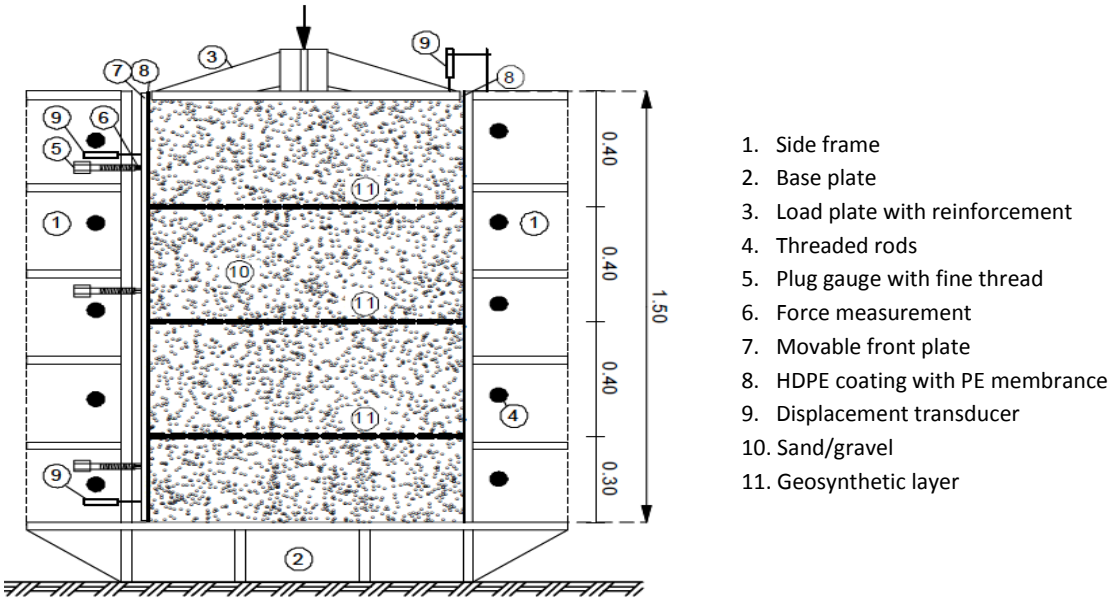

Fig. 4-5 Test setup with movable front wall (after Bussert, 2006)

The test results showed that interaction of soil and geogrid mainly depends on the geosynthetic layer spacing, soil grain size, geosynthetic aperture size as well as strength of shape and extensional stiffness of geogrids. Load plate was subjected to a load (in kPa) and strain of geosynthetics was measured based movement of movable wall. Magnitude of load

in kPa was recorded as the stress reduction at the front of the moving wall in horizontal direction caused by different geogrid products as reinforcement and also without reinforcement is shown in Fig. 4-6.

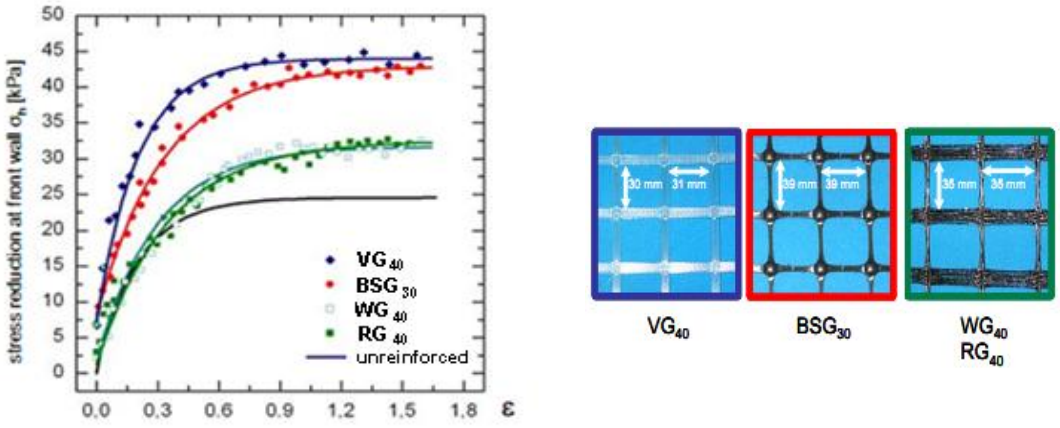

Fig. 4-6 Earth stress reduction at movable front wall with different geosynthetics and without reinforcement of soil body (after Bussert, 2006)

4.2.1.3. Geosynthetics-soil-interaction behaviour experiment

A lot of tests have been carried out in the laboratory of the Geotechnical Institute of Technical University Bergakademie Freiberg to understand the interaction-behaviour between geosynthetics and cohesive soil (Aydogmus&Klapperich, 2004; Aydogmus, 2006; Tamaskovics&Klapperich, 2010; Althoff, 2010, 2011). The geosynthetics-soil-interaction-testing device (ITD) was provided. The ITD is a large shear frame device for shear tests (ISV). It is possible to use this device for friction tests (abbreviation IRV) and pull-out tests (abbreviation IPV). Figure 4-7 gives an overview of the testing device.

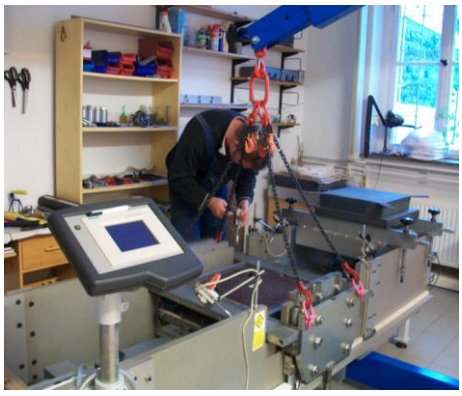

(a) preparing sample in shear box

(b) running test

Fig.4-7 Geosynthetics-soil-interaction-testing device (ITD)

The shear box consists of a lower and upper shear frame. This box can be filled with more or less 80-120 kg soil mass depending on type of soil, water content and degree of compaction. Before installing material sample in the shear box, the material is homogenized using a mixing device. The soil mass is built-in several layers and each layer is compacted with a hand compaction device. During testing, the upper shear frame can move vertically, but will not go under the pre-adjusted target value. Therefore, the shear gap can adjust itself during the experiment. The parameters of the device are listed in Table 4-1.

Table 4-1 Specification of interaction testing device

Parameters	Size and/or rate	Unit
Size of the shear box	L=500, W=500, H=200	mm
Normal stress range	0 - 600	kN/m^2
Shear and pull-out force	125	kN
Maximum shear displacement	160	mm
Maxsimum pull-out displacement	400	mm
Shear velocity	0.000001 – 12.5	mm/minute

Tests of friction and shear behaviour are costly and time-consuming. Pull-out test in particular is one of the most expensive performance tests (Koerner, 2005). Thus, in previous research a more economical technique for using the ITD (for IRV, ISV, and IPV) was investigated in the institute (Tamaskovics and Klapperich, 2010; Althoff, 2010; 2011; Widodo, 2013). Multi-Stage Large Shear-Frame test has some advantages. During installation of sample, soil in the shear box is highly compacted and then the tests are carried out at low velocity. These test series contain multi-stage tests (ISV, IRV, and IPV) using a cohesive soil (Canitz-silt) in combination with twelve different geogrids from six different producers which have some properties such as short time tensile strength (25-180 kN/m), elongation, aperture size, junction strength, surface and thickness. According to the grain size distribution, Canitz-silt is strongly sandy and slightly clayey silt.

My research activity under DFG-research project FY 2012/2013 in this laboratory was still ongoing. Multi-stage tests for ISV, IRV, and IPV have been undertaken not only for Canitz-silt soil, but also Hohen Bockär glassy sand and Kaolin soil. In order to reach maximum density for three kinds of soil, Proctor test has been done in which the measured water contents are 11.3%, 2.5%, and 28.07% for Canitz-silt soil, Hohen Bockär glassy sand and Kaolin soil, respectively. All types of geosynthetics were tested in machine direction, with and without cross-element in order to understand behaviour of geosynthetics-soil-interaction.

4.2.2. Piled Embankment

4.2.2.1. Pile-soil relative displacement experiment

Wei-Ping et al. (2007) conducted the experimental test to investigate soil arching within reinforced and unreinforced piled embankments in 2D-layout. A total of 15-model tests were conducted to evaluate the effects of pile-soil relative displacement, embankment height, cap beam width and clear spacing, and geosynthetics with different tensile strength on the stress concentraion ratio and settlements in the embankments.

Model test consisted of a bricked base, two rubber water bags and tank. Toughened glass was used for the four walls of the tank to allow observation. The system was 1500 mm long, 1000 mm wide and 1440 mm high as shown in Fig. 4-8. The base was 140 mm high, two water

bags which each water bag with a dimension of 1000 mm long, 600 mm wide and 140 mm high, were placed inside the base and filled with water.

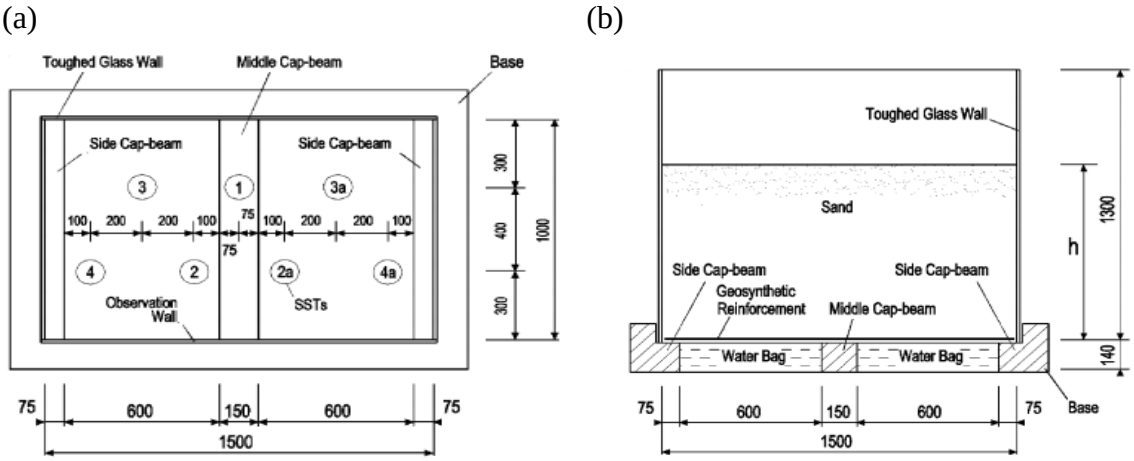

Fig. 4-8 Layout of test setup (a) Top view and (b) Side view (after Wei-ping et al., 2007)

The sand used in the model tests was come from Qiantang River Beach, China. Specific gravity G = 2.64, the coefficient of uniformity C_u = 2.5 and the coefficient of curvature C_c = 0.96. Sand grains were subangular and predominantly quartz with D_{10} = 0.1 mm, D_{60} = 0.25 mm, D_{max} = 2 mm, e_{max} = 0.89 and e_{min} = 0,54. The unit weight of the fill in the tank was 15.35-15.83 kN/m^3 and corresponded to a relative density of 55$\pm$7%. Peak secant angle of shearing resistance ϕ_{max} was 44^o. Three types of geosynthetics were used in the model tests with biaxial tensile strength 0.35, 1.40 and 22.5 kN/m at 8% axial strain.

Based on 15 model tests having a ratio of embankment height to clear spacing, h/s, from 0.7 to 2.0 they obtained some interesting results. In Test 1 through Test 4, when $h/s \leq 1.4$, the surface of the embankment was non-uniform. It implies that the differential settlement occurred on the top of an embankment. In Test 5 through Test 7, when $h/s \geq 1.6$, the settlements at the base of the embankment were non-uniform, but the embankment surface remained almost horizontal. Deformations in embankments of model Tests 1 through Test 7 also suggest that the height of equal settlement plane is about 1.4 - 1.6 times the cap beam clear spacing, i.e., $h_e = (1.4\text{-}1.6)s$. Model tests from 1 to 7 were dedicated to unreinforcement embankment whereas model tests from 8 to 13 were intended to reinforcement embankment using geosynthetic. By using geosynthetics either low embankment h/s = 0.7 or hight embankment h/s = 1.8 produces the higher stress concentration ratio, because the geosynthetics transfers the vertical load over geosinthetics to beam cap. In addition, from the experimental test that the higher embankment indicated the higher stress concentration ratio when using the same of tensile strength of geosinthetics.

4.2.2.2. Cyclic loading experiment

Zaeske (2001) conducted the experimental test for embankment over soft soil reinforced by geosynthetics. Heitz (2006) developed this experiment to observe the influence of cyclic loading on the embankment over soft soil. Fig. 4-9 and Fig. 4-10 illustrate the setup of test model of the embankment over soft soil and placement of devices respectively.

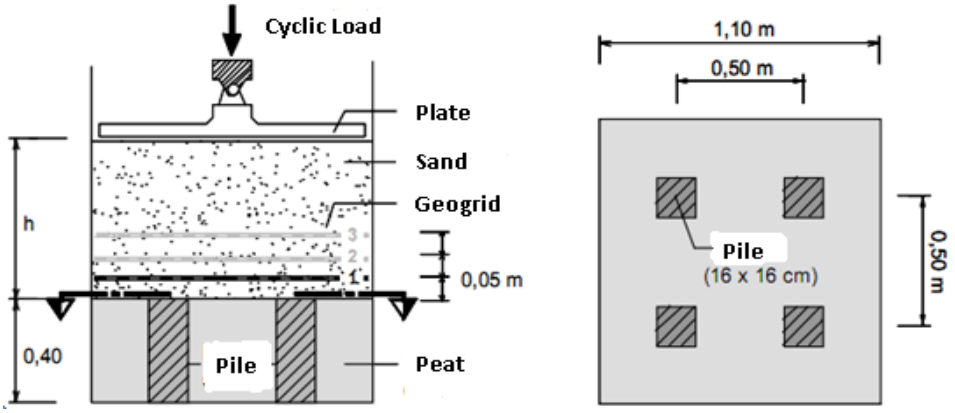

Fig. 4-9 Setup of test model under cyclic loading (after Heitz, 2006)

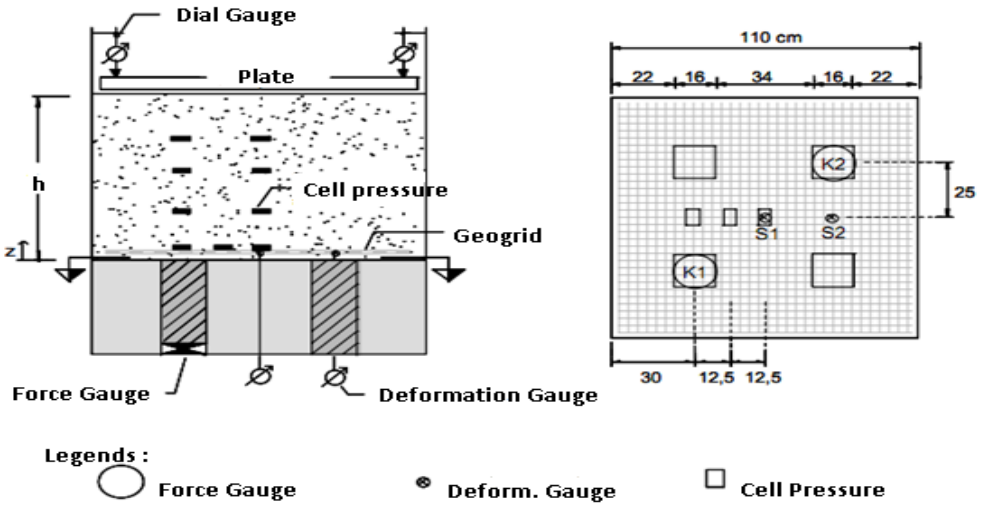

Fig. 4-10 Location of devices in laboratory test (after Heitz, 2006)

In this experiment, four cross-sectional 16×16 cm concrete piles were installed to support an embankment. The unit weight of piles γ = 24 kN/m^3, modulus of elasticity E = 23,982 MN/m^2, strain e_{max} = 0.9%, Poisson's ratio ν = 0.2, Some properties of soft soil (peat) used in the experiment consist of unit weight of piles γ = 8 kN/m^3, modulus of elasticity E = 0.85 MN/m^2 at σ' = 100 kPa, water content w = 300-350%, cohesion c = 8.5 kPa, internal friction angle ϕ' = 24^o, compression index c_c = 2.48, organic content OC = 80.2%, permeability k_i = 4.1E-7 m/s.

Geogrid used in the research were Polyester GW 60 PET and Polyvinyl GW 180 PVA. Tensile strength for longitudinal and transversal direction are 60 kN/m and 180 kN/m respectively. Elastic modulus of geogrids are 850 kN/m at a strain of 2% for GW 60 PET and 3,800 kN/m at strain of 1.25%.

Some interesting findings were obtained from the study. Settlements at surface of embankment induced by cyclic loading with the same magnitude of the load was deeper than static loading. Numerous number of geosynthetics layers were able to reduce settlement at the surface of the embankment.

Highest tensile force occurred at an interface between the pile and geosynthetics, and then the lower tensile force was located on between piles in the orthogonal direction, the lowest tensile force was at the middle of geosynthetics between piles in a diagonal direction. Moreover, maximum strain ε_{max} for low embankment (h = 0.35 m) is higher than high embankment (h = 0.70 m). Meanwhile, settlement at the surface of the embankment for low embankment was deeper than the high embankment over the increasing external load.

The influence of cyclic and dynamic loading could decrease the arching effect. Moreover, vertical stress in the embankment fill will increase over the large number of repetitions.

4.3. Case Studies in the Field

4.3.1. Geosynthetics

4.3.1.1. Weesenstein railway rehabilitation project

Klompmaker et al. (2008) showed the Elbe-river flood disaster in 2002 that destroyed approximately 80% of infrastructure in the valley of Müglitztal near Dresden. To operate the rail traffic again in the shortest possible time, the combination of geosynthetic reinforcement together with the fill material as a compound was applied to ensure the internal and external stability of the structure. The steel grid element stabilizes the slope face and geotextile non-woven separation. Filter layer was provided to prevent the erosion of fill material. The approximately 5 m high geogrid reinforced part on the bottom of the slope is constructed with 60^{o} inclination and is superposed by a 4 m-high embankment (see Fig. 4-11). Structural analysis for the reinforced slope was carried out on the basis of the German recommendations for geosynthetic reinforcements.

a) Collapsed railway embankment b) Geogrid reinforced railway embankment

Fig. 4-11 Weesenstein railway embankment (after Klompmaker et al., 2008)

The applied product Secugrid 120/40 R6 has a Federal Railway Agency's certification for this application. A 0/45 mm crushed mix acted as covering material. The geogrid was installed in 10 layers with a distance of 0.5 m. Within just a few weeks, whole structure had been completed, so that the flow of regular traffic was quickly reinstated.

4.3.1.2. Tabing-Duku road widening project

Klompmaker et al. (2008) also reported the road widening project on a section of Tebing-Duku near the town of Padang on the largest of the Indonesian island, Sumatera, required an existing road from the airport to city center. In spite of extremely problematic ground conditions on the site with low bearing capacity and a high ground-water level, the solution involved the road embankment reinforced with uniaxial Secugrid R-geogrids. Secugrid 120/40 R1 geogrids 15,200 m² made of polypropylene (PP) were installed with anchorage lengths between 6.0 m and 10.0 m. The original design envisaged geogrid reinforcement layers with 60-80 kN/m tensile strength with a layer spacing of 0.5 m as shown in Fig. 4-12.

a) Subgrade condition b) Reinforced slope c) Finished project

Fig. 4-12 Tabing-Duku road widening (after Klompmaker et al., 2008)

The Secugrid solution with geogrid width of 4.75 m allowed faster and more cost-efficient installation. The deformations were remedied as further layers of Secugrid were installed to reinforce the embankment. Measurements were taken from the upper edge of the embankment to determine the degree of deformation. Any deformations were hardly noted, which confirmed that Secugrid had allowed an existing road to be successfully and safely be widened on an extremely soft subgrade at favourable costs.

4.3.1.3. Setoko-Nipah road embankment project

Djarwadi (2006) reported the execution of road embankment using geotextile reinforcement in Setoko and Nipah islands in Province of Kepulauan Riau, Indonesia. The soil investigation shows that soft soil layer up to 15 m deep below the ground surface is present. Water table at a certain situation can achieve about 1.5 m above the elevation of subsoil. Road embankment height of 3.5 m consisting of unit weight γ = 18.5 kN/m^3, cohesion c = 18 kN/m^2, and internal friction angle ϕ = 19^o was constructed over soft soil. Peat and/or very soft marine clay height of 4.5 m was existing beneath the embankment fill consisting of unit weight γ = 14.5 kN/m^3, undrained shear strength s_u = 5 kN/m^2, and internal friction angle ϕ = 2^o. Underneath this layer, very fine sandy clay height of 1.5 m was present consisting of unit weight γ = 16.0

kN/m^3, undrained shear strength s_u = 7.5 kN/m^2, and internal friction angle ϕ = 3^o. Furthermore, marine clay consisting of unit weight γ = 18.0 kN/m^3, undrained shear strength s_u = 10.0 kN/m^2, and internal friction angle ϕ = 2^o was present beneath sandy clay. Typical cross-section of the road embankment over soft soil in Setoko and Nipah islands is depicted in Fig. 4-13.

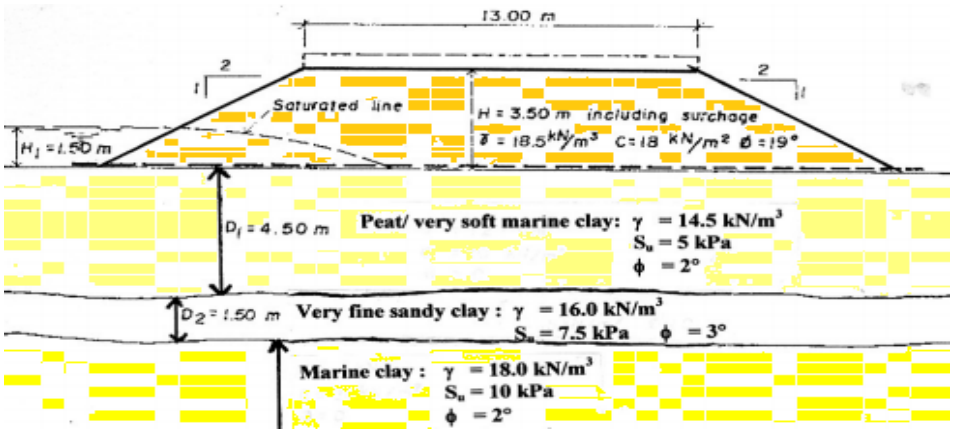

Fig. 4-13 Cross-section of road embankment in Setoko and Nipah islands (after Djarwadi, 2006)

According to Djarwadi (2006) for internal stability using the limit equilibrium method, the construction needs a tensile strength of geotextile around 87 kN/m, whereas foundation stability (external stability) needs a tensile strength of geotextile about 272,8 kN/m.

Compaction has to be done in each embankment thickness of 0.3 m using vibratory smooth drum compactor 15 ton weight until compaction degree of proctor standard ≥ 97%, in which are 8 passing with a constant speed 10 km/h. The compaction tests using the sand cone test are for each 2500 m³ volume of embankment. The observation for settlements of 400 m long road embankments is depicted in Fig. 4-14. We can see that settlements at the final elevation can be more than 1.0 m during less than 3 weeks of execution.

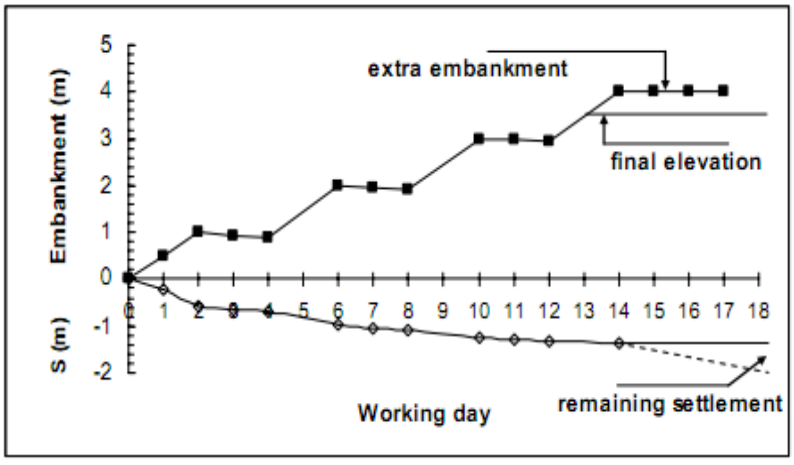

Fig. 4-14 Settlements during work execution (after Djarwadi, 2006)

4.3.1.4. Yamanote Line railway project

Palmeira et al. (2008) reported that since early 1990's reconstruction of railway that collapsed by flooding with embankments having geosynthetic-reinforced steep slope or *Geosynthetic-reinforced soil retaining walls* (GRS RWs), having a stage-constructed FHR facing or their combination, started based on successful experiences of high cost-effectiveness and high performance of GRS RWs. This construction was employed also in other similar cases after this event of flooding. The gentle slope of the embankment and conventional retaining walls that collapsed by an earthquake (the 1995 Kobe earthquake) were reconstructed using GRS RWs. The GRS RWs having a stage-constructed *full-height rigid* (FHR) facing is now the standard retaining wall construction technology for railways in Japan (Tatsuoka et al. (1997a, 2007).

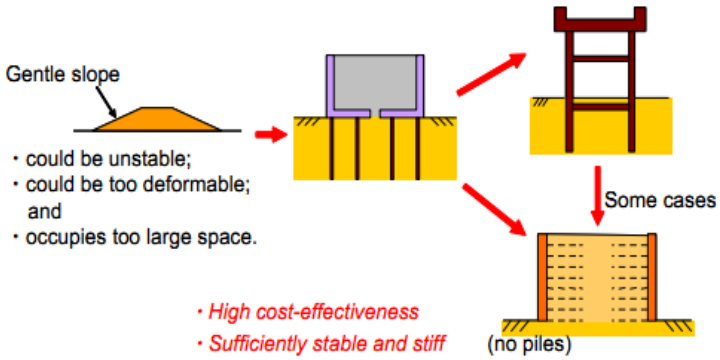

Fig. 4-15 History of elevated railway and highway structure in Japan
(after Palmeira et al., 2008)

Fig. 4-16 and 4-17 show a typical GRS RWs having a FHR facing constructed in center Tokyo, in Yamanote Line near Shinjuku station. It had been built during 1995-2000. This new type GRS RWs has been constructed in more than 600 sites in Japan and the total wall length is recently more than 100 km as of March 2008 (after Palmeira, 2008).

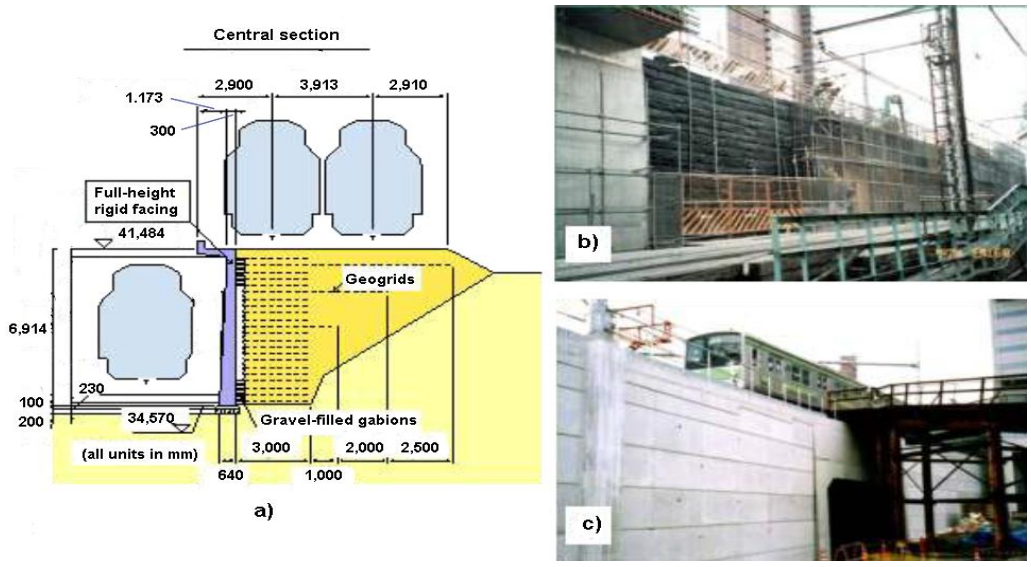

Fig. 4-16 GRS-RWs having a FHR facing in Yamanote Line, a) Typical cross-section
b) Wall under construction c) Completed wall, (after Palmeira et al., 2008)

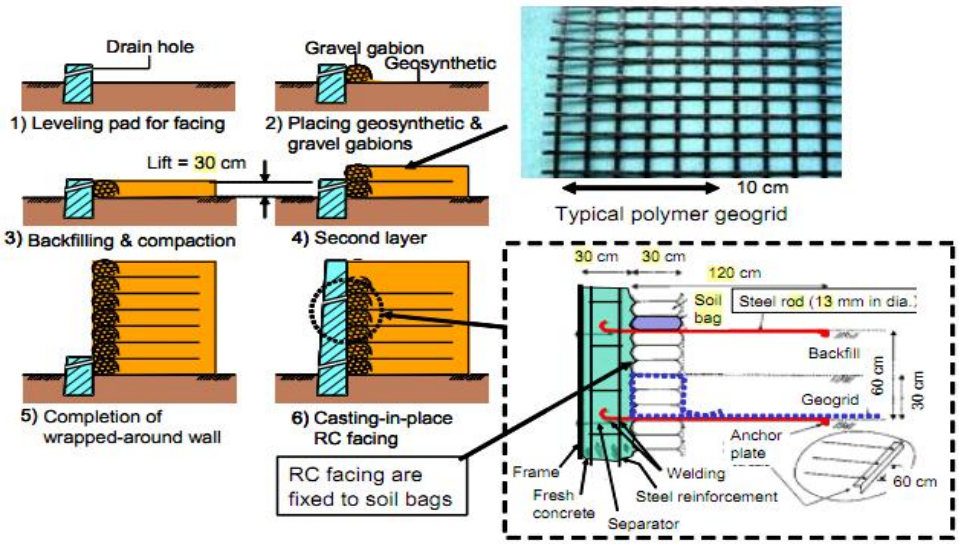

Fig. 4-17 Staged construction of GRS RWs with a FHR facing
(after Palmeira et al., 2008)

4.3.2. Piled Embankment

4.3.2.1. Barra da Tijuca field test

Almeida et al. (2008) performed a field investigation for a case ''low embankment'' at Rio de Janeiro. They investigated low embankment over a 10 m depth of soft clay at Barra da Tijuca district. The soft soil parameters consisted of water content w = 100-500%, Plasticity Index I_p = 100-250%, the average unit weight γ = 12.5 kN/m^3, the undrained shear strength s_u = 4-18 kPa, Compression ratio $CR=c_c/(1-e_o)$ = 0.5, the average coefficient of horizontal consolidation c_h = 6.5E-8 m^2/s.

There were two low embankments observed on the site. Dimensions and characteristics of two embankments are provided in Table 4-2 and illustrated in Fig. 4-18.

Table 4-2 Main characteristics of two piled embankments

Characteristics	Embankment 1	Embankment 2
Construction year	2004	2004-2005
Number of piles	1900	10000
Pile spacings, s (m)	2.5	2.8
Square pile cap, b (m)	0.8	1.0
Clear spacing, $a = s - b$ (m)	1.7	1.8
Embankment height, h (m)	1.2	1.4
Ratio h/a	0.7	0.78
Geogrid characteristics	Fortrac R, Polyester, Biaxial	Fortrac, PVA, Biaxial
Nominal geogrid strength (kN/m)	200	200 and 240
Geogrid modulus (kN/m)	3600	3600 and 4400
Fill height below the pile cap (m)	2.0	0.6 – 1.0
Soft soil deposit thickness (m)	8-10	9-11

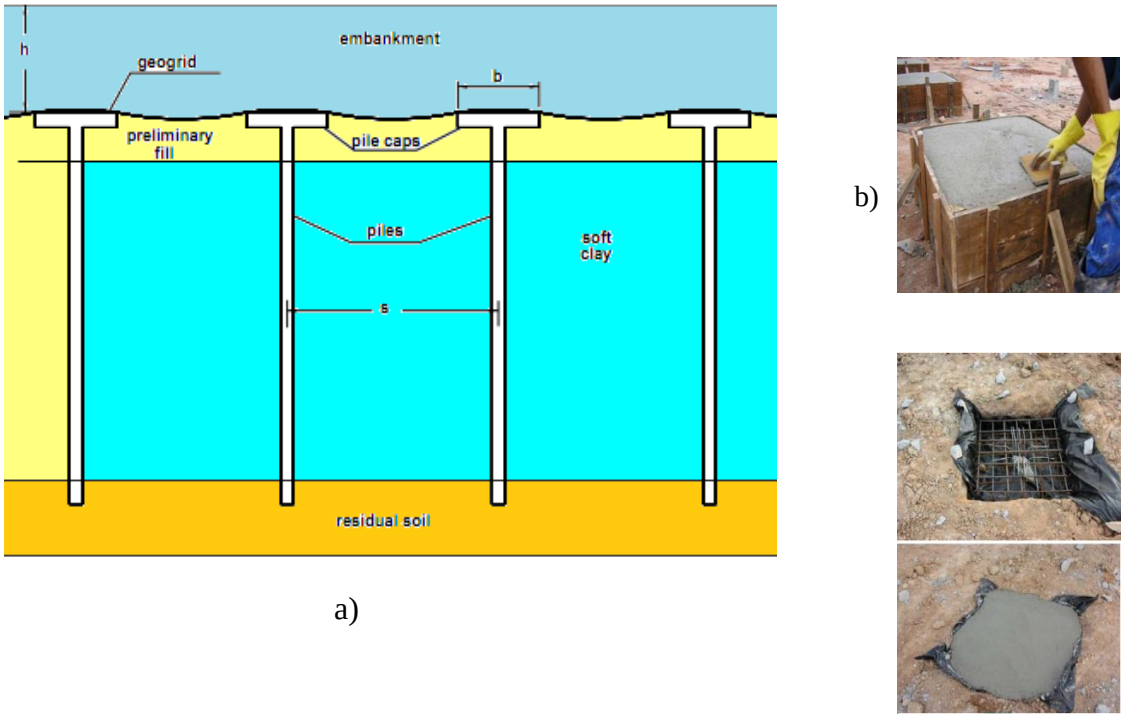

Fig. 4-18 Embankment at Barra da Tijuca, a) General scheme of piled embankment, b) Pile caps above the initial fill, c) Pile caps inside the initial fill (after Almeida et al., 2008)

Some findings are gained from the field test. The strains of geogrids at the face of the pile cap are higher than those at half distance between caps. Meanwhile, strains of geosynthetics in between pile caps at an orthogonal direction were higher than those at a diagonal direction. Based on the damaged geogrids, a circular cap could be more effective than the square caps in thoses cases. In addition, the result suggested that subgrade reaction should not be considered for designing a geogrids-piled embankment.

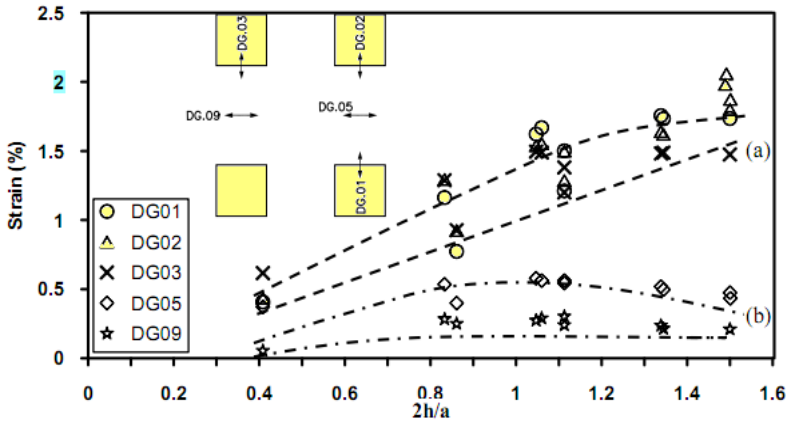

Fig. 4-19 Measured strains in geogrid in points at: a) face of the pile cap, b) half distance between caps (after Almeida et al., 2008)

4.3.2.2. Gebeng Bypass Highway field test

Hassandi and Edil (2005) reported a full scale test embankment to evaluate the performance of different types of loading platform (LTP) supported on geopiers. Three types of LTP were constructed, they include reinforced concrete LTP, geosynthetic-reinforced LTP with two layers of geogrid (catenary beam LTP), and geosynthetic-reinforced LTP with three or more layers of geogrids (beam LTP).

To evaluate the performance of the catenary and the beam LTP. A well instrumented full-scale test embankment was constructed in Gebeng, Pahang State, Malaysia as shown in Figure 4-20. The length of the embankment was approximately 90 m, 13.5 wide, and 3.5 m high. The test embankment was divided into 4 major sections (section 1 through 4) and 2 controlled sections (C1 and C2) at the two ends of embankments.

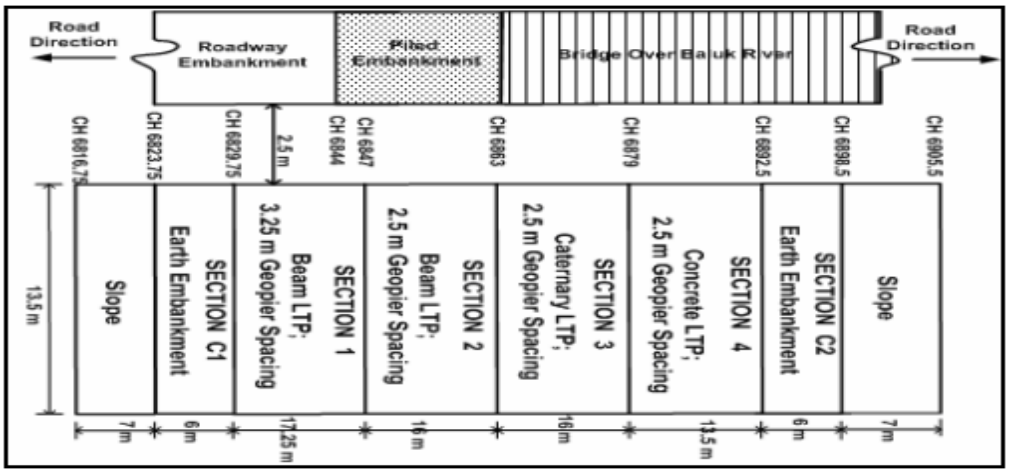

Fig. 4-20 Layout of the major and the control sections of test embankment (after Hassandi et al., 2005)

Site investigation carried out indicated a silty clay layer as deep as 15 m at some locations. However, this soft layer generally ends at approximately 5-6 m below the original ground level. The soils are composed of highly plastic clay and silt with natural water content w between 35% and 61%. The field vane tests that the shear strength S_u lies between 14 to 60 kPa with most of the values less than 25 kPa and sensitivity S varies from 3 to 11.

Geopiers were 75 cm in diameter with 5.5 m deep installed at all sections. Section 1 has the beam LTP with four layers of geogrids and 3.25 m geopier spacing designed by Collin Method. Section 2 has the beam LTP with three layers of geogrids with 2.5 m geopier spacing designed by the Collin Method. Section 3 has the catenary LTP with two layers of high strength with 2.5 m geopier spacing design by BS 8006. Section 4 has a continuous reinforced concrete slab as LTP. Settlement plates were set directly above the geopier elements and at the center between groups of geopier elements. Earth pressure cells were positioned on the geopiers and in between them. Piezometers and extenometers were placed at different depths. Vertical inclinometers were placed at the toe of the embankment in

between the geopiers, and horizontal inclinometers immediately under and across the embankment in between the geopiers.

Geogrid biaxial Tensar SS 20 was utilized for reinforcement in Section 1 and 2. The distance between each geogrid layer in this section was 300 mm. In Section 1, aggregate blanket was laid between layers of geogrid to a thickness of 1.5 m. Meanwhile in Section 2 was 1.0 m. Geogrid uniaxial Miragrid 24 XT was used for reinforcement in Section 3. The distance between the geogrid layers was 75 mm and the selected aggregate blanket thickness was 0.3 m.

According to Nordic Hanbook (2003) it recommends that the differential settlement between the subsoil and the columns shall not be more than 0.1 m and 0.2 m. Total and differential settlements of embankment test from different section was indicated in Table 4-3. We can look that the use of piled embankment would reduce total settlement. Section 3 as catenary LTP suggests the highest differential settlement and the lowest total settlement compared to other sections.

Table 4-3 Total and differential settlements at the base of the embankments

Description	Section 1	Section 2	Section 3	Section 4	C1 and C2
Total settlement (mm)	145	103	102	136	490
Differential settlement (mm)	9	14	23	6	NA
Maximum strain in geogrid (%)	1.4	1.2	0.6	NA	NA

Source: Hassandi et al., 2005

Another finding resulted from the vertical inclinometer readings indicates that the use of LTP supported on columns could reduce the lateral displacement of the subsoil at the edge of the embankment.

4.3.2.3. Kyoto road field test

For the construction of roads on very soft soils, several construction methods are available. The piled embankment using geosynthetic reinforcement (GR) is one of these methods, becoming more and more popular in the Netherlands (Eekelen et al., 2009). Until 2009, at least 20 piled embankments have been constructed underneath highways and local roads. Regarding with Dutch guideline for the design of piled embankment, a full-sclae field has been conducted.

A full-scale field test has been carried out on ''Kyoto Road" in Giessenburg, in the Netherlands (see Fig. 4-21). Results of 2 years of measurements (2005-2007) in a full-scale field test were validated. The Kyoto road was constructed on 13 m long wooden piles with square grid pile spacing of 1.27 m, concrete piles cap with a height of 0.4 m and 0.3 m in diameter. The geogrid reinforcement consisted of two layers of uniaxial geogrids, perpendicular on road axis Fortrac 400/30-30 M and along the road axis Fortrac 350/50-30 M. The embankment fill 1.15 m high made of a "Hegemann sludge mixture" was overlaid over the geogrid layers. The Hegemenn sludge mixture is a mixture of dredged material and additives containing mainly clay and cement having average unit weight γ = 18.6 kN/m^3,

natural water content w = 18.1%, permeability k_v = 2.1E-9 m/s, internal friction angle ϕ = 33.8^o and a cohesion of 11.5 kPa. The modulus of subgrade reaction of soft soil (peat), determined from compression tests on samples, is k = 477 kN/m^3.

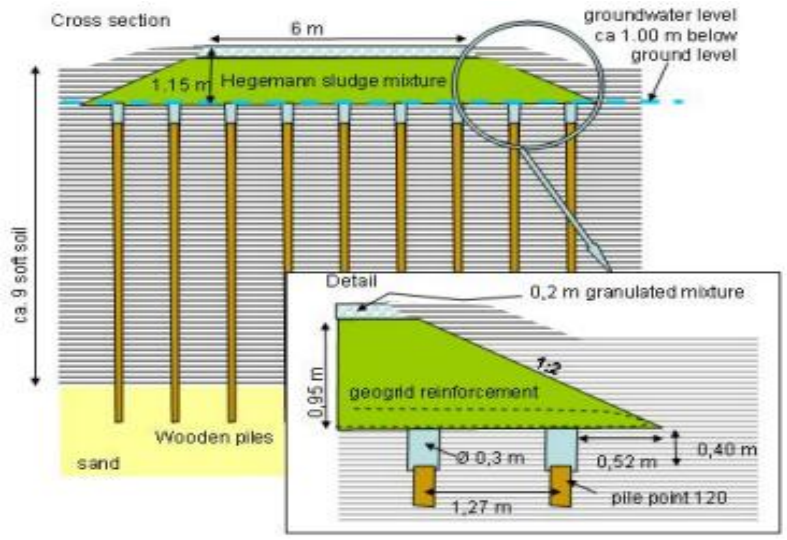

Fig. 4-21 Scheme of the full-scale test Kyoto road (after Eekelen et al., 2009)

Comparison of two and a half years of measurements on a full-scale test compared with the calculation based on German EBGEO and the British BS 8006 showed that EBGEO gives better predictions of the load distributed in the piled embankment than BS 8006. The dynamic load influences the arching and tensile stress in the geosynthetics. However, the arching can be restored during the rest period.

4.3.2.4. Büchen-Hamburg railway section field test

Schwarz and Reithel (2005) reported ground improvement of very soft organic subsoil at two sections of Hamburg-Berlin railway lines by means of installing cement columns with the mixed-in place (MIP) method, which can be characterized as a wet deep mixing technique, and by reinforcing the embankment with geogrids. The section Büchen-Hamburg was upgraded in 2003 by the German Rail company (Deutsche Bahn), to allow a train speed of 230 km/h. Due to very soft organic soil layers (peat and mud) and insufficient bearing capacity of embankment, an improvement of the railway embankment was necessary in two sections with a total length of 625 m near the railway station Büchen (see Fig. 4-22 and Fig. 4-23).

Peat soil has a water content of 80 to 330% and an organic content between 25 and 80%. Underneath these soil layers, slightly silty sand layers with a thickness up to 8 m are present, which are medium dense packed. At the base of the sand layers, boulder clay is present, which has a soft to stiff consistency and a water content of 10 to 20%.

The cemented columns (diameter 0.63 m), totally 3,260 MIP columns of a length between 5 and 8 m, were installed in square 1.5 × 1.5 m grids using the MIP-technique. Using a single auger, a cement slurry is injected continuously into the soil during penetration as well as during retrieval of the auger. On the top of the MIP-columns two layers of Fortrac R PVA

geogrid type M 400/30-30 were unrolled. To obtained an uniform bearing platform for the ballast bed, 2.5 to 3% cement was added to the filling material. A gap graded gravel-sand mixture (soil group SI according to the German Standard DIN 18196) with a coefficient of uniformity ≥6 was used. The filling material was placed in layers of maximum 30 cm thickness in accordance to the Ril 836. Each layer was compacted to a degree of compaction at least 98%.

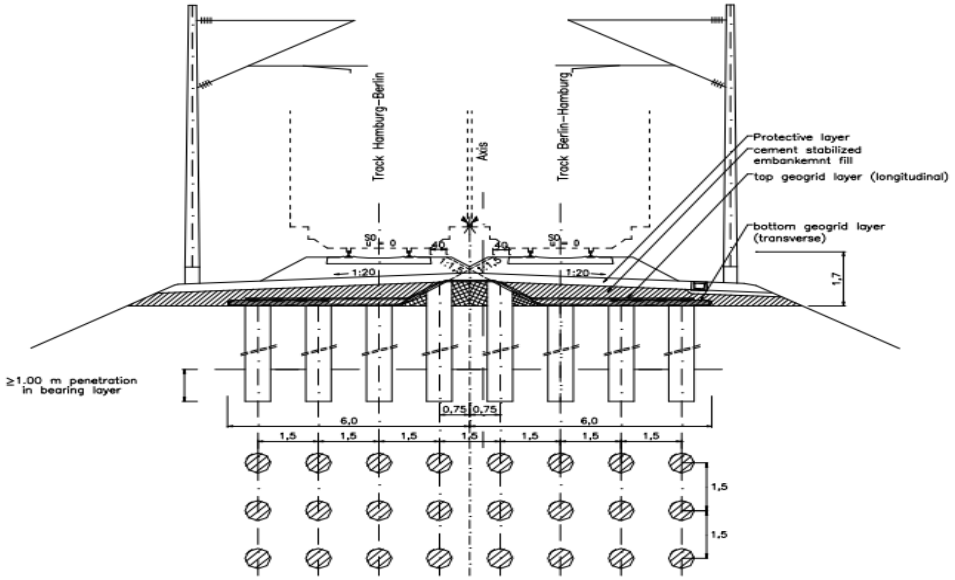

Fig. 4-22 Foundation system at section of Büchen-Hamburg (after Schwarz et al., 2005)

For laboratory testing purpose, wet grab samples were extracted from 4.5% of column every 500 m3 of treated soil, 6 unconfined compressive tests were carried out after 28 days, to determine the unconfined compressive strength q_u. According to the tests, unconfined compressive strength after 28 days of all samples exceeded the design criteria of $q_u \geq 2.2$ MN/m^2.

Fig. 4-23 Installation of MIP-columns and placing of geogrids (after Schwarz et al., 2005)

The settlement behaviour of tracks was monitored by means of geodetic measurements of the outer rail of both tracks (see Fig. 4-24). The measurements were conducted in 3 measurement sections each 20 m in length, consisting of 5 measurement points with spacing 5 m. The effectiveness of the executed improvement measures was proved by means of settlement measurements. The measurements show that the track Hamburg-Berlin has settled up 7 mm in a period of 6 months after reopening the track. This settlement can be considered as small since usually a settlement of 10 mm to 15 mm will occur, due to compaction of ballast bed, the protective layer and embankment, even if the soil condition is favourable.

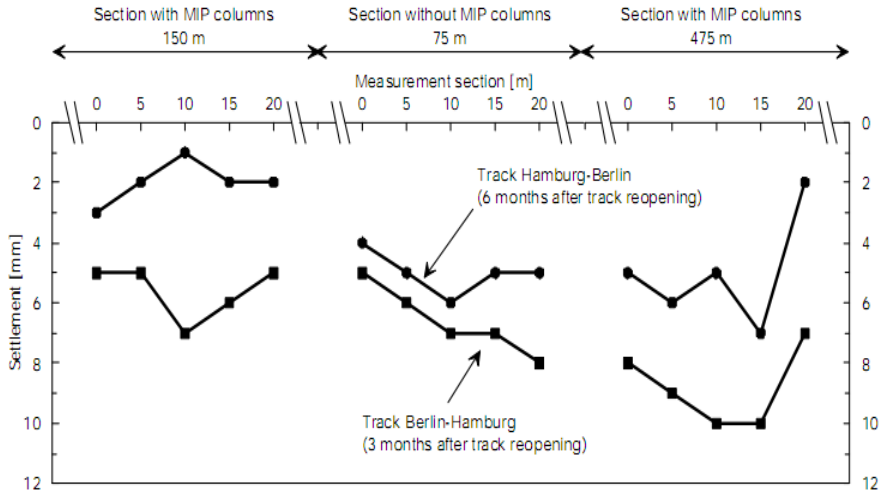

Fig. 4-24 Settlements of field measurements (after Schwarz et al., 2005)

4.3.2.5. Brogborough Lake embankment test

As reported Scottwilson (2009) that Brogborough's road embankment at A421 M1 Junction in the UK can be considered for piled embankment case. In this site, subsoil consisting of soft clay to depths up to 20 m is present. Distribution of undrained shear strength of Brogborough Lake is shown in Fig. 4-25.

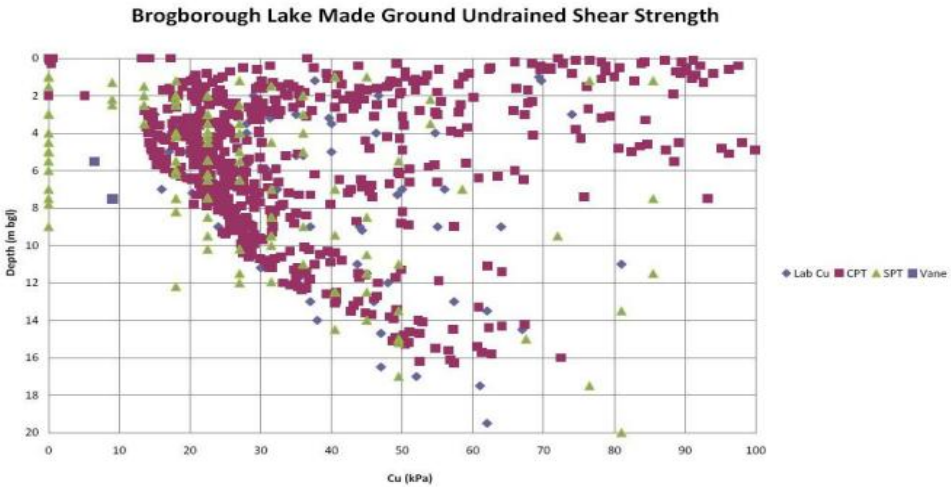

Fig. 4-25 Distribution of undrained shear strength at Brogborough Lake (after Scottwilson, 2009)

Precast driven piles of 275 mm square with 900 mm diameter of the pile cap were installed with piles spacing of 1.75 m, 2.0 m, and 2.5 m square grid pattern (see Fig. 4-26). These piles are intended to support the embankment height between 1.5 m and 7 m. Meanwhile, Huesker Fortrac R-MP with a single layer (in each direction) of high strength low strain Polyvinyl Alcohol (strain at peak strength ca. 6% was used.

Fig. 4-26 Execution of Brogborough Lake embankments (after Scottwilson, 2009)

Final erection and driving of piles have been executed in mid November 2009. Rod and plat settlement gauges above some of the pile caps with the aim of monitoring the settlement of the pile group were installed.

4.4. Summary

Some important findings regarding with experimental works in laboratories and case studies in the fields are as follows:

- Inclusion of geosynthetics into granular material can reduce horizontal outward pressure. The more amount of geosynthetic layers increases, lateral pressure will be significantly decreased. It depends on properties of geosynthetics such as tensile modulus, tensile strength, and size of aperture. Inclusion of geosynthetics in cohesive soil exhibits a reduced cohesion of compound material.
- In the field, in case of high embankment, geosynthetics can be applied using multi-layer ranging from 30 cm to 50 cm between layers. Moreover, reinforcement in soft soil using geosynthetics cannot overcome excessive settlement.
- Properties of soft soil can be easily recognized such as high water content, low undrained shear strength, low friction angle, low elasticity modulus and low compressibility.
- Piled embankment is a promising method to solve problem when constructing infrastructure over soft soil. In laboratory, it is mostly modelled as end-bearing piles that refers to shallow soft soil. Meanwhile, there is no a model has been derived for floating piles.
- Critical height of embankment is an important parameter in which differential settlement on surface of embankment is equal to zero or very few. This parameter can

be applied to determine minimum thickness of embakment in order to avoid excessive roughness of surface pavement.

- Differential settlement at surface of pavement can be reduced by utilizing a high tensile strength of geosynthetics. Particularly, in case of low embakment in which effective high of embakment is lower than critical height.
- There are various types of piles made of such as concrete pile, wooden pile, stone column or pier aggregate, stabilized column which can be used in a construction with or without pile cap. Because of these various types of piles, it will provide a little bit different final result for a construction.
- In many cases of geosynthetic-reinforced piled embankment, layer of geosynthetics functionate as a load transfer platform (LTP) which is directly laid down at base of embankment to transfer a load to piles. Multi-layer of geosynthetics can also be applied.
- Strains of geosynthetics at the face pile are higher than those at half distance between piles. Meanwhile strains at half distance between piles are higher than those at center of four piles.
- In cases of floating piles over soft soil, total settlements at surface of embankment are high enough and they are still occurred because of creep. Otherwise, differential settlement at base of embankment is small enough. Furthermore, influence of piles to reduce total settlement is really obvious.

CHAPTER 5

Modelling and Numerical Analysis

5.1. Analytical Modelling

In normal situation, the *dynamic response* of road pavements to the *moving loads* on their surface can be modeled as a beam, a plate, or the top layer of a layered soil medium. The foundation soil can be modeled as a system of elastic springs and dashpot or a homogeneous or layered half-space. The behaviour material of the pavement can be elastic or viscoelastic, whilst the foundation layers can be elastic, viscoelastic, even inelastic. The loads, concentrated or distributed of finite extent, may vary with time and move with constant or variable speed. Some methods can be done by analytical, analytical/numeric and purely numerical methods, such as finite element and boundary element methods, under conditions of plane strain or full three-dimensionality.

5.1.1. Two-layered System Elastic Theory

For flexible circular foundation under uniform load, the deflection of a two-layered soil system had been investigated by several researchers (Burmister, 1943; Meyerhof, 1978; Huang, 1969). In case axi-symmetrical problem, the basic equation to determine stress distribution satisfies equilibrium and compatibility relationships. Fig. 5-1 depicts geometry of two-layered system.

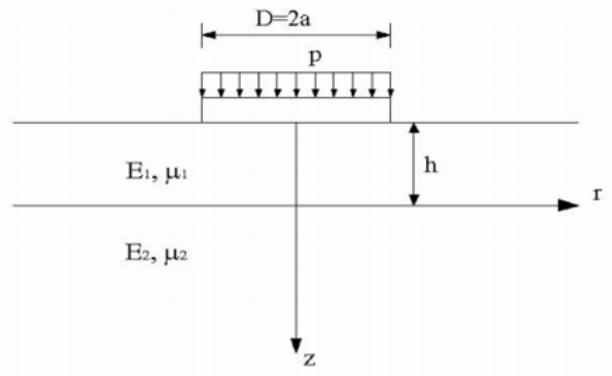

Fig. 5-1 Geometry of two-layered system (after Burmister, 1943)

For a surface load of mI_o/m_r, the vertical displacement of the surface is given as follow (Milovic, 1992):

$$w(r) = I_0(m_r)\frac{2(1-\mu_1)}{E_1} \cdot \left[\frac{1+4\,Kmh e^{-2mh} - KL e^{-4mh}}{1-(L+K+4Km^2h^2)e^{-2mh}+KL e^{-4mh}}\right] \quad (5\text{-}1)$$

Where: $n = E_2\,(1+\mu_1) / E_1(1+\mu_2)$

$K = 1\text{-}n / [1 + n\,(3\text{-}4\mu_1)]$

$L = (3\text{-}4\mu_2) - n\,(3\text{-}4\mu_1) / [(3\text{-}4\mu_2) + n]$

I_o= Bessel function of the first kind and order of zero; m = dimensionless parameter; r = horizontal distance from centerline; h = thickness of the first layer; E_1, E_2= elastic modulus of first and second layer; μ_1, μ_2= Poisson's ratio of first and second layer.

For the stress and deformation at interface between two layers, Burmister (1943) obtained the following equations:

$$\sigma_z = mI_0(m_r).\left[\frac{[1+mh-\frac{L}{2}-0.5\,K(1+2mh)]e^{-mh}+\left[KL(1-mh)-\frac{L}{2}-0.5\,K(1-2mh)\right]e^{-3mh}}{1-(L+K+4Km^2h^2)e^{-2mh}+KLe^{-4mh}}\right] \quad (5\text{-}2)$$

$$\sigma_{rz} = -mI_1(m_r).\left[\frac{[mh+\frac{L}{2}-0.5\,K(1+2mh)]e^{-mh}+\left[KLmh-\frac{L}{2}+0.5\,K(1-2mh)\right]e^{-3mh}}{1-(L+K+4Km^2h^2)e^{-2mh}+KLe^{-4mh}}\right] \quad (5\text{-}3)$$

$$w = I_0(m_r)\frac{1+\mu_1}{E_1}.\left[\frac{\begin{matrix}[2-2\mu_1+mh+\frac{L}{2}+0.5\,K(3-4\mu_1)(1+mh)]e^{-mh}- \\ \left[KL(2-2\mu_1-mh)+\frac{L}{2}+0.5\,K(3-4\mu_1)(1-2mh)\right]e^{-3mh}\end{matrix}}{1-(L+K+4Km^2h^2)e^{-2mh}+KLe^{-4mh}}\right] \quad (5\text{-}4)$$

If the elastic properties (E and μ) are equal in the two layers, the coefficient of K and L are equal to zero and the above equations reduce to Boussinesq's equations. The main assumption in layered elastic theory that the two-layer system is linear elastic and there is no relative displacement at the interface between two layers (perfectly rough interface).

Based on elastic analysis, Fox (1948) provided a solution to the vertical stress σ_z on the top of the second layer for a perfectly rough interface and perfectly smooth interface. Fig.5-2 provides the vertical stress on the axis for the case with a/h=1. Here a= radius of the circular footing, h= thickness of the first layer, d= depth, p_z= the vertical pressure on the circular footing, p_o= the pressure on the circular footing. The vertical ratio of rough interface is 0.644, 0.292, 0.081 and vertical ratio of smooth interface is 0.722, 0.305, 0.082 for E_1/E_2= 1, 10, 100 respectively.

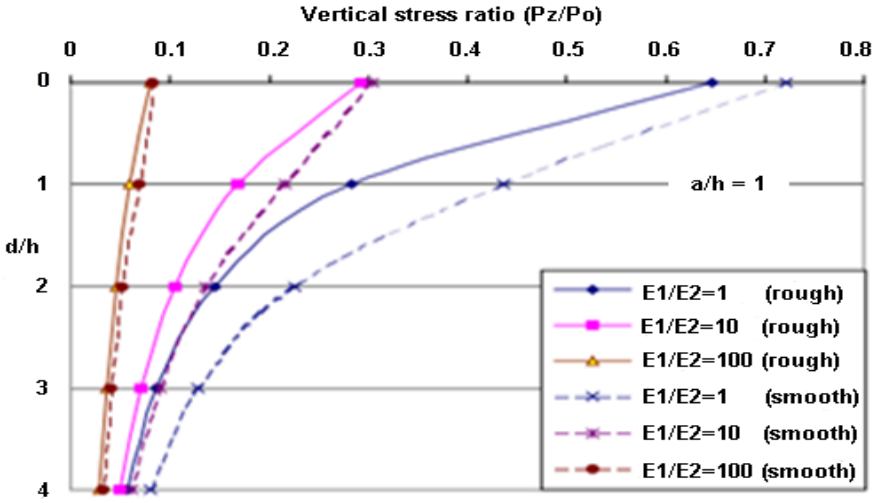

Fig. 5-2 Vertical stress distribution at the surface of second layer for two-layered system (after Fox, 1948)

5.1.2. Analytical Method for Dynamic Response of Beam and Plate on Winkler Type Elastic Foundation under Moving Loads

First of all, consider an infinitely extended elastic beam-like plate strip (modeling the pavement) on an elastic foundation (Winkler springs and daspot) under a *constant*

concentrated vertical load P moving with a *constant velocity V*. The equation of the free motion of this system is written as (Thompson, 1963):

$$D\frac{\partial^4 w}{\partial x_0^4} + kw + c\frac{\partial w}{\partial t} + \rho h\frac{\partial^2 w}{\partial t^2} = 0 \tag{5-5}$$

where $w = w(x_0,t)$ is the lateral deflection of plate strip, k and c is the foundation stiffness and damping, respectively. $D=E\cdot h^3/12(1-\nu^2)$ is the flexural rigidity of the plate strip with E and ν being the modulus of elasticity and Poisson's ratio, respectively. Mass density ρ and the thickness of plate strip h, while x_0 and z are the fixed coordinates along the length of the strip and in the vertical direction, respectively, whilst t denotes time.

Now, it is introduced a new coordinate system x, z ,which moves with the load P. Thus, one has

$$x = x_0 - V\cdot t \tag{5-6}$$

with the new coordinate system, the previous equation becomes

$$D\frac{\partial^4 w}{\partial x^4} + kw - cV\frac{\partial w}{\partial x} + \rho h V^2\frac{\partial^2 w}{\partial x^2} = 0 \tag{5-7}$$

indicating that w in the moving coordinate system is independent of time after all the transient vibrations have disappeared and the motion of the plate is said to be steady-state.

By introducing some symbols

$$\beta = \left(\frac{k}{4D}\right)^{1/4},\ \theta = \frac{V}{V_{cr}},\ \zeta = \frac{c}{c_{cr}},\ V_{cr} = \left(\frac{4kD}{\rho^2 h^2}\right)^{1/4},\ c_{cr} = 2(k\rho h)^{1/2}$$

into Eq. 5-7 above, we may rewrite the equation into the form

$$\frac{\mathrm{d}^4 w}{\mathrm{d}x^4} + 4\theta^2\beta^2\frac{\mathrm{d}^2 w}{\mathrm{d}x^2} - 8\zeta\theta\beta^3\frac{\mathrm{d}w}{\mathrm{d}x} + 4\beta^4 w = 0 \tag{5-8}$$

Therefore, the characteristic equation of the equation is

$$m^4 + 4\theta^2\beta^2 m^2 - 8\zeta\theta\beta^3 m + 4\beta^4 = 0 \tag{5-9}$$

with a discriminant Δ, which may be positive, negative or zero. For instance, at case $\Delta > 0$, after application of boundary conditions ($w=dw/dx=0$) at $x = \pm\infty$, compatible of deflection, slope and bending moment of the plate (pavement) under loading and formulation of the discontinuity in the shear load. Finally, we can obtain:

$$w = -\frac{P\beta}{2k}\left[\frac{\eta e^{\mp\eta\beta x}}{\eta^4+\theta^2\eta^2+0.5(\theta\zeta/\eta)^2}\right]\left[\frac{-\left(\frac{\theta\zeta}{\eta}\mp\eta^2\right)}{\eta(2\theta^2+\eta^2\pm 2\theta\zeta/\eta)^{1/2}}.\sin(2\theta^2+\eta^2\pm 2\theta\zeta/\eta)^{1/2}\beta x + \cos 2\theta 2+\eta 2\pm 2\theta\zeta/\eta 1/2\beta x\right] \tag{5-10}$$

where in case of double signs the upper sign correspond to $x > 0$, while the lower thing to $x<0$. In the above $\eta = A_1 / \beta$, with A_1 is the real positive part of the first root.

Now, consider an elastic beam of infinite extent (modeling the pavement) on elastic foundation (Winkler springs and dashpot) under a *vertical distributed* (over a finite length) and *time-dependent load p* (x_0,t) moving with a constant velocity V. The equation of motion of this system in fixed Cartesian coordinates (x_0,z) is (Kim and Roesset, 2003):

$$EI\frac{\partial^4 v}{\partial x_0^4} + kv + c\frac{\partial v}{\partial t} + m\frac{\partial^2 w}{\partial t^2} = p(x_0 t) \tag{5-11}$$

where $v = v(x_0,t)$ is the lateral beam deflection, I the cross-sectional moment of inertia, m the mass per unit length of the beam, k the foundation stiffness per unit length and c is the viscous damping constant. By using coordinate system (x,y), which moving load during a time $x = x_0 - V \cdot t$, we may rewrite the Eq. 5-11 in another form:

$$EI\frac{\partial^4 v}{\partial x^4} + kvc\left(\frac{\partial v}{\partial t} - V\frac{\partial v}{\partial x}\right) + m(\frac{\partial^2 v}{\partial t^2} - 2V\frac{\partial^2 v}{\partial x \partial t} + V^2\frac{\partial^2 v}{\partial x^2}) = p(x,t) \qquad (5\text{-}12)$$

When a distributed load p moves harmonically with time, i.e., $p(x,t) = p_0(x)e^{i\Omega t}$, where $i = \sqrt{-1}$ and Ω the operational load frequency, one has that $v(x,t) = v_0(x)\, e^{i\Omega t}$, the Eq. 5-12 becomes:

$$EI\frac{\partial^4 v_0}{\partial x^4} + kv_0 + c\left(i\Omega v_0 - V\frac{\partial v_0}{\partial x}\right) + m(-\Omega^2 v_0 - 2i\Omega V\frac{\partial v_0}{\partial x} + V^2\frac{\partial v_0}{\partial x^2}) = p_0(x) \qquad (5\text{-}13)$$

For the general case of time variation of the load p, one can apply onto the double *Fourier transform* with respect to x and t and then we obtain:

$$[EI\xi^4 + k + ic(\omega - V\xi) - m(\omega - V\xi)^2]\bar{\bar{v}}(\xi,\omega) = \bar{\bar{p}}(\xi,\omega) \qquad (5\text{-}14)$$

where: $\bar{\bar{v}}, \bar{\bar{p}} = \int_{-\infty}^{\infty}\int_{-\infty}^{\infty}(v,p)e^{-i\xi x}e^{i\omega t}dxdt$

Finally, consider the three-dimensional extension for an elastic plate of infinite extent on an elastic foundation (Winkler springs and dashpots) under a vertical distributed (over a finite surface) and time-dependent load $p(x_0,y_0,t)$ moving with a constant velocity V along the x-direction. The equation of motion of this system in fixed Cartesian coordinates (x_0,y_0,z) is (Kim and Roesset, 2003):

$$D\left(\frac{\partial^4 w}{\partial x_0^4} + 2\frac{\partial^4 w}{\partial x_0^2 \partial y^2} + \frac{\partial^4 w}{\partial y^4}\right) + kw + c\frac{\partial w}{\partial t} + m\frac{\partial^2 w}{\partial t^2} = p(x_0,y,t) \qquad (5\text{-}15)$$

where D is the flexural rigidity of plate, w is deflection along the z-direction and x_0,y is the middle plane of the plate.

5.1.3. Analytical Method for Dynamic Response of Layered Half-space under Moving Loads

Firstly, consider an elastic layered three-dimensional half-space (whose top layer can model the pavement) under a concentrated vertical time-dependent load moving on its surface with constant velocity V (Grundmann et al., 1999). For a homogeneous elastic layer, the equations of motion may be written:

$$\mu u_{i,jj} + (\lambda + \mu)u_{j,ij} - \rho\ddot{u}_i = 0 \qquad (5\text{-}16)$$

where u_i (i=1,2,3) is the displacement vector, λ and μ are the *Lame elastic constants*, ρ is the mass density, commas and overdots denote space and time differentiation, respectively. Axes x and y corresponding to i=1 and i=2 denote the two horizontal directions, while axis z for i=3 denotes the vertical direction. The Eq. 5-16 above can be expressed using the aid of Helmholtz's decomposition as:

$$u_i = \emptyset_i + \varepsilon_{ijk}\psi_{kj} \qquad (5\text{-}17)$$

where the scalar ϕ and vector ψ_i functions satisfy the wave equations

$$\emptyset_{jj} - \frac{1}{c_p^2}\ddot{\emptyset} = 0\,, \quad \psi_{i,jj} - \frac{1}{c_s^2}\ddot{\psi}_i = 0 \qquad (5\text{-}18)$$

with ε_{ijk} being the alternating tensor and $c_p = \sqrt{(l+2\mu)/\rho}$ and $c_s = \sqrt{\mu/\rho}$ the dilatational and shear wave velocities.

5.1.4. Critical Velocity

The velocity of high-speed train can approach or exceed the characteristic wave velocity of the dynamic system comprising of the underlying soft ground, trackbed/embankment, and the moving load. As the train's velocity approaches some *'critical velocity'* large deformation can occur. These motions could be dangerous for train and the integrity of the structure. The velocity of Rayleigh surface in soft sandy soils may be vary low (90-130 m/s) even such wave velocity in some soft soils in Netherlands can be as low as 29-47 m/s, which is considerably lower than the railway's proposed design speed, the matter clearly required investigation.

Kenney (1954) gave some insight into parameters that seem to be of importance to the critical velocity, v_{cr}, as the equation below:

$$v_{cr} = \sqrt[4]{\frac{4kEI}{\rho^2}} \tag{5-19}$$

where k = spring constant per unit length of beam
E = modulus of elasticity of beam
I = moment of inertia of beam
ρ = mass per unit length of beam

Kinney discusses a point load moving with constant velocity over an *Euler-Bernoulli* beam on visco-elastic Winkler medium. In Kenney's analytical solution, the embankment sub-soil system has to be simplified as a single beam supported by linear springs.

5.1.5. Explicit Model for Cyclic Accumulation

In the implicit procedure, each cycle is calculated at a rate of σ–ε constitutive model. The accumulation results as a by-product due to the not perfectly closed stress or strain loops. Elastoplastic multi-surface models (Mroz et al., 1978; Chaboche, 1994), endochronic model (Valanis&Lee, 1984) or hypoplastic model intergranular strain (Kolymbas, 1991; Gudehus, 1996; Wolffersdorf, 1996; Niemunis&Herle, 1997) can be used. The applicability of the implicit method is restricted to a low number of cycles (N<50) because with each increment an accumulation of systematic errors of constitutive model or the integration scheme takes places (Niemunis, 2005). Even small errors accumulate significantly (e.g. with a factor 10^6, if 10^4 cycles are calculated each with 100 increments). Therefore, a constitutive model of an unreachable perfection would be necessary. Also the large calculation effort sets boundaries to the application of the implicit method. Wolffersdorff & Schwab (2001) had to restrict their implicit FE calculation of Watergate 'Uelzen 1' to less than 25 cycles.

For high-cyclic loading, in general, explicit models are the better choice. Treatment of the process of accumulation under cyclic loading is similar to a process governed by viscosity. The number of cycles N replaces the time t. First, two are calculated implicity with strain increments (see Fig. 5-3) using a rate of σ–ε constitutive model. This implicit calculation can be performed quasi-static or dynamic. During the second cycle in each integration point the strain loop is recorded as a series of discrete strain points. The recording follows some predefined criteria. The strain amplitude $\varepsilon^{\text{ampl}}$ is determined from this strain loop. The first cycle is not suitable for the determination of $\varepsilon^{\text{ampl}}$, since the deformation in the first cycle can significantly differ from those in the subsequent cycles (the first quarter of the first cycle up to the maximum load is a first loading). The amplitude of the second cycle is more representative for the amplitudes in the following cycles.

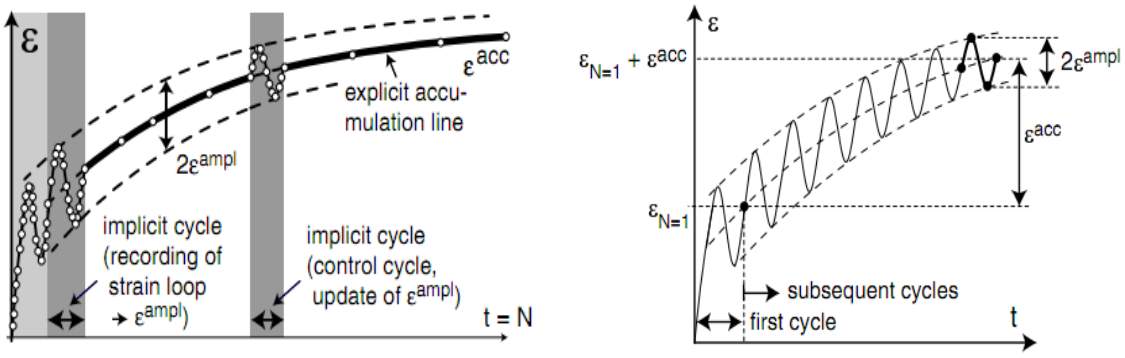

(a) (b)

Fig. 5-3 Cyclic loading (a) Procedure of an explicit calculation of accumulation (b) Evolution of total strain in a cyclic triaxial test (after Wichtmann, 2005)

The accumulation starting from the second cycle is calculated directly by means of an equation of the shape:

$$\dot{\mathbf{T}} = E : (\mathbf{D} - \mathbf{D}^{acc}) \tag{5-20}$$

where: $\dot{\mathbf{T}}$: Jaumann stress rate, $\mathbf{D}$: strain rate, $\mathbf{D}^{acc}$: given accumulation rate, E: elastic stiffness, without following the strain path during the particular cycles. The equation leads to an accumulation of stress (e.g. $\dot{\mathbf{T}}$= -E: D^{acc} at D=0) and/or strain (D= D^{acc} at $\dot{\mathbf{T}}$=0). When $\dot{\mathbf{T}}$=0 the strain follows the average accumulation curve $\varepsilon^{acc}(N)$.

The strain amplitude ε^{ampl} is assumed constant for the explicit calculation. The explicit calculation may be interrupted after definite numbers of cycles and ε^{ampl} can be updated in the an implicit so-called *control cycle*.

5.1.5.1. Model of Sawicki & Swidzinski

Sawicki and Swidzinski (1989) basing on experimental results from their simple shear device, proposed for the cyclic accumulation a purely volumetric accumulation rule

$$\epsilon_{ij}^{acc} = \frac{1}{3}\epsilon^{acc\,v}\delta_{ij} \tag{5-21}$$

in which the volumetric strain, $\epsilon^{acc\ v}$, was described by a so-called '*universal densification curve*'

$$\Phi(\tilde{N}) = C_1 \ln(1 + C_2\tilde{N}) \tag{5-22}$$

with the state "compaction" $\Phi = \Delta n / n_0$, with n = porosity, the number of cycles weighted by the amplitude

$$\tilde{N} = \int J\, dN = \int \frac{1}{2}\left|\varepsilon^{*}_{ampl}\right|^2 dN = \frac{1}{4}\left(\gamma^{ampl}\right)^2 N \tag{5-23}$$

and the material constant C_1 and C_2. The tensor ε^{ampl} contains the amplitudes of the particular strain component. The latter transformation in Eq. (5-23) is valid for the case of cyclic simple shear tests with a constant shear strain amplitude γ^{ampl}. The compaction rate $\Phi = \delta\Phi/\delta N$ is obtained from Eq. 5-24:

$$\Phi = \frac{C_1 C_2\, J}{(1 + C_2 N)} = C_1 C_2\, J^{\left(\frac{-\Phi}{C_1}\right)} \tag{5-24}$$

The model of Sawicki & Swidzinski was performed on tests with a relatively low number of cycles ($N < 10^3$). A major drawback of the model is that only the volumetric accumulation, whereas the deviatoric one not be considered.

5.1.5.2. Model of Bouckovalas et al.

The model of Bouckovalas et al. (1984) presents both the accumulation of volumetric and the accumulation of deviatoric strains as depicted the equation below:

$$\dot{\varepsilon}_v^{acc} = A(2\gamma^{ampl})^a I^c f \tag{5-25}$$

$$\dot{\varepsilon}_q^{acc} = \pm B(\eta^{av}/2)^b (2\gamma^{ampl})^a I^c \tag{5-26}$$

The value of average stress ratio η^{av} can be positive or negative, whilst *A*, *B*, *a*, *b* and *c* are material constants. The dependence of the accumulation rates on the historiotropy is expressed:

$$I = \int_0^N (2\gamma^{ampl} N)^a N^c dN \tag{5-27}$$

For cycles with a constant shear strain amplitude, the rates are proportional to $N^{c(c+1)}$. The parameter *f* is stress-dependent. It takes the value 1 on the *p*-axis and is zero on the critical-state line.

The model of Bouckovalas et al. (1984) predicts the cyclic flow rule correctly: ε_v^{acc} vanishes on the critical state line, while ε_q^{acc} becomes zero at $\eta^{av} = 0$. A power law is used for the dependence of the accumulation rates on the number of cycles. In the model, a constant $a = 3$ and $c = -1.5$ are chosen and factor *f* remains vague in the mathematical definition. The model uses a state variable for the historiotropy which considers also the amplitude of the cycles. The model gives a too strong amplitude-dependence with approximate value $\varepsilon^{acc} \sim (\varepsilon^{ampl})^3$.

5.2. Consitutive Models in Numerical Analysis

5.2.1. Mohr Coulomb Model

Plasticity has a relationship which strain is irreversible. To evaluate the plasticity in a calculation, a yield function *f*, can be used as a function between stress and strain. Generally, a plastic perfectly model is a constitutive model with a certain yield surface, a yield surface defined by model parameters and not influenced by plastic strain. For the stresses under yield surface, they behave fully elastic and strains are reversible.

5.2.1.1. *Elastic Perfectly Plastic Behaviour*

A basic principle of elastic plasticity model is that strain and strain rate are devided by elastic and plastic parts:

$$\underline{\varepsilon} = \underline{\varepsilon}^e + \underline{\varepsilon}^p \;\; and \;\; \underline{\dot{\varepsilon}} = \underline{\dot{\varepsilon}}^e + \underline{\dot{\varepsilon}}^p \tag{5-28}$$

Hooke law is used to correlate the elastic stress rate and strain rate. Substituting the equation above into Hooke‘s law gives:

$$\underline{\sigma'} = \underline{D}^e . \underline{\dot{\varepsilon}}^e = \underline{D}^e . \left(\underline{\dot{\varepsilon}} - \underline{\dot{\varepsilon}}^p\right) \tag{5-29}$$

According to classical plasticity theory (Hill, 1958), a plastic strain rate is proportional to a derivative of stress yield function. It means that the plastic strain rate may be expressed as a vector perpendicularly with the yield surface (see Fig. 5-4). The classical form of plasticity

theory is so-called as *associated plasticity*. But, for Mohr-Coulomb yield function, this theory will give overestimate dilatancy prediction. Therefore, besides yield function *f*, it is used a plastic potential function *g*. At case $g \neq f$, it is so-called as *non-associated plasticity*. Generally, strain rate can be written as:

$$\underline{\dot{\varepsilon}}^p = \lambda \frac{\partial g}{\partial \sigma'} \tag{5-30}$$

where λ is a plastic multiplied factor. For pure elastic, λ is equal to zero and for plastic behaviour, λ is a positive value.

$$\lambda = 0\,,\ for: f < 0\ or: \frac{\partial f^T}{\partial_{\sigma'}} \cdot D^e \cdot \dot{\varepsilon} \leq 0\ )\ elastic \tag{5-31}$$

$$\lambda > 0\,,\ for: f = 0\ and: \frac{\partial f^T}{\partial_{\sigma'}} \cdot D^e \cdot \dot{\varepsilon} > 0\ )\ plastic \tag{5-32}$$

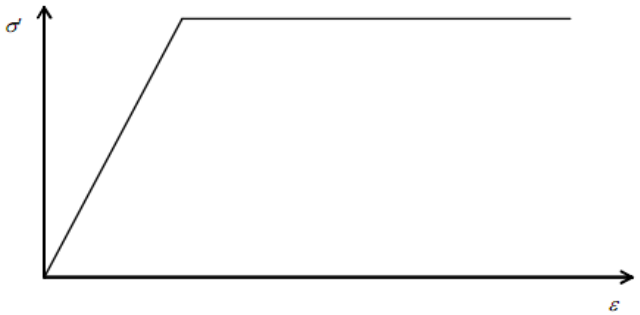

Fig. 5-4 Basic principle of elastic perfectly plasticity (after Hill, 1958)

The equations can be used to obtain a relationship between effective stress rate and strain rate for elastoplastic model (Smith & Griffith, 1982; Vermeer, 1982):

$$\underline{\dot{\sigma}}' = \left(\underline{\underline{D}}^e - \frac{\alpha}{d}.\underline{\underline{D}}^e.\frac{\partial_g}{\partial_{\sigma'}}.\frac{\partial f^T}{\partial_{\sigma'}}.\underline{\underline{D}}^e\right).\underline{\dot{\varepsilon}} \tag{5-33}$$

with: $d = \frac{\partial f^T}{\partial_{\sigma'}} \underline{\underline{D}}^e \frac{\partial_g}{\partial_{\sigma'}}$

Parameter α can be used as a switch. If material behaviour is elastic, α value is equal to zero, whilst α value is one when material behaviour is plastic. Plastic theory above is limited only for a continuous and smooth yield surface, and not included into a multi-surface of yield likes MC model. For multi-yield surface, Koiter (1960) took into consider to flow vertices involving two or more plastic potential functions:

$$\underline{\dot{\varepsilon}}^p = \lambda_1 \frac{\partial g_1}{\partial_{\sigma'}} + \lambda_2 \frac{\partial g_2}{\partial_{\sigma'}} + \cdots \tag{5-34}$$

5.2.1.2. *Formulation of Mohr-Coulomb Model*

The yield condition of Mohr-Coulomb encompasses six yield functions when formulated in context of main stress (Smith & Griffin, 1982):

$$f_{1a} = \frac{1}{2}(\sigma'_2 - \sigma'_3) + \frac{1}{2}(\sigma'_2 - \sigma'_3)\sin\emptyset\ - c.\cos\emptyset \leq 0 \tag{5-35a}$$

$$f_{1b} = \frac{1}{2}(\sigma'_3 - \sigma'_2) + \frac{1}{2}(\sigma'_3 - \sigma'_2)\sin\emptyset\ - c.\cos\emptyset \leq 0 \tag{5-35b}$$

$$f_{2a} = \frac{1}{2}(\sigma'_3 - \sigma'_1) + \frac{1}{2}(\sigma'_3 - \sigma'_1)\sin\emptyset\ - c.\cos\emptyset \leq 0 \tag{5-35c}$$

$$f_{2b} = \frac{1}{2}(\sigma'_1 - \sigma'_3) + \frac{1}{2}(\sigma'_1 - \sigma'_3)\sin\emptyset - c.\cos\emptyset \leq 0 \quad (5\text{-}35d)$$

$$f_{3a} = \frac{1}{2}(\sigma'_1 - \sigma'_2) + \frac{1}{2}(\sigma'_1 - \sigma'_2)\sin\emptyset - c.\cos\emptyset \leq 0 \quad (5\text{-}35e)$$

$$f_{3b} = \frac{1}{2}(\sigma'_2 - \sigma'_1) + \frac{1}{2}(\sigma'_2 - \sigma'_1)\sin\emptyset - c.\cos\emptyset \leq 0 \quad (5\text{-}35f)$$

two parameters of plastic model emerge into yield function are the friction angle ϕ and cohesion *c* well known in geotechnical engineering. These yield functions together will form a hexagonal cone in main stress space as shown in Fig. 5-5.

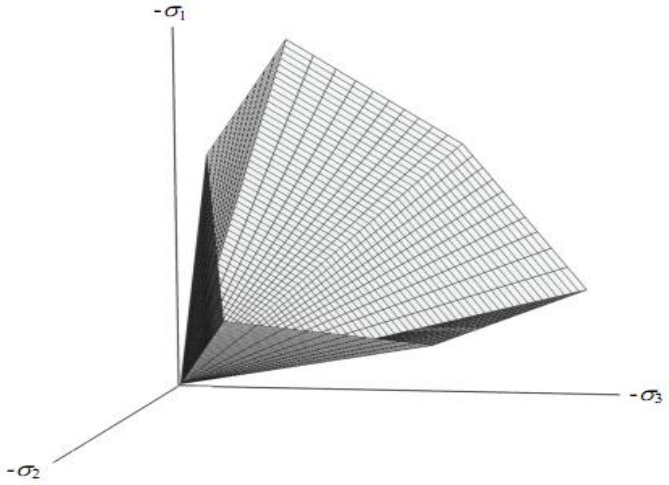

Fig. 5-5 Mohr-Coulomb yield surface in main stress space (*c*=0) (after Smith et al., 1982)

Besides yield functions, there are six plastic potential functions for MC model:

$$g_{1a} = \frac{1}{2}(\sigma'_2 - \sigma'_3) + \frac{1}{2}(\sigma'_2 - \sigma'_3)\sin\psi \quad (5\text{-}36a)$$

$$g_{1b} = \frac{1}{2}(\sigma'_3 - \sigma'_2) + \frac{1}{2}(\sigma'_3 - \sigma'_2)\sin\psi \quad (5\text{-}36b)$$

$$g_{2a} = \frac{1}{2}(\sigma'_3 - \sigma'_1) + \frac{1}{2}(\sigma'_3 - \sigma'_1)\sin\psi \quad (5\text{-}36c)$$

$$g_{2b} = \frac{1}{2}(\sigma'_1 - \sigma'_3) + \frac{1}{2}(\sigma'_1 - \sigma'_3)\sin\psi \quad (5\text{-}36d)$$

$$g_{3a} = \frac{1}{2}(\sigma'_1 - \sigma'_2) + \frac{1}{2}(\sigma'_1 - \sigma'_2)\sin\psi \quad (5\text{-}36e)$$

$$g_{3b} = \frac{1}{2}(\sigma'_2 - \sigma'_1) + \frac{1}{2}(\sigma'_2 - \sigma'_1)\sin\psi \quad (5\text{-}36f)$$

Plastic potential function has a third plastic parameter, namely dilation angle ψ. This parameter is needed to model an increment of plastic volumetric strain positively as it actually occurs on stiff soil.

For $c > 0$, Mohr-Coulomb criteria allow to tensile stress, but in fact, soil only reminds this stress very small, even nothing. Plaxis software can model by using constraint of tensile stress. This constraint incorporates with three additional yield function:

$$f_4 = \sigma'_1 - \sigma_t \leq 0 \quad (5\text{-}37a)$$

$$f_5 = \sigma'_2 - \sigma_t \leq 0 \quad (5\text{-}37b)$$

$$f_6 = \sigma'_3 - \sigma_t \leq 0 \quad (5\text{-}37c)$$

The allowable tensile stress σ_t can be setup (default) as zero. For three yield functions, these can be used with an associated flow rule. The Mohr-Coulomb model needs five parameters. Generally, these parameters can be obtained from laboratory tests as follows:

E : Young‘s modulus [kN/m^2]

ν	: Poisson's ratio	[-]
ϕ	: friction angle	[^{o}]
c	: cohesion	[kN/m^2]
ψ	: dilation angle	[^{o}]

5.2.2. The Hardening Soil (HS) Model

In this model the total strains are calculated using a stress-dependent stiffness, different for both virgin loading and un-/reloading. The plastic strains are calculated by introducing a multi-surface yield criterion. Hardening is assumed to be isotropic depending on both the plastic shear and volumetric strain. For the frictional hardening a non-associated and for the cap hardening an associated flow rule is assumed. First the model is written in its rate form. Therefore the essential equations for the stiffness modules, the yield, failure and plastic potential surfaces are given.

In contrast to an elastic perfectly-plastic model, the yield surface of the Hardening Soil model is not fixed in the principal stress space, but it can expand due to plastic straining. Distinction is made between two main types of hardening, namely *shear hardening* and *compression hardening*. Shear hardening is used to model irreversible strains due to primary deviatoric loading, whereas compression hardening is used to model irreversible plastic strains due to primary compression in oedometer loading and isotropic loading.

5.2.2.1. *Constitutive Equations for Standard Drained Triaxial Test*

A basic idea for the formulation of the Hardening Soil model is the hyperbolic relationship between the vertical strain ε_1 and the deviatoric stress q in primary triaxial loading (see Fig. 5-6). In case a drained triaxial test, the observed relationship between the axial strain and the deviatoric stress can be well approximated by a hyperbola (Kondner&Zelasko, 1963). Standard drained triaxial test tends to yield curves that can be described by:

$$\varepsilon_1 = \frac{q_a}{2E_{50}} . \frac{(\sigma_1-\sigma_3)}{q_a-(\sigma_1-\sigma_3)} \quad for: \; q < q_f \tag{5-38}$$

The ultimate deviatoric stress q_f and quantity q_a in Eq.5-38 are defined as:

$$q_f = \frac{6\sin\varphi_p}{3-\sin\varphi_p}\left(p + c.\cot\varphi_p\right) , \quad q_a = \frac{q_f}{R_f} \tag{5-39}$$

The above relationship for q is derived from the Mohr-Coulomb failure criteria, which involves the strength parameters c and ϕ_p. As soon as $q = q_f$, the failure criterion is satisfied and perfectly plastic yielding occurs. The ratio between q_f and q_a is given by the failure ratio R_f , which should obviously be smaller than 1. R_f = 0,9 often is a suitable default setting.

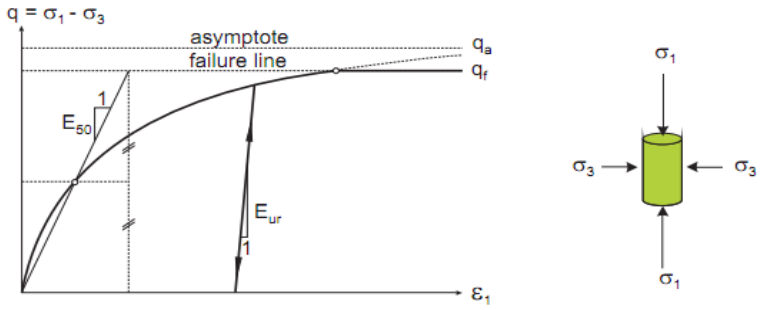

Fig. 5-6 Hyperbolic stress-strain relation in primary loading for a standard drained triaxial test (after Schanz et al.,1999)

5.2.2.2. *Stiffness for Primary Loading*

The stress strain behaviour of primary loading is highly nonlinear. The parameter E_{50} is the confining stress dependent stiffness modulus for primary loading. E_{50} is used instead of the initial modulus E_i for *small strain* which, as a tangent modulus, is more difficult to determine experimentally. It is given by equation:

$$E_{50} = E_{50}^{ref} \left(\frac{\sigma_3 + c.\cot\varphi_p}{\sigma^{ref} + c.\cot\varphi_p} \right)^m \tag{5-40}$$

E_{50}^{ref} is a reference stiffness modulus corresponding to the reference stress p^{ref}. The actual stiffness depends on the minor principal stress σ_3', which is the effective confining pressure in a triaxial test. The amount of stress dependency is given by the power *m*. Von Soos (2001) showed that *m* values range between 0.4 and 1.0. In order to simulate a logarithmic stress dependency, as observed for soft clay, the power should be taken equal to 1.0 and for *m* value sands is 0.5. As a secant modulus E_{50}^{ref} is determined from a triaxial stress-strain-curve for a mobilization of 50% of the maximum shear strength q_f.

5.2.2.3. *Stiffness for un-/reloading*

The stress paths for unloading and reloading, another stress-dependent stiffness modulus is used:

$$E_{ur} = E_{ur}^{ref} \left(\frac{\sigma_3 + c.\cot\varphi_p}{\sigma^{ref} + c.\cot\varphi_p} \right)^m \tag{5-41}$$

where E_{ur}^{ref} is the reference Young's modulus for unloading and reloading, corresponding to the reference pressure σ^{ref}. The un-/reloading path is modeled as purely (non-linear) elastic. The elastic components of strain ε^e are calculated according to a *Hookean* type of elastic relation.

$$G_{ur} = \frac{1}{2(1+v_{ur})} E_{ur} \ , \ \sigma^{ref} = 100\ kPa \tag{5-42}$$

For drained triaxial test stress paths with $\sigma_2 = \sigma_3$ = constant, the elastic Young's modulus E_{ur} remains constant and the elastic strain are given by equations:

$$\varepsilon_1^e = \frac{q}{E_{ur}} \ , \ \ \varepsilon_2^e = \varepsilon_3^e = v_{ur} \frac{q}{E_{ur}} \tag{5-43}$$

5.2.2.4. *Yield Surface, Failure Conditions, Hardening Law*

For the triaxial case, the two yield functions f_{12} and f_{13} are defined according to Eq. 5-38 and 5-39. Here the measure of the plastic shear strain γ^p is used as the relevant parameter for the frictional hardening.

$$f_{12} = \frac{q_a}{E_{50}} . \frac{(\sigma_1 - \sigma_2)}{q_a - (\sigma_1 - \sigma_2)} - \frac{2(\sigma_1 - \sigma_2)}{E_{ur}} - \gamma^p \tag{5-44}$$

$$f_{13} = \frac{q_a}{E_{50}} . \frac{(\sigma_1 - \sigma_3)}{q_a - (\sigma_1 - \sigma_3)} - \frac{2(\sigma_1 - \sigma_3)}{E_{ur}} - \gamma^p \tag{5-45}$$

with the definition:

$$\gamma^p = \varepsilon_1^p - \varepsilon_2^p - \varepsilon_3^p = 2\varepsilon_1^p - \varepsilon_v^p \approx 2\varepsilon_1^p \tag{5-46}$$

In reality, plastic volumetric strains ε_v^p will never precisely equal to zero, but for hard soils plastic volume changes tend to be small when compared with the axial strain, so that the approximation in Eq. 5-46 will generally be accurate. For a given constant value of the

hardening parameter, the yield condition $f_{12} = f_{13} = 0$ can be visualized in p'-q-plane by means of a yield locus. For m = 1.0 straight line is obtained, but for slightly curved yield loci correspond to lower of the exponent. Fig. 5-7 shows the shape of successive yield loci for m = 0.5, being typical for hard soils.

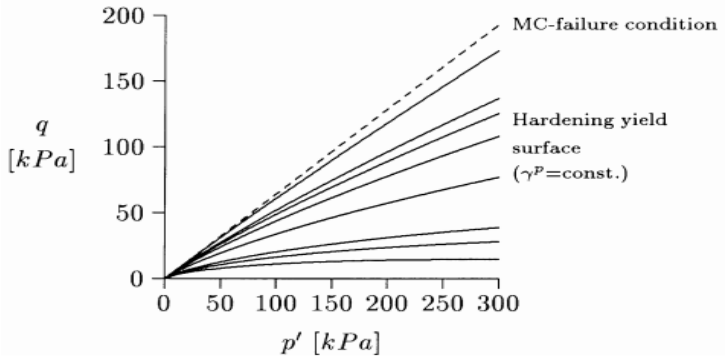

Fig. 5-7 Successive yield loci for various values of the hardening parameter γ^{p} and failure surface (after Schanz et al., 1999)

In contrast to elastic perfectly Mohr-Coulomb (MC) model, in the Hard Soil (HS) model, plastic strains may occur before the limit MC-failure stress reached. The HS model incorporates two other yield surfaces, which are not fixed in principal stress space, but they may expand and soil hardening is simulated due to plastic straining. As illustrated in Fig. 5-8, distinction is made between two types of hardening, which are shear hardening and compression hardening. For the shear hardening law, a yield function f_s is introduced, which is a function of the triaxial loading stiffness E_{50} and for the compression hardening a yield function f_c is formulated.

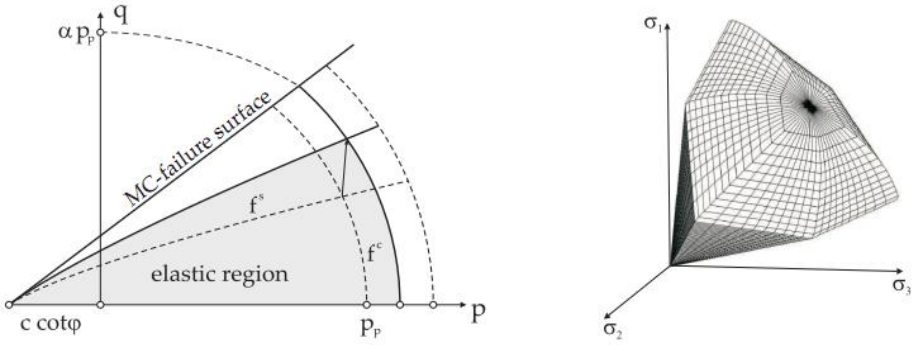

Fig. 5-8 Yield surface of HS model, a) Successive yield loci for shear hardening and compression hardeing in *p-q* space, b) Total yield contour in principal stress space (after Schanz et al., 1999)

5.2.2.5. *Flow Rule, Plastic Potential Functions*

As for all plasticity model, the HS model involves a relationship between *rates of plastic strain*, i.e. a relationship between ε_v^{p} and γ^{p}. This flow rule has the linear form:

$$\dot{\varepsilon}_v^p = \sin\psi_m \dot{\gamma}^p \tag{5-47}$$

The expression of the mobilized dilatancy angle ψ_m is:

$$\sin\psi_m = \frac{\sin\varphi_m - \sin\varphi_{cv}}{1 - \sin\varphi_m \sin\varphi_{cv}} \tag{5-48}$$

where ϕ_{cv} is the critical state friction angle, being a material constant independent of density (Schanz & Vermeer, 1996), and ϕ_m is the mobilized friction angle:

$$\sin\psi_m = \frac{\sigma_1 - \sigma_3}{\sigma_1 + \sigma_3 - 2c.\ \cot\varphi_p} \tag{5-49}$$

The above equations correspond to the well-known stress-dilatancy theory (Rowe 1962, Rowe, 1971). The essential property of the stress-dilatancy theory is that the material contracts for small stress ratio $\phi_m < \phi_{cv}$, whilst dilatancy occurs for high stress ratio $\phi_m < \phi_{cv}$. At failure, when the mobilized friction angle is equal to the failure angle, ϕ_p, it is found the previous equation, that:

$$\sin\psi_{cv} = \frac{\sin\varphi_p - \sin\psi_p}{1 - \sin\varphi_p \sin\psi_p} \tag{5-50}$$

Hence, the critical state angle can be computed from failure angle ϕ_p and ψ_p . The definition of flow rule is equivalent to the definition of the plastic potential functions g_{12} and g_{13} according to:

$$g_{12} = \frac{1}{2}(\sigma_1 - \sigma_2) - \frac{1}{2}(\sigma_1 - \sigma_2)\sin\psi_m \tag{5-51a}$$

$$g_{13} = \frac{1}{2}(\sigma_1 - \sigma_3) + \frac{1}{2}(\sigma_1 - \sigma_3)\sin\psi_m \tag{5-51b}$$

By using the *Koiter-rule* (Koiter 1960) for yielding depending on two yield surface (*Multi-surface plasticity*) one finds:

$$\dot{\varepsilon}^p = \dot{\Lambda}_{12}\frac{\partial_{g_{12}}}{\partial_\sigma} + \dot{\Lambda}_{13}\frac{\partial_{13}}{\partial_\sigma} = \dot{\Lambda}_{12}\begin{bmatrix}\frac{1}{2} - \frac{1}{2}\sin\psi \\ -\frac{1}{2} - \sin\psi \\ 0\end{bmatrix} + \dot{\Lambda}_{13}\begin{bmatrix}\frac{1}{2} - \frac{1}{2}\sin\psi \\ 0 \\ -\frac{1}{2} - \frac{1}{2}\sin\psi\end{bmatrix} \tag{5-52}$$

5.2.2.6. *Parameters of the HS model*

Some parameters of the present hardening model coincide with those of classical non-hardening Mohr-Coulomb model. These are the failure parameters ϕ_p, c and ψ_p. Additionally we used the basic parameters for the soil stiffness:

E_{50}^{ref}, secant stiffness in standard drained triaxial test
E_{oed}^{ref}, tangent stiffness for primary oedometer loading
m, power for stress-level dependency of stiffness

This set of parameters is completed by the following advanced parameters:

E_{ur}^{ref}, unloading/reloading stiffness
ν_{ur}, Poisson's ratio for unloading/reloading
p^{ref}, reference stress for stiffness
K_o^{NC}, K_o-value for normal consolidation
R_f, failure ratio q_f / q_a

Experimental data on m, E_{50} and E_{oed} for granular soils is given in (Schanz & Vermeer, 1998).

5.2.3. The Hardening Soil Small (HS Small) Model

The Hardening Soil Small (HS-Small) model is an extension of the HS model to incorporate the small strain stiffness behaviour of soils. The behaviour of soil at small strains has been studied by some researchers (Seed&Idriss, 1970; Burland, 1989; Atkinson, 2000; Benz

2007). At small strain levels, most soil exhibit a higher stiffness than at strain levels. The soil stiffness decays with increasing strain. Figure 5-9 shows a small unloading-reloading stress-strain paths result in a considerably higher elastic modulus E_o.

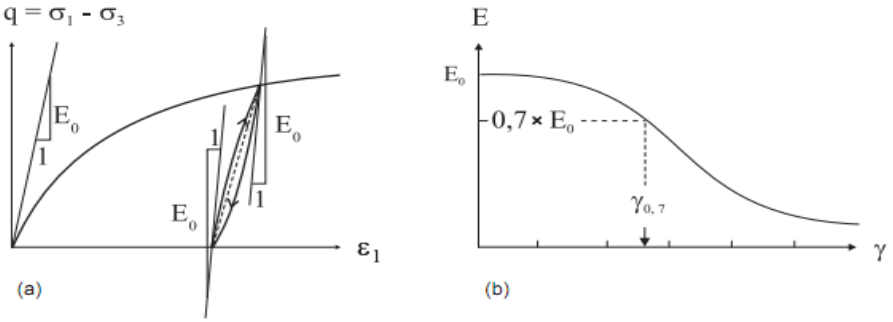

Fig. 5-9 HS-small model, a) Initial stiffness modulus E_0 in a triaxial test
b) Small strain parameters E_0 and $\gamma_{0.7}$ (after Benz, 2007)

In fact, maximum soil stiffness is observed at very low strain levels, e.g. Strains smaller than 10^{-5} (Atkinson and Sällfors, 1991). Special devices is needed to identify stiffness at very small strain. Biarez and Hicher (1994) gave a simple correlation for quarts sand as follows:

$$E_0 = \frac{140}{e} \cdot \left(\frac{p}{p^{ref}}\right)^{0.5} \tag{5-53}$$

where e is the void ratio of the soil and p is the mean stress. Alphan (1970) also estimated preliminary estimation of the E_0. Hardin and Drnevich (1972) formulated the decay of stiffness when strains increase.

$$E = \frac{E_0}{1+\frac{3}{7}\frac{\gamma}{\gamma_{0.7}}} \tag{5-54}$$

where E is the actual secant modulus at the corresponding shear strain γ , E_0 is the initial stiffness of soil and $\gamma_{0.7}$ is the shear strain at 70 percent from the initial stiffness E_0 .

The initial shear modulus G_0 is determined from the relationship between E_0 and Poisson's ratio v as in the following equation

$$G_0 = \frac{E_0}{2(1+v)} \tag{5-55}$$

Whilst, the shear strain is expressed using the strain invariant

$$\gamma = \frac{1}{\sqrt{2}} \cdot \sqrt{(\varepsilon_1 - \varepsilon_2)^2 + (\varepsilon_2 - \varepsilon_3)^2 + (\varepsilon_3 - \varepsilon_1)^2} \tag{5-56}$$

The stiffness degradation due to plastic straining is modelled by involving material hardening. Therefore, before reaching plastic material behaviour, the formulation of small strain stiffness is cut off at the unloading-reloading stiffness E_{ur}. There are two additional input parameters are required for the HS-Small model: the elastic small-strain shear modulus G_0^{ref} at reference pressure p^{ref} and the curve-decay value $\gamma_{0.7}$ in primary loading.

5.2.4. The Soft Soil Creep Model

Soft Soil Creep model distinguishes between primary loading and unloading/reloading behaviour and in this respect the model is similar to the Hardening Soil model. In the HS model, there is no time dependency in the model. The cap expandeds instaneously if an increase in the load would cause the stress state to fall outside the current cap. In the Soft Soil

Creep (SSC) model, this shift of the cap needs time. If a higher load is applied, the cap will not follow immediately, but it will take a day to adapt to the new stress state.

The SSC model is suitable for estimating the viscous effects, i.e. creep and stress relaxation. In fact, all soils exhibit some creep and primary compression is more often than not followed by a certain amount of secondary compression. Buisman (1936) proposed the following equation to describe creep behaviour under constant effective stress.

$$\varepsilon = \varepsilon_c - c_B \log\left(\frac{t}{t_c}\right) \ , \ for: t > \ t_c \tag{5-57}$$

where ε_c is the strain up to the end of consolidation, t is the time measured from the beginning of loading, t_c is the time to end of primary consolidation and C_B is a material constant (see Fig. 5-10). Rewriting above the equation as:

$$\varepsilon = \varepsilon_c - c_B \log\left(\frac{t+t\prime}{t_c}\right) \ , \ for: t > \ 0 \tag{5-58}$$

where $t' = t - t_c$ being the effective creep time.

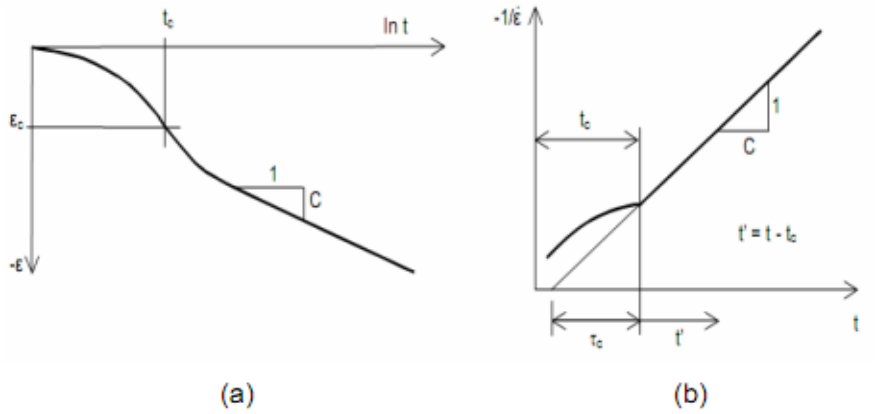

Fig. 5-10 Consolidation and creep behaviour in a standard Oedometer test
(After Vermeer and Neher, 1999)

Garlanger (1972) proposed the creep equation as follows:

$$e = e_c - c_B \log\left(\frac{\tau_c+t\prime}{\tau_c}\right) \ , \ for: t' > \ 0 \tag{5-59}$$

where: $C_\alpha = C_B\,(1 + e_o)$

Butterfield (1979) alsodescribed a slightly different possibility for secondary compression as:

$$\varepsilon^H = \varepsilon_c^H - C \ln\left(\frac{\tau_c+t\prime}{\tau_c}\right) \tag{5-60}$$

where ε^H is the logarithmic strain defined as:

$$\varepsilon^H = \ln\left(\frac{V}{V_0}\right) = \ln\left(\frac{1+e}{1+e_0}\right) \tag{5-61}$$

Originally, Hencky (1928) used the subscript '0' denoting initial values whilst the superscript '*H*' for denotating logaritmic strain. For small strains it is possible to show that:

$$C = \frac{C_\alpha}{(1+e_0)\ln 10} = \frac{C_B}{\ln 10} \tag{5-62}$$

1D Creep model

The SSC model described here is on the basis of the work done by Vermeer and Neher (1999) on elastic visco-plastic creep model. Vermeer and Neher (1999) adopted Bjerrum's idea to find an analytical expression for quantity of τ_c. For the one dimensional creep, two strain components need to be modelled as shown in Fig. 5-11.

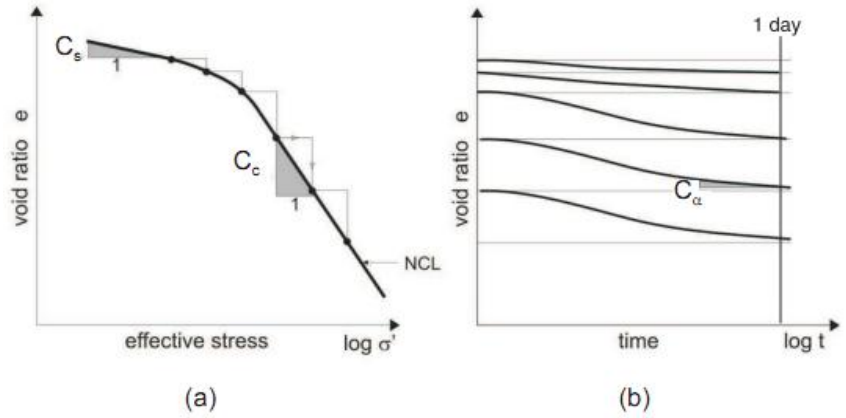

Fig. 5-11 Standard Oedometer Test, a) Stepwise loading in *e*-log vs. σ' plot
b) Void ratio vs. Time (After Vermeer and Neher, 1999)

First of them is the more or less elastic deformation, as directly observed in unloading and reloading condition. The other component of strain is irreversible and time dependent. Volumetric strain implies a change of void ratio and it is convenient to formulate the deformation in terms of void ratio *e*, and the change of void can be expressed by a equation below:

$$\dot{e} = \dot{e}^e + \dot{e}^c \tag{5-63}$$

where the superscripts *e* and *c* refer to the elastic and creep component respectively. The elastic change of void ratio is formulated as follows:

$$\dot{e}^e = -\frac{C_s}{\ln 10}.\frac{\dot{\sigma}'}{\sigma} \tag{5-64}$$

where C_s is the swelling index, which can be the unloading-reloading index C_{ur}. Whilst the creep deformation is represented using power law

$$\dot{e}^c = -\frac{C_\alpha}{\tau.\ln 10}\left(\frac{\sigma'}{\sigma_p}\right)^\beta = -\frac{C_\alpha}{\tau.\ln 10}\left(\frac{1}{OCR}\right)^\beta, \quad \beta = \frac{C_c - C_s}{C_\alpha} \tag{5-65}$$

where τ is a particular reference time, which can mostly be taken equal to one day. C_α is the secondary compression index that is also referred to as the creep index and C_c is the compression index obtained from an oedometer test. From the equation above that the creep rate depends on the *OCR* value. Some typical soil data give $C_s = C_c/10$ and $C_\alpha = C_c/30$. This will give β of about 27.

The preconsolidation stress σ_p increases during creep according to the differential equation

$$\frac{\dot{\sigma}_p}{\sigma_p} = -\frac{\ln 10}{C_c - C_s}.\dot{e}^c \tag{5-66}$$

By integrating the equation (5-66), we will get the preconsolidation stress:

$$\sigma_p = \sigma_{p0}.\exp -\frac{\ln 10.\Delta e^c}{C_c - C_s}, \quad with\ \Delta e^c = e^c - e_0^c \tag{5-67}$$

where σ_{p0} is the initial preconsolidation stress for $e^c = e_0^c$. Subscript '0' denotes the initial value. Finally, the creep rate formulation can be obtained as the equation below:

$$\dot{e}^c = -\frac{C_\alpha}{\tau.\ \ln 10}\left(\frac{\sigma'}{\sigma_{p0}}\right)^\beta \exp\frac{e^c - e_0^c}{C_\alpha/\ln 10} \tag{5-68}$$

The effective stress σ' may be either larger or smaller than σ_{p0}. For a special case of a constant effective stress, the differential creep formulation can be integrated analytically to obtain the logarithmic creep law

$$\Delta e^c = e^c - e_0^c = -C_\alpha \log\left(1 + \frac{t}{t^*}\right) \tag{5-69}$$

where $t = 0$ for $e = e_0$, and then

$$\tau^* = \tau.\left(\frac{\sigma_{p0}}{\sigma'}\right)^\beta = \tau.OCR_0^\beta \tag{5-70}$$

3D Soft Soil Creep model

On extending the 1-D model to general states of stress and strain, the well-known stress invariants p and q for mean and deviatoric stress are adopted. These invariants are used to define a new stress measure named p^{eq}, namely:

$$p^{eq} = p' + \frac{q^2}{M^2 p'} \tag{5-71}$$

with $p' = \frac{1}{3}(\sigma_1' + \sigma_2' + \sigma_3')$ *and* $q = \frac{1}{\sqrt{2}}.\sqrt{(\sigma_1' - \sigma_2')^2 + (\sigma_2 - \sigma_3)^2 + (\sigma_2 - \sigma_2)^2}$

Fig. 5-12 shows that the stress measure p^{eq} is constant on the ellipse in the p-q plane. In fact, the ellipses are from the Modified Camclay Model as introduced by Roscoe and Burland (1968).

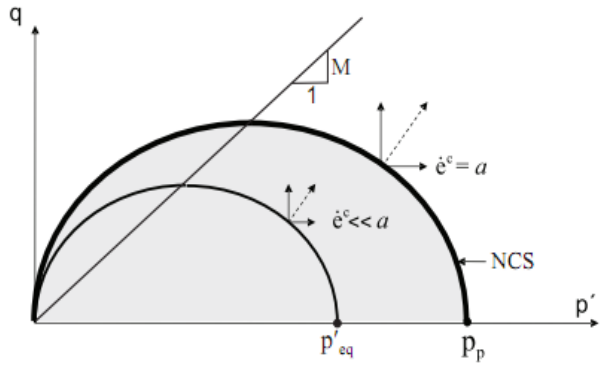

Fig. 5-12 Diagram of p^{eq}-ellipse in a p-q plane (after Vermeer and Neher, 1999)

Soil parameter M represents the slope of the so-called '*critical state line*' and it is defined as:

$$M = \frac{6\sin\varphi_{cv}}{3 - \sin\varphi_{cv}} \tag{5-72}$$

where ϕ_{cv} is the constant volume friction angle, also referred to as critical-state friction angle. The preconsolidation pressure changes during creep according to the law

$$p_p = p_{po}.\exp\frac{\Delta\varepsilon_{vol}^c}{\lambda^* - \kappa^*} \tag{5-73}$$

where λ^* and κ^* are a modified compression index and a modified swelling index respectively. In case of small strain, it gives

$$\lambda^* = \frac{C_c}{\ln 10} \cdot \frac{1}{1+e_0} \tag{5-74}$$

and

$$\kappa^* \approx \frac{3(1-v)}{1+v} \cdot \frac{C_s}{\ln 10} \cdot \frac{1}{1+e_0} \approx \frac{2C_s}{\ln 10} \cdot \frac{1}{1+e_0} \tag{5-75}$$

Volumetric creep strain rate define as

$$\dot{\varepsilon}_{vol}^{c} = \frac{\mu^*}{\tau} \cdot \left(\frac{p_{eq}}{p_p}\right)^{\frac{\lambda^*-\kappa^*}{\mu^*}} , with\ \mu^* = \frac{C_\alpha}{\ln 10} \cdot \frac{1}{1+e_0} \tag{5-76}$$

Whilst the elastic volumetric strain rate can be expressed as

$$\dot{\varepsilon}_{vol}^{c} = \frac{\dot{p}'}{K_{ur}} = \kappa^* \frac{\dot{p}'}{p'} \tag{5-77}$$

where bulk modulus $K_{ur} = p'/\kappa^*$

The total volumetric strain rate in 3D Soft Soil Creep model can be written as

$$\dot{\varepsilon}_{vol} = \dot{\varepsilon}_{vol}^{e} + \dot{\varepsilon}_{vol}^{c} = \kappa^* \frac{\dot{p}'}{p'} + \frac{\mu^*}{\tau} \cdot \left(\frac{p_{eq}}{p_p}\right)^{\frac{\lambda^*-\kappa^*}{\mu^*}} \tag{5-78}$$

Parameter used in Soft Soil Creep model has a relationship with Camclay parameters model. The modified compression index λ^* is $\lambda / (1+e)$, the modified swelling index κ^* is $\kappa / (1+e)$, and the modified creep index μ^* is $C_\alpha / 2.3(1+e)$. The ratio of the unloading/primary loading stress, λ^* / κ^*, cannot be smaller than 1 and should normally be between 2 and 10. Users should be very wary of values outside this range' for most practical cases the value falls within the range of 3 to 7. Secondly, there is the creep ratio, $(\lambda^*-\kappa^*)/\mu^*$, to consider. This ratio can have a wide range of values, normally between 5 and 25, where high values represent stiff soil with little creep and small values represent soft soils with a considerable amount of creep. For most practical cases the ratio falls within the range of 10 to 20 and if the creep ratio is over 25 one could reconsider the use of the creep model.

Table 5-1 Material parameters for the Soft Soil Creep model
(after Vermeer and Neher, 1999)

Symbols	Name of parameters
λ^*	a modified compression index
$\kappa^* = \lambda^* / 2\text{-}10$	a modified swelling index
$\mu^* = (\lambda^*-\kappa^*) / 10\text{-}20$	a modified creep index
$\nu_{ur} = 0.15$	un-/reloading Poisson's ratio
c'	effective cohesion
ϕ'	effective friction angle
K_0^{NC}	height of normal consolidation surface
OCR	the state of preconsolidation stress

5.2.5. The Hypoplastic Model

Hypoplasticity is a particular class of incrementally non-linear constitutive models. The basic structure of the hypoplastic models has been developed during 1990's at the University of Karlsruhe. It is unlike in elasto-plasticity, in hypoplasticity, the strain rate is not decomposed into elastic and plastic parts, and the models do not use explicitly the notions of the yield surface and plastic potential surface. But the models are still capable in predicting an

important feature of soil behaviour. This is achieved by the hypoplastic equation being non-linear in the strecthing tensor **D**. The basic equation may be expressed as:

$$\dot{\mathbf{T}} = \mathcal{L} : \mathbf{D} + \mathrm{N}\,\|\mathbf{D}\| \tag{5-79}$$

where $\dot{\mathbf{T}}$ is the objective (Jaumann) stress rate, **D** is the Euler's stretching tensor and $\mathcal{L}$ and **N** are fourth- and second order constitutive tensors, respectively. The early hypoplastic model was developed by trial and error (Kolymbas, 1991). Gudehus (1996) proposed a modification to include the stress level (barotropy) and density (pyknotropy), as the modified equation below:

$$\dot{\mathbf{T}} = f_s \mathcal{L} : \mathbf{D} + f_s f_\mathrm{d} \mathrm{N}\,\|\mathbf{D}\| \tag{5-80}$$

with f_s and f_d are scalar factors expressing the influence of barotropy and pyknotropy. Hereafter, Wolffersdorf (1996) refined it with incorporating Matsuoka-Nakai critical state stress condition. Nowadays, this model is considered as a standard hypoplastic model for granular materials.

5.2.5.1. Hypoplastic Model for Granular Materials

The hypoplastic model for granular material has eight material parameters, consisting of ϕ_c, h_s, n, $e_{\mathrm{d}0}$, $e_{\mathrm{c}0}$, $e_{\mathrm{i}0}$, α and β. The critical state friction angle ϕ_c can be obtained directly by the measurement of the angle of repose. Two parameters h_s and n can be directly computed from oedometric loading curves. The parameter n controls the curvature of oedometer curve, whilst h_s controls the slope of oedometric curve (see Fig. 5-13).

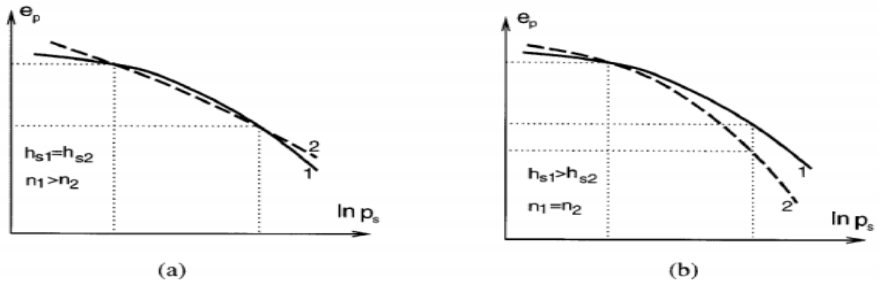

Fig. 5-13 Influence of n (a) and h_s (b) on Oedometric curves (after Herle and Gudehus, 1999)

The parameter n can be written using an equation:

$$n = \frac{ln\left(e_{p1} C_{e2} / e_{p2} C_{e1}\right)}{ln(p_{s2}/p_{s1})} \tag{5-81}$$

where mean stress $p_{\mathrm{s}1}$ and $p_{\mathrm{s}2}$ may be calculated from axial stresses using the Jaky formula $K_0 = 1 - \sin \phi_\mathrm{c}$, and $e_{\mathrm{p}1}$ and $e_{\mathrm{p}2}$ are the void ratios corresponding to the stress $p_{\mathrm{s}1}$ and $p_{\mathrm{s}2}$. Tangent compression indices corresponding to the limit values of interval $p_{\mathrm{s}1}$ and $p_{\mathrm{s}2}$ ($C_{\mathrm{c}1}$ and $C_{\mathrm{c}2}$) can be approximated by secant moduli between loading steps preceding and following steps $p_{\mathrm{s}1}$ and $p_{\mathrm{s}2}$. The parameter h_s can be expressed as:

$$h_s = 3\, p_s \left(\frac{n\, e_p}{C_c}\right)^{1/n} \tag{5-82}$$

where C_c is a secant compression index calculated from limiting values of the calibration interval $p_{\mathrm{s}1}$ and $p_{\mathrm{s}2}$, in which p_s and e_p are averages of the limit values of p and e in this range.

Further model parameters are the reference void ratio $e_{\mathrm{d}0}$, $e_{\mathrm{c}0}$ and $e_{\mathrm{i}0}$, corresponding to the densest, critical state and loosest particle packing at the zero mean stress. Bauer (1996)

formulated the reference void ratio e_d, e_c and e_i corresponding to the non-zero stress depending on the mean stress, as the Eq. 5-83 and then shown in Fig. 5-14.

$$e_c = e_{c0}\, exp\left[-\left(\frac{3p}{h_s}\right)^n\right] \tag{5-83}$$

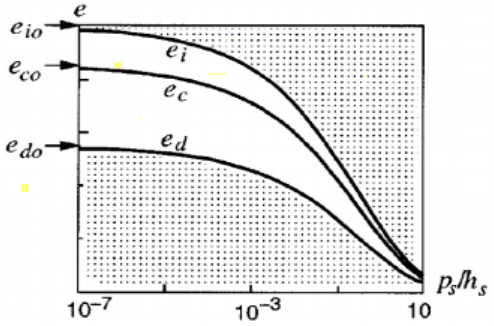

Fig. 5-14 Dependency of the reference void ratio of e_{d0}, e_{c0} and e_{i0} on the mean stress (after Herle and Gudehus, 1999)

The initial void ratio e_{max} can be considered equal to the critical state void ratio at zero presure e_{c0}. Void ratio e_{d0} and e_{i0} can approximately be obtained from empirical relations. The physical meaning of e_{d0} is the void ratio at maximum density, void ratio e_{i0} represents intercept of the isotropic normal compression line with $p = 0$ axis. The ratio $e_{i0}/e_{c0} \approx 1.2$ was derived from considering skeleton consisting of ideal spherical particles (Herle and Gudehus, 1999). Whereas the minimum void ratio e_{d0} should be obtained by densification of a granular material by means of cyclic shearing with small amplitude under constant pressure. If there are no data, it can be estimated using an empirical relation $e_{d0}/e_{c0} \approx 0.4$.

The last two parameters α and β should be calibrated by means of single-element simulations of the drained triaxial tests. Parameter β controls independently the shear stiffness and α controls the peak friction angle.

5.2.5.2. Intergranular Strain Concept (Small Strain Behaviour)

The hypoplastic models can predict successfully the soil behaviour in the medium to large strain range. However, in the small strain range and upon cyclic loading, they fail in predicting the high quasi-elastic soil stiffness. To overcome this problem, Niemunis and Herle (1997) proposed an extension of the hypoplastic equation considering additional state variable "*intergranular strain*" determine the direction of the previous loading. This modification, often denoted as the "*intergranular strain concept*", can be used for both the model for granular materials and the model for clay.

The rate formulation of the enhanced model is given by the equation:

$$\dot{\mathbf{T}} = \boldsymbol{M} : \mathbf{D} \tag{5-84}$$

where $\boldsymbol{M}$ is the fourth-order tangent stiffness tensor of the material. Strain can be thought of as the sum of a component related to the deformation of interface layers at intergranular contacts, quantified by the intergranular strain tensor δ; and a component related to the rearrangement of the soil skeleton.

Intergranular strain concept requires five additional parameters, R controlling the size of the elastic range, β_r and χ controlling the rate of stiffness degradation, m_R controlling the initial

shear stiffness for the initial and reverse loading conditions and m_T controlling the stiffness upon neutral loading conditions.

5.3. Geometrical Idealization

There are some geometrical idealizations used for the FE-calculations such as axisymmetric, plane strain according to Bergado and Long (1994), plane strain with equivalent stiffness and 3D geometry (Fig. 5-15).

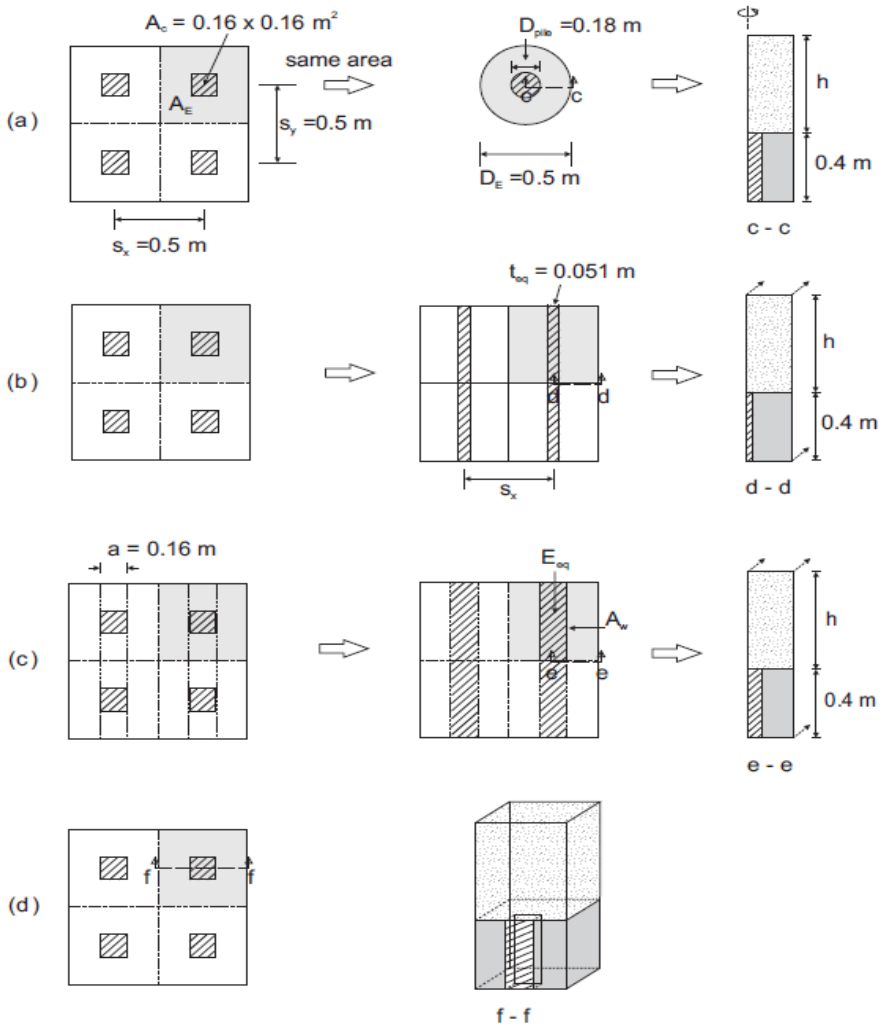

Fig. 5-15 Geometrical idealizations of one cell piled embankment (a) Axisymmetric idealization (b) Idealization for plane strain after Bergado (c) Idealization plane strain using equivalent stiffness (d) 3D geometry (after Satibi, 2009)

For *Axisymmetric*, the three dimensional one cell of the piled embankment is transformed in to a circular cell using the area of the pile and the soil the same. Fig. 5-15(a) shows the transformation of the squared cell to a circular cell which one radian of the circular piled embankment cell is used.

Plane strain after Bergado: The three dimensional grid of piles can be transformed into continuous walls with an equivalent thickness t_{eq} in plane strain model as indicated in Fig. 5-15(b). By keeping an improved area ratio (A_c/A_E) is constant, the thickness of the continuous

wall is calculated based on the consideration of this ratio. Due to symmetrical geometry, only a half of the plane strain geometry is used for the FE calculations.

$$\frac{A_c}{A_E} = \frac{t_{eq} . s_y}{s_x . s_y} \tag{5-85}$$

Plane strain with equivalent pile stiffness: An alternative method to transform the three dimensional grid of piles into a continuous wall in plane strain condition is by assuming equivalent wall stiffness. The equivalent stiffness of the wall E_{eq} is taken as the proportional average of the pile and soil stiffness. Hence,

$$E_{eq} = \frac{E_c . A_c + E_s (A_w - A_c)}{A_w} \tag{5-86}$$

where E_c, E_s and A_w are pile stiffness, soft soil stiffness and wall area as illustrated in Fig.5-15(c). It is worthy to note that when using this approach, the improved area ratio becomes larger.

3D geometry: Three dimensional dimension of the actual case can be best analyzed using 3D geometry. Here, half of the piled embankment cell is considered the 3D FE analysis as described in Fig. 5-15(d).

According to Irsyam et al. (2008) he modeled bamboo piles in the Bamboo piles-Mattress system as soil reinforcement for embankment on soft clay, and results of FE-analysis was in a good agreement with field measurement. To model pile he applies 'node-to-node anchor' in which it was commonly used and available in Plaxis. By modelling pile using elasto-plastic 'node-to-node anchor', soil in between wooden piles is not confined and then actual vertical pile capacity can be obtained. The stiffness of elasto-plastic 'node-to-node anchor' is taken from the estimated displacement of wooden piles in the vertical direction.

5.4. Summary

To explain distribution of stress, strain due to a load on surface of pavement, it can be grouped into two types. First point of view is static load and another is dynamic one. Analitical approach can be used to solve simple problem. Then, a numerical analaysis provides more advance models that offers a good solution for modelling behaviour of material. Some drawbacks and advantages of these approaches as a consideration in analyzing a problem can be explained as follows:

- For a simple case which layers behave elastic material, two layered system can be used which has two homogeneous material consisting of pavement and subgrade subjected to a circular load. Hence, elasticity modulus and Poisson'ratio are important parameters.
- Dynamic response of pavement and subgrade under moving load is derived from an equation of free motion which pavement modeled as a plate and subgrade as an elastic foundation.
- Motion of a load will emerge large deformation on a structure integrity and could be dangerous when approaching or higher than wave velocity of soil foundation.
- In implicit procedure, each cycle is calculated at a rate of σ–ε constitutive model. This model is to estimate strain due to stress and is restricted to a low number of cycles (N<50).

- For high cyclic loading, in general, explicit models are the better choice. Accumulation process under cyclic loading is similar to a process that is governed by viscosity. The number of cyclic *N* replaces the time *t*.
- Constitutive models in numerical analysis provide some models that are able to model the behaviour of material in which it behaves not simply elastic material . Plasticity has a σ–ε relationship which can be non-linear and strain is irreversible.
- When undertaking finite element analysis, idealization of geometry is needed. Some geometrical idealization, such as axisymmetric, plane strain, and 3-D geometry, can be applied in dealing with several cases of geometry in laboratory or in the field. Particularly, it would be important part, when available software for analysis is limited merely two dimensional package software.

CHAPTER 6

Discussion Using Finite Element Calculations

6.1. Introduction

This chapter discusses some findings resulted from some experimental works and several field case studies. Most of the results are directly obtained from observations through devices installed both in the laboratories and in the field. By using FE-calculations, the results are then verified with the main aim to do comparisons in order to be able to properly understand the behavior of material.

6.2. Optimal Vertical Distance of Geosynthetics

Granular materials in pavement engineering such as sub-base course and/or base course play an important role in bearing a load on it and then distribute downward to surface of subgrade. When thickness of base course and/or sub-base course is deep enough, inserting geosynthetics is possible to enhance the bearing capacity and simultaneously reduce the horizontal thrust.

With reference to Ruiken's work procedure in laboratory (Ruiken&Ziegler, 2008), now we use axisymmetrical approach of FE-analysis. It will be presented the results for the purpose of the effectiveness of vertical distance of geosynthetics to support a load. Fig. 6-1 explains the work procedure used in FE-analysis.

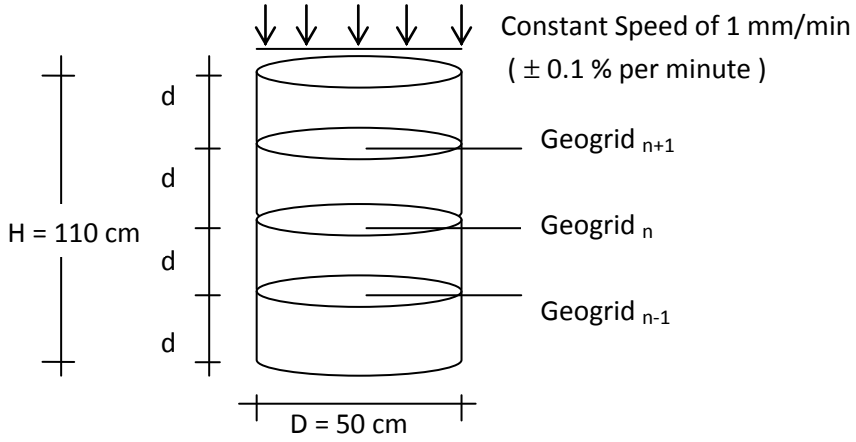

Fig. 6-1 Schematic work procedure for FE analysis

Inclusion of geosynthetics in granular material will enhance bearing capacity. By inserting geosynthetics in tubular sample soil, it will increase the confining pressure of material and results in smaller horizontal strain. In other words, it means that the soil stiffness will be higher and sample soil has eventually higher bearing capacity.

To prove this hypothesis, FE-analysis using Plaxis software with axisymmetric configuration is presented. Tubular sample soil with 110 cm high and 50 cm in diameter is subjected to a vertical compressive load with a constant speed of 1 mm/minute. In this model, number of geosynthetics layer used is up to 4 layers with two types of tensile strength 30 kN/m and 300 kN/m respectively. Tensile strength of 30 kN/m represents a low tensile strength, whilst tensile strength of 300 kN/m represents a moderate tensile strength.

Strength of granular material for the base course or subbase course can be expressed by *CBR* (California Bearing Ratio) or resilient modulus (M_r). Table 6-1 provides a correlation between *CBR* and M_r using Eq. 3-2 through Eq. 3-5, as explained in Chapter 3.

Table 6-1 Resilient moduli of base course and subbase course

Source(s)	Equations	Resilient moduli (M_r)		
		CBR 40	CBR100	CBR150
Heukelom&Klomp (1962)	M_r (psi) = 1500 CBR M_r (MPa) = 10.34 CBR	60 ksi 413 MPa	150 ksi 1034 MPa	225 ksi 1551MPa
Webb&Campbell (1986)	M_r (psi) = 3116 CBR $^{0.4779707}$ M_r (MPa) = 21.485 CBR $^{0.4779707}$	18 ksi 125 MPa	28 ksi 194 MPa	34 ksi 235 MPa
Sasongko (1996)	M_r (MPa) = 10 CBR M_r (MPa) = 4 CBR	400 MPa 160 MPa	1000 MPa 400 MPa	1500 MPa 600 MPa
NCHRP (2004)	M_r (psi) = 2555 CBR $^{0.64}$ M_r (MPa) = 17.6 CBR $^{0.64}$	27 ksi 186 MPa	48 ksi 335 MPa	63 ksi 435 MPa

According to Sasongko (1996), resilient modulus correlates to 4 times CBR value when CBR>28%. This is quite close with NCHRP's equation. Whilst Heukelom's equation extensively developed for fine grained soil with maximum CBR of 10% provides too high estimation, whereas Webb's equation gives too small estimation. Based on data in Table 6.1, the appropriate values of subbase course with CBR of 40% correlates to the resilient modulus between 160 MPa and 190 MPa. Meanwhile, base course with CBR of 100% correlates to the resilient modulus between 335 MPa and 400 MPa and base course very dense with CBR of 150% correlates to the modulus resilient between 435 MPa and 600 MPa.

In this FE analysis, three resilient moduli are used for representing resilient moduli of pavement materials, namely 200 MPa, 400 MPa and 600 MPa respectively. Mohr-Coulomb (MC) and the Hardening Soil (HS) model are used for analyzing this work. Besides elastic modulus represented by resilient modulus, other parameters are also introduced for FA-analysis, namely friction angle (ϕ) and dilation angle (ψ). Dilation angle is an important parameter because pavement material is a compacted soil. Material properties are shown in Table 6-2.

Table 6-2 Material properties used in finite element analysis

Properties	Unit	Element and model		
		Granular material		Geogrid
		MC	HS	Elastic
Unit weight, γ	kN/m^3	18	18	-
Friction angle, ϕ	[^{o}]	38, 45	38, 45	-
Dilation angle, ψ	[^{o}]	8, 15	8, 15	-
Cohesion, c	kPa	0.5	0.5	-
Young's modulus, E	MPa	200, 600	-	-
Secant modulus, E_{50}	MPa	-	50, 100 , 150	-
Oedometer comp. modulus, E_{oed}	MPa	-	50, 100 , 150	-
Un-/reloading modulus, E_{ur}	MPa	-	200, 400, 600	-
Poisson's ratio, v_{ur} /v	[-]	-/0.3	0.2/-	-
Tensile strength, EA	kN/m	-	-	30, 300
Drainage		Drained	Drained	Non-porous
Calculation type		Stage construction, plastic calculation		

Pictures in the Table 6-3 through Table 6-6 show the patterns of failure which indicate zones having the maximum horizontal displacements (red colour) when being subjected to a load

using MC-model for the elastic modulus of 200 MPa and 600 MPa. In Table 6-3 and Table 6-4, some findings are resulted from FE-analysis using MC model, which the elastic modulus of granular soil of 200 MPa and 600 MPa with tensile strength of geosynthetics of 30 kN/m. It is clearly shown that granular material with high friction angle of 45^o and dilation angle of 15^o is able to support higher stress (around 37 kPa) than lower friction angle and dilation angle, 38^o and 8^o respectively, which can support the vertical stress around 34 kPa. Moreover, by using material with a higher friction angle and dilation angle can reduce horizontal displacement smaller than lower one. Another important finding is that the number of inclusion of geosynthetics in granular material contributes to reduce horizontal displacement.

Table 6-3 Horizontal displacements for MC-model, E=200 MPa and EA= 30 kN/m

Elastic modulus	MC-model for E = 200 MPa , EA= 30 kN/m							
Friction angle and dilatant angle	$\phi = 45^o$, $\psi = 15^o$				$\phi = 38^o$, $\psi = 8^o$			
Number of geosynthtetics layer	0	1	2	3	0	1	2	3
Patterns of horizontal displacements	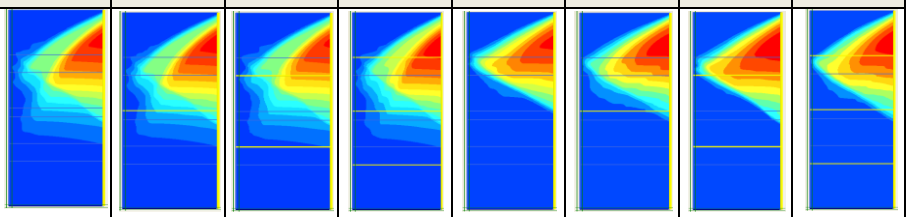							
Remarks	More load step	More load step	More load step	More load step	More load step	More load step	More load step	More load step
Horizontal displacement (mm)	0.0697	0.0541	0.0527	0.0557	0.1118	0.1071	0.1065	0.1061
Vertical displacement (mm)	0.0697	0.0700	0.0686	0.0713	0.1497	0.142	0.1529	0.1482
Force (kN)	0.819	0.82	0.819	0.825	0.77	0.777	0.775	0.775
Stress (kPa)	37.27	37.381	37.296	37.774	34.3	34.711	34.472	34.668

Table 6-4 Horizontal displacements for MC-model, E=600 MPa and EA= 30 kN/m

Elastic modulus	MC-model for E = 600 MPa , EA= 30 kN/m							
Friction angle and dilatant angle	$\phi = 45^o$, $\psi = 15^o$				$\phi = 38^o$, $\psi = 8^o$			
Number of geosynthtetics layer	0	1	2	3	0	1	2	3
Patterns of horizontal displacements	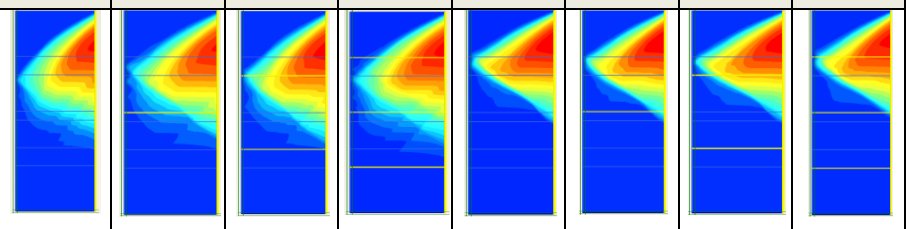							
Remarks	More load step	More load step	More load step	More load step	More load step	More load step	More load step	More load step
Horizontal displacement (mm)	0.0408	0.0405	0.0415	0.0390	0.0396	0.0418	0.0417	0.0431
Vertical displacement (mm)	0.0498	0.0499	0.0525	0.0499	0.0543	0.0565	0.0563	0.0580
Force (kN)	0.827	0.827	0.827	0.825	0.775	0.777	0.783	0.784
Stress (kPa)	37.91	37.889	37.951	37.794	33.628	33.882	34.304	34.564

Similar trend in previous findings, by inclusion of higher tensile strength of 300 kN/m in granular material with elastic modulus of 200 kPa, it is able to support the vertical stress enormously, particularly when granular material has the higher friction angle and dilation angle, as indicated in Table 6-5. However, inclusion tensile strength of 300 kN/m in granular material with an elastic modulus of 600 MPa only contributes slightly vertical stress, as shown in Table 6-6.

Table 6-5 Horizontal displacements for MC-model, E=200 MPa and EA= 300 kN/m

Elastic modulus	MC-model for E = 200 MPa , EA= 300 kN/m							
Friction angle and dilation angle	$\phi = 45^o$, $\psi = 15^o$				$\phi = 38^o$, $\psi = 8^o$			
Number of geosynthtetics layer	0	1	2	3	0	1	2	3
Patterns of horizontal displacements	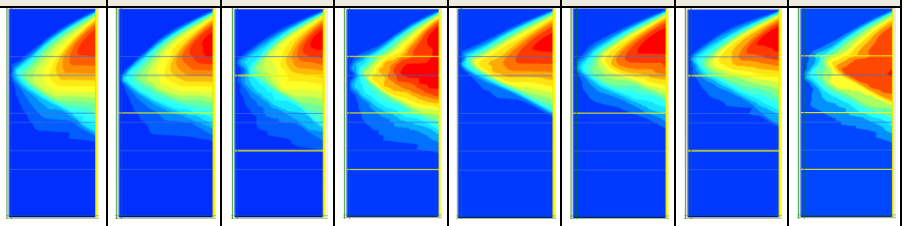							
Remarks	More load step	More load step	More load step	More load step	More load step	More load step	More load step	More load step
Horizontal displacement (mm)	0.160	0.167	0.168	0.140	0.133	0.137	0.135	0.100
Vertical displacement (mm)	0.190	0.192	0.200	0.197	0.178	0.82	0.178	0.169
Force (kN)	0.900	0.918	0.961	0.978	0.772	0.781	0.803	0.820
Stress (kPa)	45.526	47.042	51.058	52.419	34.724	35.529	37.386	38.701

Table 6-6 Horizontal displacements for MC-model, E=600 MPa and EA= 300 kN/m

Elastic modulus	MC-model for E = 600 MPa , EA= 300 kN/m							
Friction angle and dilation angle	$\phi = 45^o$, $\psi = 15^o$				$\phi = 38^o$, $\psi = 8^o$			
Number of geosynthtetics layer	0	1	2	3	0	1	2	3
Patterns of horizontal displacements	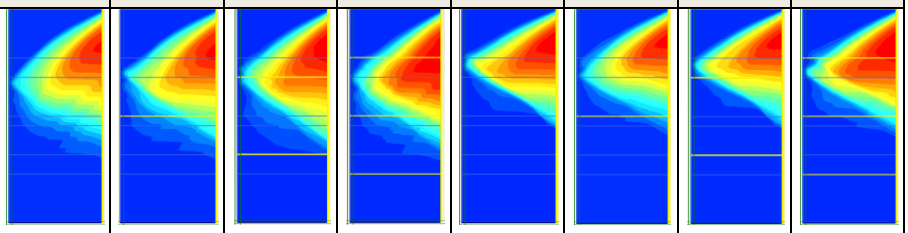							
Remarks	More load step	More load step	More load step	More load step	More load step	More load step	More load step	More load step
Horizontal displacement (mm)	0.0408	0.044	0.0397	0.0376	0.0396	0.0409	0.0437	0.0559
Vertical displacement (mm)	0.0498	0.0541	0.0526	0.0517	0.0543	0.0539	0.0581	0.0558
Force (kN)	0.827	0.826	0.847	0.849	0.775	0.791	0.795	0.804
Stress (kPa)	37.910	37.832	39.599	39.774	33.628	34.965	35.376	36.072

We may resume some findings as presented in Table 6-3 through Table 6-6 that smaller horizontal displacement can be obtained when we apply higher elastic modulus, higher friction angle and dilation angle, higher tensile strength and number of geosynthetics.

Table 6-7 through Table 6-12 show some important results using HS-model for granular material with an elastic modulus of 200, 400 and 600 MPa respectively. We may notice results as shown in Table 6-7 through Table 6-9 that the higher values of elastic moduli, friction angle and dilation angle provide higher vertical stress. When we apply the elastic modulus of 200 MPa with tensile strength of geosynthetics around 30 kN/m, at least 3 layers of geosynthetics is needed for granular materials having friction angle of 45^o and dilation angle of 15^o whereas using lower friction angle and dilation angle (38^o and 8^o respectively), sample soil fails even applied for 4 layers of geosynthetics.

Table 6-7 Horizontal displacements for HS-model, E=200 MPa and EA= 30 kN/m

Elastic modulus	HS-model for E = 200 MPa , EA= 30 kN/m							
Friction angle and dilation angle	$\phi = 45^o$, $\psi = 15^o$				$\phi = 38^o$, $\psi = 8^o$			
Number of geosynthtetics layer	0	1	2	3	0	1	2	3
Patterns of horizontal displacements	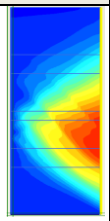	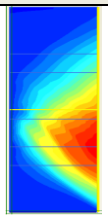	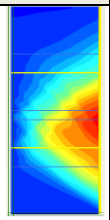	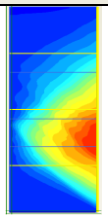	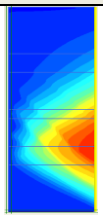	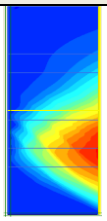	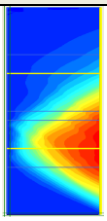	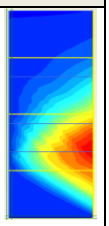
Remarks	Soil body collapses	Soil body collapses	More load step	More load step	Soil body collapses	Soil body collapses	Soil body collapses	Soil body collapses
Horizontal displacement (mm)	0.720	0.753	0.845	0.858	0.521	0.544	0.589	0.634
Vertical displacement (mm)	1.228	1.303	1.375	1.422	1.111	1.121	1.268	1.250
Force (kN)	0.633	0.634	0.637	0.64	0.634	0.634	0.633	0.636
Stress (kPa)	40.302	39.578	39.325	39.491	35.846	34.051	35.491	36.315

Table 6-8 Horizontal displacements for HS-model, E=400 MPa and EA= 30 kN/m

Elastic modulus	HS-model for E = 400 MPa , EA= 30 kN/m							
Friction angle and dilation angle	$\phi = 45^o$, $\psi = 15^o$				$\phi = 38^o$, $\psi = 8^o$			
Number of geosynthtetics layer	0	1	2	3	0	1	2	3
Patterns of horizontal displacements	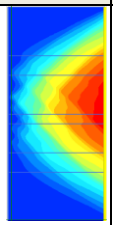	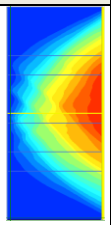	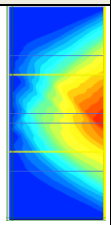	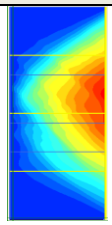	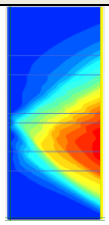	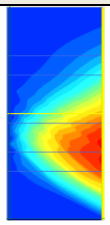	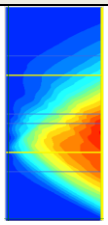	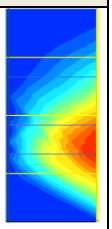
Remarks	More load step	More load step	More load step	More load step	Soil body collapses	More load step	More load step	More load step
Horizontal displacement (mm)	0.339	0.323	0.361	0.348	0.357	0.330	0.346	0.324
Vertical displacement (mm)	0.693	0.698	0.682	0.699	0.709	0.643	0.685	0.637
Force (kN)	0.726	0.735	0.743	0.748	0.062	0.650	0.649	0.659
Stress (kPa)	39.614	39.925	40.427	42.273	30.267	35.026	36.017	35.798

At least a layer of geosynthetics has to be used when the elastic modulus of sample soil is 400 MPa with a friction angle of 38^o and a dilation angle of 8^o as shown in Table 6-8. Another important finding is that use of the higher friction angle and dilation angle can slightly reduce the horizontal displacement.

Table 6-9 Horizontal displacements for HS-model, E=600 MPa and EA= 30 kN/m

Elastic modulus	HS-model for E = 600 MPa , EA= 30 kN/m							
Friction angle and dilation angle	$\phi = 45^o$, $\psi = 15^o$				$\phi = 38^o$, $\psi = 8^o$			
Number of geosynthtetics layer	0	1	2	3	0	1	2	3
Patterns of horizontal displacements	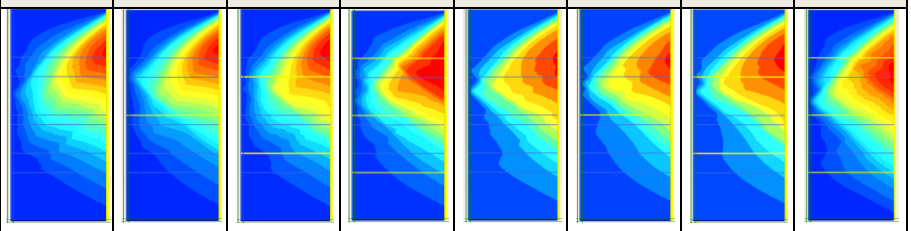							
Remarks	More load step	More load step	More load step	More load step	More load step	More load step	More load step	More load step
Horizontal displacement (mm)	0.367	0.390	0.358	0.316	0.206	0.227	0.211	0.197
Vertical displacement (mm)	0.642	0.657	0.651	0.639	0.467	0.483	0.473	0.453
Force (kN)	0.823	0.822	0.83	0.84	0.741	0.737	0.745	0.75
Stress (kPa)	42.342	41.861	43.118	43.586	35.664	34.661	35.647	35.91

Table 6-10 through Table 6-12 are the results using HS-model for granular materials with elastic modulus of 200, 400 and 600 MPa respectively and inclusion of geosynthetics with tensile strength of 300 kN/m. Similar result as previous findings that higher values of elastic modulus, friction angle, dilation angle and number of layers are able to reduce the horizontal displacement and simultaneously increase the vertical stress.

Table 6-10 Horizontal displacements for HS-model, E=200 MPa and EA= 300 kN/m

Elastic modulus	HS-model for E = 200 MPa , EA= 300 kN/m							
Friction angle and dilation angle	$\phi = 45^o$, $\psi = 15^o$				$\phi = 38^o$, $\psi = 8^o$			
Number of geosynthtetics layer	0	1	2	3	0	1	2	3
Patterns of horizontal displacements	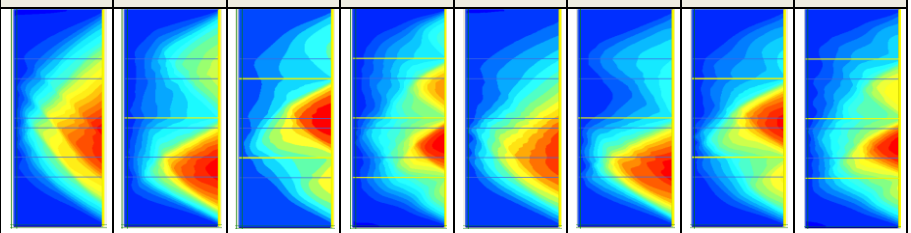							
Remarks	Soil body collapses	Soil body collapses	More load step	More load step	Soil body collapses	Soil body collapses	More load step	More load step
Horizontal displacement (mm)	0.780	0.931	1.09	0.995	0.521	0.689	0.744	0.707
Vertical displacement (mm)	1.549	1.756	1.882	1.914	1.111	1.267	1.459	1.451
Force (kN)	0.630	0.654	0.722	0.817	0.634	0.635	0.678	0.725
Stress (kPa)	39.048	46.547	41.453	43.401	35.846	36.987	35.500	35.745

Table 6-11 Horizontal displacements for HS-model, E=400 MPa and EA= 300 kN/m

Elastic modulus	HS-model for E = 400 MPa , EA= 300 kN/m							
Friction angle and dilation angle	$\phi = 45^o$, $\psi = 15^o$				$\phi = 38^o$, $\psi = 8^o$			
Number of geosynthtetics layer	0	1	2	3	0	1	2	3
Patterns of horizontal displacements	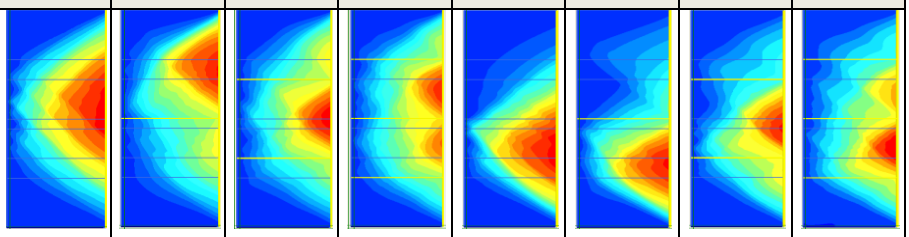							
Remarks	More load step	More load step	More load step	More load step	Soil body collapses	More load step	More load step	More load step
Horizontal displacement (mm)	0.337	0.364	0.355	0.340	0.357	0.326	0.308	0.278
Vertical displacement (mm)	0.690	0.726	0.687	0.729	0.709	0.641	0.641	0.639
Force (kN)	0.726	0.776	0.826	0.868	0.622	0.677	0.694	0.718
Stress (kPa)	39.551	44.254	47.231	50.274	30.267	37.434	33.885	35.517

Table 6-12 Horizontal displacements for HS-model, E=600 MPa and EA= 300 kN/m

Elastic modulus	HS-model for E = 600 MPa , EA= 300 kN/m							
Friction angle and dilation angle	$\phi = 45^o$, $\psi = 15^o$				$\phi = 38^o$, $\psi = 8^o$			
Number of geosynthtetics layer	0	1	2	3	0	1	2	4
Patterns of horizontal displacements	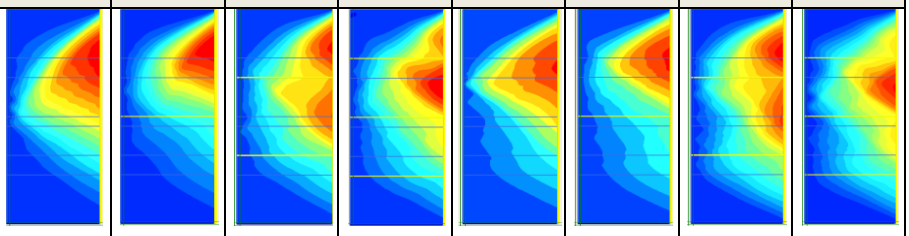							
Remarks	More load step	More load step	More load step	More load step	More load step	More load step	More load step	More load step
Horizontal displacement (mm)	0.313	0.389	0.269	0.299	0.206	0.227	0.168	0.192
Vertical displacement (mm)	0.585	0.584	0.596	0.632	0.453	0.454	0.446	0.461
Force (kN)	0.819	0.859	0.910	0.952	0.738	0.756	0.787	0.806
Stress (kPa)	37.287	41.241	46.197	52.024	36.297	37.173	40.901	41.554

If we compare patterns of horizontal displacements between MC-model and HS-model, we may notice that the influence of geosynthetics inclusion in granular material using MC-model is not quite obvious compared with HS-model, particularly when using a moderate tensile strength.

By inserting geosynthetics layers on material pavement, the horizontal thrust will be reduced. It is a correct assumption that number of layer inserted in pavement material will reduce the horizontal thrust. In other words, it the reduced horizontal displacement. Figure 6-2 shows an influence of the number of geosynthetics layers inserted on granular material.

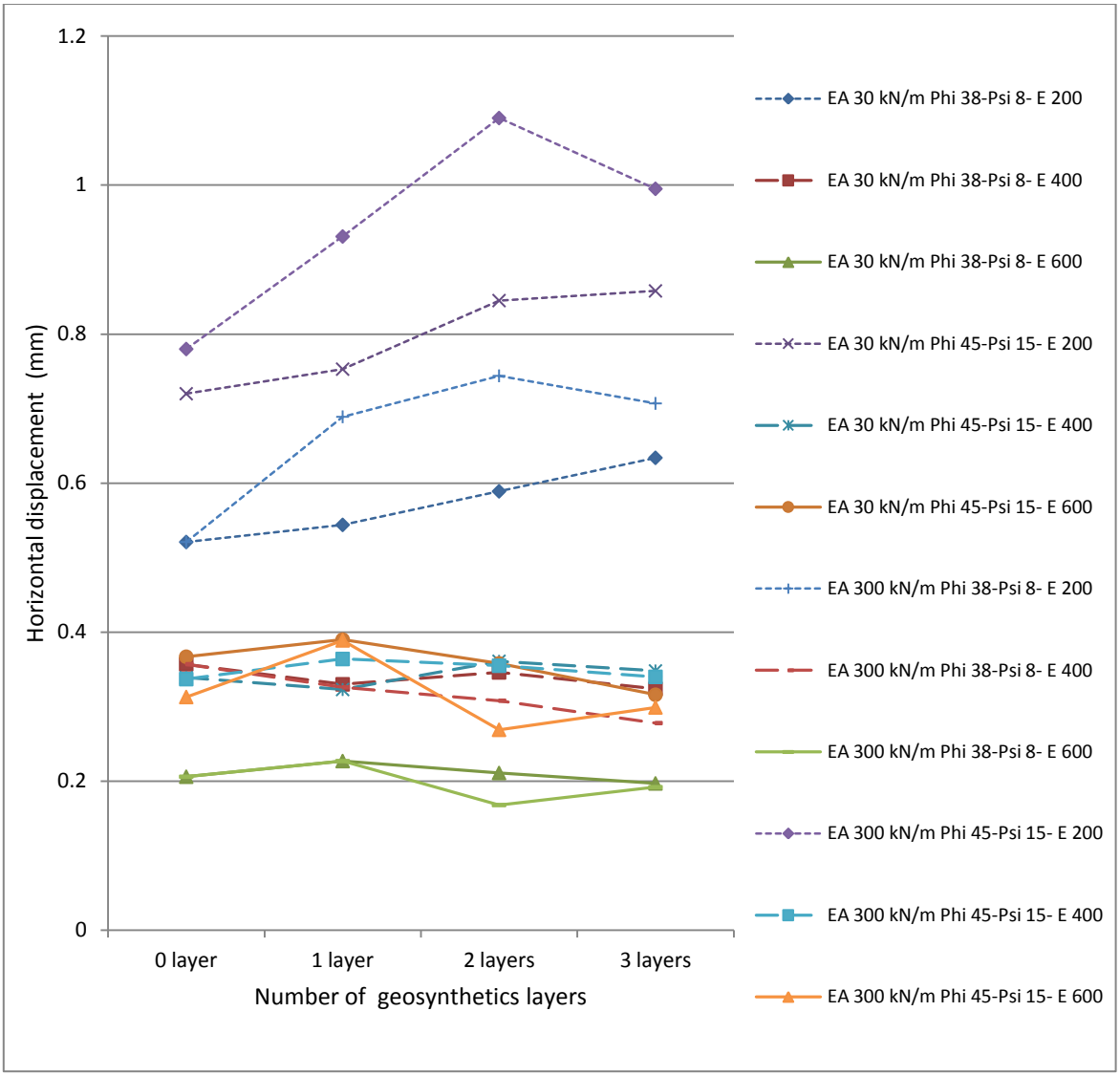

Fig. 6-2 Horizontal displacements vs. Number of geosynthetics layers

Fig. 6-2 suggests that at least two geosynthetics layer (vertical distance of 36.7 cm) of 300 kN/m tensile strengths on the elastic modulus of 200 MPa pavement material are needed, if not soil sample will be collapsed. Whereas use of low tensile strength of 30 kN/m does contribute stability of a soil sample. Meanwhile, at least a layer of geosynthetics (vertical distance of geosynthetics around 55 cm) is needed when applying the elastic modulus of 400 MPa with friction angle of 38^{o} and dilation angle of 8^{o}. Another finding using material with the elastic modulus of 600 MPa without the geosynthetics layer (soil sample height of 110 cm), soil sample does not fail. It is worthly to mention here that the best result is the use of 300 kN/m-tensile stiffness with the soil stiffness, phi, psi are 400 MPa, 38 degree, 8 degree respectively. The reason is that the increased number of geosynthetics layers applied causes horizontal displacements is smaller.

No doubt, the base course or subbase course material must be compacted on a construction. Hence, this material has a dilation angle and also the material should have a friction angle at least 30^{o}. Fig. 6-3 presents some findings using MC-model. Generally, the higher values of friction angle, dilation angle, tensile strength of geosynthetics and number of geosynthetics layers will provide the higher vertical stress as shown in Fig. 6-3. In x-axis, the numbers for

the first, second and third are the friction angle, dilation angle, and number of geosynthetics layers respectively.

(a)

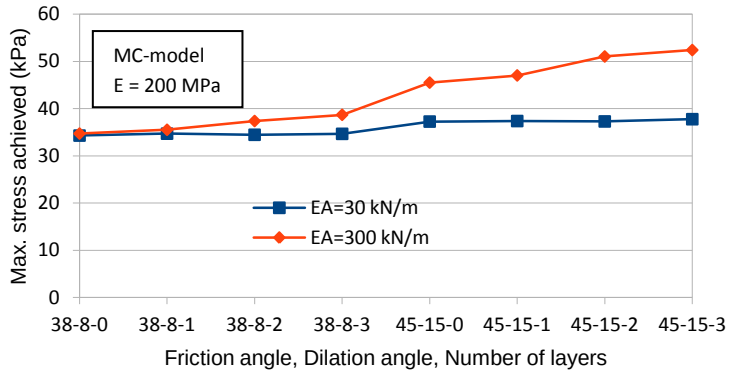

(b)

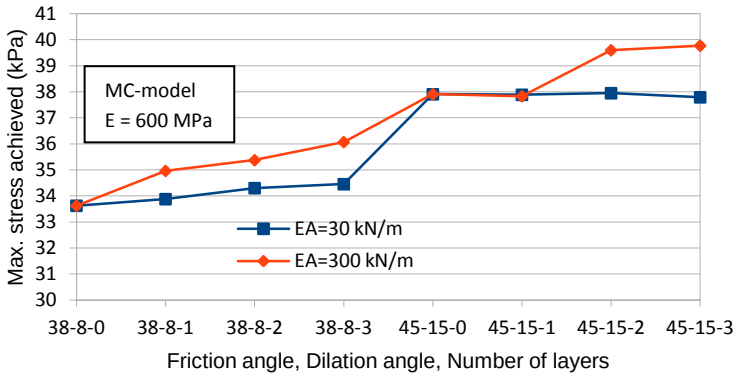

Fig. 6-3 Maximum stress using MC-model at different elastic modulus of base course (a) E=200 MPa (b) E= 600 MPa

Fig. 6-4(a) through Fig. 6-4(c) reveal some findings using HS-model as given in Table 6-7 through 6-12. When using MC-model, the model did not show stability of sample during subjected by a load. Vertical stresses are influenced by the elastic modulus of granular material, friction angle, dilation angle, tensile strength of geosynthetics and number of layer inserted in granular soil as shown in Fig. 6-4. In x-axis, number of first, second and third is the friction angle, dilation angle and number of geosynthetics layers respectively.

(a)

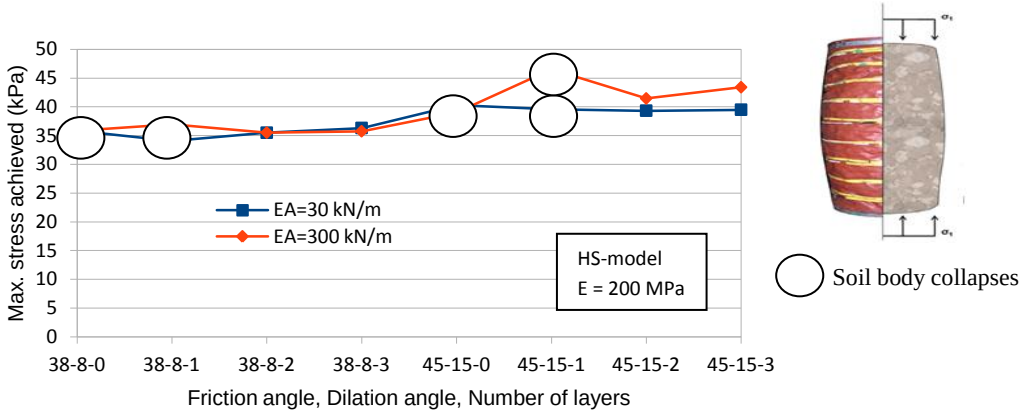

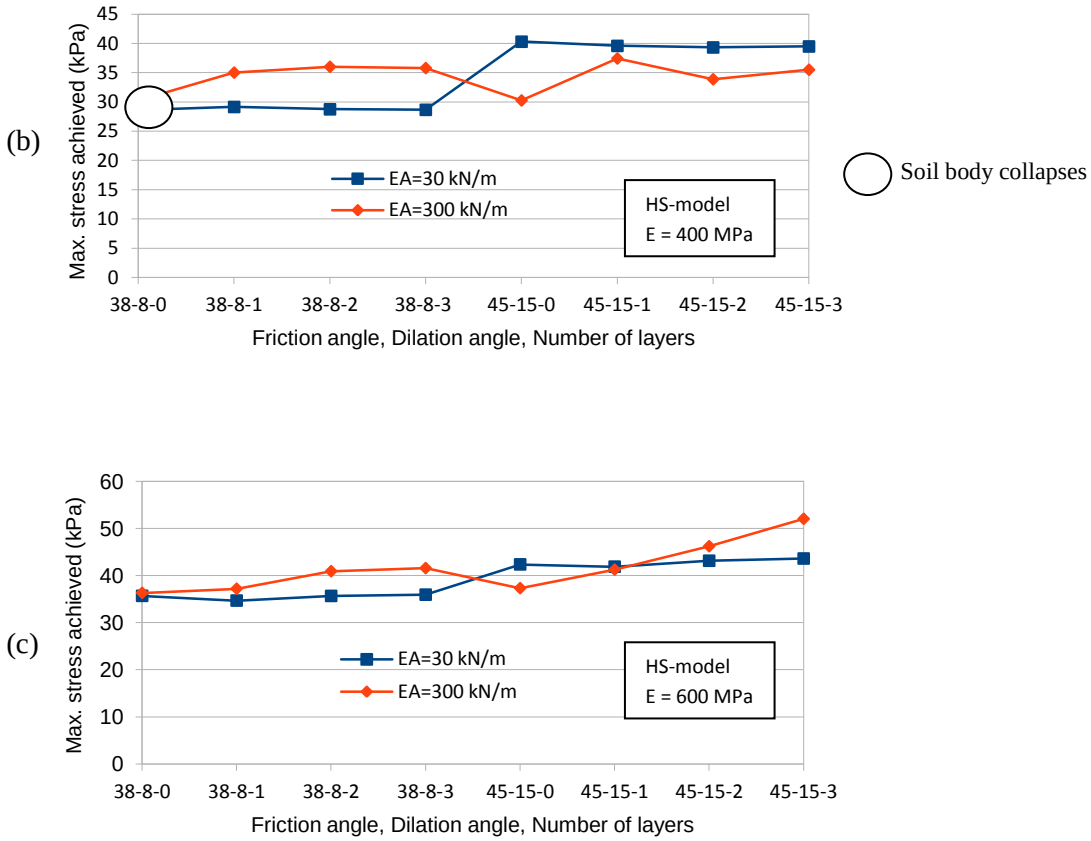

Fig. 6-4 Maximum stress using HS-model at different elastic modulus of base course

Circles signs designated in Fig. 6-4 are the stresses achieved when the soil sample is subjected to a vertical load. It can be seen that the higher friction angles can bear the higher stresses as well as higher tensile strength of geosynthetics.Though it is not so obvious for the elastic modulus of 400 MPa when geosynthetics with tensile strength of 300 kN/m is applied.

No doubt, the higher elastic modulus suggests higher stability when being subjected to a load. Fig. 6-4 shows that the elastic modulus of 200 MPa needs at least 2 layers of geosynthetics (36.7 cm-vertical distance of layers which the soil sample is 110 cm high) to withstand the loading. Whilst, materials having the elastic moduli of 400 MPa with a friction angle of 38^{o} needs at least one layer of geosynthetics (55 cm vertical distance). Granular soils having the elastic modulus of 600 MPa can withstand a load with vertical stress around of 35 kPa without using a layer of geosynthetics.

6.3. Stress Concentration Ratio

The simplest starting point for analysis of arching is a two-dimensional plane strain model. Some findings of Cao Wei-Ping's experimental work and then the use of finite element as a comparison are a good description to understand well the arching behavior. One of important parameters when soil arching occurred is stress concentration ratio, *n*.

Cao Wei-Ping et al. (2007) conducted experimental work for 15 test models (as explained in Chapter 4). The Plaxis finite element software using MC model based on soil material of Qiantang River Beach will be compared with the experimental work. Furthermore, material properties are listed in Table 6-13.

Table 6-13 Material properties used in finite element analysis

Properties		Element and model		
		Brick	Fill material	Water bag
Symbol	Unit	Linear elastic	MC	Linear elastic
Unit weight, γ	kN/m^3	22	15.6	15
Friction angle, ϕ	[^{o}]	-	34/44	-
Dilation angle, ψ	[^{o}]	0	0	-
Cohesion, c	kPa	-	0.5	0.5
Young's modulus, E	MPa	16000	160	50
Poisson's ratio, v	[-]	0.2	0.33	0.33
Permeability, k_i	m/s	-	-	100

6.3.1. Influence of Embankment Height on Stress Concentration Ratio

During running test, the soft soil support was imitated by using the water bag. Test 7 describes the vertical stress both on above soft soil and top pile during embankment filling as shown in Fig. 6-5. The stresses increase linearly with height of embankment. Moreover, the stresses on top pile will be higher than those of subsoil.

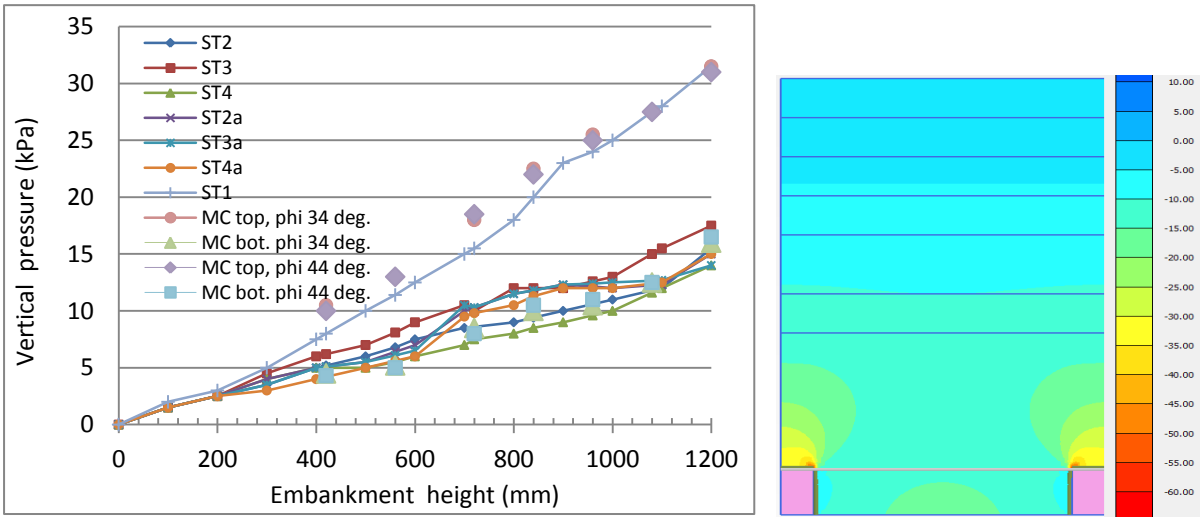

(a) Vertical stress resulted from Test 7 and model (b) Vertical stress using FEM

Fig. 6-5 Influence of embankment height due to vertical stress during embankment filling of Test 7

During the consolidation process, in this model, imitated by discharging water gradually from the water bags, the surface of subsoil will go downward, and it means that the reduced vertical support occurs over the surface of subsoil. In FE-analysis the process applies prescribed displacement. It turns out that the stresses at the top pile increase until certain maximum value and then gradually going down and more stable circumstance afterwards. It means that the stress concentration ratio, n, would be changing during the consolidation process. The stress concentration ratio for higher value of h/s will result in the stress concentration ratio to be higher than those of smaller h/s (see Fig. 6-6). There is strongly dependent on pile-subsoil relative displacement Δ_{Sc}, which the soil arching is developed at maximum value when Δ_{Sc}=8-13 mm, whilst beyond this range the soil arching may be less.

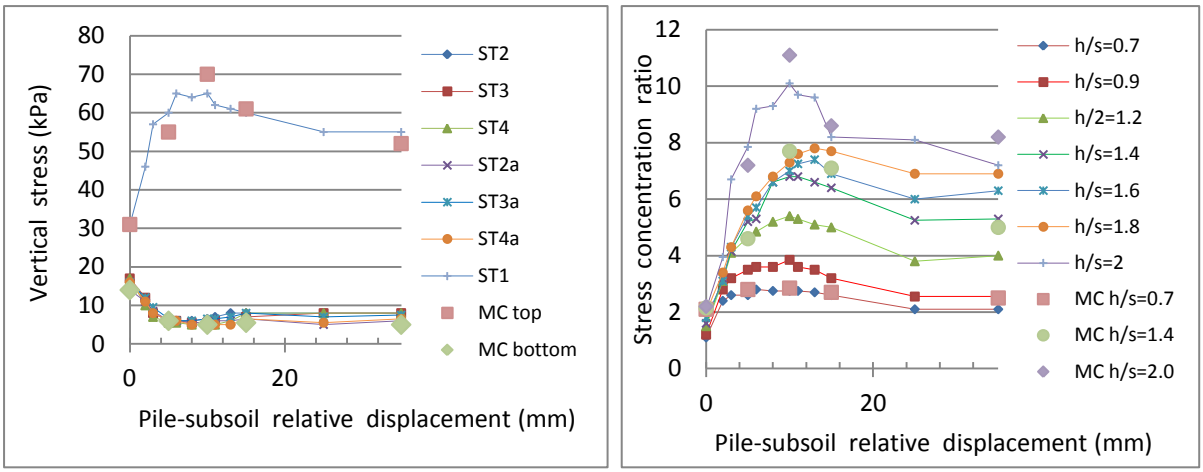

(a) (b)

Fig. 6-6 Variations of vertical stresses and stress concentration ratios, (a) Vertical stress during water discharge Test 7, (b) Influence *h/s* on stress concentration ratios

6.3.2. Differential Settlement and Critical Height of Embankment

Test 1 through Test 4, when $h/s \leq 1.4$, the embankment height was relatively 'low' and not completed soil arching. It shows that the surface of the embankment was non-uniform implying differential settlement occurred on the top of the embankment. Furthermore, in Test 5 through Test 7, when $h/s > 1.6$, the embankment height was relatively 'high', the settlements at the base of the embankment were non-uniform, but at the surface of the embankment remained almost flat. Both situations when pile-soil relative displacement Δ_S =35 mm are depicted in Fig. 6-7.

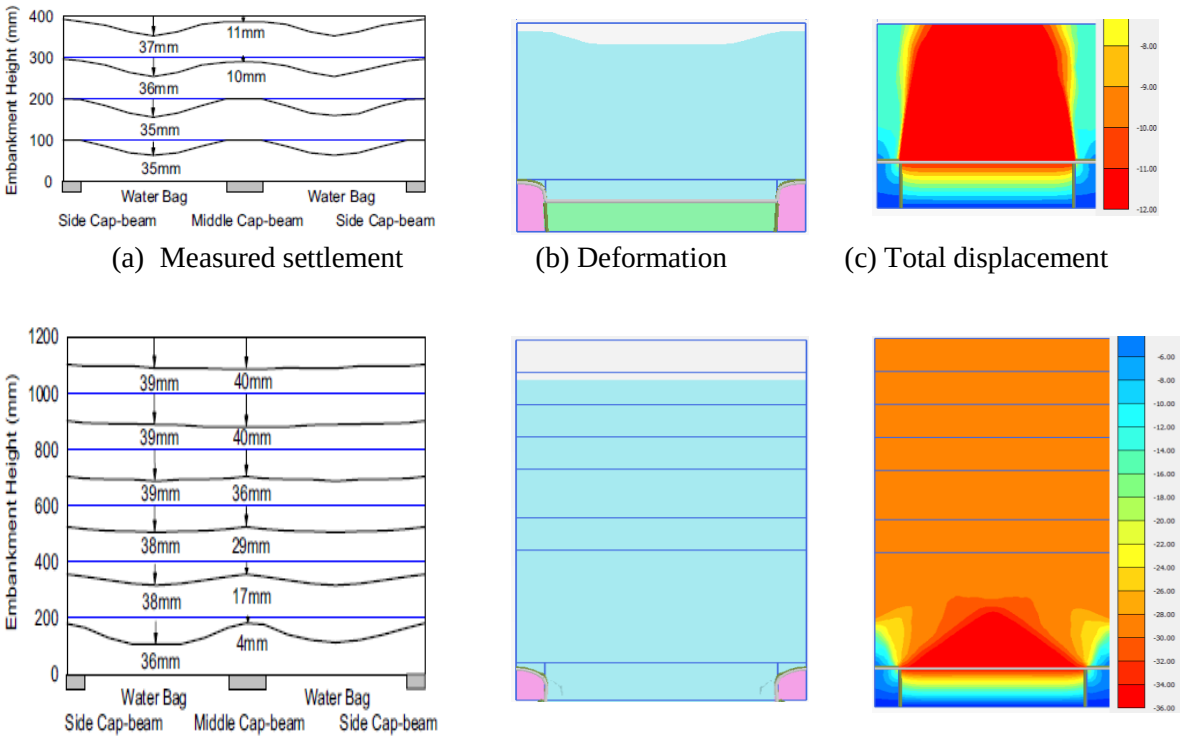

(a) Measured settlement (b) Deformation (c) Total displacement

(a) Measured settlement (b) Deformation (c) Total displacement

Fig. 6-7 Differential settlements of Test 1 (above) and Test 7 (below)

A comparison for settlement at the surface of the embankment between measurement and finite element analysis for Test 1 (C) and Test 7 (h/s=2) is shown in Table 6-14.

Table 6-14 Settlements at surface of embankment using FE-analysis

Test number	Settlements at surface of embankment (mm)					
	Measurement		Finite element method			
			$\phi = 34^{o}$		$\phi = 44^{o}$	
	Above of pile	Between piles	Above of pile	Between piles	Above of pile	Between piles
Test 1 (h/s=0.7)	11	37	13.73	35	13.5	34.5
Test 7 (h/s=2.0)	40	39	29.63	29.63	29.75	29.77

Experimental work and FE-analysis suggest that the height of the equal settlement plane, h_c, is about 1.4-1.6 times of the cap beam clear spacing or h_c=(1.4-1.6)s. Furthermore, to ensure that no differential settlement occurs at the surface of embankment, the embankment height of 1.6s is necessary. Fig. 6-8 presents some deformation of embankment including mesh deformation, the total vertical displacement, total vertical and horizontal strain for h/s=1.4 using FE analysis when subsoil is moved downward 35 mm.

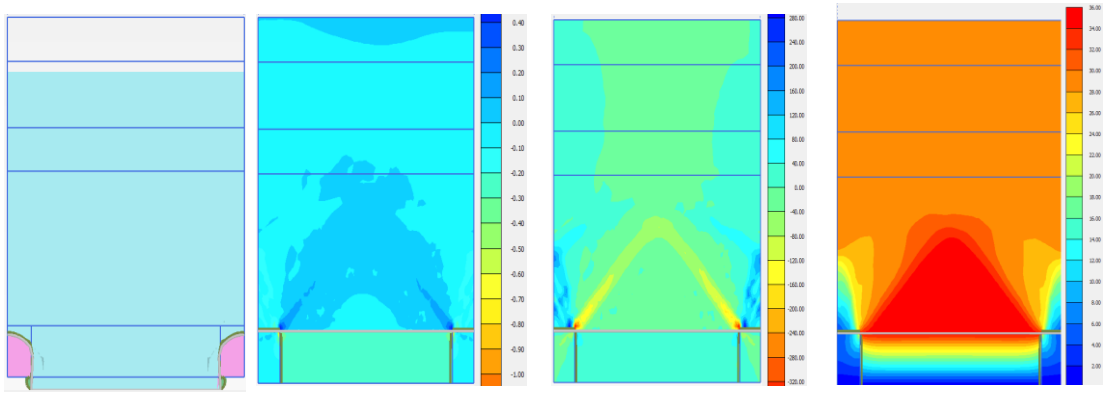

(a) Deformation (b) Vertical strain (c) Horizontal strain (d) Vertical displacement

Fig. 6-8 Shapes of deformation for h/s=1.4

6.3.3. Comparison of Stress Concentration Ratio between Experimental Work and Several Analytical Methods

It is useful to understand the parameter of stress concentration ratio on arching phenomenon between experimental results and some analytical methods as well as the finite element method. Several analytical methods have already been existed such as Method of Low et al. (1994), Method of Terzaghi (1943), British Standard BS 8006 (1995).

There are seven model tests with different ratios of embankment height to clear spacing (h/s). Test 1 has the smallest ratio of 0.7, whereas Test 7 has the highest ratio of 2. Meanwhile, some values in between are 0.9, 1.2, 1.4, 1.6, and 1.8 respectively. Results of Test 1 through Test 7 are then compared with analytical methods and also the finite element method. Parameters of material fill are assumed for c=0 kPa, ϕ=44^{o} and γ=15.5 kN/m^{3}. Resume of equations for 2D-analytical methods are shown in Table 6-15.

Table 6-15 Equations in analytical method of two-dimension

Method	Stress on pile, σ_p	Stress on subsoil, σ_s	Remarks
Low et al.(1994)	$\sigma_p = \frac{(s+a)h\gamma - \sigma_s s}{a}$	$\sigma_s = \alpha\gamma\left\{\frac{(K_p-1)(1-\delta)(s+a)}{2(K_p-2)} + (1-\delta)^{K_p-1}\left[h - \frac{s+a}{2} - \frac{s+a}{2(K_p-2)}\right]\right\}$	δ=$a/(s+a)$ α=0.8 a= width of pile cap s = piles clear spacing h=high of embankment
Terzaghi (1943)	$\sigma_p = \frac{(s+a)h\gamma - \sigma_{vh}s}{a}$	$\sigma_{vh} = \sigma_v \mid_{z=h} = \frac{s\gamma}{2Ktan\,\emptyset}\left(1 - e^{-2K\left(\frac{h}{s}\right)tan\emptyset}\right)$	K= 0.7 Valid for $h/s \leq 2$
BS8006 (1995)	$Case\ 2D \ldots \frac{\sigma_p}{\gamma h} = \frac{C_c a}{h}$ $Case\ 3D \ldots \frac{\sigma_p}{\gamma h} = \left(\frac{C_c a}{h}\right)^2$	$\sigma_s = \frac{(s+a)h\gamma - \sigma_p a}{s}$	C_c=1.95 h/a- 0.18 for end-bearing piles C_c=1.55 h/a- 0.07 for friction piles h_c=1.4s

Then, stress concentration ratio can be easily obtained which $n = \sigma_p / \sigma_s$. Herein, the comparison is only intended for embankment without reinforcement namely from Test 1 with h/s=0.7 to Test 7 with h/s=2.0 as depicted in Fig. 6-9.

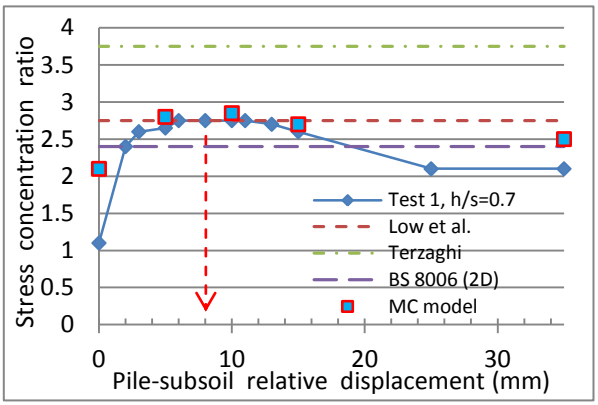

(a)

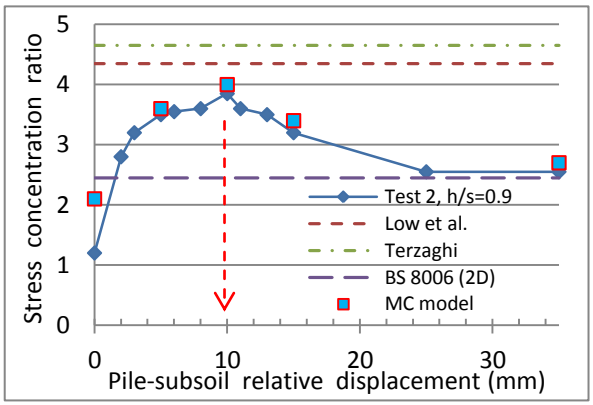

(b)

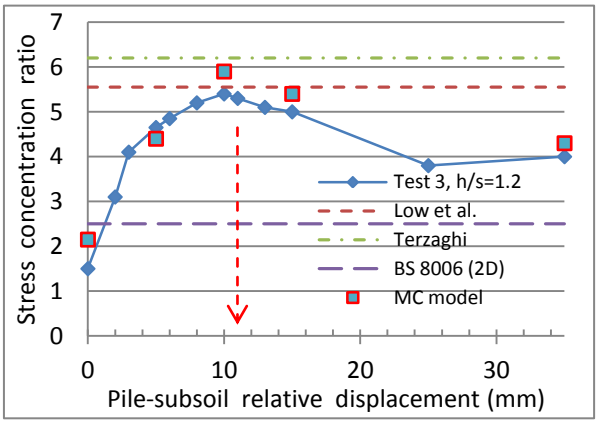

(c)

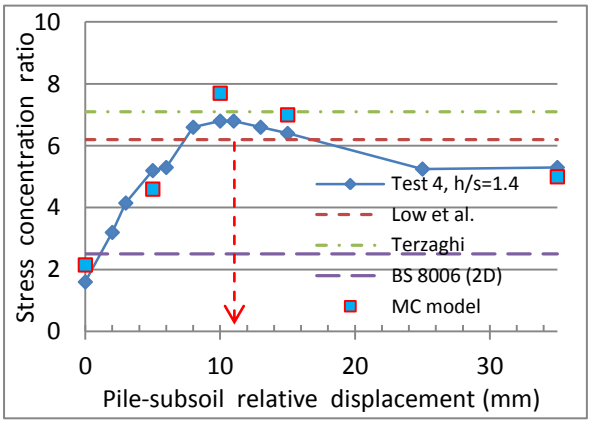

(d)

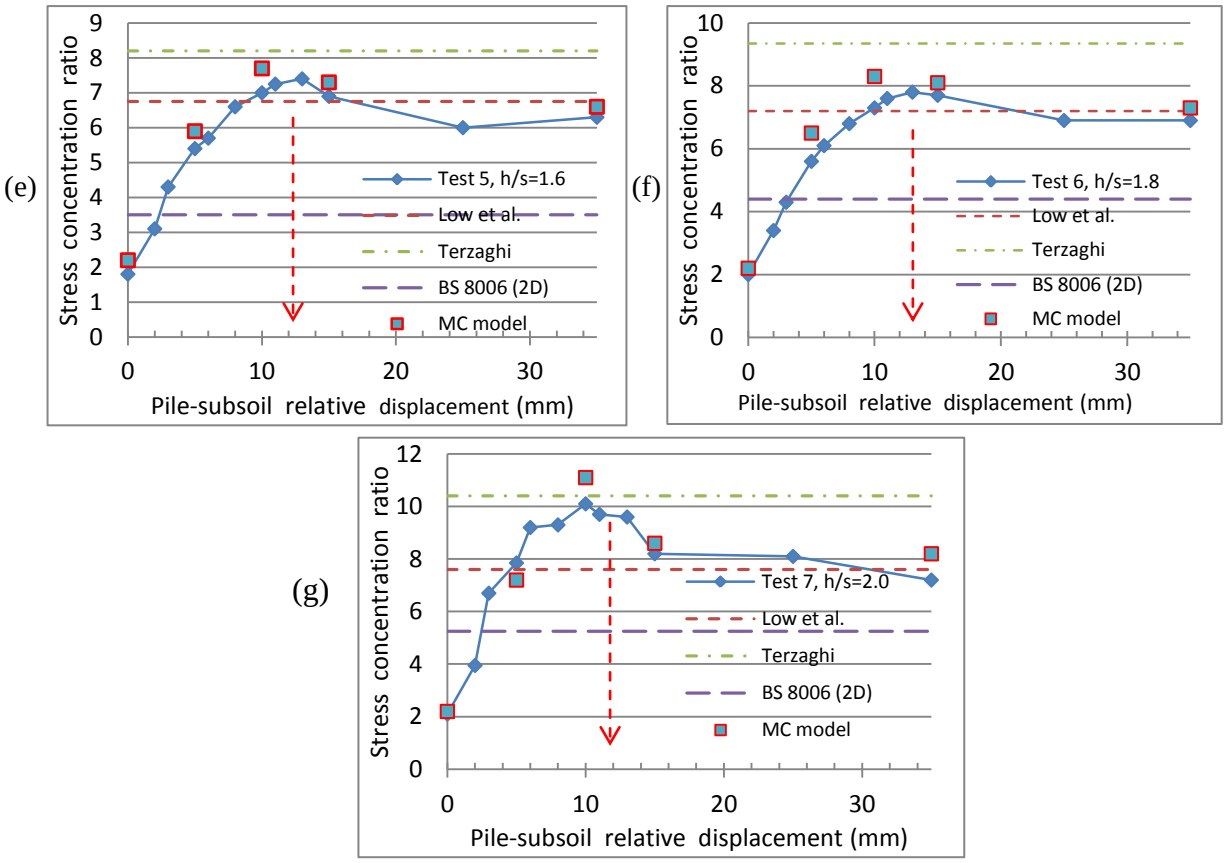

Fig. 6-9 Comparison between test results, Analytical methods and Finite element analysis for stress concentration ratio: (a) Test 1, (b) Test 2, (c) Test 3, (d) Test 4, (e) Test 5, (f) Test 6, (g) Test 7

The figures show that Terzaghi method is always over-prediction in the stress concentration ratio whereas the BS8006 method suggests strongly under-estimate. Meanwhile, Low et al. method gives slightly larger result for low embankment $h/s \leq 1.4$ but this method good agrees with high embankment $h/s > 1.4$. Iglesias et al. (1999) have introduced a terminology namely Ground Reaction Curve by means of normalising subsoil movement downwards to pile clear spacing. This curve describes a curve of vertical stress over subsoil. When stress on top of the piles is at a maximum value, the vertical stress over subsoil is at a minimum value. Meanwhile, the curves above show that the critical values are between 8-13 mm. By using pile clear spacing of 60 cm, it means that the critical values are from 1.3% to 2.2%.

6.4. Load Transfer Platform

In Malaysia particularly nearby Gebeng Highway, Hassandi et al. (2007) carried out a field test using the various load transfer platform (LTP) on top of aggregate piers (called 'geopiers') on soft soil. It would have shown the performance of several load transfer platform used in the field test. The rammed aggregate piers as columns used in the field test are 'floating piles' over soft soil. Test embankment was approximately 90 m long, 14.5 m wide, and 3.5 m high. The side slopes of the embankment were 1V:1.5 H.

There are three types of load transfer platform (LTP) performed in the field test, namely:

- Geosynthetics-reinforced LTP with two layers of geogrids (catenary LTP)
- Geosynthetics-reinforced LTP with three or more layers of geogrids (beam LTP)
- Reinforced concrete LTP

Two control sections were also provided at the edge of the field test. These sections are embankment without reinforcement. Layout and dimension of different LTP are shown in Fig. 6-10.

The geosynthetic-reinforced LTPs consist of an aggregate layer with geogrid reinforcement within the aggregate. Section 1 has a 1.5 m thick beam LTP with four layers of biaxial extruded polypropylene geogrid (Tensar SS20) reinforcement spaced at 0.3 m apart vertically within the LTP, and supported on geopiers spaced in a 3.25 m center-to-center square pattern. Section 2 has a 1.0 m thick beam LTP spaced at 0.3 m apart vertically, and supported on geopiers in spaced a 2.5 m center-to-center square patterns. Section 3 has a catenary LTP with two layers of uniaxial woven polyester high-strength geogrid coated with polyvinyl chloride (Miragrid 24XT) spaced at 75 mm apart vertically placed in a different direction (longitudinal and transverse) of embankment. This section was also supported on geopiers spaced at 2.5 m. Last section (section 4) was supported on 0.3 m thick continuous steel-reinforced concrete LTP over geopiers spaced of 2.5 m.

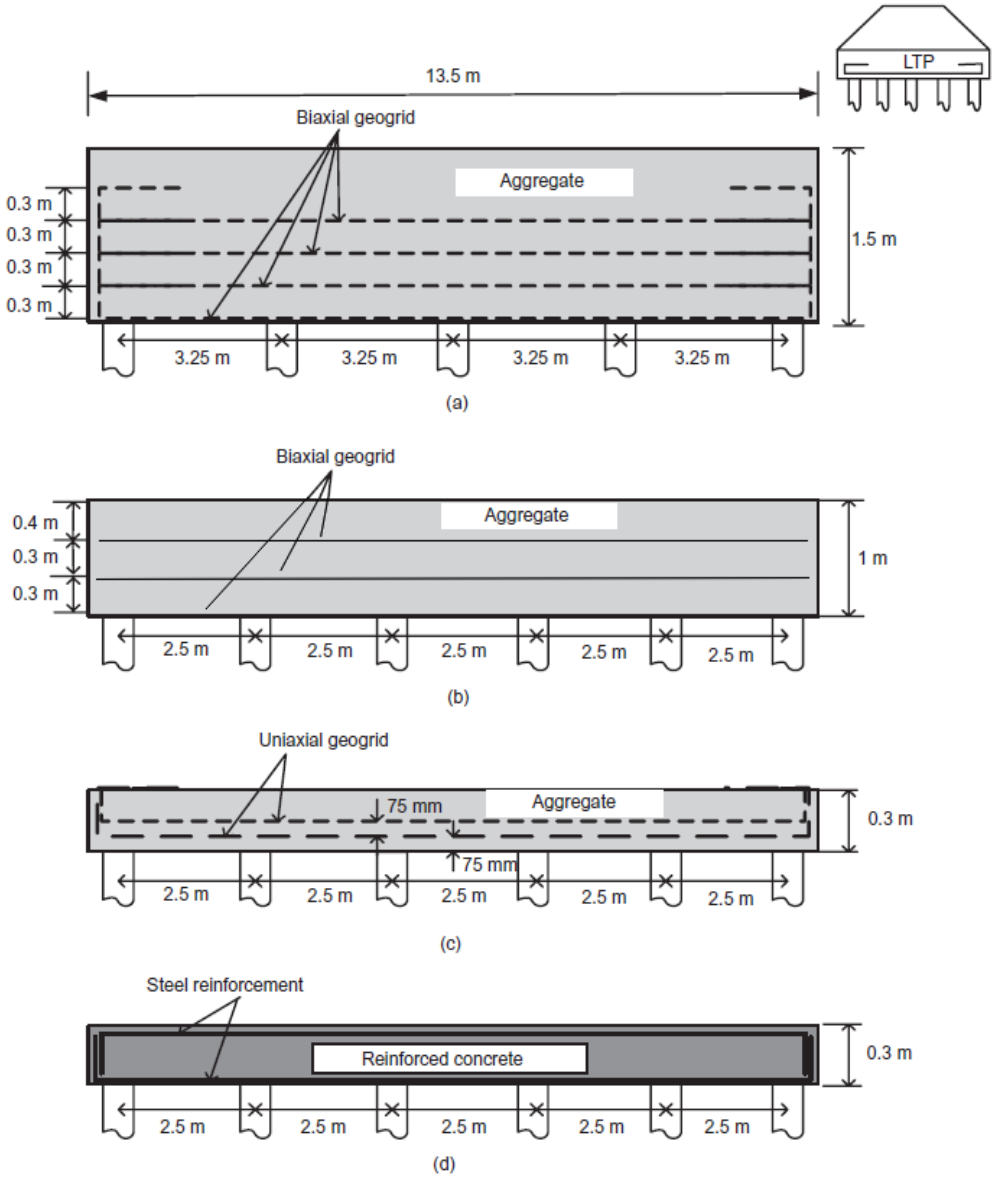

Fig. 6-10 Schematic sections of LTP (after Hassandi et al., 2007)

Table 6-16 Properties of geogrids used in the field test (after Hassandi et al., 2007)

Properties	Biaxial extruded geogrid		High-strength uniaxial geogrid	
	Machine direction	Cross-machine direction	Machine direction	Cross-machine direction
Tensile strength at ultimate (kN/m)	20	20	370.3	43.6
Tensile strength at 5% strain (kN/m)	14	14	93.3	17.5
Tensile modulus (kN/m)	280	280	1870	350
Grid aperture (mm)	39	39	101	17.8
Mass/unit area (kg/m2)	0.220		1.289	

The selected aggregate used in the LTPs consisted of well-graded crushed granitic rock with fine material that was less than 3%. This aggregate is normally used as a sub-base layer for road pavements. Then, over this aggregate blanket, the embankment was constructed using gravelly sandy clay.
The rammed aggregate pier, called geopier, is a relative the new intermediate-depth columnar foundation introduced in the construction industry (Fox and Cowell, 1998). Typically, drilled holes were extended between 2 and 8 m below subsoil surface. In this field test, the initial drilled diameter of the geopiers was 0.75 m and the initial depth of the drilled hole for the geopier was 5.5 m.

Site investigation provides a soft silty clay/clayey silt layer as deep as 15 m at some location. This layer is composed of highly plastic clay with natural content between 35% and 61%. Field vane tests indicated that the shear strength ranges from 14 to 60 kPa, with most of the values less than 25 kPa. Moreover, its value of sensitivity varies from 3 to 11.

6.4.1. Settlement of the Embankment over Floating Piles

This embankment is high embankment ($h/s \geq 1.4$). Therefore, differential settlement at the surface of the embankment may be omitted because it is very small. Then, total settlement and differential settlement at the bottom of the embankment are the important things to be discussed. Table 6-17 provides material properties are used in FE-analysis.

Table 6-17 Material properties used in finite element analysis of embankment test on Gebeng highway

Properties		Element and model						
		Geopier	Fill material	Aggregate blanket	Subsoil		Geogrid	Concrete Slab
		MC	MC	MC	MC	SSC	Elasto-plastic	Elastic
Unit weight, γ	kN/m^3	19	18.5	21	14	14	-	24
Friction anle, ϕ	[^{o}]	48	35	38	8	8	-	-
Dilation angle, ψ	[^{o}]	0	0	4	0	0	-	-
Cohesion, c	kPa	1	1	1	15	15	-	-
Young's modulus, E	MPa	100	200	300	0.75	0.75	280, 1870	19650
Modified comp. index, λ^*	[-]	-	-	-	-	0.1183	-	-
Modified swelling index, κ^*	[-]	-	-	-	-	0.0229	-	-
Modified creep index, μ^*	[-]	-	-	-	-	0.0058	-	-
Poisson's ratio, ν_{ur} /ν	[-]	-/0.3	-/0.3	-/0.3	-/0.4	0.15/-	-	-/0.15

The total settlement resulted from field test and calculation using finite element method is compared. Treatment between compaction and no compaction using a load of 550 kPa generated from wheels roller during the compaction process is presented. In addition, Mohr Coulomb model for whole soil material (embankment and subsoil) and Mohr Coulomb model for embankment combined with Soft Soil Creep (SSC) model for soft soil are also presented.

Figure 6-11(a) through Figure 6-11(d) show a comparison between field measurement and finite element calculation for several types of LTP. Fig. 6-11(a) and Fig. 6-11(b) show that the total settlement of geogrid from field measurement at the bottom layer would be deformed deeper than at the upper layer of geogrid. Mohr Coulomb model using plastic calculation with compaction load of 550 kPa can be used to predict the total settlement only for the final step of compaction at the end of project execution. Although, it cannot follow the creep phenomenon on soft soil after completion of project execution. Meanwhile, the SSC-model for the soft soil is better and can follow the creep phenomenon when using the consolidation calculation type and no compaction load.

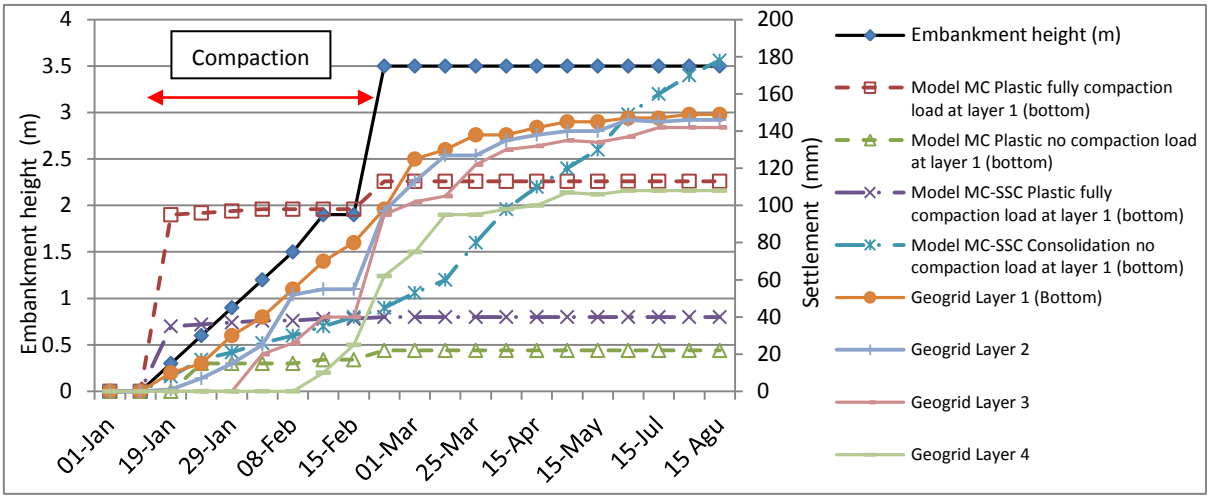

(a) Section 1

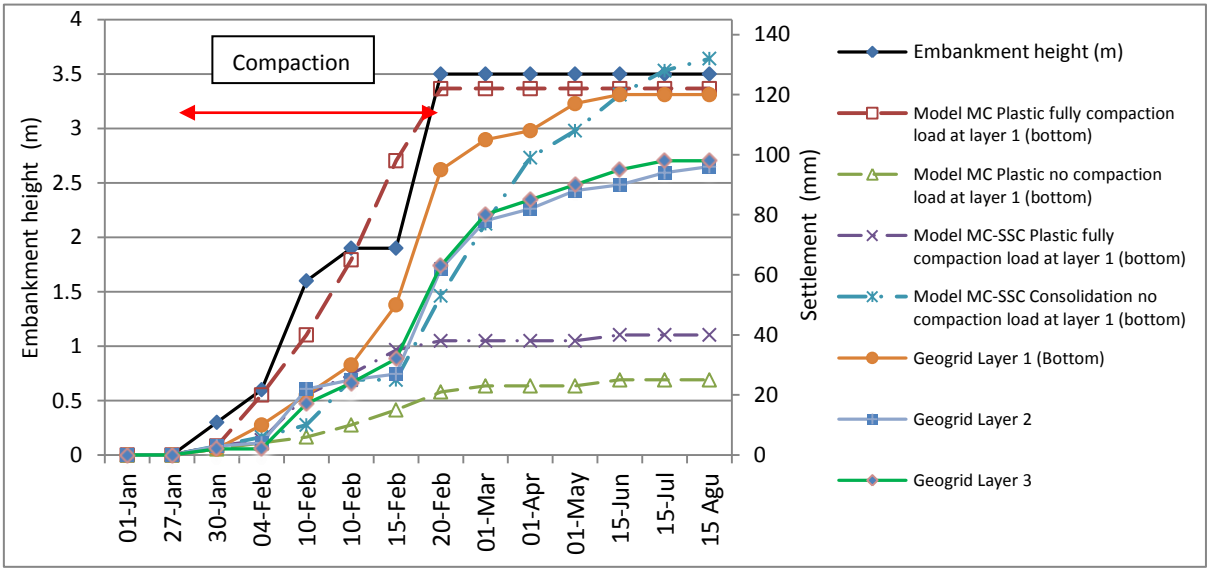

(b) Section 2

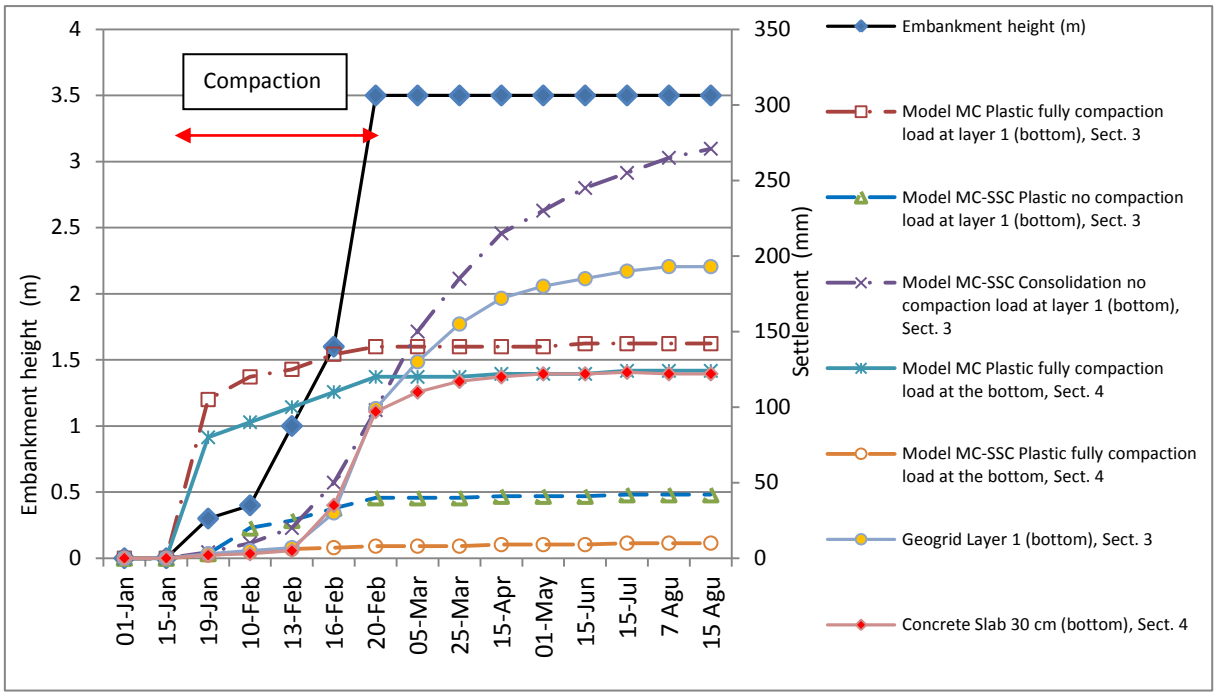

(c) Section 3 and 4

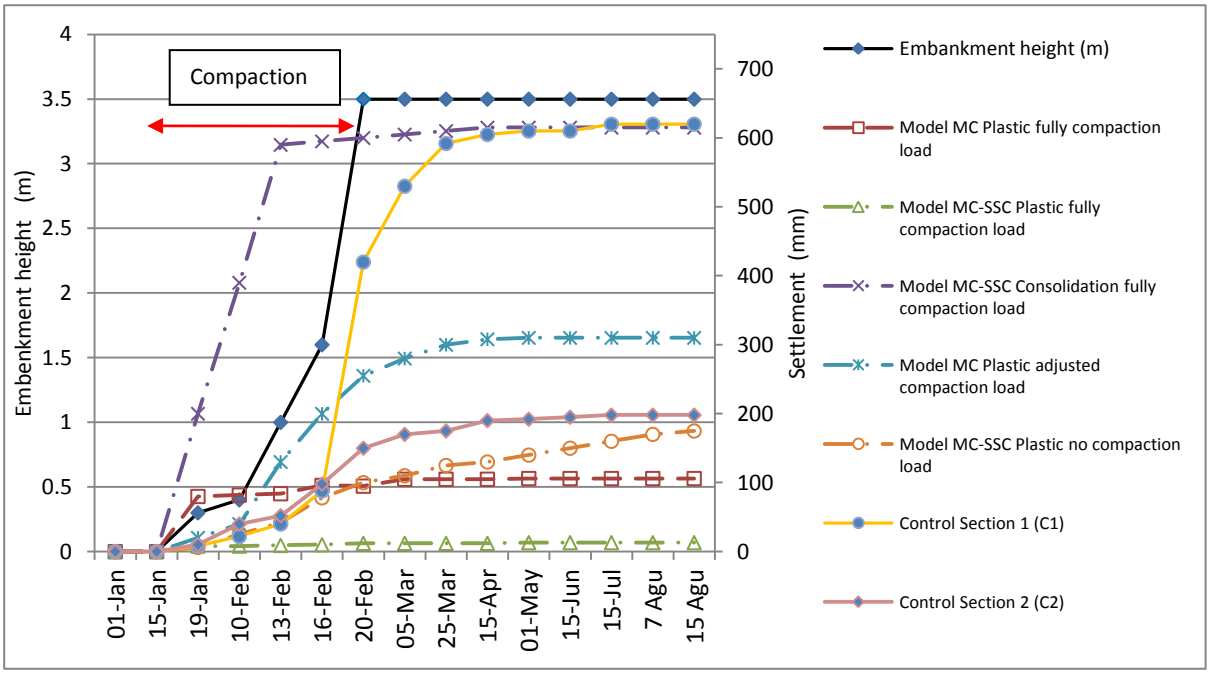

(d) Control sections

Fig. 6-11 Total settlement of LTP sections (at centre of square pattern of geopiers) and control sections: (a) Section 1 (b) Section 2 (c) Section 3 and 4 (d) Control sections

Similarly, settlement for a catenary LTP over the floating piles will be better predicted with consolidation calculation type without compaction process regarding with creep as shown in Fig. 6-11(c). Although, plastic calculation type can be used without considering creep with compaction at the final of embankment hight. Meanwhile, Fig. 6-11(d) suggests that settlement without piles will be deeper than those of using piles.

6.5. Low Embankment on the End-bearing Piles

In case, the use of end-bearing pile and load transfer platform of catenary (1 or 2 layers of geosynthetics) Almeida et al. (2008) performed a field test of a low embankment (h/s <1.4) at Barra da Tijuca district in Brazil. Two situations had already been done by means of excavated and non-excavated zones. Purpose of the excavated zone is to know the influence soil support on pile embankment. Lay out for the field test is described in Fig. 6-12.

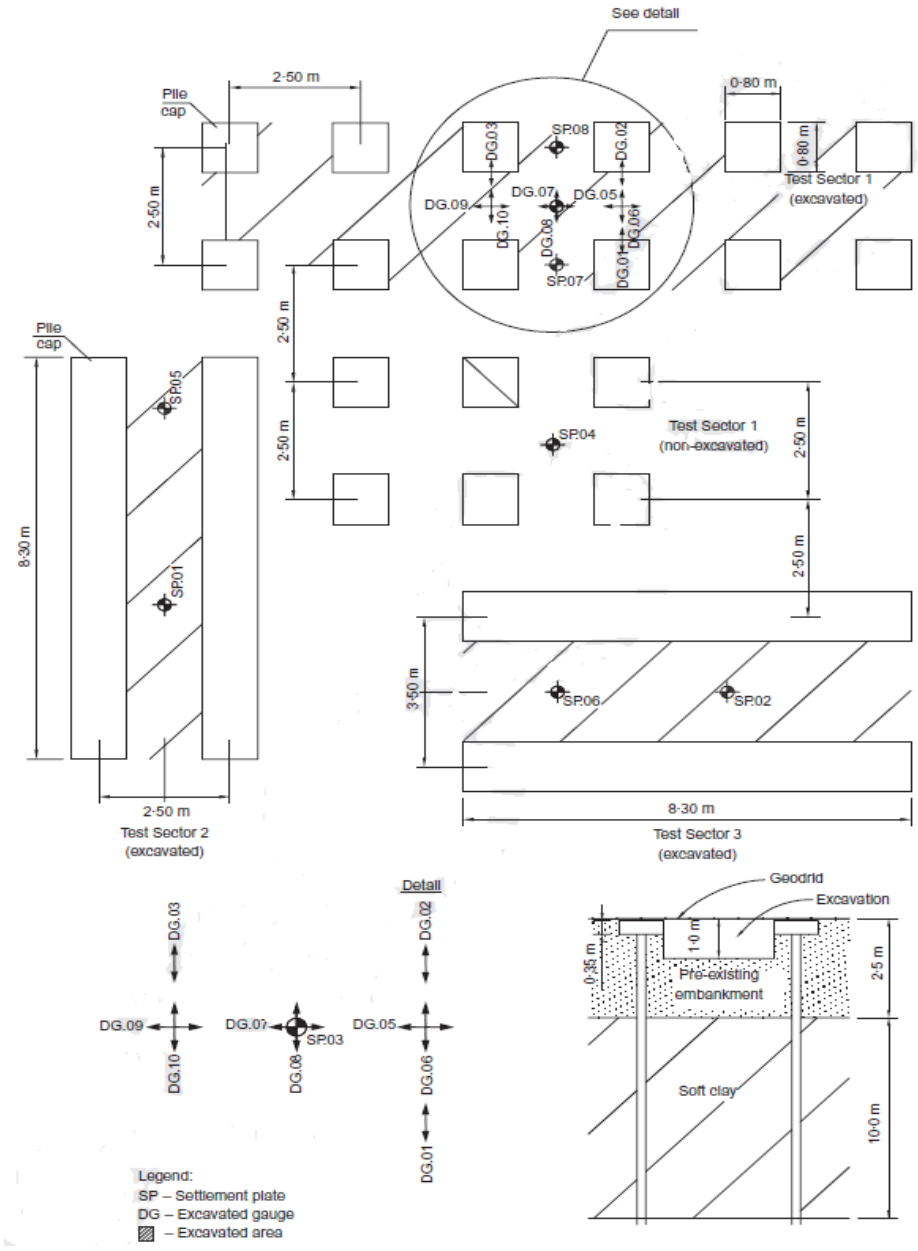

Fig. 6-12 Layout of field test at Barra da Tijuca district in Brazil (after Almeida et al., 2008)

Properties of materials are shown in Table 6-18 and FE-calculation uses 2-D axisymmetric and plane strain model. Pavement materials are approached with MC and HS-model and subsoil with SSC-model. While, linear elastic model is applied for pile and geosynthetics.

Table 6-18 Material properties used in finite element analysis at Barra da Tijuca district in Brazil

Properties		Element and model					
		Concrete pile	Working platform	Fill embankment		Subsoil	Biaxial Geogrid
		Linear elastic	MC	MC	HS	SSC	Linear elastic
Unit weight, γ	kN/m^3	24	17.5	18	18	12.5	-
Friction angle, ϕ	[^{o}]	-	33.8	37	17	5	-
Dilation angle, ψ	[^{o}]	-	0	0		0	-
Cohesion, c	kPa	-	11	11	11	11	-
Young's modulus, E	MPa	24000	300	400	-	0.75	-
Secant modulus, E_{50}	MPa	-	-	-	130	-	-
Oedometer comp. modulus, E_{oed}	MPa	-	-	-	150	-	-
Un-/reloading modulus, E_{ur}	MPa	-	-	-	400	-	-
Modified compression index, λ^*	[-]	-	-	-	-	0.226	-
Modified swelling index, κ^*	[-]	-	-	-	-	0.012	-
Modified creep index, μ^*	[-]	-	-	-	-	0.005	-
Poisson's ratio, v_{ur} /v	[-]	-/0.15	-/0.3	-/0.3	0.2/-	0.15/-	-
Tensile strength, EA	kN/m	-	-	-	-	-	1400

Settlements resulted from field measurement and FE-calculation can be looked into in Table 6-19 both 2D and 3D layout for various positions. Meanwhile, Fig. 6-13 shows the settlement using FE-calculation with the model using both the MC model and HS model for pavement material and SSC model for the soft soil at the centre of 4 piles.

Table 6-19 Comparison of settlements between at base of embankment from field measurement and FE-calculation

Plates	Layout	Position	Embankment height, h (m)	Half distance between pile caps, b (m)	h / b	δ / b	Settlements till end of construction , δ (m)		
							Field measurement	FE-calculation	
								MC-SSC	HS-SSC
SP 01	2D	Midpoint	1.10	0.85	1.30	0.37	0.032	0.027	0.030
SP 05	2D	between	1.14	0.85	1.33	0.27	0.022	0.027	0.030
SP 02	2D	adjacent	1.28	1.35	0.95	0.27	0.037	NC	NC
SP 06	2D	pile caps	1.25	1.35	0.93	0.30	0.040	NC	NC
SP 03	3D	Centre of	1.28	0.85	1.49	0.43	0.360	0.720	0.060
SP 04	3D	4 piles	1.08	0.85	1.27	0.12	0.025	0.015	0.020
SP 07	3D	Midpoint	1.23	0.85	1.45	0.19	0.017	NC	NC
SP 08	3D	between pile caps	1.24	0.85	1.45	0.20	0.017	NC	NC

Remarks: NC = *no calculated*

Unfortunately, FE-analysis finds the difficulties when modeling the excavated sector which suggests huge deformation. Whereas, on non-excavated sector the settlements could be approached using the plastic calculation type with involving loading during the compaction process or consolidation calculation type . Fig. 6-13 shows settlements at the centre of 4 piles between field measurement and FA-analysis. It can be seen that several weeks after the end of construction, the settlement in the field was developed highly huge because of traffic and weak anchorage.

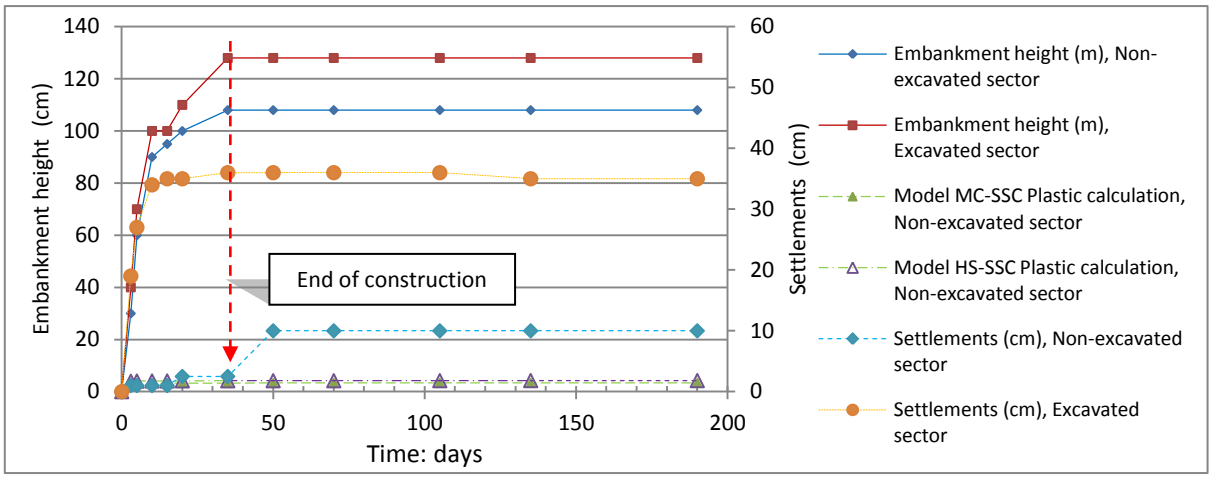

Fig. 6-13 Settlements at the centre of 4 piles

Strains of 3D layout resulted from field measurement particularly on the excavated zone and compared with axisymmetric configuration are shown in Table 6-20.

Table 6-20 Comparison of tensile strains for geosynthetics between field measurement and FE-analysis

Deformation gauge	Layout	Position	*h* / *b*	Strain (%)		
				Field measurement	FE-analysis	
					MC-SSC	HS-SSC
DG 01	3D	Face of pile caps	1.5	2.05	1.14	1.52
DG 02	3D		1.5	1.73	1.14	1.52
DG 03	3D		1.5	1.51	1.14	1.52
DG 05	3D	Half distance between pile	1.5	0.51	0.27	0.36
DG 09	3D	caps, parallel to pile face	1.5	0.32	0.27	0.36
DG 06	3D	90° to DG 05	1.5	1.50	0.85	1.14
DG 10	3D	90° to DG 09	1.5	1.36	0.85	1.14
DG 07	3D	Centre of four pile caps,	1.5	1.14	0.63	0.83
DG 08	3D	align to pile array	1.5	0.97	0.63	0.83

It is clear that the maximum tensile strength of geosynthetics would be occurred at zone of adjacent piles, and then the lower tensile strength would be found at half distance between piles with parallel to pile face. This zone is so-called *'primary reinforcement'*, whereas other as *'secondary reinforcement'*.

6.6. Influence of Traffic Load on Arching Effect

A full-scale test of a low embankment using the end-bearing wooden piles had been carried out in Giessenburg (so called 'Kyoto Road') in the Netherlands. Suzanne van Eekelen at al. (2008) have observed the influence of loading induced by traffic load during 3 ½ years after completion of construction by installing cell pressures at the surface of piles located above and below geosynthetics to measure vertical stress on the top of piles.

The Kyoto road was constructed on 13 m long wooden piles and configured using piles spacing of 1.27 m grid pattern, concrete pile caps with a height of 0.4 m and 0.3 m diameter. The geogrid reinforcement consisted of two layers uni-axial grids, perpendicular on road axis Fortrac 400/30-30 M and along the axis Fortrac 350/50-30 M (see Fig. 6-14). On top of that, a 1.15 m high compacted embankment fill of a 'Hegemann' (sandy) sludge mixture was constructed.

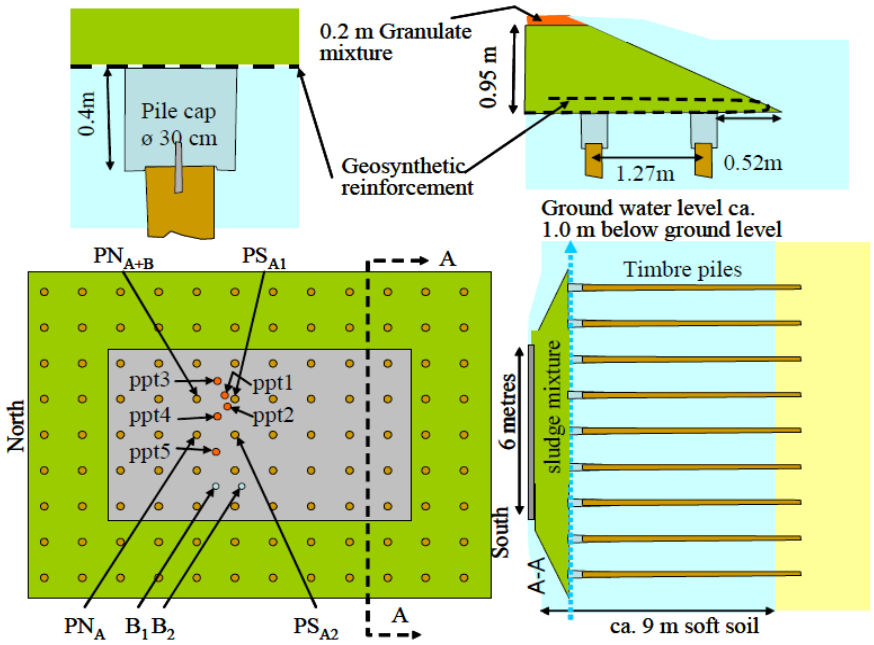

Fig. 6-14 Layout of the Kyoto road field test (after Eekelen, 2009)

The Hegemann sludge mixture is a mixture of dredged material and additives containing mainly clay and cement with the following properties: average unit weight γ=18.6 kN/m^3, a friction angle of ϕ=33.8^o and a cohesion of 11.5 kPa. The Kyoto road was built over a 9 m deep of soft soil with a reaction modulus k= 477 kN/m^3. Table 6-21 shows soil properties used in Kyoto road embankment.

Table 6-21 Properties of fill material used in Kyoto road embankment

γ_{wet}	γ_{dry}	γ_{avg}	w	k_v	ϕ	c
kN/m^3	kN/m^3	kN/m^3	%	m/s	^{o}	kPa
22.2	17.0	18.6	18.1	2.1E-9	33.8	11.5

Source: van Eekelen, 2009

Table 6-22 shows Young's moduli of subsoil used for analysis. These values are found from soil investigation on site and then tested in the laboratory.

Table 6-22 Young's moduli of Kyoto road's subsoil

Position	Material	Thickness (m)	E (kN/m^2)
Top layer	peat	d_1= 1.45	1077
Lower layer	clay	d_2= 1.50	2000

Source: van Eekelen, 2009

The modulus of subgrade reaction, k, can be calculated as follows: $k = (E_1.E_2)/ (E_1.d_2+E_2.d_1)$ = 477kN/m^3.

Performance of gosynthetics is time-dependent, so time will influence the performance of material in construction along its life service. Fig. 6-15 shows their isocrones: time dependent tensile stiffness J can be evaluated for a strain 2%.

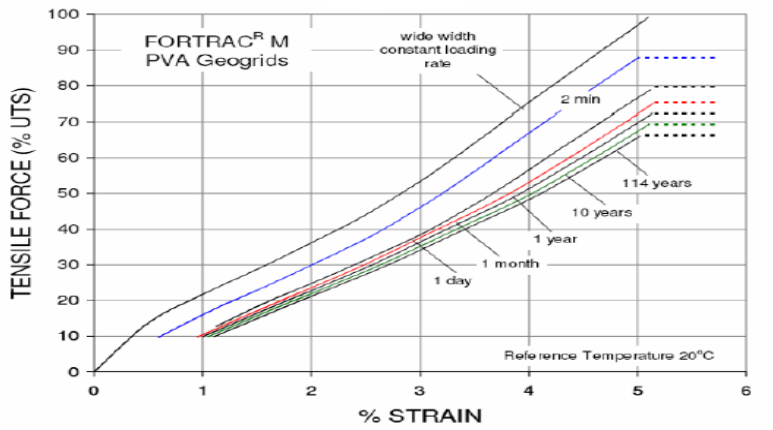

Fig. 6-15 Isochrones of geogrids (after Eekelen, 2009)

By using Fig. 6-15, tensile stiffness of material used on the test of road embankment can be estimated for long-term as indicated in Table 6-23.

Table 6-23 Tensile stiffnesses of geogrids (after Eekelen, 2009)

Direction on road construction	Time under load	Ultimate tensile strength, UTS (kN/m)	Tensile stiffness J (kN/m^2) J=(% of UTS/strain) x UTS Herein values at 2 % strain
Longitudinal	1 day	350	(25.0/2)x350=4375
Perpendicular	1 day	400	(25.0/2)x400=5000
Longitudinal	1 year	350	(22.8/2)x350=3990
Perpendicular	1 year	400	(22.8/2)x400=4560
Longitudinal	10 years	350	(22.1/2)x350=3868
Perpendicular	10 years	400	(22.1/2)x400=4420

6.6.1. Load Distribution

To compare the calculated and measured load distributions, load parts *A*, *B*, and *C* are defined as (Fig. 6-16):

- Load part *A* is directly transferred to the pile caps through arching effect,
- Load part *B* is transferred through the reinforcement to the pile caps,
- Load part *C* is resting on the subsoil

Unity for load *A*, *B* and *C* are given in kN.

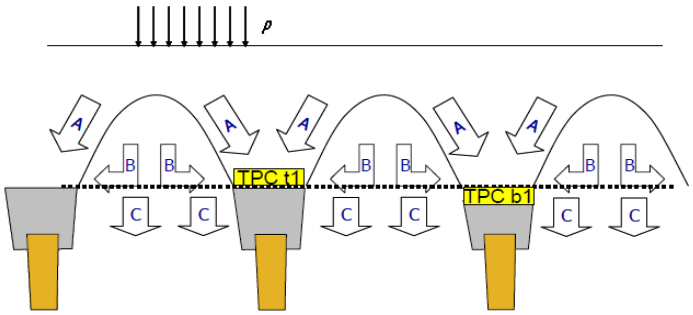

Fig. 6-16 Load distribution in geosynthetics-reinforced piled embankment (after Eekelen et al., 2008)

Devices TPC t1, t2 and t3 were installed on top of reinforcement. These TPCs measured the pressure imposed directly on the piles. The total pressure cells above reinforcement layer (TPCt1, TPCt2, TPCt3) measure load *A*, whereas total pressure cell below reinforcement layer (TPCb1) for measuring load (*A*+*B*). The vertical load *B*, which is the load carried by the geosynthetics reinforcement (GR). By means of tensile forces in the geosynthetics, this load is transferred to the piles. The curve presenting load B was determined by subtracting the average measured pressure of TPC t1, TPC t2 and TPC t3 from TPC b1.

The transferred vertical load on each pile was calculated using the equation of γ^*H+p=18.6*1.15+p= 21.39+p kPa, where p is a surcharge. As soon as arching occurred, the load was transferred laterally to the piles. Therefore, the pressure measured at TPCs would be more than 21.39+p. The vertical distance between TPCs and the horizontal line at 21.39 kPa was an indication of arching.

There are various kinds of material used in the model such as embankment fill, pavement, subsoil, geosynthetics, pile cap, and pile. Therefore, the behaviour of the material also varies. HS model is used to model granular and embankment fill. Linear elastic is applied for modeling concrete pile, wooden pile, and hotmix asphalt. Elastoplastic is used to model geogrid. Futhermore, SSC model is applied for subsoil. Properties of materials in axisymmetric configuration of FE-analysis are shown in Table 6-24.

Table 6-24 Material properties used in finite element analysis of Kyoto road

Properties		Element and model							
		Concrete Pile caps	Wooden piles	Hotmix asphalt	Granular mixture	Fill embkmnt	Subsoil		Biaxial geogrid
							upper	lower	
		Linear elastic	Linear elastic	Linear elastic	HS	HS	SSC	SSC	Elasto-plastic
γ	kN/m^3	24	9.75	23	20	18.6	10.3	13.4	-
ϕ	[^{o}]	-	-	-	44	33.8	20.3	17.43	-
ψ	[^{o}]	-	-	-	8	0	0	0	-
c	kPa	-	-	-	1	11.5	2.05	4.53	-
E_{50}	MPa	-	-	-	160	6.215	1.07	2.36	-
E_{oed}	MPa	-	-	-	130	4.975	-	-	-
E/E_{ur}	MPa	24000/-	12500/-	4000/-	-/400	-/14.92	-	-	-
λ^*	[-]	-	-	-	-	-	0.176	0.138	-
κ^*	[-]	-	-	-	-	-	0.032	0.010	-
μ^*	[-]	-	-	-	-	-	0.011	0.006	-
ν_{ur} /ν	[-]	-/0.2	-/0.2	-/0.2	-/0.2	-/0.2	0.15/-		-
EA	kN/m	-	-	-	-	-	-		4100
k_v	m/s	-	-	-	0.1	1.728E-4	6.86E-4	4.1E-4	-
K_o^{nc}	[-]	-	-	-	-	-	0.653	0.700	-
Drainage		Non Porous	Non Porous	Non Porous	Drained	Drained	Undrained		Non Porous

Distribution of load *A*, *B*, and *C* along 2 ½ years for both field measurement and finite element analysis is shown in Fig. 6-17. Herein, there are three important parts of field measurement. The first part is the fluctuation of vertical stress on the top pile over geogrid along 2 ½ years. Secondly, it is the distribution of vertical stress on the top pile below geogrid. This stress is additional stress due to load below the soil arching which geogrid bring it to top pile. Last part is a fluctuation of vertical stress on the surface of subsoil below geogrid. Each part is also compared with results using the analytical method and finite element method.

(a)

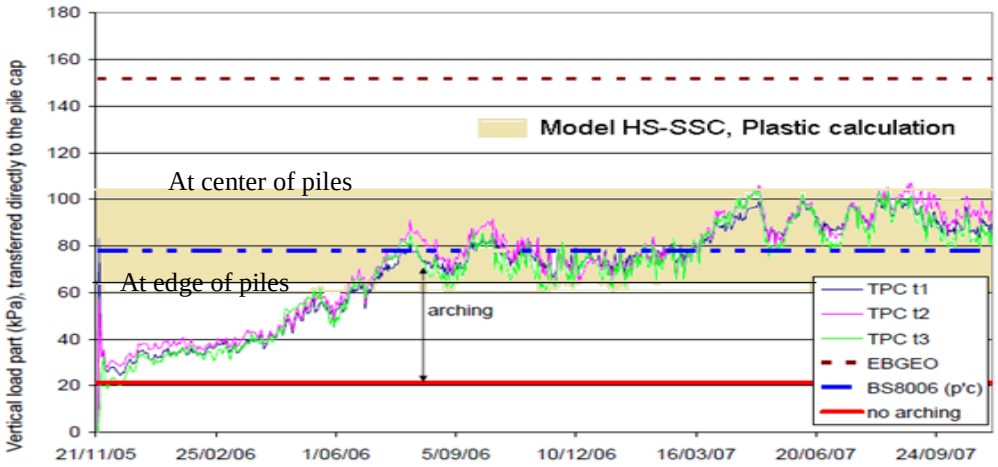

(b)

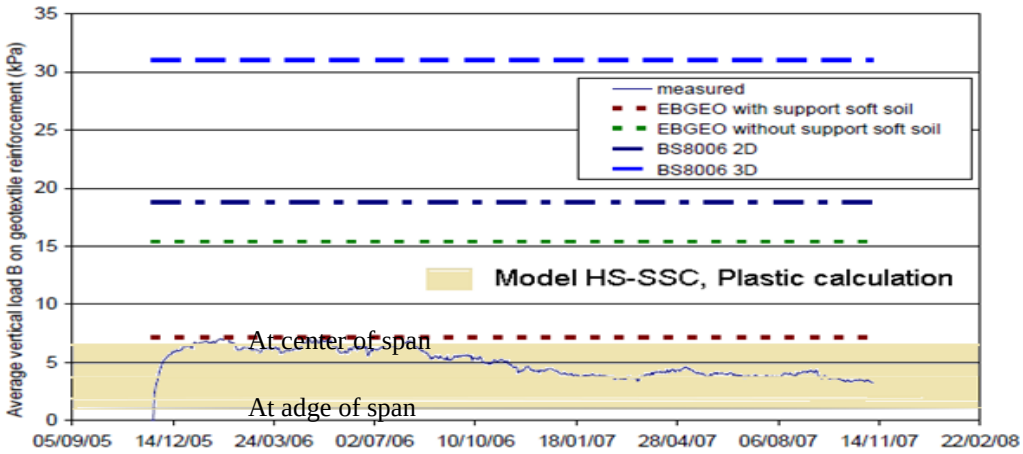

(c)

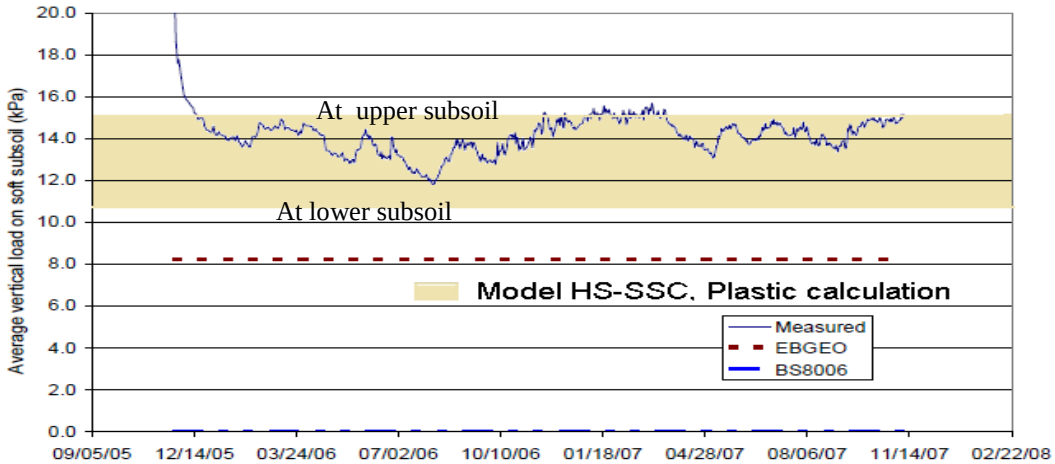

Fig.6-17 Load Distribution for *A*, *B* and *C* of vertical stresses observed throughout 2 ½ years, Prediction using analytical method and FE-calculation (a) Vertical stress (load A) directly on pile above geosynthetics, (b) Vertical stress (load B) under geosynthetics, (c) Vertical stress (load C) on subsoil

Fig. 6-17 shows that it took several months to develop the arching fully. Perhaps, this phenomenon was caused by cementation and settlement process of the fill material. From July 2006 onward, the arching measurements were relatively constant. The fluctuations were mostly due to variation in the weather, moisture content and the alternating periods of traffic. The prediction of the load acting directly on the piles using BS8006 is better than that of EBGEO, which is much higher than the measured values. However, this value is not so important because for the design purpose for piles the total load is conservatively assumed as the applied load on piles.

When taking into account the support of the subsoil, the EBGEO gives a better approach for predicting the vertical load on geosynthetics compared to BS8006. It is an utmost important thing that the imposed load on geosynthetics directly determines the tensile forces on the geosynthetics reinforcement.

By using HS model for fill material and SSC model for soft soil, also using plastic calculation type with 550 kPa as traffic load to predict distribution of vertical stresses for load A, B, and C, it shows that the vertical stresses resulted from field measurement is in range of FE-analysis. Furthermore, contour images of stresses from axisymmetrical approach of FE-analysis with1651 elements are depicted in Fig.6-18. As shown in the figure, critical stress on pile is at the edge of the piles which punch take place.

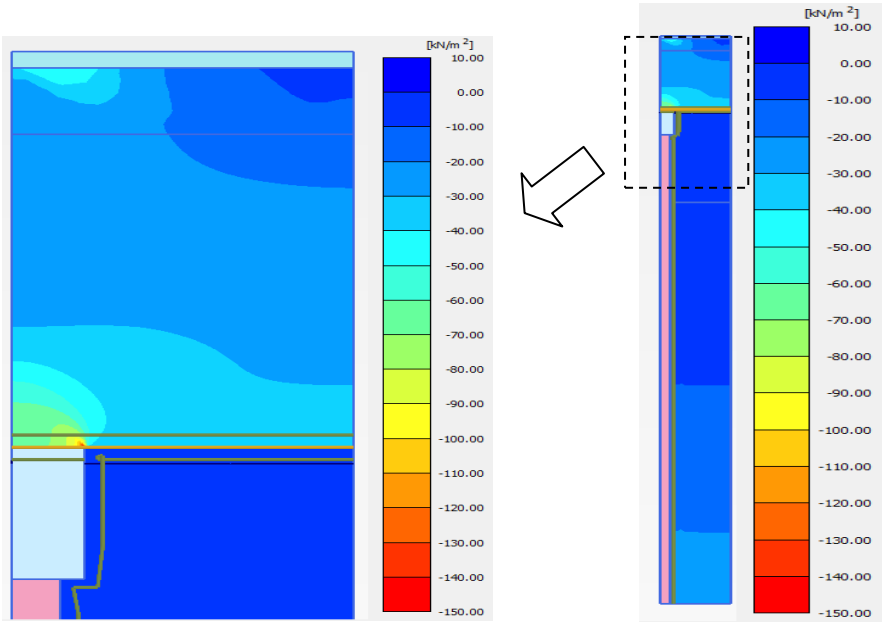

Fig. 6-18 Vertical stresses on piled embankment

6.6.2. Influence of Traffic Load

Traffic started immediately after the completion of construction. Arching needed several months to develop completely (increasing of load *A*, decreasing of load *B*, *C* and pore pressures).

A heavy dynamic load induced by vehicular traffic, however, can cause a sudden short-term decrease of arching (load A decreases and load B increase suddenly). This construction only serves traffic during working hours. Fig. 6-19 shows a daily arching reduction during the first

passages of the day. However, during periods without traffic or rest period so the geosynthetics reinforcement has an opportunity to restore again.

(a)

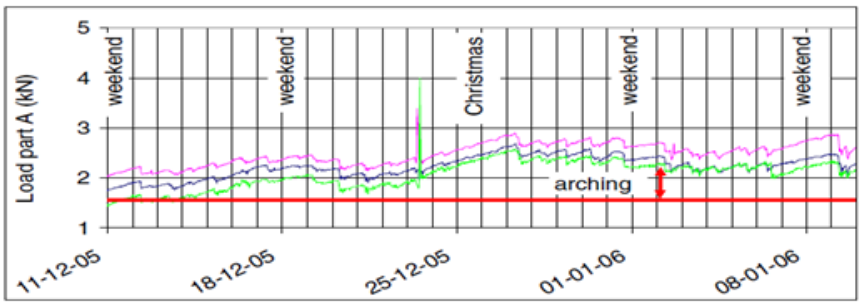

(b)

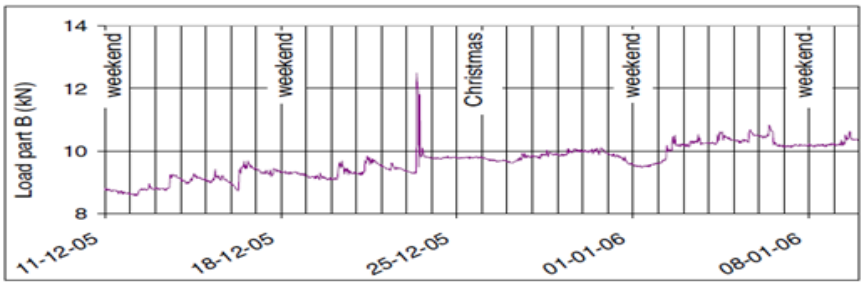

Fig. 6-19 Daily arching cycle on the Kyoto road, (a) Load A, (b) Load B (after Eekelen et al, 2008)

The following Fig. 6-20 shows the increasing of load B after a passage of a rather heavy truck, but the arching generally recovers during the rest of the day or weekend, although other passage is still occurred.

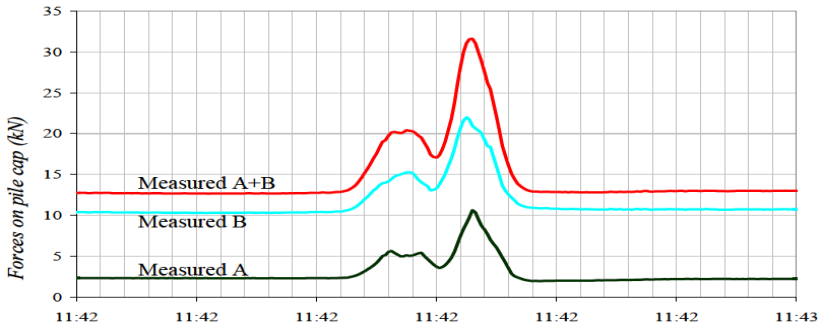

Fig. 6-20 Passage of a truck of 397 kN with 2x2-axles (after Eekelen et al, 2008)

It is clear that higher loading implies the alteration of soil arching. When load at the surface of the embankment is increased, geosynthetics will bear the additional load and then to be transferred to pile.

6.7. Summary

Finite element analysis has huge ability and some advantages to solve a lot of problem in geotechnical engineering. In Chapter 6, some interesting topics regarding with experimental

works and some field case studies in Chapter 4 were readily solved using 2D Plaxis software. Some important findings can be explained as follows:

- In case of high embakment, because of certain circumstance, utilizing multi-layer of geosynthetics provides some benefits. Effectiveness of vertical distance of geosynthetics depends on properties of geosynthetics mainly tensile strength and tensile modulus. That is also influenced by elasticity modulus of granular soil, friction angle and dilation angle. By inserting geosynthetics into granular soil, compound material is able to bear a higher load and simultaneously reduces the horizontal outward thrust. For a compacted soil, HS-model provides a good agreement with soil behaviour. It can reveal the influence of number of layer and pattern of horizontal displacement. By using this model, it is clearly described that maximum lateral outward thrust will be occurred at the lower part of embankment for low elasticity modulus of granular soil, and then at the middle and the upper part for medium and very high elasticity modulus, respectively.
- Vertical stress at top pile and on surface of subsoil will be increased in line with high of embankment.
- When subsoil is moving downward because of consolidation process or low bearing capacity, vertical stress at top pile will be increased until reaching a maximum value and then goes slow down and stable afterwards. Otherwise, on surface of subsoil it will be decreased before getting a stable stage.
- Stress concentration ratio (SCR) is influenced by a height of embankment. The more higher of embankment, it will be increased. Maximum stress concentration ratio or this critical value is reached when ratio relative displacement between pile and subsoil to clear spacing of piles ranges from 1.3 to 2.2%.
- Maximum SCR using Low et al.'s method suggests more close to the measured findings in experimental works compared to others (Terzaghi and BS8006). Terzaghi method provides upper limit, and otherwise BS8006 as lower limit.
- Differential settlement at surface of embankment can be minimized or equal to be nearly zero, when ratio height of embankment to clear spacing of piles is at least 1.4.
- Shape of soil arching for a low relative density (55±7%) is isosceles triangle.
- Load transfer platform (LTP) can be provided using catenary and/or beam system. Placement of inclusion these materials must be inside of soil arching.
- Using soft soil creep (SSC) model with consolidation calculation type agrees with behaviour of soft soil compared to other model (MC) and other type of calculation (plastic).
- Influence of loading on piled embankment over undrained soft soil during a compaction stage is slightly small.
- In case of embankment over end-bearing piles, plastic calculation type can be applied and behaviour of embankment material is better modelled using HS-model. Meanwhile, for soft soil it can be applied the SSC-model.
- Maximum strain of geosynthetics occurs at the face of the piles, and then the lower one is at the half distance between piles. Meanwhile the lowest is at the centre of four piles.

- Finite element provides good results. For instance, in case study of Kyoto road, by using the HS-model to model the embankment and the SSC-model to model the subsoil which agree with the field results. Here, axisymmetric configuration with a load of 550 kPa is applied and plastic calculation type is used for FE-analysis. In comparison with another analytical method (BS8006), the EBGEO method suggests better result which is close to the measured findings in the field.
- When surcharge load induced by vehicular traffic passes through on surface of pavement, shape of soil arching will be changed. Not only an increasing vertical stress or increasing load at the top piles will be increased, but it also happens on surface of subsoil.
- For an embankment with stabilized material, for instance using cement, soil arching effect fully starts after a period of time.

CHAPTER 7

Case Studies Using FEM

This chapter presents analyses of two sites encountered in the field measurement on Supadio airport projects, namely runway reconstruction work and Apron widening project. My works was included in these sites which my role was as a pavement engineer during design stage and intensively as supervision team when executing the project. The first one is a small part of Runway Overlay Project in 2009 to level up PCN 50 of Supadio airport runway in order to be able to serve heavier airplane. Latter is a project that was completed in 2006 to expand the apron to anticipate high demand of air traffic in the future. Furthermore, finite element method is applied and then compared with some results of field measurements. Main topic of this chapter is to discuss settlement of pavement construction over soft soil.

7.1. Location

For purpose of case studies, Supadio airport is chosen regarding with settlement of pavement construction over soft soil. There are two sites for these case studies. The first site is located in the middle of the runway and the second one is situated on the new apron. Main problem in the first site is the settlement of partial weak segment of runway, particularly on wheel track of the airplane, because of the heavier kind of airplane. Whilst, discussion at the second site is different settlement in adjacent segment between new construction and existing construction as well as creep impact for pavement construction over deep soft soil. Aerial view of location for case studies is presented in Fig. 7-1.

Fig. 7-1 Aerial view of Supadio airport

In the airport, there is a runway with 2500 m long and 30 m wide which direction of the runway is 33-15. Whilst, the widening concrete apron with 80×100 m is located in northern part of existing asphaltic apron. Everyday the airport serves air traffic started from 7 a.m to 10 p.m which the heaviest airplane is Boeing 737-400 with a maximum wheel load around 30 tonnes.

7.2. Runway Reconstruction Work of Supadio Airport

Since several months of commencing and the airplane Boeing 737-400 was operated, it appeared a weak section on the runway with 35 m long and 5 m wide that was started at station 1+150. To overcome this problem, wooden piles of 12 cm in diameter and 5 m long using a square pattern of 40 cm pile spacing were applied to support the weak section. The heave was around 4 cm even more that was occurred on this weak spot of runway. The reconstruction work had been completed in April 2009.

Soft clay underlying pavement of runway has the undrained shear strength varying from 7 to 20 kPa and the values of the unconfined compressive strength ranging from 8 to 65 kPa collected from 10 boreholes with depth between 3 m and 20 m. Natural water content of this type of soil is between 35 and 90 percent. Plasticity index is around 20 percent and internal friction is laid between 3% and 13.6% with mean value of 8%.

During undertaking this work, time is very important and limited. Starting from digging and removing of pavement around 90 cm deep until the finishing work of the bituminous layer as runway surface had to be done within a night because at 7 am the runway has to be able to operate the air traffic as the normal situation. Fig. 7.2 is showing the cross-section of Supadio airport runway.

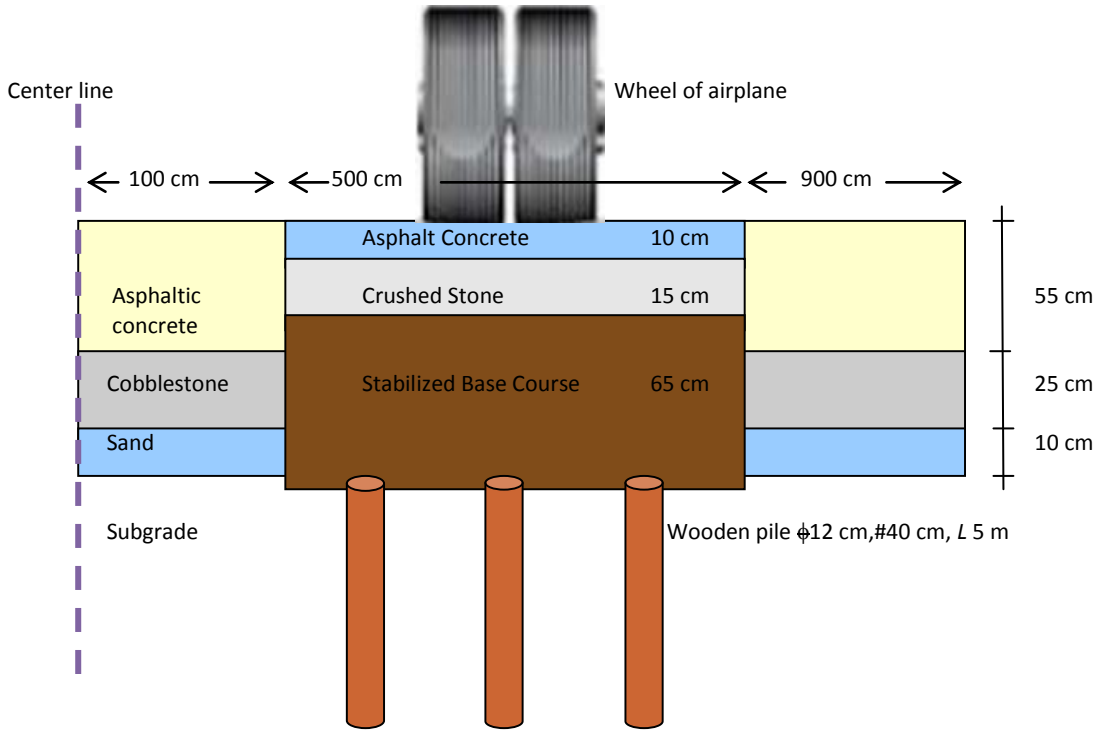

Fig. 7-2 Cross-section of Supadio airport runway (reconstruction pavement in the middle and existing pavement on left-right side)

Wooden piles were driven downward as soon as possible after excavation was completed. Base course as an important part of this work has to be stabilized. Stabilized base course using cement content of 6% and then each more or less 30 cm deep of the base course layer was compacted in this site to get maximum density until the whole depth of base course. Above the stabilized layer, crushed stone with 15 cm thick was poured and then compacted. This layer serves to prevent the poor impact of water contacting directly with the bottom asphaltic surface on the top surface of stabilized base course due to an oxidation process during curring time. Top layer of pavement is 10 cm thick asphaltic surface course with Marshall stability 1000 kg. Fig. 7-3 shows the execution steps of runway reconstruction work.

(a) (b) (c)

Fig. 7-3. Execution of Supadio airport runway reconstruction work (a) Driving piles (b) Pouring base course (c) Compaction

The aim of reconstruction work of Supadio airport runway in Indonesia is to provide a stable surface for the operation of the airplane B737-400 which this kind of airplane is heavier than B737-300 operated before. After about 4 months airplane B737-400 was operated, a deflection appears around 2 cm that occured in this weak spot of runway. To overcome this problem, wooden piles 12 cm in diameter and 4 m long using a square pattern of 40 cm piles spacing was applied to support the weak section and also stabilize base course using 6% cement.

Everyday the airport serves more or less 30 departures, and if during ramping of airplane to apron the wheels of airplane touch an observed point around 0.5 second, hence during airplanes passing through 4 months is equivalent to an hour of parking load and similarly for 36 months around a half day. It is relatively difficult to ensure a settlement caused by the moving load using finite element method. Though, the settlement coming from an airplane is very significant. No load means that there is no loading at the surface, whereas fully load is similar to an airplane that parks at the parking stand all time. Hence, the moving load may take a value in between.

There are various kinds of material used in the model such as embankment fill, pavement, subsoil, and pile. Therefore, the behaviour of the material also varies. MC model is used to model sand, cobble stone, and gravel. Linear elastic behaviour is applied to model wooden pile, stabilized base course, and hotmix asphalt. Furthermore, SSC model is applied for subsoil. Properties of material for FE-analysis is shown in Table 7-1. In the FE-analysis the plane strain after Bergado (1994) was applied to transform from 3D to 2D.

Table 7-1 Material properties used in FE-analysis on Supadio airport runway reconstruction work

Properties		Element and model						
Symbol	Unit	Wooden piles	Asphaltic concrete	Gravel	Stabilized base course	Subsoil	Coble stone	Sand
		Linear elastic	Linear elastic	MC	Linear elastic	SSC	MC	MC
Unit weight, γ	kN/m^3	9.5	22.5	20	20	15.5	20	18
Friction angle, ϕ	[^{o}]	-	-	35	44	13.7	33	30
Dilation angle, ψ	[^{o}]	-	-	0	-	0	0	0
Cohesion, c	kPa	-	-	1	210	8	1	1
Young's modulus, E	MPa	12000	4000	400	660	-	300	120
Modified compression index, λ^*	[-]	-	-	-	-	0.1008	-	-
Modified swelling index, κ^*	[-]	-	-	-	-	0.0202	-	-
Modified creep index, μ^*	[-]	-	-	-	-	0.00350	-	-
Poisson's ratio, v_{ur} /v	[-]	-/0.33	-/0.2	-/0.33	-/0.2	0.15/-	-/0.33	-/0.33
Drainage		Non-porous	Non-porous	Drained	Non-porous	Undrained	Drained	Drained
Calculation type		Stage construction, Plastic calculation						

Characteristic of soft soil is low bearing capacity and high compressibility when being subjected by a load. Table 7-2 presents FE-analysis for settlement of the pavement that is reinforced by wooden piles.

Table 7-2 Settlements and types of loading for pavement reinforced by wooden piles

Description	Settlements and types of loading	
	Parking load	Moving load
Settlement estimated for 4 months	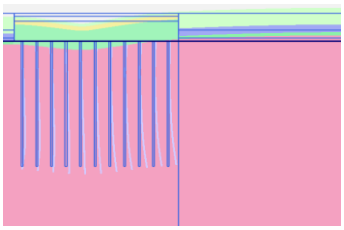 6.60 mm	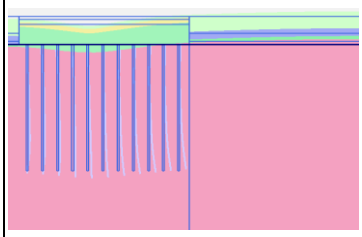 6.16 mm
Settlement estimated for 3 years	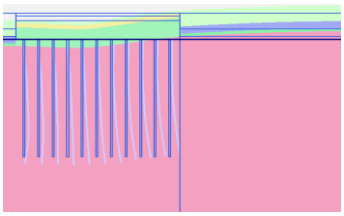 17.70 mm	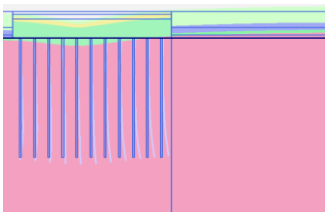 6.23 mm

Table 7-3 presents FE-analysis for settlement of pavement without wooden piles. Settlements of pavement without wooden piles are deeper than those of with wooden piles. It means that piles contribute to reduce the settlement of the pavement.

Table 7-3 Settlements and types of loading for pavement unreinforced by wooden piles

Description	Settlement and types of loading	
	Parking load	Moving load
Settlement estimated for 4 months	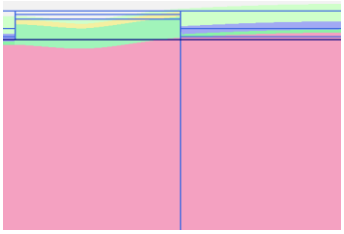 14.87 mm	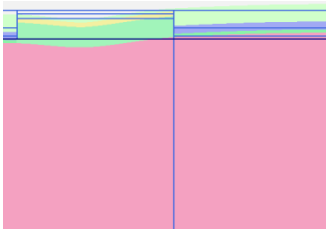 13.93 mm
Settlement estimated for 3 years	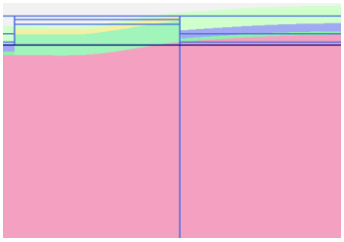 33.07 mm	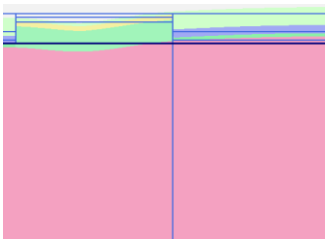 14.06 mm

During the settlement process, soil body beneath a load will shove the outer of adjacent soil to heave up. It can be seen some pictures in Table 7-2 and Table 7-3. Furthermore, Fig.7-4 describes clearly this phenomenon by looking into incremental displacement.

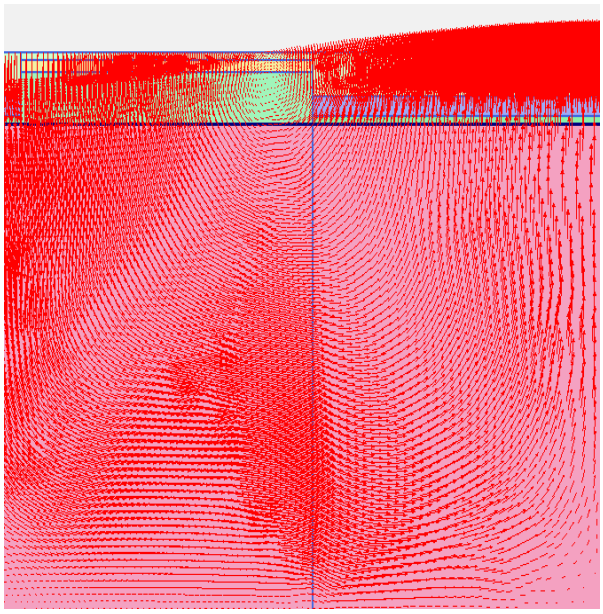

Fig. 7-4 Incremental displacement

Fig. 7-5 provides settlements on the weak spot of runway both reinforced by wooden piles and without piles. These results are compared to each other, as well as a comparison with the settlement of existing pavement construction.

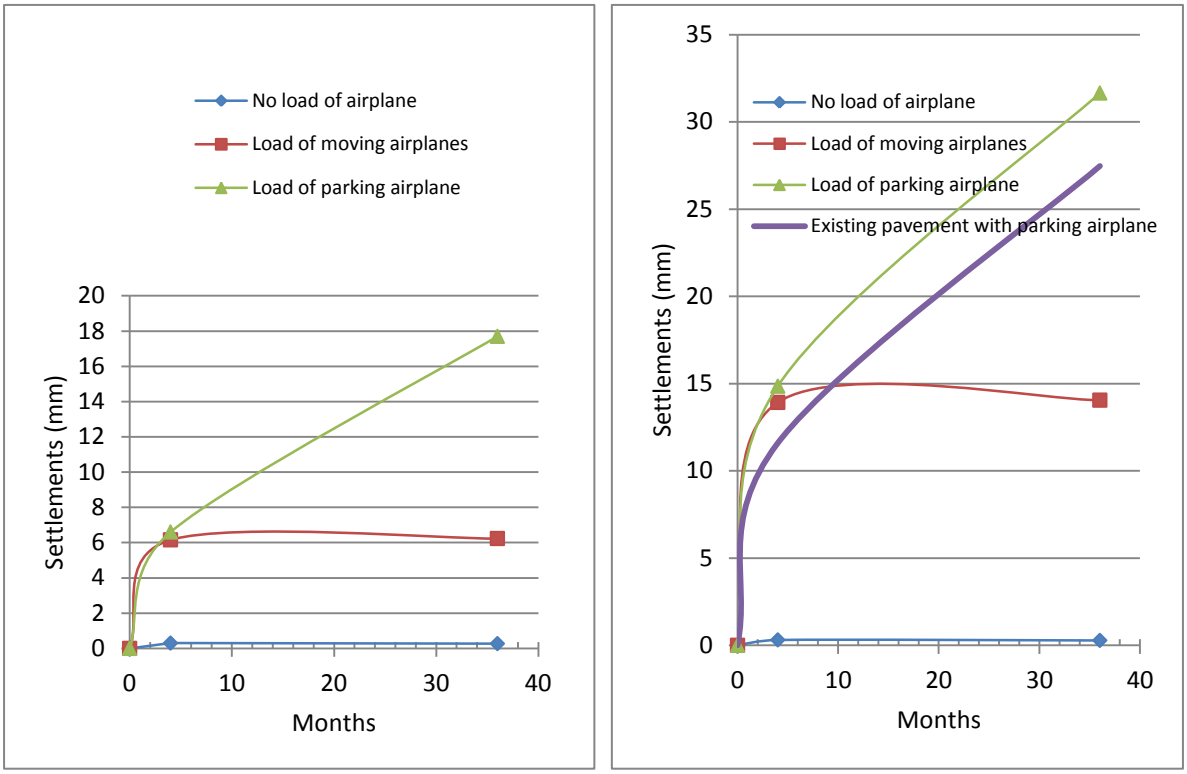

(a) with piles (b) without piles

Fig. 7-5 Settlements on weak-spot surface of Supadio airport runway (a) with piles (b) without piles

It is clear that by using piles to support the pavement construction contributes smaller settlements than those of no piles. Fig. 7-5 (b) indicates that a new type of construction for the reconstruction work is not better than the type of the existing pavement construction when the piles do not be applied to support it. For settlements induced by the moving airplanes, the FE calculation suggests that after the reconstruction work is completed. The settlement is more or less 6 mm and this value is stable until 36 months.

7.3. Apron Widening Project of Supadio Airport

This project is as an effort to fulfill the increasing demand at Supadio airport in Indonesia. A 30 cm-slab concrete has already been chosen for apron expansion 80×100 square meters at western side and 40×80 square meters at eastern side, respectively. To support the pavement, totally 120 cm high, wooden piles with diameter 12 cm and 10 meter long had been arranged on a square pattern of 50×50 cm.

This project was completed in August 2006 and everyday this facility is able to serve airplane B737-400. There are two parking stands operated in the new apron. The occupancy level of parking stand that close to existing apron is higher than other because this place is quite easy for maneuver of airplanes. The whole structure of the pavement on the widening apron as illustrated in Fig.7-6.

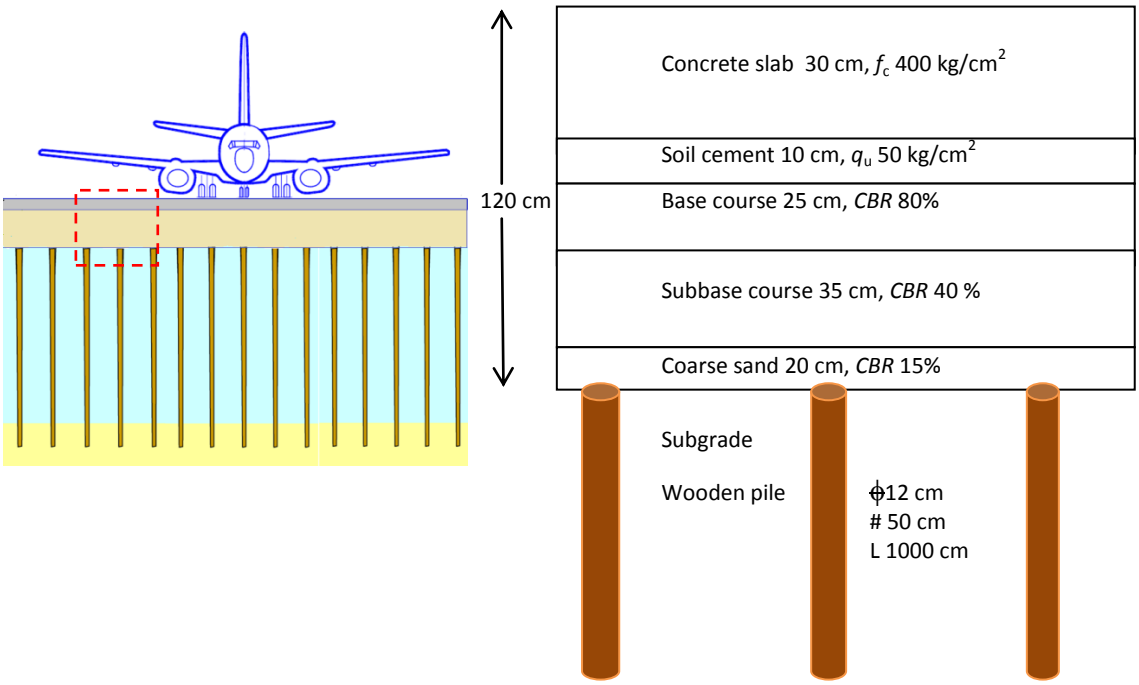

Fig.7-6 Cross-section of Supadio airport apron

In airport pavement engineering, there are two important classification values, the values for airplane and pavement. Value for pavement is so-called PCN (Pavement Classification Number). Meanwhile value for airplane is so-called ACN (Aircraft Classification Number). The PCN value must be higher than the ACN value. It means that the pavement is able to serve a certain airplane. Characteristic of airplane weight and Aircraft Characteristic Number (ACN) for airplane of Boeing 737-400 is briefly listed in Table 7-4.

Table 7-4 Weight and ACN for airplane of Boeing 737-400 (after ICAO, 1999)

Aircraft Model	All-up mass/ mass empty (kg)	Load on one main gear leg (%)	Tire pressure (MPa)	ACN for Rigid Pavement Subgrade (MN/m^3)				ACN for Flexible Pavement Subgrade (CBR)			
				High	Med	Low	Ultra low	High	Med	Low	Ultra low
				150	80	40	20	15	10	6	3
737-400	68.266 33.643	46.91	1.27	42 18	44 19	47 20	48 21	37 16	39 17	44 18	48 21

From data above we know that the maximum weight of one main gear leg is 68,266×46.91% (32,000 kg or 30 tonnes). For taking an assumption that the shape of the tire imprint is a circle, the radius of the circle is around 28.32 cm.

Finite element analysis is used to estimate settlements on apron pavement. The consolidation calculation type is chosen in estimating settlement for soft soil. The SSC model is applied to model the soft soil. For soft soil which creep phenomenon is really obvious, the model is able to imitate the creep behavior when being subjected by a load. The MC model is applied for granular soil. Meanwhile, elastic linear model is applied for wooden piles and concrete slab. Material properties of some elements for FE-analysis are shown in Table 7-5.

Table 7-5 Material properties used in finite element analysis of Supadio airport apron widening project

Properties		Element and model						
		Wooden pile	Portland cement concrete	Soil cement	Base course	Sub-base course	Sand	Subsoil
Symbol	Unit	Linear elastic	Linear elatic	MC	MC	MC	MC	SSC
Unit weight, γ	kN/m^3	9.5	24	19	20	19.5	18	15.5
Friction angle, ϕ	[^{o}]	-	-	44	40	38	35	13.7
Dilation angle, ψ	[^{o}]	-	-	-	8	5	3	0
Cohesion, c	kPa	-	-	210	1	1	1	8
Young's modulus, E	MPa	12000	30000	200	500	300	15	-
Modified compression index, λ^*	[-]	-	-	-	-	-	-	0.1008
Modified swelling index, κ^*	[-]	-	-	-	-	-	-	0.0202
Modified creep index, μ^*	[-]	-	-	-	-	-	-	0.0035
Poisson's ratio, v_{ur} /v	[-]	-/0.33	-/0.2	-/0.2	-/0.33	-/0.33	-/0.33	0.15/-
Permeability, k_i	m/day	-	-	-	1	1	1	0.0001
OCR	[-]	-	-	-	-	-	-	1.5
Drainage	[-]	Non-porous	Non-porous	Non-porous	Drained	Drained	Drained	Un-drained
Calculation type		Stage construction, Consolidation calculation						

7.3.1. Settlement at Surface of Pavement

After completion of the apron widening project was around 5 years ago, settlement resulted from field measurement on the surface of concrete pavement at the first parking stand is around 22.7 cm and the second parking stand is 16.7 cm. Meanwhile, settlement at the edge of the apron that no load is 16 cm. Generally, operation time of apron is started at 7.00 a.m to 10.00 p.m, and then at the first parking stand there will be an airplane that overnight until 7.00 a.m the next day. If there are two airplanes at that night, the second parking stand is provided for parking the other. The first parking stand bears a load of airplane around 12 hours. Fig. 7-7 depicts the total settlements on the surface of new apron.

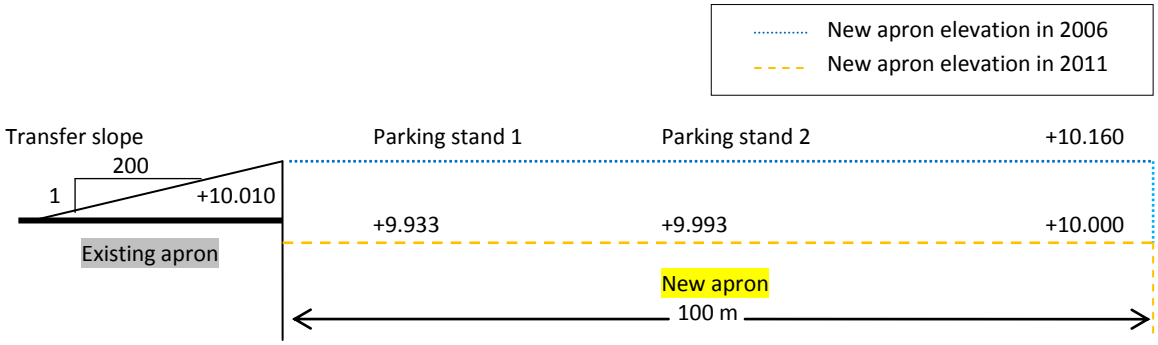

Fig. 7-7 Total settlements on the surface of new apron

Settlements of apron pavement at the 5th year using 2D Plane strain of FE analysis is described in the Fig.7-8. We can see that the estimated total settlement is around 25.0 cm and there is no differential settlement (too small) at the base of the embankment between top piles and surface of subsoil.

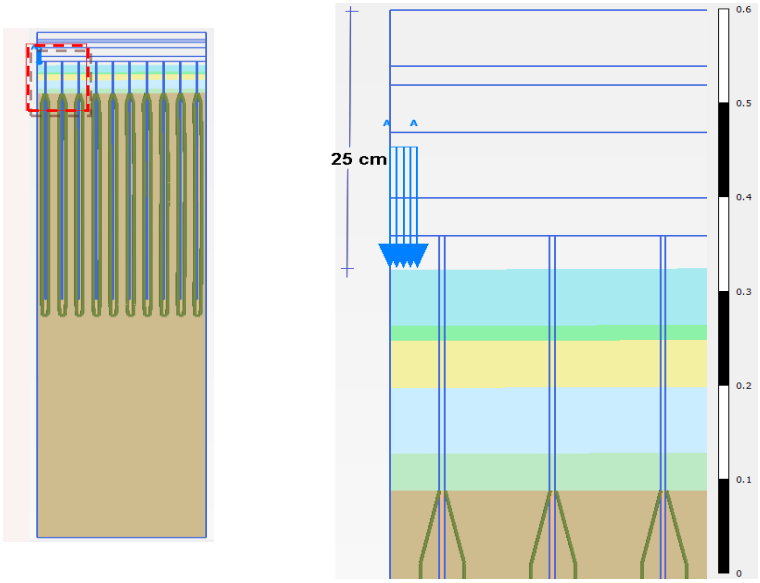

Fig. 7-8 Predicted settlement at surface of parking stand 1

Comparison of settlements between the settlement at the first parking stand resulted from field measurement and settlements from FE-analysis with different time and type of loading can be seen in Fig. 7-9.

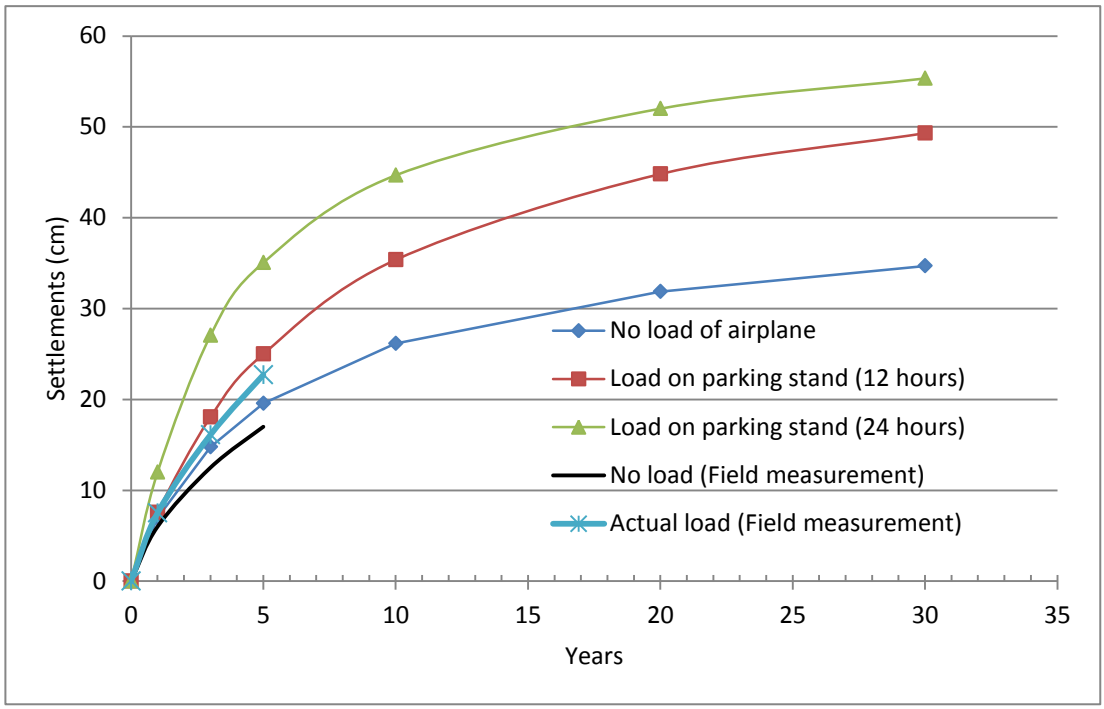

Fig. 7-9 Settlements on the surface of concrete apron at Supadio airport

Fig. 7-9 presents total settlements at surface of parking stand 1 during the 5 years. The measured values from field measurement are located between settlements with no load of airplane and those of 50% occupancy level of parking stand. Of course, actual settlements from field measurement are higher than those of when no airplane that parks at the surface of pavement. It is over-estimated when predicting the total settlement with airplanes fully park on the apron which actually airplanes are coming, parking and then leaving alternately.

7.3.2. Block Behaviour of Settlements

When improving the weak-ground using piles, Pile spacing-Diameter pile ratio (s/D) is an important parameter. Commonly, to keep the structure is able to behave block behavior so the ratio is less than 5. Here, with s=50 cm and D=12 cm or (s/D=4.17), this work is presented using 2D Plane strain of FE-analysis. When settlements at top piles are equal or relatively close to settlements at the surface of soft soil in the middle of between piles, the settlements behave as a block.

Fig. 7-10(a) through 7-10(d) show settlements at different length of piles either no load or maximum load of airplane that parks on the surface of concrete pavement. From these figures, we may notice settlements both on top piles and middle between piles at the base of the pavement for two cases, namely no airplane parks at the parking stand and airplane parks whole day at the parking stand. Firstly, settlements due to airplane that parks on the surface of the pavement are deeper than those of no airplane. Secondly, use of longer piles is able to reduce the settlement for two cases. Thirdly, it is very important to note that the pavement structure behaves as a block because differential settlement on top piles and in the middle point between piles is very small for 2 cases. Lastly, settlements on the surface and bottom of the pavement are very small, it means that the material pavement does not deform.

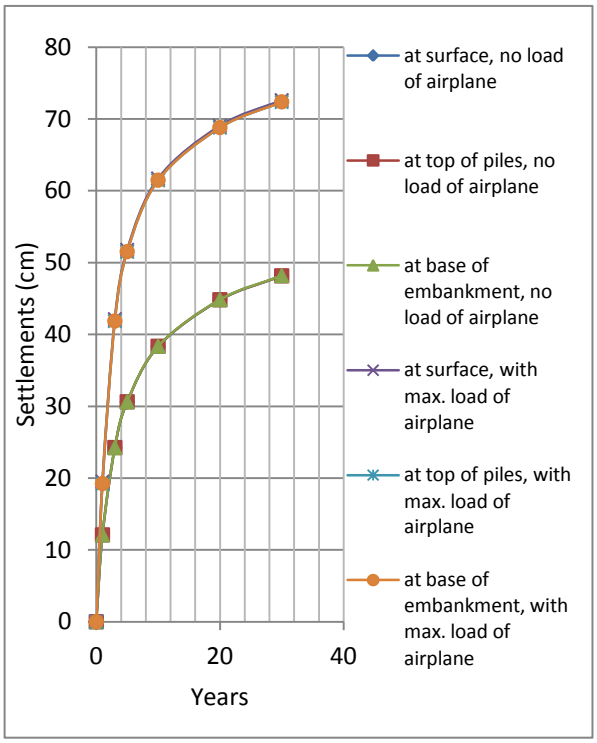

(a) Pile length of 2.5 m

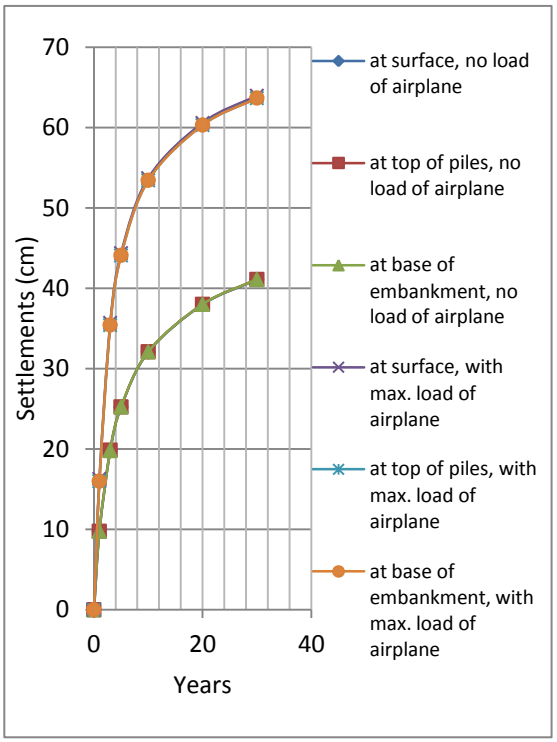

(b) Pile length of 5 m

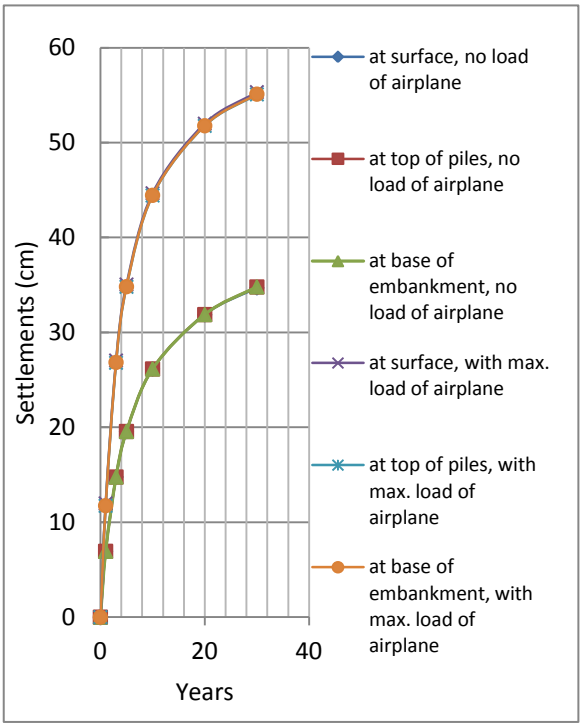

(c) Pile length of 10 m

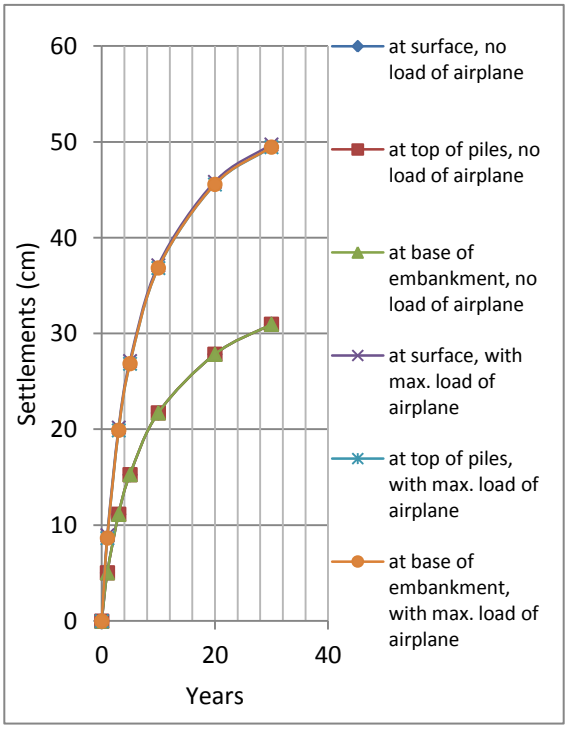

(d) Pile length of 15 m

Fig. 7-10 Predicted settlements at different length of piles and years, (a) Pile length of 2.5 m (b) Pile length of 5.0 m (c) Pile length of 10 m (d) Pile length of 15 m

Fig.7-11 below presents the estimated settlements of apron pavement without using piles. These settlements at 30th year for no loading and maximum loading are 50.4 cm and 76.6 cm respectively. Whilst, for the 5th year, the settlements are 31.9 cm and 54.9 cm respectively. Of course, settlements without using piles in construction give the deepest value compared to those of using piles. All settlements in different length of piles show that settlements behave '*block*' where differential settlements at top piles and subsoil in the middle of between piles are very small.

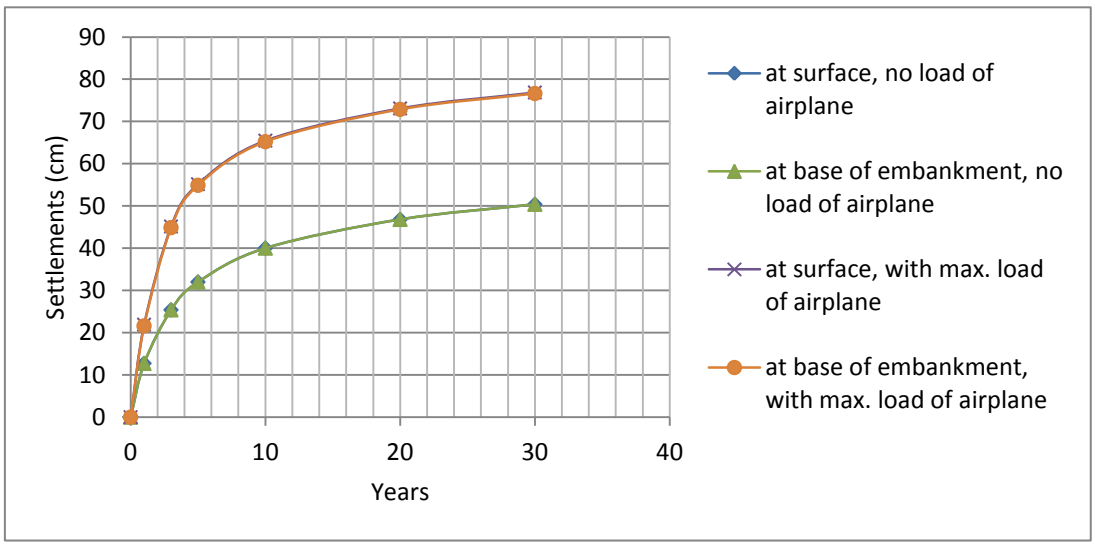

Fig. 7-11 Predicted total settlements of apron pavement without piles

7.3.3. Effectiveness of Piles Length on Floating Piles

No doubt that use of longer piles on a construction over soft soil contributes a smaller settlement. For construction over soft soil which creep behavior is really obvious, it is worth to note that the effectiveness of piles length that is penetrated in soft soil must be taken into account. Relative Settlement Reduction (RSR) can be used to describe the effectiveness of pile length when constructing the floating pile group on soft soil. The RSR is a ratio for a deviation of settlements between no piles and piles to settlement no piles or $(S_o\text{-}S_L)/S_o$. Where S_o is settlement without using piles and S_L is a settlement with a pile at certain length of piles.

Fig. 7-12 provides the effectiveness of pile length using RSR parameter for case no load of airplane and parking load of airplane. It shows when a ratio of pile length to soft soil thickness is less than 0.2, the length of the piles will not quite significant reduce settlement. Moreover, time of period and magnitude of loading are an important aspect when observing the effectiveness of pile length. Short-term monitoring is more effective than long-term period to know the effectiveness. Whilst, higher load implies that longer pile is needed to reduce the excessive settlement. In other words, the use of pile length more than 0.2 of soft soil thickness is an important consideration to overcome the creep behaviour.

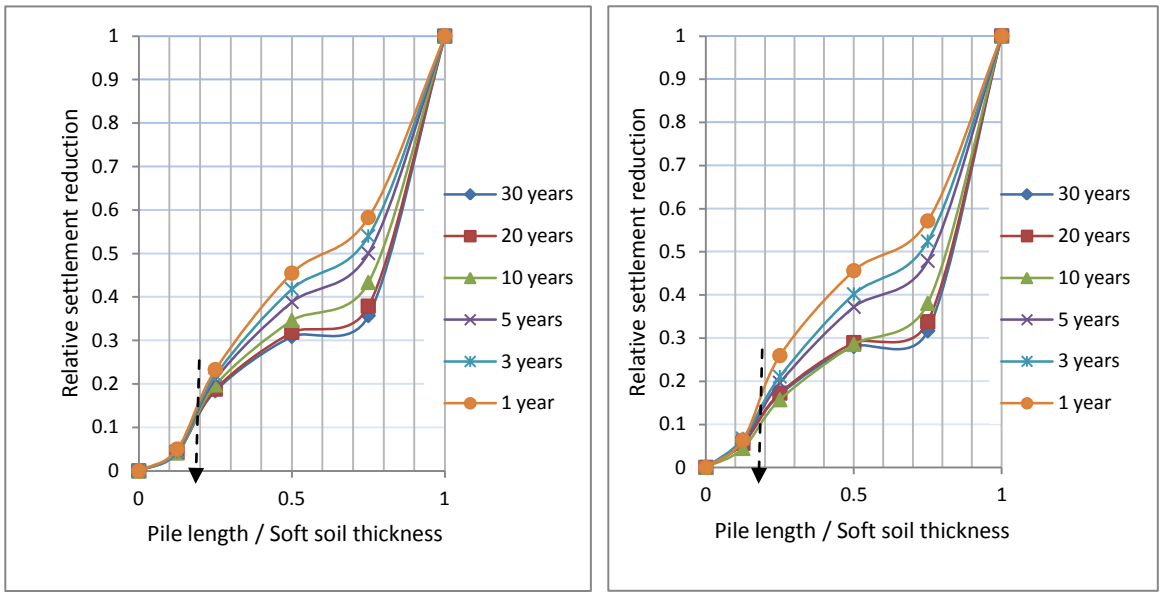

(a) (b)

Fig. 7-12 Effectiveness of pile length, (a) No load of airplane (b) Parking load of airplane

CHAPTER 8

Conclusions and Recommendations

In the framework of research on analysis of dynamic loading behaviour for pavement on soft soil, several research topics have been presented. The research can be divided into six main topics consisting of the effective distance of geosynthetics for reinforcement, analysis of stress concentration ratio on high compressibility of soil, various types of load transfer platforms on floating columns, performance of low embankment on end-bearing piles, the influence of traffic load on arching effect, settlement on floating piles under traffic load. The most important findings of the research are summarized in the following sections and then followed by recommendations for further research.

8.1. Clonclusions

The research that has been presented is aimed to establish the behaviour of pavement material under traffic load over soft soil that being supported by piles including both with geosynthetics reinforcement and without geosynthetics reinforcement. The findings have been discussed in the previous chapters, and they can be concluded in several topics below:

The effective distance of geosynthetics for reinforcement

- Vertical distance of geosynthetics depends on the stiffness of pavement material. Pavement material with low elastic modulus around of 200 MPa (e.g. sandy gravel) needs at maximum distance of 36.7 cm each other of geosynthetics layers. Whereas, higher modulus elastic around of 400 MPa (e.g. crushed stone) can achieve a longer distance around of 50 cm to support the same load.
- Hardening Soil (HS) model can predict better than Mohr Coulomb (MC) model, in this case in which it can reveal the influence of number of layer and pattern of horizontal displacement.
- The higher value of the elastic modulus, higher friction angle and higher value of the dilation angle are able to reduce horizontal strain.

Analysis of stress concentration ratio on high compressibility of soil

- The higher embankment fill will increase the stresses at the top surface of piles for both low embankment ($h/s \leq 1.4$) and high embankment ($h/s > 1.4$).
- During consolidation process because of high compressibility of soft soil, stress at the top surface of the pile will increase up to a certain level and then decrease slowly and stable afterwards. It is in contrary with the vertical stress at the surface of subsoil. In the test, peak situation is developed when pile-subsoil relative displacement (Δ_{Sc}/s) is between 8 mm and 13 mm. By using the pile clear spacing of 60 cm, it means that the critical values range from 1.3% to 2.3%.
- In the test in which the sample has low relative density, MC-model can be well performed to predict stress concentration ratio. When estimating the stress concentration ratio, Terzaghi's model always suggests overestimate than others, and otherwise BS8006, but Low'smodel provides quite close with the test model.

- From laboratory work of Ping et al. (2007) and FE-calculation, *h/s* value around of 1.4 can be used to distinguish between low embankment and high embankment based on the equal plane strain at the surface of the embankment.

Various types of load transfer platforms on floating columns

- Load transfer platform (LTP) can be a catenary (max. 2 geosynthetics layers), a beam (at least 3 geosynthetics layers) and the reinforced concrete. All of them will give high total settlements when being applied on the floating piles, even only within 6 months of observation time, namely:
  - Catenary LTP: 181 mm
  - Beam LTP: 147 mm at Section 1 and 119 mm at Section 2
  - Reinforced concrete: 132 mm
  - Without Piles: 198 mm at Control 1 and 628 mm at Control 2
- Differential settlement at the base of the embankment (difference settlement between at top surface of column and surface of subsoil) is quite small, namely:
  - Catenary LTP: 29 mm
  - Beam LTP: 4 mm at Section 1 and 11 mm at Section 2
  - Reinforced concrete: 16 mm
  - Without Piles: 0 mm
- To model embankment over floating piles using FE-calculation, the use of SSC-model for soft soil and consolidation calculation type without load during compaction process can be taken into account.
- For construction with load transfer platform using more than a layer, the lower geosynthetics is deformed deeper than the upper layer.

The low embankment performance on end-bearing piles

- The differential settlement at the base of the embankment using the end-bearing piles on the shallow soft soil will be relatively greater than on floating piles. By using MC-model or HS-model for pavement material and SSC-model for soft soil, plastic calculation type with involving compaction load agrees with result of the field test.
- Regarding with zones for geosynthetics reinforcement, maximum tensile strength of geosynthetics is occurred at the zone of adjacent piles and at the half distance between piles with parallel to pile face. It is primary reinforcement, whereas other as secondary reinforcement.

The influence of traffic load on arching effect

- Traffic load at the surface of pavement is always changing by time. By observing the change of the vertical load on top piles for both upper and lower part of geosynthetics inserted at the base of the embankment of Kyoto road, it is possible to monitor the change of vertical stress over time. The vertical stress at top pile and on surface of subsoil would be increased during surcharge load. It means that shape of soil arching was changing.
- By using HS model for granular material of the pavement and SSC model for soft soil with plastic calculation type and traffic load around of 550 kPa at the surface of the pavement, this model agrees with the field test. Furthermore, for calculating the vertical load directly transferred on top of piles, BS8006 method is better than

EBGEO method, but for vertical stress over subsoil. Moreover, EBGEO method gives better results than BS 8006 method.

- Another important finding is that the soil arching is changing when surface of pavement is subjected to a traffic load and pavement material is able to restore its self to an initial phase during a rest period.

The settlements on floating piles under traffic load

- Total settlement on construction over soft soil using floating piles is too huge. Though, there is no traffic load. Because of creep, settlement still happens over a long time.
- SSC-model for soft soil with the consolidation calculation type can be accurately applied for predicting the settlement of a pavement construction over soft soil supported by the floating piles.
- In practice, always keeping value of s/d <5 to obtain block behaviour in pile group.
- Relative settlement ratio (RSR) can be used to describe the effectiveness of pile length when constructing the floating pile group. In this case of the apron at Supadio airport, the ratio of pile length to soft soil thickness is around 0.20.

Furthermore, for practical purpose it is important to note here that main conclusions below are utmost important thing to keep in mind. Firstly, height of the embankment must be more than 1.4 times of clear spacing between piles to avoid differential settlement at the surface of the embankment. Secondly, because floating piles foundation works as a pile group, it is important to remember that ratio pile spacing to pile diameter must be kept always less than 5. Thirdly, the use of small size for diameter of the pile is an useful way when being applied to low embankment construction. Last thing, when we construct an embankment over soft soil supported by floating piles using FEM and estimate settlement because of creep, consolidation calculation type must be run without taking into consider a load compaction during construction period. However, plastic calculation type can be used to predict settlement with involving a static traffic load. This type of calculation is relatively faster than consolidation calculation type.

8.2. Recommendations for Further Research

Further research related to behaviour of embankment material over soft soil under the traffic load for both end-bearing piles and floating piles is required to investigate the following topics:

- The embankment supported by basally piles reinforcement is widely used for shallow depth of soft soil but floating piles is rear encountered in the literature study. It is the promising realm to be developed in the future for treating it on deep soft soil.
- Resistance of soil arching under cyclic loading and long-term condition for cemented material is necessary to be observed. Because in some circumstances the pavement material is stabilized with cement.
- It is also a good idea to study soil interaction with inclusion geosynthetics on a cemented material using pull-out test.

- The phenomenon of increasing bearing capacity of displacement piles along the increasing time after installation is well known and these findings are based on some empirical field experiments. However, its mechanical behaviour has not been fully understood yet.

REFERENCES

Adhi, W. (1984), *''Masalah Tanaman di Tanah Gambut''*, Prosiding Pertemuan Teknis Penelitian Pola Usahatani Menunjang Transmigrasi, Badan Penelitian dan Pengembangan Pertanian, Jakarta.

Almeida, M.S.S., Ehrlich, M., Spotti, A.P. and Marques, M.E.S. (2007), *''Embankment supported on piles with biaxial geogrids''*, Journal of Geotechnical Engineering, Institution of Civil Engineers, ICE, UK, Vol. 160, No. 4, pp. 185-192.

Almeida, M.S.S., Marques, M.E.S., Almeida, M.C.F., and Mendonca, M.B. (2008), *''Performance of Two 'Low' Piled Embankments with Geogrids at Rio de Janeiro''*, The First Pan American Geosynthetics Conferences & Exhibition, Cancun, Mexico, pp.1285-1295.

Alphan, I. (1970), *''The geotechnical properties of soils'',* Earth-Science Review, Vol.6, pp. 5-49.

Althoff, S. (2010), *''Contribution to use Multi-stage Large Shear-Frame tests to Investigate the Interaction-Behaviour between Geosynthetics and Cohesive Soil''*, Technische Universität Bergakademie, Freiberg.

Althoff, S. et al. (2011), *''Bestimmung der verbundeigenschaften-innovatives versuchskonzept mit 12 geogittern''*, FS-KGEO 2011, München.

Althoff, S. (2011), *''Forschung am Institut für Geotechnik, neue Erkenntnisse beim Verbund- & Systemverhalten von Geokunststoffen in bindigen Böden''*, Geotechnisches Seminar, January 2012, Technische Universität Bergakademie, Freiberg.

Alwi, A. (2007), *''Ground Improvement on Malaysian Peat Soils Using Stabilised Peat-Column Techniques''*, PhD thesis, University of Malaya, Kuala Lumpur, Malaysia.

Anonim (1978), *''Peraturan Konstruksi Kayu Indonesia''*, NI-5 PKKI 1961, Penerbit Departemen Pekerjaan Umum, Direktorat Jenderal Cipta Karya, Direktorat Penyelidikan Masalah Bangunan, Bandung, Indonesia.

Archer, S. (2008), *''Subgrade Improvement for Paved and Unpaved Surefaces using Geogrids''*, Tensar International, Construction Products inc.

Atkinson, J.H. and Sällfors, G. (1991), *''Experimental determination of soil properties''*, Proceedings of 10th ECSMFE, Vol.3, pp. 915-956, Florence.

Atkinson, J.H. (2000), *''Non-linear soil stiffness in routine design''*, Geotechnique, Vol. 50, pp. 487-508.

Aydogmus, T. and Klapperich, H. (2004), *''The next generation: Enhanced shear-pullout-testing device''*, ECI int'l conference, Schloss Pillnitz, Dresden.

Aydogmus, T. (2006), *''Beitrag zum Interaktionsverhalten von Geokunstoff und Lockergestein''*, Dissertation, TU-Bergakademie Freiberg.

Baker, S. (2000),*''Deformation Behaviour of Lime/Cement Column Stabilized Clay''*, Swedish Deep Stabilization Research Centre, Rapport 7, Chalmers University of Technology.

Barenberg, E. J., Hales, J. and Dowland, J. (1975), *''Evaluation of Soil-AggregateSystems with MIRAFI Fabric*", University of Illinois Report No. UILU-ENG-75-2020, prepared for Celanese Fibers Marketing Company.

Barenberg, E.J. (1992), *''Subgrade stabilization, in A Design Primer'',* Geotextiles and Related Materials, IFAI, 10-20.

Barry, A. J., Bambang, T., Symes ,T. & Younger, J. S. (1992), *''Piling for roads over peat in Sumatra''*, Geotropika 92 International Conference on Geotechnical Engineering, Johor Bahru.

Barry, A. J. & Rachlan, A. (2001), *''Embankments on soft soils in North Java''*, Proceedings International Conference on In Situ Measurement of Soil Properties and Case Histories, Bali, Parahyangan Catholic University, Indonesia.

Bauer, E.(1996), *''Calibration of a comprehensive constitutive equation for granular Materials''*, Soils and Foundations 36, pp. 13–26.

BB Litbang (2008), *''Konsorsium Penelitian dan Pengembangan Perubahan Iklim pada Sektor Pertanian*'', Balai Besar Penelitian dan Pengembangan Sumberdaya Lahan Pertanian, Laporan Tahunan 2008, Bogor.

Bell, A. L., Jenner, C., Maddison, J.D. and Vignoles, J. (1994), *''Embankment support using geogrids with vibro concrete columns''*, Proceedings, 5th International Conference on Geotextiles, Geomembranes, and Related Products, 335-338.

Bender, D.A. and Barenberg, E.J. (1980), *''Design and Behavior of Soil-Fabric-Aggregate Systems''*, Transportation Research Record 671, TRB, National Research Council, Washington DC, USA, pp. 64-75.

Benz, T. (2007), *''Small strain stiffness of soils and its numerical consequences''*, PhD Thesis, Institute of Geotechnical Engineering, University of Stuttgart.

Bergado, D.T. and Long, P.V.(1994),''*Numerical analysis of embankment on subsiding ground improved by vertical drains and granular piles*'', Proceeding of the XIII International Conferences on Soil Mechanics and Foundation Engineering, Vol.4, Morgantown, Balkema, pp.1361-1366.

Bergado, D. T., Ruenkrairergsa, T., Taesiri, Y., and Balasubramaniam, A.S. (1999), *''Deep soil mixing used to reduce embankment settlement''*, Ground Improvement 3:145-162.

Beskou, N.D and Theodorakopoulos, D.D.(2011), *''Dynamic effects of moving loads on road Pavement''*: A review, Soil Dynamics and Earthquake Engineering 31(2011), Elsevier Ltd, p.547-567.

Biarez, J. And Hicher, P.-Y. (1994), *''Elementary Mechanics of Soil Behaviour''*, Balkema.

Bjerrum, L. (1967), *''Engineering geology of Norwegian normally-consolidated marine clays as related to settlements of buildings''*, Geotechnique, 17,2, p.81-118.

Bouckovalas, G.,Whitman, R.V. and Marr, W.A.(1984), *''Permanent displacement of sand with cyclic loading''*, Journal of Geotechnical Engineering, ASCE, 110(11): pp.1606-1623.

Broms, B. B. (2003), *''Deep soil stabilization: design and construction of lime and lime/cement Columns''*, Royal Institute of Technology, Stockholm, Sweden.

Broms, B. B., and Boman, P. (1979), *''Stabilization of soil with lime columns''*, GroundEngineering 12, no. 4: 23-32.

BS8006 (1995), *''Berehcmung und Dimensionierung von Erdkörpern mit Bewehrungens-einlagen aus Geokunststoffen''*, Deutsche Gesellscahft für Geotechnik e.V.

Burland, J.B. (1989),''*Small is beautiful-the stiffness of soils at small strains''*, Canadian Geotechnical Journal, 26, pp.499-516 .

Burmister, D. M. (1943), *''The Theory of Stresses and Displacements in Layered Systems and Applications to the Design of Airport Runways",* Proceedings, Highway Research Board, Vol. 23, pp. 126-144.

Bussert, F. (2006), *''Verformungsverhalten geokunststoffbewehrter Erdstützkörper Einflussgrößen zur Er-mittlung der Gebrauchstauglichkeit''*, Schriftenreihe des Instituts für Geotechnik und Markscheidewesen der TU Clausthal. Heft 13/2006.

Bussinesq (1936), *''Stress distribution in elastic solids''*, Proceeding of 1. ICSMFE Cambridge, Vol. 2, S. 157.

Bustamante, M.& Gianeselli, L. (1981), *''Prévision de la capacité portante des pieux isolés sous charge verticale. Règles pressiométriques et pénétrométriques (Prediction of the bearing capacity of single piles under vertical load. Pressuremeter and penetrometer rules)*'', Bull. Liaison Labo. P. et Ch., no.113, May-June, Réf. 2536, 83-108 (in French).

Butterfield, R.(1979), *''A natural compression law for soils''*, Geotechnique 29.

Cabalar, A.F. and Cevik, A. (2008), *''Modelling damping ratio and shear modulus of sand-mica mixtures using neural networks''*, Engineering Geology, doi: 10.1016/ j.enggeo. 2008. 08.005.

Cabalar, A.F. (2009), *''Dynamic Properties of Various Plasticity Clay''*, EJGE Vol. 14, Bund. B.

Cabalar, A.F. (2010), *''Applications of the oedometer, triaxial and resonant column tests to the study of micaceous sands''*, Engineering Geology 112 (21010), pp.21-28.

Carlsson, B. (1987), *''Reinforced soil, principles for calculation''*, Terratema AB, Linköping (in Schwedish).

Carlsten, P. and Ekstrom, J. (1997), *''Lime and lime cement columns, guide for project planning, construction and inspection''*, Swedish Geotechnical Society, SGF Report 4:95 E.

CDIT (Coastal Development Institute of Technology). (2002), *''The Deep Mixing Method: Principle, Design and Construction''*, A.A. Balkema: The Netherlands.

Chaboche, J.L.(1994), *''Modelling of ratchetting: evaluation of various approaches''*, European Journal of Mechanics, 13(4):501-781.

Chen, F.H. (1975), *''Foundation on expansif soils''*, Elsevier Scientifik Publishing Company, Amsterdam .

Clayton, C.R.I., Milititsky, J. & Woods, R.I.(1993), *''Earth Pressure and Earth-Retaining Structures''*, Blackie Academic & Professional, Glasgow, UK, 2nd Edition

Collin, J.G., Watson, C.H., Han, J. (2004), *''Column-Supported Embankments DesignConsideration''*, Proceedings of Minnesota 52nd Annual Geotechnical Engineering Conference, Minneapolis, Minnesota.

Collin, J.G.; Watson, C.H.; Han, J. (2005), *''Column-Supported Embankments solves time Constraint for new road construction''* , Proceedings of the Geo-Frontiers 2005 Congress, Austin, Texas.

Cox, J. B. (1970), *''The distribution and formation of recent sediments in South East Asia''*, Proceedings of 2nd South East Asian Conference on Soils Engineering, p.30-47.

Das,B.M. (1985), *''Principles of Geotechnical Engineering''*, The Univesity of Texas at El Paso, USA.

Dawson, A., Kolisoja, P. And Vuorimies, N. (2008), *''Understanding Low-Volume Pavement Response to Heavy Traffic Loading''*, Roadex III Project: Northern Periphery, The Swedish Road Administration.

DB Netz AG, (1999), *''Ril 836 – Erdbauwerke planen, bauen und instand halten''*, Fassung vom 20.12.1999.

Djarwadi, D. (2006), *''Konstruksi Jalan di Atas Tanah Lunak dengan Perkuatan Geotextile (Geotextile Reinforcement for Road Construction on Soft Soil)''*, International Civil Engineering Conference 'Towards Sustainable Civil Engineering Practice', Surabaya, Indonesia.

Dunlap, W.S. (1963), *''A report on a mathematical model describing the deformation characteristics of granular materials''*, Technical Report 1, Project 2-8-62-27, TTI, Texas A & M University.

EBGEO (2010), *''Berehcmung und Dimensionierung von Erdkörpern mit Bewehrungenseinlagen aus Geokunststoffen''*, Deutsche Gesellscahft für Geotechnik e.V.

Eekelen, S.J.M. van, Bezuijen, A. (2008a), *''Design of piled embankments, considering the basic starting points of the British Standard''*, Proceedings of EuroGeo4, Edinburgh.

Eekelen, S.J.M. van, Bezuijen, A. Alexiew, D. (2008b), *''Piled Embankments in the Netherlands: a full-scase test, comparing 2 years of measurements with design calculations''*, Proceedings of EuroGeo4, Edinburgh.

Eekelen, S.J.M. van ,Bezuijen, A. , Duijnen, P. Van and Jansen, H.L. (2009), *''Piled embankments using geosynthetic reinforcement in the Netherlands:design, monitoring & evaluation''*, Proceedings of the 17th International Conference on Soil Mechanics and eotechnical Engineering M. Hamza et al. (Eds.) pp. 1690-1693.

Eekelen, S.J.M. van and Bezuijen, A. (2010), *''The Kyoto road piled embankment: 3 ½ years of measurements''*, 9th International Conferences on Geosynthetics, Brazil.

Eekelen, S.J.M. van, Bezuijen, A., and Tol, A.F. van (2011), *''Analysis and modification of the British Standard BS8006 for the design of piled embankments''*, Geotextiles and Geomembranes 29 (2011) pp. 345-359.

Esrig, M. I., and MacKenna, P.E. (1999), *''Lime cement column ground stabilization for I-15 in Salt Lake City''*, 34th Annual Symposium on Engineering Geology and Geotechnical Engineering.

Etezad, M., Hanna, A.M. and Ayadat, T. (2006), *''Bearing capacity of groups of stone columns''*, Proceedings of the 6thEuropean Conference on Numerical Methods in Geotechnical Engineering, Graz, pp. 781-786.

EuroSoilStab (2002), *''Development of design and construction methods to stabilise soft organic soil''*, Design Guide Soft Soil Stabilization, CT97-0351 Project No. BE 96-3177.

Exxon (1989), *''Designing for Soil Reinforcement''*, Exxon Chemical, GeoPolymers Ltd.

Fang, Y. S., Chung, Y. T., Yu, F. J., and Chen, T. J. (2001),*''Properties of soil-cement stabilised with deep mixing method''*, Ground Improvement 5, no. 2: 69-74.

Farrell, E. R., O'Neill, C. & Morris, A. (1994), *''Changes in the mechanical properties of soils with variations in organic content''*, Advances in Understanding and Modelling the Mechanical Behaviour of Peat, Balkema Rotterdam.

Fox, L. (1948), *''Computation of Traffic Stresses in a Simple Road Structure",* Proc. 2nd Int. Conf. Soil Mech. Found. Eng. Vol. 2, pp. 236-246.

Garlanger, J. (1972), *''The consolidation of soils exhibiting creep under constant effective Stress''*, Geotechnique, Vol.22, pp. 71-78.

GEC (2012), *''Global Environment Centre''*, www.peat-portal.net

Giroud, J.P. and Noiray, L. (1981), *''Design of geotextile reinforced unpaved road''*, Journal of Geotechnical Engineering, ASCE, 107, 1233-1254.

Giroud, J. P., Ah-Line, C., and Bonaparte, R. (1984), *''Design of Unpaved Roads and Trafficked Areas with Geogrids"*, Polymer Grid Reinforcement: A Conference Sponsored by SERC and Netlon, Ltd., Thomas Telford, London, England, pp.116-127.

Giroud, J.P., 1995, *''Determination of Geosynthetic Strain due to Deflection"*, Geosynthetics International, Vol. 2, No. 3, pp. 635-641.

Giroud, J.P., and Han, J., 2004, *''Design Method for Geosynthetic-Reinforced Unpaved Roads:Part I–Development of Design Method"*, Journal of Geotechnical and Geoenvironmental Engineering, in press, ASCE.

Gorsel, J.T.v. (2012), *''Bibliography of the Geology of Indonesia and Surrounding Areas''*, Edition 4.1., www.vangorselslist.com.

Grundmann, H.(1999), *''Dynamic interaction of structures with the subsoil''*, In:Frybal, Naprstek J., editors. Structural Dynamics—EURODYN'99, 1.Rotterdam:AA Balkema; 1999, p.31–41.

Gudehus, G. (1996), *''A comprehensive constitutive equation for granular materials''*, Soils and Foundations 36, pp. 1–12.

Guido, V. (1987), *''Plate loading tests on geogrid-reinforced earth slabs''*, Proceedings of Geosynthetics 1987 Conf., New Orleans.

Haley & Aldrich and Virginia Geotechnical Services, P.C. (2000), *''Final Data Report on Ground Improvement for Embankment Construction''*, I-95/Route 1 Interchange, VDOT Project No. 0095-96A-106, PE-101.

Han, J. (1999), *''Design and Construction of Embankments on Geosynthetic Reinforced Platforms Supported by Piles''*, Invited Speaker, Proceedings, 1999 ASCE Geotechnical Seminar, Hershey, PA.

Han, J., and Wayne, M.H,(2000), *''Pile-Soil-Geosynthetic Interactions in Geosynthetic Reinforced/Piled Embankments over Soft Soil''*, Presentation and CD-Rom Paper at 79th Annual TRB meeting.

Han, J., Gabr, M.A. (2002), *''Numerical Analysis of Geosynthetic-Reinforced and Pile-Supported Earth Platforms over Soft Soil''*, Journal of geotechnical and geoenvironmental engineering, Vol. 128, No. 1, S. 44-53.

Han, J. (2003), *''Development of Design Charts for Geosynthetically Reinforced Embankments on Deep Mixed Columns''*, Interim Report, Literature Review, Principal Investigator, funded by the FHWA National Deep Mixing Program, 2002-2003, Widener University, Chester, PA.

Han, J., Collin, J.G. (2005), *''Geosynthetic Support Systems over Pile Foundations''*, Proceedings of the Geo-Frontiers 2005 Congress, Austin, Texas.

Handy, R.L. (1985), *''The arch in soil arching''*, ASCE Journal of Geotechnical Engineering, Vol. 111, No. 3, pp. 302-318.

Hardin, B.O. and Drnevich, V.P. (1972), *''Shear Modulus and Damping in Soils: Measurement and Parameter Effects"*, Journal of Soil Mechanics and Foundations, ASCE, 98, SM6, 603-624.

Hassandi, A.C. and Edil, T.B. (2005), *''Full scale Geosynthetic-Reinforced Column-Supported Test Embankment''*, University of Wisconsin-Madison.

Hassandi, A.C. and Edil, T.B. (2007), *''Behaviour of Geogrid-reinforced load transfer platforms for embankment on rammed aggregate piers''*, Geosynthetics International, Vol. 14 No. 3. Pp. 141-153.

Heitz, C. (2006), *''Bodengewölbe unter ruhender und nichtruhender Belastung bei Berücksichtigung von Bewehrungseinlagen aus Geogittern''*, Schriftenreihe Geotechnik, University of Kassel, Heft 19.

Hencky, H. (1928), *''Über die form des elastizitätsgesetzes bei ideal elastischen stiffen''*, Zeitschrift fur Technische Physik 9, pp. 214–247.

Herle, I. and Gudehus, G.(1999), *''Determination of parameters of a hypoplastic constitutive model from properties of grain assemblies''*, Mechanics of Cohesive-Frictional Materials 4: pp. 461–486.

Heukelom, W. and A.J.G. Klomp (1962), *''Dynamic Testing as a Means of Controlling Pavements During and After Construction"*, Proceedings of the First International Conference on Structural Design of Asphalt Pavements, University of Michigan.

Hewlett, W.J., Randolph, M.F., Aust, M.I.E. (1988), *''Analysis of piled embankments''*, Ground Engineering Vol.21, pp. 12-17.

Hill, R. (1950), *''A general theory of uniqueness and stability in elastic-plastic solids''*, Journal of the Mechanics and Physics of Solids 6, pp. 236–249.

Hobbs, N.B. (1986), *''Mire Morphology and the Properties and Behaviour of some British and Foreign peats''*, Quarterly Journal of Engineering Geology, London, Vol. 19, pp.7-80.

Hobbs, N. B. (1987), *''A note on the classification of peat''*, Geotechnique, 37, 3, p. 405-407.

Holm, G. (1999), *''Keynote lecture:Applications of dry mix methods for deep soil stabilization''*, International Conference on Dry Mix Methods: Dry Mix Methods for Deep Soil Stabilization, Balkema, Rotterdam: 3-13.

Holtz, R.D & Sivakugan, N. (1987), *''Design charts for roads with geotextiles''*, Journal of Geotextile and Geomembranes, 5, pp. 191-199.

Huang, Y. H. (1969), *''Computation of Equivalent Single-wheel Loads Using Layered Theory''*, Proceedings, Highway Research Board.

Hughes, J.M.O. and Withers, N.J. (1974), *''Reinforcing of soft cohesive soils with stone columns''*, Ground Engineering, Vol. 7, No. 3, pp 42-49.

ICAO (1999), *''Aerodrome Design and Operations''*, Aerodrome Standards, Juli 1999, COSCAP South Asia.

Iglesia, G.R., Einstein, H.H. & Whitman, R.V. (1999), *''Determination of vertical loading on underground structures based on an arching evolution concept''*, Proceedings 3rd National Conference on Geo-Engineering for Underground Facilities, pp. 495-506.

Indonesian Public Works (1999), *''Guidance of timber pile foundation over soft soils and peat soils''*, (translated), Publisher Mediatama Saptakarya, Jakarta.

Irsyam, M. & Krisnanto, S. (2008), *''Pengujian Skala Penuh dan Analysis Perkuatan Cerucuk Matras Bambu untuk Timbunan Badan Jalan Diatas Tanah Lunak di Lokasi Tambak Oso Surabaya''*, Forum Teknik Sipil, Universitas Gadjah Mada, Vol. XVIII/1, Januari, 2008.

Jacobson, J. R., Filz, G. M. and Mitchell, J. K. (2003), *''Factors Affecting Strength Gain in Lime-Cement Columns and Development of a Laboratory Testing Procedure''*, Report prepared for the Virginia Transportation Research Council, Virginia Polytechnic Institute and State University.

Jafari,M.K., Shafiee, A., Razmkhah, A. (2002), *''Dynamic Properties of Fine Grained Soils in South of Tehran''*, JSEE: Spring 2002, Vol.4, No.1, pp. 25-35.

Jenner, C. G., Austin, R. A., and Buckland, D. (1998), *''Embankment support over piles using Geogrids''*, Proceedings of 6th International Conference on Geosynthetics Vol. 1: pp.763-766.

John, N. W. M. (1987), *''Geotextiles''*, Glasgow and London: Blackie & Son Ltd.

Jones, C. J. F. P., Lawson, C. R., and Ayres, D. J. (1990), *''Geotextile reinforced piled Embankments''*, Proceedings, 5th International Conference on Geotextiles, Geomembranes, and Related Products, 155-60.

Kaiqiu, L. (2000), *''Behaviour of DCM Columns under Highway Embankment at Bridge Approaches''*, Thesis for the Degree of Doctor of Philosophy, Nanyang Technical University.

Kawasaki, T., Nina, A., Saitoh, S., Suzuki, Y., Honjyo Y. (1981), *''Deep Mixing Method Using Cement Hardening Agent''*, Proceedings of the 10th International Conference on Soil Mechanics and Foundation Engineering, Stockholm: pp.721-24.

Kempfert, H.-G., Stadel, M., Zaeske, D. (1997), *''Design of geosynthetic-reinforced bearing layers over piles''*, Bautechnik 74 Heft 12: 818-25.

Kempfert, H.G., Hu, Y. (1999), *''Measured dynamic loading of railway underground''*, Proceedings of the XI. Panamerican Conference on Soil Mechanics and Geotechnical Engineering, Foz do Iguacu, Brazil.

Kempfert, H.G., Hu, Y. (1999), *''Numerical modeling of the deformation in railway foundation– A case study'',* Proceedings of the International Symposium on Numerical Models in Geomechanics, NUMOG VII, Graz, A.A. Balkema, S 669-674.

Kempfert, H.-G., Gobel, C., Alexiew, D., and Heitz, C. (2004), *''German recommendations for reinforced embankments on pile-similar elements''*, EuroGeo3 - Third European Geosynthetics Conference, Geotechnical Engineering with Geosynthetics, 279-84.

Kempfert, H.G. and Raithel, M. (2005), *''Soil Improvement and Foundation Systems with Encased Columns and Reinforced Bearing Layers''*, Elsevier Geo-Engineering Book Series, Volume 3, pp. 923-946.

Kempton, G., and Naughton, P. (2002), *''Piled embankments with basal reinforcement: development of design methods and state of the art''*, Proceedings of the XV Italian Conference on Geosynthetics.

Kenney, J.T. (1954), *''Steady-state vibrations of beam on elastic foundation for moving load''*, Journal Appl. Mech. ASCE 1954;21:359–364.

Kenney, T. C. (1976), *''Formation and geotechnical characteristics of glacial-lake varved soils''*, In Laurits Bjerrum Mem Vol, eds N Janbu, F Jorsted & B Kjaernsli, pp.15-39, Norwegian Geotech Inst, Oslo.

Kepmenhub (2000), *''Keputusan Menteri Perhubungan Tentang Jalur Kereta Api''*, KM 52 Tahun 2000, Departement Perhubungan republik Indonesia.

Kim, S.M. and Roesset, J.M. (2003), *''Dynamic response of a beam on a frequency-independent damped elastic foundation to moving load''*, Can. J. Civ. Eng. 2003;30:460–7.

Kivelo, M. (1997), *''Undrained shear strength of lime/cement columns''*, Proceedings, 14th International Conference on Soil Mechanics and Foundation Engineering, 1173-80.

Kivelo, M. (1998), *''Stabilization of embankments on soft soil with lime/cement columns''*, Doctoral Thesis, Royal Institute of Technology.

Klapperich, H. (2004), *''The Use of Geosynthetics in Soil Reinforcement and Dynamics''*, ECI International Conference, Schloss Pilnitz, Dresden.

Klompmaker, J. and Bishop, D. (2008), *''Improving the bearing capacity of soils with Geosynthetics''*, NAUE GmbH & Co. KG, Germany.

Koerner, R.M. (2005), *''Designing with Geosynthetics''*, 5th Edition, Pearson Prentice Hall, pp. 331-348.

Koiter, W.T. (1960), *''General theorems for elastic-plastic solids''*, Sneddon&Hill, Eds, Progress in Solid Mechanics, North Holland Publishing Co., Amsterdam, pp.165-221

Kolymbas, D. (1991), *''An outline of hypoplasticity''*, Archive of Applied Mechanics 61, pp. 143–151.

Kondner, R.L. & Zelasko, J.S. (1963), *''A hyperbolic stress-strain formulation for sands''*, Proc. 2nd Pan-American Conference of Soil Mechanics and Foundation Engineering, Vol.1, pp. 289-394.

Krynine, D.P. (1945), *''Discussion of Stability and stiffness of cellular cofferdams''*, Transactions, ASCE, Vol. 110, pp. 1175-1178.

Landva, A. O., et al (1983), *''Geotechnical classification of peats and organic soils''*, in Testings of Peats and Organic Soils, ASTM STP 820 ed. P Jarrett, 37-51.

Lawson, C. R. (1992), *''Soil reinforcement with Geosynthetics, Applied Ground Improvement Techniques''*, Southeast Asian Geotechnical Society (SEAGS): 55-74.

Low, K., Tang, S.K., Choa, V. (1994), *''Arching in Piled Embankments''*, Journal of geotechnical engineering, Vol. 120, No. 11, S. 1917-1938.

Maddison, J.D., Jones, D.B., Bell, A.L. & Jenner, C.G. (1996), *''Design and performance of an embankment supported using low strength geogrids and vibro concrete columns,*

Geosynthetics – Applications'', Design and Construction, De Groot, Den Hoedt & Termaat, pp. 325-332.

Mandolini, A. & Viggiani, C. (1997), *''Settlement of piled foundations"*, Géotechnique, 47(4): 791-816.

Marston, A.& Anderson, A.O. (1913), *''The theory of loads on pipes in ditches and tests of cement and clay drain tile and sewer pipe''*, Bulletin No. 31, Iowa Engineering Experiment Station, Ames, Iowa.

Matsuoka, H. and Nakai, T. (1982), *''A new failure for soils in three-dimensional stresses, In: Deformation and Failure of Granular Materials''*, Proc. IUTAM Symp. In Delft, pp. 253-263.

May, R. W. and Witczak, M.W. (1981), *''Effective Granular Modulus to Model PavementResponse"*, Transportation Research Record 810, TRB, National Research Council, Washington, D.C.

McKelvey, D., Sivakumar, V., Bell, A. and Graham, J. (2004), *''Modelling vibrated stone columns in soft clay''*, Proceedings of the Institute of Civil Engineers Geotechnical Engineering, Vol. 157, Issue GE3, pp 137-149.

McKelvey, J.A. (1994), *''The anatomy of soil arching''*, Geotextiles and Geomembranes 13, pp. 317-329.

MacKinnon, K., Hatta, G., Halim, H. & Mangalik, A. (1996), *''The Ecology of Indonesia Series''*, Vol. III: The Ecology of Kalimantan; Periplus Editions (HK) Ltd.

McNulty, J.W. (1965), *''An Experiment study of arching in sand''*, Technical Report No. I-674, U.S. Army Engineer Waterways Experiment Station, Corps of Engineers, Vicksburg, Mississippi, 170.

Meyerhof, G.G. and Hanna, A.M. (1978), *''Ultimate bearing capacity of Foundation on Layaered Soil under Inclined Load''*, Canadian Geotechnical Journal , Vol. 15 No. 4, pp. 565-572.

Milovic, D. (1992), *''Stress and Displacements for Shallow Foundations''*, Elsevier Science Publisher, Amsterdam, The Netherlands.

Mirafi, T., (2010), *''Geosynthetic Reinforcement of the Aggregate Base/Subbase courses of Pavement Structures''*, Technical Note.

Moossazadeh, J. and Witczak, M.W. (1981), *''Prediction of Subgrade Moduli for Soil that Exhibits Nonlinear Behavior"*, Transportation Research Record 810, TRB, National Research Council, Washington, D.C., pp. 9-17.

Mroz, Z., Norris, V.A. and Zienkiewicz,O.C.(1978), *''An anisotropic hardening model for soils and its application to cyclic loading''*, International Journal For Numerical and Analytical Methods in Geomechanics, 2: pp. 203-221.

Muench, S. (2006), *''Pavement engineering''*, http://www.pavementinteractive.org

Muncke, M., Meinlschmidt, A., Hillig, J. (1999), *''Neue Erkenntnisse und Lösungen im Brücken-,Tunnel-, Erd- und Grundbau''*, Eisenbahntechnische Rundschau, Band 48, Heft 10, S. Pp. 622-638.

Muslihat, L.(2003), *''Teknik Pengukuran Bobot isi Tanah Gambut di Lapangan dan di Laboratorium''*, Buletin Teknik Pertanian Vol. 8 Nomor 2, 2003.

Navin, M. P. and Filz, G. M. (2005), *''Statistical Analysis of Strength Data from Ground Improved with DMM Columns''*, Proceedings of the International Conference on Deep Mixing, Stockholm.

Niemunis, A. & Herle, I. (1997), *''Hypoplastic model for cohesionless soils with elastic strain Range''*, Mechanics of Cohesive-Frictional Materials 2: pp. 279–299.

Niemunis, A., Wichtmann, T., Triantafyllidis, T. (2005), *''A high-cycle accumulation model for sand''*, Computers and Geotechnics, 32(4): pp. 245-263.

Nordic Guidelines (2003),''Nordic Guidelines for Reinforced Soils and Fills'', The Nordic Geotechnical Societies Nordic Industrial Fund.

Ooi, T.A., Chan, S.F., Wong, S. N. (1987), *''Design, Construction, and Performance of Pile Supported Embankments''*, 9th Southeast Asian Geotechnical Conference: 2-1 to 2-12.

Palmeira, E.M., Tatsuoka, F., Bathurst, R.J., Stevenson, P.E. and Zornberg, J.G. (2008), *''Advances in Geosynthetics Materials and Applications for Soil Reinforcement and Environmental Protection Works''*, EJGE, Bouquet 08, pp. 1-37.

Park, D. & Stewart, H.E. (2001), *''Suggestion of Empirical Equations for Damping Ratio of Plastic and Nonplastic Soils based on the Previous Studies''*, Proc. Fourth Internat. Conf. on Recent Advances in Geotech. Earthquake Eng. and Soil Dynamics, San Diego, California, Paper No. 1.21.

Paul, M.A, & Barras, B.F. (1999), *''Role of organic content in the plasticity of Bothkennar Clay''*, Geotechnique (Technical Note), 49, 4, pp. 529-535.

Perkins, S.W. and Ismeik, M. (1997), *''A Synthesis and Evaluation of Geosynthetic Reinforced Base Layers in Flexible Pavements: Part I"*, Geosynthetics International, Vol. 4, No. 6, pp. 605-621.

Porbaha, A. (2000), *''State of the art in deep mixing technology: Part IV''*, Design Considerations, Ground Improvement 3: 111-125.

Potts, V.J. & Zdravkovic, L. (2008), *''Assessment of BS8006: 1995 design method for reinforced fill layers above voids''*, Proceddings of the 4th European Geosynthetics Conference, Edinburgh, UK, Paper number 116.

Poulos, H.G. (1968), *''Analysis of the settlement of pile groups"*, Geotechnique,18:449-471.

Poulos, H. G., (1971), *''Behaviour of Laterally Loaded Piles I-Single Piles"*, Journal of SoilMechanics and Foundation Division, ASCE, Vol. 97, No. 5, pp. 711-732.

Poulos, H.G. (1993), *''Settlement of bored pile groups"*, Proc. BAP II, Ghent, Balkema, Rotterdam, pp. 103-117.

Poulos, H. GC and Davis, E. H. (1974), *''Elastic Solutions for Soil and Rock Mechanics''*, Wiley, New York.

Poulos, H.G. and Davis, E.H. (1980), *''Pile foundation analysis and design''*, New York, John Wiley.

Poulos, H.G. (1994a), *''An approximate numerical analysis of pile-raft interaction"*, IJNAMG, 18, pp.73-92.

Poulos, H.G. (1994b), *''Settlement prediction for driven piles and pile groups"*, Spec.Tech. Pub. 40, ASCE, 2, pp. 1629-1649.

Poulos, H.G. (2002), *''Simplified Design Procedure for Piled Soil Raft Foundations"*, Deep Foundations 2002, ASCE, Reston, Virginia, 441-458.

Poulos, H.G. (2005), *''Pile behaviour-Consequences of Geological and construction imperfections"*, 40th Terzaghi Lecture, Jnl. Geot. & Geoenv. Eng., ASCE, 131(5), pp. 538-563.

Priadi, E. (2008), *''Behaviour of Tiang Tongkat Foundation over Pontianak Soft Organic Soil using 3D-Finite Element Analysis''*, PhD Thesis, Geotechnical Institute of Technische Universität Bergakademie Freiberg, Germany.

Priebe, H. J. (1993), *''Design Criteria for Ground Improvement by Stone Columns''*, Proceedings of the Fourth National Conference on Ground Improvement.

Priebe, H. J. (1995), *''The design of vibro replacement''*, Ground Engineering, 28, No. 10: pp. 31-37.

PrEN ISO 10318 (2001), *''Geosynthetics-Geotextiles, geotextile-related products, geomembranes and geosynthetic clay liners, Terms and their definitions''*, Trilingual version, February 2001.

Puslitbang Prastrans (2001), *''Timbunan Jalan pada Tanah Lunak''*, (Indonesian Geotechnical Guidance-4) Panduan Geoteknik-4: Desain dan Konstruksi, WSP International, Bandung, Indonesia.

Puslitbang Prastrans (2001), *''Timbunan Jalan pada Tanah Lunak''*, (Indonesian Geotechnical Guidance-1) Panduan Geoteknik-1: Proses Pembentukan dan Sifat-sifat Dasar Tanah Lunak, WSP International, Bandung, Indonesia.

Puslitbang Prastrans (2002), *''Timbunan Jalan pada Tanah Lunak''*, (Indonesian Geotechnical Guidance-2) Panduan Geoteknik-2: Penyelidikan Tanah Lunak, Desain & Pekerjaan Lapangan, WSP International, Departemen Permukiman dan Prasarana Wilayah,Bandung, Indonesia.

Radjagukguk, B. (1991), *''Utilization and management of peatlands in Indonesia for Agriculture''*, Tropical Peat-Proceedings of the International Symposium on Tropical Peatland, Kuching 6 - 10 May 1991, pp. 21-27.

Rahadian, H. (1992), *''Comparison of Engineering Properties of Soft Marine Clays and Soft Lacustrine Clays from Indonesia''*, M.Sc. Thesis, University of Strathclyde.

Rahadian, H. et al. (2001), *''Field and laboratory data interpretation of peats at Berengbenkel trial site''*, International Conference on In situ Measurement of Soil Properties and Case Histories, Bali, Volume: Embankments on Soft Soils.

Raju, D.M. and Fannin, R.J. (1998), *''Load-strain-displacement Response of geosynthetics in Monotonic and Cyclic Pullout''*, Canadian Geotechnical Journal, Vol. 35, pp. 946-956.

Raju, V.R., Hari Krishna, R. and Wegner, R. (2004), *''Ground improvement using Vibro Replacement in Asia 1994 to 2004 – a 10 year review''*, Proceedings of 5th Int. Conf. on Ground Improvement Techniques, Kuala Lumpur, Malaysia.

Raithel, M., Küster, V. & Lindmark, A., (2004), *''Geotextile encased Column-a Foundation System for Earth Structures''*, Illustrated by a Dyke Project for a Works Extension inHamburg, Nordic Geotechnical Meeting, Sweden.

Raithel, M., Kirchner, A., Schade, C. & Leusink, E., (2005), *''Foundation of Constructions On Very Soft Soils with Geotextile Encased Columns-State of the Art''*, ASCE-Conference Geo-Frontiers, Austin, USA.

Randolph, M.F. (1994), *''Design methods for pile groups and piled rafts''*, Proc. 13th Int. Conf. S.M. & Found. Eng., 5, pp. 61-82.

Reid, W.M., Buchanan, N.W. (1983), *''Bridge approach support piling; Proceedings of Conference on Advances in Piling and Ground Improvement''*, London, S. 267-274.

Rodin, S. (1965), *''Ability of a clay fill to support construction plant''*, Journal of Terramchanics, 2, pp. 51-68.

Rogbeck, Y., Gustavsson, S., Södergren, I., Lindquist, D. (1998), *''Reinforced Piled Embankments in Sweden – Design Aspects''*, Proceedings of the 6th International Conference on Geosynthetics, S. 755-762.

Roscoe, K.H. and Burland, J.B. (1968), *''On the generalised stress-strain behaviour of wet Clay''*, Engineering Plasticity, Vol.1, London, UK. Cambridge University Press, pp. 535-609.

Rosenqvist, I. Th. (1953), *''Considerations on the sensitivity of Norwegian quickclays''*, Geotechnique, 3, 5, pp. 195-200.

Rowe, P.W. (1962), *''The stress-dilatancy relation for static equilibrium of an assembly of particles in contact''*, Proc. Roy. Soc. A. 269, pp. 500-527.

Rowe, P.W. (1971), *''Theoretical meaning and observed values of deformation parameters for soil''*, Proc. of Roscoe memorial symposium, Foulis, Henley-on-Thames, pp. 143-194.

Ruiken, A. & Ziegler, M. (2008), *''Effect of Reinforcement on the Load Bearing Capacity of Geosynthetic Reinforced Soil"*, Proc., 4th European Geosynthetics Conf., igs, Edinburgh, UK.

Ruiken, A., Ziegler, M., Vollmert, L. And Duzic, I. (2010), *''Recent findings about the confining effect of geogrids from large scale laboratory testing''*, 9th International Conference on Geosynthetics, Brazil.

Russell, D., Naughton, P. J., and Kempton G. (2003), *''A new design procedure for piledEmbankments''*, Proceedings of the 56th Canadian Geotechnical Conference and the NAGS Conference, 858-65.

Russel, D., Pierpoint, N., MacDonald, M. (1997), *''An assessment of design methods for piled Embankments''*, Ground Engineering, Nov. 1997, S. 39-44.

Sasongko, H. (1996), *''Determination of Subgrade Moduli under Repeated Triaxial Loading Tests''*, M.Sc Thesis, Bandung Institute of Technology, Indonesia.

Satibi, S. (2009), *''Numerical Analysis and Design Criteria of Embankments on Floating Piles''*, PhD Thesis, Mitteilung 62 des Institüts fur Geotechnik, Universität Stuttgart.

Sawicki, A. and Swidzinski, W. (1989), *''Mechanics of a sandy subsoil subjected to cyclic Loadings''*, International Journal for Numerical and Analytical Methods in Geomechanics, 13: pp. 511-529.

Schanz, T., and Vermeer, P.A. (1996), *''Angles of friction and dilatancy of sand''*, Geotecnique 46, No.1, pp. 145-151.

Schanz, T., Vermeer, P.A., and Bonnier, P.G.(1999), *''The hardening soil model: Formulation and verification''*, Beyond 2000 in Computational Geotechnics-10 years of Plaxis, Rotterdam, Balkema.

Schwarz, W. and Raithel, M. (2005), *''Stabilization of soft organic soils with cement columns using the Mixed-in-Place technique (MIP) for a railway embankment''*, Bauingenieur Band 79.

Scottwillson (2009), *''Bassaly Reinforced Platforms for Piled Embankments-Two Case Studies''*, Joint UK-IGS EGGS Meeting London 08 Dec 2009,www.scottwilson.com.

Seed, H. B. and Chan, C.K. (1959), *''Structure and Strength Characteristics of Compacted Clays"*, Journal of Soil Mechanics and Foundation Engineering Division, ASCE, Vol. 85, No. 5, pp. 87-128.

Seed, H.B., Mitry, F.G., Monismith, C.L., and Chan, C.K., (1967), *''Prediction of pavement deflection from laboratory repeated load tests''*, NCHRP Report 35, USA.

Seed, H.B. and Idriss, I. (1970), *''Soil moduli and damping factors for dynamic response analysis''*, Report, Eartquake Engineering Research Center, University of California, Barkeley.

Sellmeijer, J. B. and Kenter, C. J. (1983), *''Increase in Bearing Capacity due to the Application of Geolon Fabric below Granular Base of Road''*, Delft Soil Mechanics Laboratory, Delft.

Sellmeijer, J. B. (1990), *''Design of Geotextile Reinforced Paved Roads and Parking Areas"*, Proceedings of the Fourth International Conference on Geotextiles, Geomembranes, and Related Products, Balkema, Vol. 1, The Hague, Netherlands, pp. 177-182.

Simandjuntak, T. O. (1993), *''Neogene tectonics and orogenis of Indonesian''*, Jurnal Geologi dan Sumberdaya Mineral, Geological Research & Development Centre.

Skempton, A. W. (1970), ''The Consolidation of clays by gravitational compaction'', Quarterly Journal of Engineering Geology, p. 373-411.

Slocombe, B.C. & Bell, A.L. (1998), *''Setting on a dispute: discussion on Russell and Pierpoint paper''*, Ground Engineering,pp. 34-36.

Smith, I.M. and Griffith, D.V. (1982), *''Programming the Finite Element Method"*, Second Edition. John Wiley & Sons, Chisester, U.K.

Smith, M.E. (2005), *''Design of bridging layers in geosynthetic-reinforced column-supported embankments''*, PhD Thesis, Virginia Polythechnic Institute and State University.

SNI (2002), *''Tata Cara Perencanaan Struktur Kayu Untuk Bangunan Gedung''*, Beta Version, SK SNI 03-2000, Bandung, Indonesia.

Soong, T.-Y. & Koerner, R.M. (1997), *''On the Required Connection Strength of Geosynthetically Reinforced Walls''*, Journal of Geotextiles and Geomembranes, Vol. 15, pp. 377-393.

Steward, J.E., Williamson, R., and Mohney, J. (1977), *''Guidelines for Use of Fabrics in Construction and Maintenance of Low-Volume Roads''*, USDA, Forest Service Report PB-276 972, Portland, OR.

Suherman, M. et al. (2003), *''Guidance for Roadway Construction over Expansive Soil''*, Final Report, Puslibang Penelitian dan Pengembangan Prasarana Transportasi, Bandung, Indonesia.

Suryolelono ,K.B. (1997), *''Soil Stabilization and Reinforcement, Compaction, Accelerated Consolidation''*, Penataran Soil Improvement and Reinforced Earth, University of Lambung Mangkurat, Banjarmasin, Indonesia.

Tamáskovics, N. & Klapperich, H. (2010), *''Verbundverhalten von Geokunststoffen in bindigem Boden''*, 9.Sächsisches Bautextilien-Symposium BAUTEX 2010 Bauen mit Geokunststoffen, Chemnitz, pp. 1-6.

Takenaka, D. and Takenaka, K. (1995), *''Deep chemical mixing method-using cement ashardening agent''*, Takenaka Corporation, Tokyo.

Tatsuoka, F. (1993), *''Role of facing rigidity in soil reinforcing''*, Keynote Lecture, Proc. Int. Sym. On Earth reinforcement Practice, IS Kyushu '92. Balkemia, 2: 831-870.

Tatsuoka, F., Tateyama, M. Uchimura, T., Koseki, J. (1997), *''Geosynthetic-Reinforced Soil retaining Walls as Important permanent Structures''*, Geosynthetics International 1997, Volume 4, No. 2.

Tatsuoka, F., Tateyama, M., Mohri, Y. and Matsushima, K. (2007), *''Remedial treatment of soil structuress using geosynthetic-reinforcing technology''*, Geotextiles and Geomembranes, Vol. 25, Nos. 4 & 5.

Tatsuoka, F. and Kobayashi, A. (1983), *''Triaxial strength characteristics of cement-treated soft clay''*, Proceedings of the 8th European Conference of SMFE, 421-26.

Tenax (2001), *''Design of Soft Soil stabilization with Tenax geogrids''*, Technical Reference GRID-DE-1.

Tenax (2001), *''Design of unpaved roads with Tenax geogrids''*, Technical Reference TDS007,GRID-DE-3.

Terashi, M. (2003), *''The state of practice in deep mixing methods''*, Grouting and GroundTreatment, Proceedings of the 3rd International Conference, ASCE Geotechnical Special Publication No. 120, New Orleans: 25-49.

Terzaghi, K. (1943), *''Theoretical Soil Mechanic''*, John Wiley & Sons, New York.

Thompson, W.E. (1963), *''Analysis of dynamic behavior of roads subject to longitudinally moving loads''*, Highway Res. Rec. 1963;No. 39:1–24.

Tomlinson, M.J. (1977), *''Pile design and construction practice''*, London: Cement and Concrete Association.

Uzan, J. (1985), *''Characterization of Granular Material''*, Transportation Research Record 345, Washington, D.C. 1022, TRB, National Research Council, Washington, D.C., pp 52-59.

Valanis, K.C and Lee, C.F. (1984), *''Endochronic theory of cyclic plasticity with applications''*, Journal of Applied Mechanics, 51:367-374.

Van Impe, W. F., Madhav, M. R., Vandercruyssen, J. P. (1997), *''Considerations in stone column design''*, Ground Improvement Geosystems, Densification and Reinforcement, 190-196.

Vermeer, P. (1982), *''A five constant model unifying well established concepts''*, In: Constit. Relat. for Soils, Balkema, Holland, Proceedings of the International Workshop in Grenoble, pp. 175-198.

Vermeer, P.A. and Neher, H.P.(1999), *''A soft soil model that accounts for creep''*, Proceeding of International Symposium Beyond 2000 in Computational Geotechnics, Balkema, pp. 249-261.

Von Soos, P. (2001), *''Eigenscfahten von Boden und Fels-ihne Ermittung im Labor''*, Gundbau-Taschenbuch, Vol.1. chapter 1.4, pp. 117-201, Ernst and Sohn, Berlin.

Webb, W.M., and Campbell, B.E. (1986), *''Preliminary Investigation into Resilient Modulus Testing for new AASHTO Pavement Design Guide''*, Office of Materials and Research, Georgia Department of Transportation.

Wei-ping, C.,Yun-min, C., Ren-peng, C. (2007), *''An experimental investigation of soil arching within basal reinforced and unreinforced piled embankments''*, Geotextiles and Geomembranes 26 (2008), Science Direct, Elsevier, pp. 164-174.

Wichtmann, T.(2005), *''Explicit accumulation model for non-cohesive soils under cyclic Loading''*, Doctoral Dissertation, Heft-38, Ruhr-Universität Bochum.

Widodo, S. et al. (2013), *''Zwischenbericht des DFG-Forschungsprojektes: Verbundverhalten von Geokunststoffen in bindigen Böden''*, TU-Bergakademie Freiberg (unpublished).

Wilson and Huesker (2009), *''Basally Reinforced Platforms for Piled Embankments-Two Case Studies''*, Joint UK-IGS EGGS Meeting London 08 Dec 2009.

Wolffersdorff, P.A.v.(1996), *''A hypoplastic relation for granular materials with a predefined limit state surface''*, Mechanics of Cohesive-Frictional Materials 1: pp. 251–271.

Wood, D.M., Hu, W., Nash, D.F.T. (2000), *''Group effects in stone column foundations-model tests''*, Geotechnique, Vol. 50, No. 6, pp. 689-698.

Yang, G., Zhang, B. & Zhou, Q. (2009), *''Behaviour of Geogrid Reinforced Soil Retaining Wall with Concrete-Rigid Facing''*, Journal of Geotextiles and Geomembranes (2009), article in press, doi: 10.1016/j.geotexmem. 2009.03.001.

Zaeske, D. (2001), *''Zur Wirkungsweise von unbewehrten und bewehrten mineralischen Tragschichten über pfahlartigen Gründungselementen''*, Schriftenreihe Geotechnik, Universität Kassel, Heft 10.

Ziegler, M., Heerten, G., Retzlaff, J. (2007), *''A new dimensioning approach for junction stiff Geogrids''*, XIV European Conference on Soil Mechanics and Geotechnical Engineering, Madrid, Spain.

Zornberg, J.G and Grupta, R. (2010), *''Geosynthetics in pavements: North America Contributions''*, The 9th International Conference on Geosynthetics, Brazil.

Zhuang, Y.F. (2006), *''Model test study on soft clay reinforced with electro-kinetic geosynthetics''*, Geosynthetics, J. Kuwano & J. Koseki (eds), p.531-534, Rotterdam.

Zhuang, Y. (2009), *''Numerical Modelling of Arching in Piled Embankments Including the Effect of Reinforcement and Subsoil''*, PhD Thesis, University of Nottingham.